New insights into the allosteric regulation of *Arabidopsis* PI4Kβ1 and effects of phosphorylation on protein function

Dissertation

zur Erlangung des

Doktorgrades der Naturwissenschaften
„doctor rerum naturalium“

der

Naturwissenschaftlichen Fakultät I – Biowissenschaften –

MARTIN-LUTHER-UNIVERSITÄT
HALLE-WITTENBERG

vorgelegt von
Frau Angela Liliana Meza López

Gutachter: -Prof. Dr. Ingo Heilmann
-Prof. Dr. Mike Schutkowski
-Prof. Dr. Ivo Feußner

Eingereicht am: 11.12.2024
Tag der Verteidigung: 10.03.2025

Table of contents

Abbreviations

ACN	Acetonitrile
ADP	Adenosine diphosphate
AP	Alkaline phosphatase
APS	Ammonium persulfate
prefix At	from *Arabidopsis thaliana*
AtPI4Kβ1	Phosphatidylinositol 4-kinase beta1 from *Arabidopsis thaliana*
ATP	Adenosine triphosphate
BCIP	5-bromo-4-chloro-3-indolyl phosphate
BSA	Bovine serum albumin
$CaCl_2$	Calcium chloride
CA	Constitutively Active
CA-MPK4	Constitutively Active Mitogen Activated Protein Kinase 4
CA-MPK6	Constitutively Active Mitogen Activated Protein Kinase 6
Cas	Casein
Cat	Catalytic domain
CBL	Calcineurin B-like protein
cDNA	Complementary deoxyribonucleic acid
CDPK11	Calcium-dependent protein kinase
DMSO	Dimethyl sulfoxide
DNA	Deoxyribonucleic acid
dNTPs	Desoxynucleotides
DTT	Dithiotreitol
E. coli	*Escherichia coli*
EDTA	Ethylene diamine tetraacetic acid

ER	Endoplasmic reticulum
EYFP	Yellow fluorescent protein
HCl	Hydrochloric acid
IPTG	Isopropyl β-D-1-thiogalactopyranoside
KanR	Kanamycin resistance
KCl	Potassium chloride
KD	"Kinase dead", catalytically inactive protein variant
KD-MPK4	catalytically inactive Mitogen Activated Protein Kinase 4
KD-MPK6	catalytically inactive Mitogen Activated Protein Kinase 6
KOH	Potassium hydroxide
LC/MS/	Liquid-chromatography coupled to tandem mass-spectrometry
Lin	Linker domain
LKU	Lipid kinase Unique Domain
m/z	Mass-to-charge ratio
MAPK	Mitogen-activated protein kinase
MBP	Maltose binding protein
MCS	Multiple cloning site
$MgCl_2$	Magnesium chloride
MORN	Membrane occupation and recognition nexus
MyBP	Myelin Basic Protein
Na_2MoO_4	Sodium molybdate
NaCl	Sodium chloride
NBT	Nitro blue tetrazolium chloride
NH	Novel homology domain
NH_4OH	Ammonium hydroxide
PCR	Polymerase chain reaction
PDB	Protein data base

PI 4-Kinase	Phosphatidylinositol 4-kinase
PI 3-Kinase	Phosphatidylinositol 3-kinase
PI4Kβ1- WT	Wild Type Phosphatidylinositol 4-kinase beta1
PI4Kβ1- S186A	Phosphatidylinositol 4-kinase beta1 phospho-ablation variant
PI4Kβ1- S454A	Phosphatidylinositol 4-kinase beta1 phospho-mimicking variant
PI4Kβ1- S186D	Phosphatidylinositol 4-kinase beta1 phospho-ablation variant
PI4Kβ1- S454D	Phosphatidylinositol 4-kinase beta1 phospho-mimicking variant
PI4Kβ1- S186A-S454A	Phosphatidylinositol 4-kinase beta1 phospho-ablation variant
PI4Kβ1- S186D-S454D	Phosphatidylinositol 4-kinase beta1 phospho-mimicking variant
PI4Kβ1- R626A	Phosphatidylinositol 4-kinase beta1 ablation variant
PI4Kβ1- L1117A	Phosphatidylinositol 4-kinase beta1 ablation variant
PI4Kβ1- C-terminus	Phosphatidylinositol 4-kinase beta1 c-terminus tail deleted
PI4Kβ1- Cat-domain	Catalytic domain of phosphatidyl-inositol-4-kinase-beta1
PIs	Phosphoinositides
PI Soy	Phosphatidylinositol derived from Soy
PIPK	Phosphatidylinositol-bisphosphate kinase
PPC	Plant Partially charged (PPC) or repetitive domain
PtdIns	Phosphatidylinositol
PtdIns3P	Phosphatidylinositol 3-phosphate
PtdIns4P	Phosphatidylinositol 4-phosphate
PtdIns5P	Phosphatidylinositol 5-phosphate
PtdIns(3,4)P_2	Phosphatidylinositol 3,4-bisphosphate

PtdIns(3,5)P_2	Phosphatidylinositol 3,5-bisphosphate
PtdIns(4,5)P_2	Phosphatidylinositol 4,5-bisphosphate
PtdIns(3,4,5)P_3	Phosphatidylinositol 3,4,5-trisphosphate
SDS-PAGE	Sodium dodecyl sulfate polyacrylamide gel electrophoresis
RNA	Ribonucleic acid
SnRK2.6-WT	Wild type sucrose non-fermenting-1-related protein kinase 2.6
TEMED	Tetramethylethylenediamine
TLC	Thin layer chromatography
TRIS	2-Amino-2-hydroxymethyl-propane-1,3-diol
UniProt	Universal Protein Resource

Summary

Phosphatidylinositol 4-kinase β1 (PI4Kβ1) is a key enzyme of plant phosphoinositide biosynthesis at endosomal membranes, where it mediates the ATP-dependent conversion of phosphatidylinositol (PtdIns) to PtdIns 4-phosphate (PtdIns4P). *Arabidopsis* PI4Kβ1 is important for endomembrane trafficking, and at a larger scale for plant development, for instance for correct progression of cytokinesis or for root hair growth. PI4Kβ1 colocalizes and interacts with the mitogen-activated protein kinase (MAPK) MPK4 at the trans-Golgi-network (TGN) and is a known phosphorylation substrate for the MAPKs, MPK4 and MPK6. So far, biochemical features of PI4Kβ1 and effects of phosphorylation have not been characterized. The aim of this dissertation was to investigate the biochemical features of purified recombinant MBP-PI4Kβ1 produced in *E. coli* BL21 (DE3), to elucidate the orientation PI4Kβ1 towards the (substrate) membrane, and to characterize the effects of phosphorylation of PI4Kβ1 *in vitro.* Radioactive *in vitro* lipid phosphorylation assays suggest that PI4Kβ1 kinetics is regulated upon binding to both substrate and product. Upon increasing PtdIns substrate concentration PI4Kβ1 is allosterically regulated through product (PtdIns4P) binding, and PI4Kβ1 exhibits a positive cooperativity indicated by a sigmoidal kinetic profile. The kinetic data indicate that PI4Kβ1 contains distinct product binding sites that are different from the active site and are located in regulatory domains of the protein. By contrast, a hyperbolic kinetic behavior was obtained for PI4Kβ1 upon increasing concentrations of ATP, in line with only one ATP-binding site involved in catalysis. Based on protein homology modeling and molecular dynamics simulations performed in cooperation with the group of Prof. Dr. Panagiotis Kastritis, a 3D model of PI4Kβ1 was obtained that indicates a likely membrane-orientation of the protein. The obtained model for PI4Kβ1 exhibited a well conserved c-terminal tail helix, possibly interacting with the PtdIns4P product. A predicted involvement of the c-terminal tail helix in catalysis was confirmed by i*n vitro* lipid phosphorylation assays, suggesting an essential role of this c-terminus helix for either binding the substrate or for product release.

Protein function and catalysis can also be regulated by PI4Kβ1 phosphorylation by MPK4 or MPK6. We confirmed that PI4Kβ1 is a target for phosphorylation by upstream MAPKs and that S186 and S454 are key phosphorylation sites. To elucidate the role of these target phosphosites on protein function, substitution variants of PI4Kβ1 were created in which the respective residues were altered to alanine or aspartic acid to mimic the dephosphorylated or phosphorylated states, respectively. The kinetic characterization of the PI4Kβ1 substitution variants indicated a regulatory effect of S186D (activating) and S186A (inactivating), whereas both S454D and S454A had similar reaction kinetics to Wild Type-PI4Kβ1. The data indicates that MAPK-mediated phosphorylation of MBP-PI4Kβ1 at position S186 may contribute to the regulation of catalytic activity of PI4Kβ1. Taken all together, a model for the orientation of PI4Kβ1 at the membrane is presented. Experimental data establish a novel mechanism of regulation of PI4Kβ1 through product binding and indicate activating/inactivating effects of MAPK-mediated phosphorylation of PI4Kβ1.

1. Introduction

1.1. Membranes and membrane-associated processes in plants

Membrane structure and lipid composition

Biological membranes are highly ordered structures consisting of an asymmetric lipid bilayer with integral and associated proteins (Jaillais et al., 2024). In 1972, the Fluid-Mosaic model of cell membranes was presented based on thermodynamic principles. The mosaic structure was proposed to be dynamic rather than static with evidence of lateral mobility within the membrane matrix (Singer & Nicolson, 1972). This model remains important to this day and has been expanded to accommodate more complex membrane structures, such as specialized membrane nanodomains, protein/glycoprotein complexes, cytoskeletal fences, and links to extracellular matrix components that limit the lateral diffusion of membrane components (Nicolson, 2014).

Biological membranes of eukaryotic organisms act as a barrier not only controlling the exchange of molecules between the two sides of the membrane but also serve as a primary contact site between cellular spaces (Nicolson, 2014). While the plasma membrane surrounds the cell, endomembranes allow the cell to compartmentalize into sub-structured organelles like nucleus, endoplasmic reticulum, Golgi, endosomes, chloroplasts and mitochondria (Alberts et al., 2002).

In plants, the main components of all membranes are glycerolipids (mainly phospholipids), sterols and sphingolipids (Figure 1 A-B). Glycerolipids are molecules consisting of a head group nucleated by a glycerol moiety to which two fatty acyl chains are esterified at positions *sn1* and *sn2*. The third position consists of a hydroxyl group to form diacylglycerol (DAG) and can be further modified to form the different classes of phospholipids. Phosphatidylcholine (PtdCho) and phosphatidylethanolamine (PtdEtn) represent up to 68–80% of structural phospholipids. Other structural lipids, such as phosphatidylglycerol (PtdGly), phosphatidylinositol (PtdIns), phosphatidylserine (PtdSer), or phosphatidic acid (PtdOH), are also present in plant membranes (Murphy et al., 2010). Sterols are further crucial structural components of membranes because they control lipid chain order and increase the bilayer permeability. Sterols are isoprenoids, made up of four rigid rings. Free sterols represent 70–90% of total sterols in the plasma membrane.

Additionally, sphingolipids consist of a long-chain base amidated by a fatty acid and a polar head attached to the alcohol residue of the long chain base (Murphy et al., 2010).

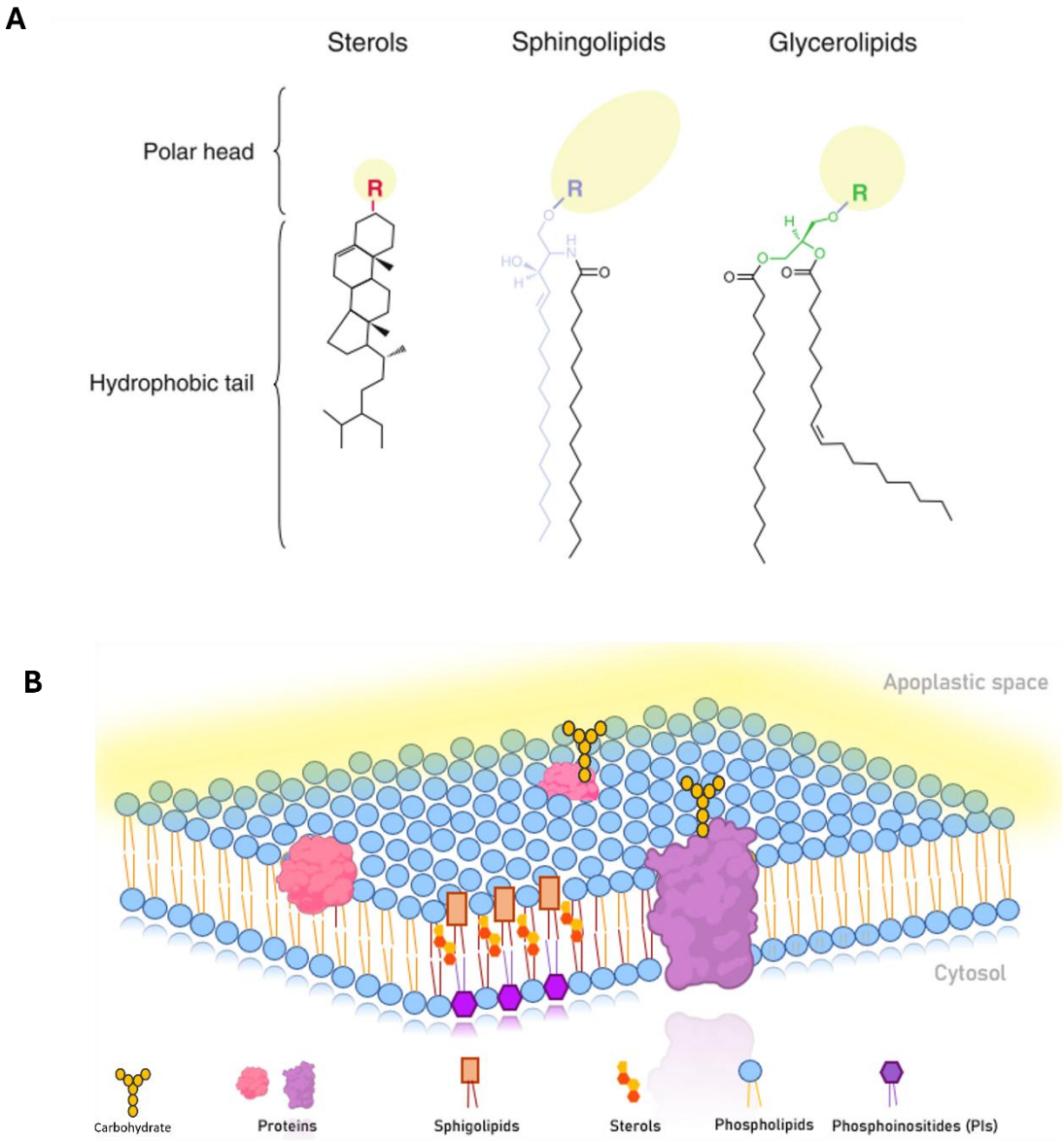

Figure 1. Representation of a plant plasma membrane. **A.** The main components of membranes are glycerolipids, sterols and sphingolipids. **B.** Biological membranes contain structural and regulatory lipids, proteins (integral and associated) and carbohydrates (e.g. glycolipids, glycoproteins). This figure was designed here, based on lipid compositions previously reported (Mamode Cassim et al., 2019).

On the other hand, phosphoinositides (PIs) represent a minority of total cellular lipids and play an important regulatory role in membrane trafficking in plants. Their functional effects can be mediated by their headgroups, which can be reversibly phosphorylated to generate up to five species in plants (I. Heilmann, 2016; Sussman & Harper, 1989). PIs are derived from the membrane phospholipid, phosphatidylinositol (PtdIns), which contains

D-myo-inositol, a cyclic polyol, linked via a phosphodiester bond in the C1 position to the glycerol backbone as a lipid head group. Derivatives emerges from the PtdIns phosphorylation of hydroxyl groups in the positions 3, 4 and 5 to form three PtdIns monophosphates, PtdIns3P, PtdIns4P and PtdIns5P, and two PtdIns bisphosphates, PtdIns(3,5)P_2 and PtdIns(4,5)P_2. PtdIns5P has been detected in plants, but there is no candidate for a PI 5-kinase mediating its biosynthesis by direct phosphorylation of PtdIns (Figure 2).

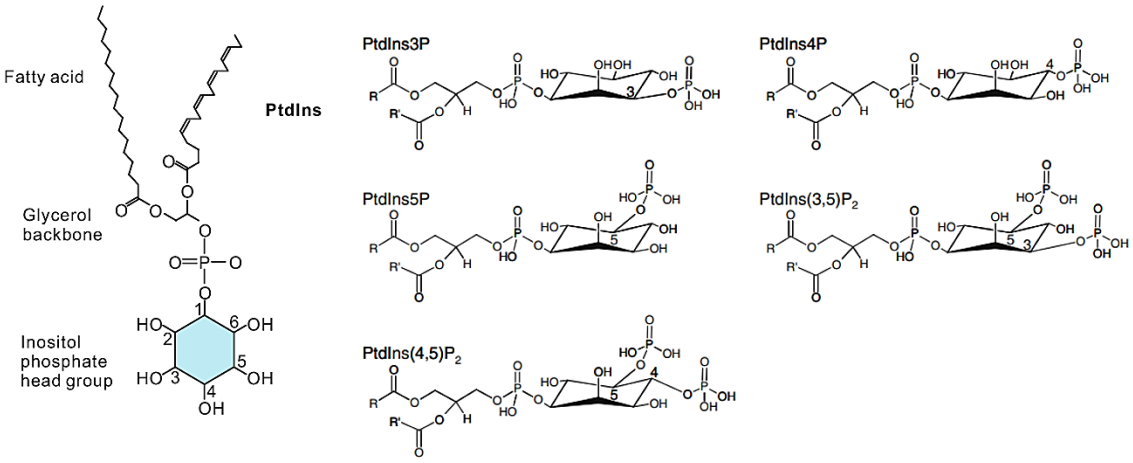

Figure 2. The *Arabidopsis* phosphoinositide structures. PIs are derived from the membrane phospholipid, phosphatidylinositol (PtdIns), which contains D-myo-inositol ring that can be phosphorylated at particular positions giving rise to five known PIs in plants: phosphatidylinositol-3-phosphate (PtdIns3P); phosphatidylinositol-4-phosphate (PtdIns4P); phosphatidylinositol-5-phosphate (PtdIns5P); phosphatidylinositol-3,5-bisphosphate (PtdIns(3,5)P_2) and phosphatidylinositol-4,5-bisphosphate (PtdIns(4,5)P_2) (Hirano & Sato, 2019; Ischebeck, Seiler, et al., 2010).

This project was focused on understanding the function of PI 4-Kinase, which catalyzes the phosphorylation of PtdIns to PtdIns4P, because recent findings suggest that is an essential enzyme for plant growth and cytokinesis in *Arabidopsis* roots (Lin et al., 2019; Preuss et al., 2006; Starodubtseva et al., 2022).

Membrane-associated processes in plants

Membranes can initiate signal transduction and regulate enzyme activities, trigger the formation of secondary messengers and eventually control gene expression. One way is through the presence of micro- and nanodomains that consist of either short-lived clusters of proteins and lipids, or of large, organized domains that facilitate cell signaling processes, cell adhesion and membrane trafficking events. In addition, vesicular trafficking pathways are also fundamental to modulate cell signaling and the homeostasis of membrane-enclosed organelles (Groves & Kuriyan, 2010; Laude & Prior, 2004).

Membrane trafficking events like exocytosis and endocytosis are critical for cellular homeostasis, tissue function and cell survival. Exocytosis is the final step of the secretory pathway, which starts at the endoplasmic reticulum (ER), goes to the Golgi, then to the trans-Golgi network (TGN) and finishes with the fusion of secretory vesicles with the plasma membrane. The process of secretion employs vesicular trafficking basically to transport cargo from the inside of the cell to the extracellular space. The cargo can be either intrinsic membrane proteins that are distributed between membranes as part of vesicles; or cargoes can represent secreted substances, such as cell wall components, that are released to the apoplast upon secretion. By contrast, endocytosis is characterized by the fission of vesicles from the plasma membrane and its further transport through the endocytic pathway to the early endosomes (EE). The TGN works as a central sorting station in vesicle trafficking. From the TGN, inbound vesicles can be directed to the vacuole via pre-vacuolar compartments (PVC) or to the Golgi apparatus, based on the sorting function of the endosomal retromer complex (Le Roy & Wrana, 2005) (Figure 3).

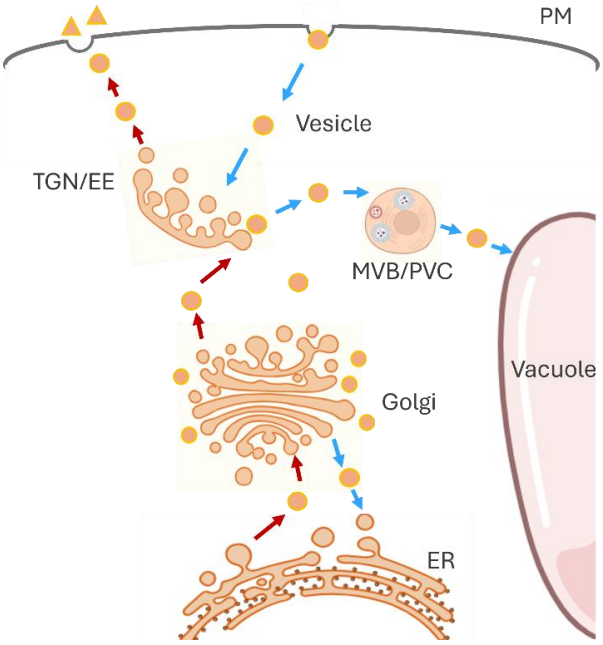

Figure 3. Exocytosis and endocytosis pathways in plants. The exocytic pathway is indicated with red arrows. The endocytic pathway is shown by blue arrows. ER: endoplasmic reticulum, TGN: trans-Golgi network, EE: early endosome, MVB: multivesicular body, PVC: pre-vacuolar compartment and PM: plasma membrane. Picture produced here adapted from (Bandman, 2011), using Biorender program.

In plants the TGN functionally overlaps with the EE, being called TGN/EE. The TGN/EE can be found in proximity to Golgi stacks but plays a crucial role as the central sorting hub to direct newly synthesized and endocytosed cargo to the cell surface or vacuole. It is also responsible for the transport of endocytosed cell surface proteins to late endosomes/multivesicular bodies (LE/MVB) for degradation in the vacuole, the recycling

of endocytosed proteins to the plasma membrane and finally the retrograde transport to the Golgi (LaMontagne & Heese, 2017).

Plants must cope with different environmental stresses, but cells can quickly remodel their cell surface and vacuolar contents through synthesis and re-localization of the incoming molecules. To achieve this, plants use vesicular trafficking pathways to transport proteins between intracellular membrane compartments or to their correct location at the plasma membrane (LaMontagne & Heese, 2017). PIs are essential elements of controlling membrane-positioning of proteins. Even though the complexity of the plant PI network is just being elucidated, the current knowledge indicates that PIs are also involved in membrane trafficking events to help plants meet their cellular requirements.

1.2. Control of membrane function by regulatory lipids: protein recruitment

The biological activity of a cellular membrane is mainly a consequence of the presence of proteins that enable membrane-associated processes like transport, signal transduction, cytoskeletal attachment, protein recruitment or membrane trafficking events. Even though the majority of the membrane consists of structural lipids, a minority of membrane lipids comprises lipids that have a regulatory function. The regulatory effects are mediated by lipids acting as ligands for protein partners or through effects on the biophysical properties of membranes, such as rigidity, surface charge and curvature Figure 4 (Gerth et al., 2017; I. Heilmann, 2016).

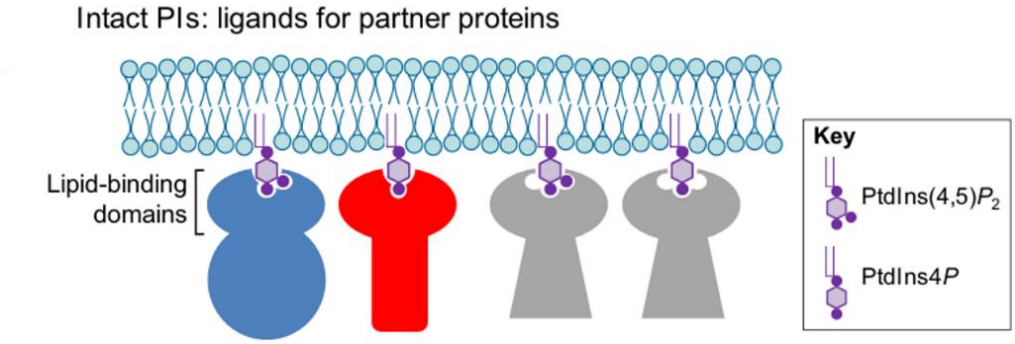

Figure 4. Control of membrane function by PI action. PIs can act through the binding of their characteristic head groups to partner proteins containing specific PI recognition domains. Protein binding to a PI ligand, can serve as a recruitment signal or alter the activity or function of the target protein upon PI binding. Proteins with different lipid binding regions colored in blue, red and grey. Figure taken from (I. Heilmann, 2016)

PIs are mainly localized in the cytosolic side but can occasionally also occur in the luminal/extracellular leaflets of vesicles or the plasma membrane (Gonorazky et al., 2012). The recruitment of peripheral membrane proteins to membrane areas enriched in PIs, occurs mainly through PIs head groups, which protrude from the plane of the membrane into the cytosol and are available for phosphorylation by lipid kinases (Takenawa & Itoh, 2006). These phosphorylated head groups can be recognized by PI-binding domains like pleckstrin homology (PH) domain, Fab1 YOTB Vac1 EEA1 (FYVE) domains and phagocytic oxidase (PX) domains or also by polybasic protein regions found in numerous cellular proteins (Lemmon, 2003).

Some PI-binding domains have shown to be highly specific towards their substrates, but their specificity can depend on increased levels of certain PIs. For example, the PH domain of human PLCδ1 displays a strong preference for PtdIns(4,5)P_2, whereas the PH domain of human four-phosphate adaptor protein 1 (FAPP1), binds specifically to PtdIns4P (Takenawa and Itoh, 2006). However, lipid binding domains are not always well conserved at the sequence level and further bioinformatic analysis of protein secondary structures may be required for their identification. *Arabidopsis thaliana* encodes numerous proteins containing putative or *de facto* PI-binding domains (M. Heilmann & Heilmann, 2024).

1.3. The plant phosphoinositide (PI) system: Enzymes mediating biosynthesis or degradation of PIs

PI biosynthesis and degradation

PIs represent a minor group of phospholipids in all eukaryotes, in plants accounting for less than 1% of the total (Vermeer et al., 2009a). PIs are derived from the membrane phospholipid, phosphatidylinositol. PtdIns can be phosphorylated by lipid kinases in the D-3, D4 and – as monophosphates – also in the D-5 positions of the inositol head group (A. Balla & Balla, 2006; Munnik & Nielsen, 2011). The D-2 and D-6 positions of the inositol ring are not accessible for phosphorylation, probably due to steric constraints (I. Heilmann, 2016; Vermeer et al., 2009b). In plants only five PI species have been detected, compared to up to seven species found in other eukaryotes. Plants contain three PtdIns monophosphates, PtdIns3P**,** PtdIns4P and PtdIns5P, and two PtdIns bisphosphates, PtdIns(3,5)P_2 and PtdIns(4,5)P_2 (Figure 5 A)**.** Even though PtdIns5P has been detected in plants, there is currently no candidate for a PI 5-kinase mediating its biosynthesis by direct

phosphorylation of PtdIns (Meijer et al., 2001), so PtdIns5P is likely formed by dephosphorylation of a PtdIns-bisphosphate. The presence of PtdIns (3,4)P_2 or PtdIns (3,4,5)P_3 in plants is still under debate (Mueller-Roeber & Pical, 2002).

PtdIns is synthesized by the PtdIns synthase (PIS) from D-myo-inositol and cytidine diphosphate diacylglycerol (CDP-DAG). *Arabidopsis* encodes two PIS isoforms, PIS1 and PIS2, which are both integral membrane proteins. PIS1 and PIS2 differ in their preferences for CDP-DAG substrate species with varying degrees of unsaturation in their fatty acyl tails. Once PtdIns is formed, hydroxyl groups in the inositol head group of PtdIns can be phosphorylated by specific lipid kinases, giving rise to the PtdIns monophosphates and in a separate phosphorylation step also of the PtdIns bisphosphates (I. Heilmann, 2016) (Figure 5 A).

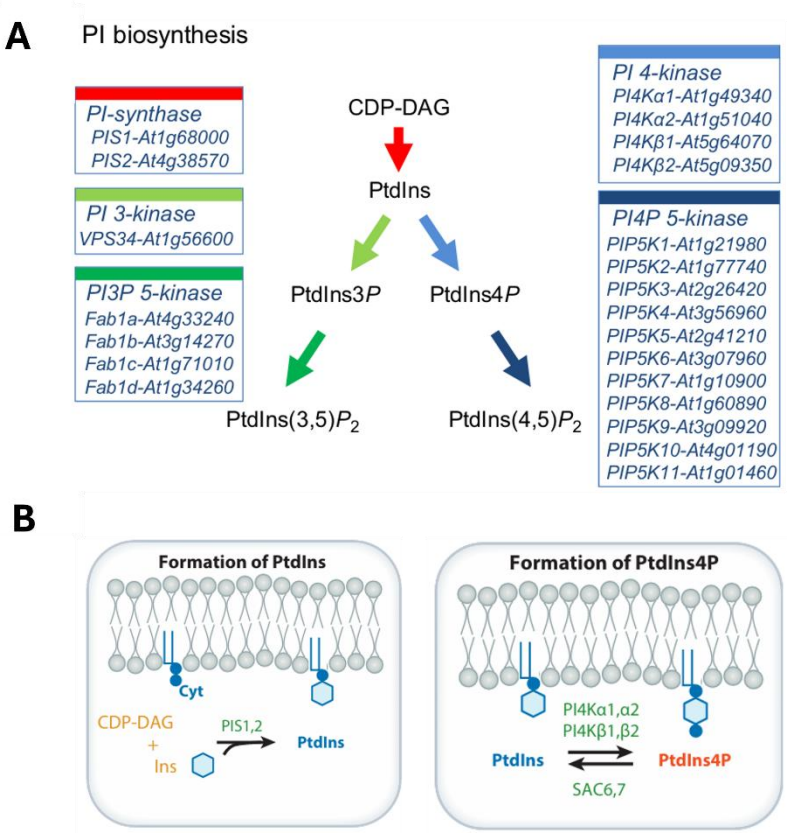

Figure 5. PI biosynthesis. **A.** Schematic representation of the PI biosynthesis. Arrows showing the individual enzymatic steps. Colored boxes indicating the *Arabidopsis* genes encoding enzymes that catalyze each step. **B.** PtdIns is formed mainly by phosphatidylinositol synthase (PIS 1,2) from D-myo-inositol and cytidine diphosphate diacylglycerol (CDP-DAG). PtdIns can be phosphorylated by PI4Kα or PI4Kβ subfamilies in the D4 position of the inositol ring, resulting in the formation of phosphatidylinositol 4-phosphate (PtdIns4P). Figure taken from (Gerth et al., 2017; I. Heilmann, 2016).

PI-Kinases

Phosphorylation of PtdIns by PI-kinases produces PtdIns3P and PtdIns4P. In *Arabidopsis thaliana* the PI 3-Kinase (AtVPS34) catalyzes the phosphorylation of PtdIns to PtdIns3P. The reaction takes place only in the D-3 position of the inositol ring of PtdIns and not on any PtdIns monophosphate or biphosphate. PI 4-Kinase catalyzes the phosphorylation of PtdIns to PtdIns4P (Figure 5 B). PI 4-Kinases are classified based on their sensitivity to the inhibitors adenosine and wortmannin, as type-II and type-III, respectively. They are further grouped in alpha, beta and gamma isoforms depending on their similarities and domain structures (Balla & Balla, 2006; Mueller-Roeber & Pical, 2002).

The *Arabidopsis* genome contains 12 putative PI 4-Kinase loci (Mueller-Roeber & Pical, 2002). The type II group is represented by eight isoforms (PI4Kγ1– PI4Kγ8), but no lipid substrate has been identified for PI4Kγ3, PI4Kγ4, PI4Kγ5 and PI4Kγ7 from *Arabidopsis*. Autophosphorylation and protein kinase activities have been reported, raising doubts whether the PI 4-kinase gamma subfamilies in fact represents lipid kinases, due to absence of *in vitro* lipid kinase activities (Akhter et al., 2016; Galvão et al., 2008; Preuss et al., 2006). By contrast, PI 4-kinases of type III represented by the remaining four PI4Kα1, PI4Kα2, PI4Kβ1 and PI4Kβ2 are likely true PI 4-kinases. The absence of expressed sequence tags for *PI4Kα2* suggests this gene may be a pseudogene (Mueller-Roeber & Pical, 2002).

The PI 4-kinase α-isoform contains a lipid kinase unique domain, a catalytic domain and a PH-domain that can bind to the product of the reaction, PtdIns4P (Stevenson et al., 1998). Deletion of the PH-domain results in inhibition of PI4Kα1 activity from *Arabidopsis* and mislocalization of the enzyme, indicating a role of the PH-domain in controlling localization and activity of PI4Kα1 (Stevenson-Paulik et al., 2003). The β-family of PI4Ks consists of PI4Kβ1 and PI4Kβ2, which are 1121 and 1116 aa in length, respectively. Both hold different domains well conserved in yeasts, animals and plants, as well as a plant-specific protein domain: a Lipid Kinase Unique (LKU) domain, a novel homology (NH) domain, plant partially charged (PPC) domain, and the catalytic domain (further discussed below) (M. Heilmann & Heilmann, 2015; Lou et al., 2006; Preuss et al., 2006; Xue et al., 1999a).

The catalysis performed by PI 4-Kinases represents a crucial point for the regulation of PIs pathways, and recent findings suggest that PI4Kβ1 is essential for plant growth and cytokinesis in *Arabidopsis* roots. Importantly, PI4Kβ1 acts synergistically with protein partners to control cytoskeletal rearrangements, phragmoplast dynamics and ultimately successful completion of cytokinesis (Lin et al., 2019; Preuss et al., 2006; Starodubtseva et al., 2022). Plant PI metabolism also includes the degradation of PIs, represented by PI

phosphatases and phospholipases (Mueller-Roeber & Pical, 2002). For example, families of PI phosphatases like the suppressor of actin (SAC) phosphatases, degrade PtdIns biphosphates at the plasma membrane or the tonoplast, and the phosphatase and tensin-homolog deleted on chromosome 10 (PTEN)-related enzymes, which control the degradation of D-3-phosphorylated PtdIns-monophosphates and PtdIns-bisphosphates. Other important phosphatases include the PI 5-phosphatase (5PTase) family, which act both on PI lipids and on soluble inositol polyphosphates (IPPs). In addition, PI-specific phospholipase C (PI PLC) enzymes, encoded in the *Arabidopsis* genome by nine isoforms can mediate PIs degradation by cleavage of phospholipids on the diacylglycerol (DAG) side (I. Heilmann, 2016; Mueller-Roeber & Pical, 2002). As these enzymes are not immediately relevant for this thesis, they shall not be discussed in more detail.

1.4. PI4Kβ1 role in plant phosphoinositide biosynthesis: mutant phenotypes, root hair defects, cytokinetic defects

The main focus of this study is the biochemical characterization of PI4Kβ1, and the need for this characterization is a consequence of previous, mostly cell-biological studies. PI4Kβ1 plays a key role in the phosphorylation of PtdIns to produce PtdIns4P, the most abundant PI in plants, representing approx. 80% of total PIs. PtdIns4P has established functions in the regulation of polarized membrane trafficking in growing root hairs and pollen tubes (Gerth et al., 2017; Ischebeck et al., 2008; Lin et al., 2019; Munnik & Nielsen, 2011). The role of PI4Kβ1 and PtdIns4P was first uncovered by root hair defects exhibited in *Arabidopsis pi4kβ1 pi4kβ2* double mutant plants (Preuss et al., 2006) which additionally exhibited a dwarf phenotype proposed to be related to cytokinetic defects (Kang et al., 2011; Preuss et al., 2006). Later, the molecular mechanisms of the cytokinesis defects became clearer when (Lin et al., 2019) found that cytokinetic defects were accompanied by overstabilization of phragmoplast microtubules, which guide membrane trafficking at the cell plate. The impaired trafficking of proteins at the cell plate, including decreased clathrin recruitment and endocytosis, results in incomplete cytokinesis. In addition, a synergistic regulation of MPK4 and PI4Kβ1 was reported to control phragmoplast dynamics and successfully complete cytokinesis, and the interplay of PI4Kβ1 with MAPKs was the basis for studying the biochemical features of PI4Kβ1 and how these features were controlled by MAPK-mediated phosphorylation. The previous findings underlying the

motivation to study the biochemistry of PI4Kβ1 in detail will be outlined in the following paragraphs.

Phenotypes of the *Arabidopsis pi4kβ1 pi4kβ2* double mutant

Initially, transfer DNA (T-DNA) insertional mutants *Arabidopsis* plants were investigated by (Kang et al., 2011; Preuss et al., 2006), where both *pi4kβ1* and *pi4kβ2* were knocked out. As a result, double-mutant plants were smaller than the wild type exhibiting a dwarf phenotype and displaying altered aberrant root hair accompanied by cytokinetic defects. Later, (Lin et al., 2019) confirmed the dwarf phenotype and expressed the coding sequences of *PI4Kβ1* and *PI4Kβ2* under their endogenous promoters in the *pi4kβ1 pi4kβ2* mutant background. As a result, the dwarf phenotype of the double mutant was fully rescued by the ectopic expression of either gene, suggesting that the phenotypes were a result of mutations in *pi4kβ1* and *pi4kβ2* (Figure 6 A) and enabling the study of the subcellular localization of a functional fluorescent fusion of PI4Kβ1.

Cytokinetic defects of the *pi4kβ1 pi4kβ2* double mutant

As *pi4kβ1 pi4kβ2* double mutant plants displayed abnormal growth, cytokinetic defects were further analyzed (Lin et al., 2019) by propidum iodide (PI) staining in single, double mutants and in complemented lines. The *pi4kβ1 pi4kβ2* double mutants roots showed cell wall stubs indicating failure to complete cytokinesis, but the complemented plants did not show cytokinetic defects indicating that plants were successfully complemented by ectopic expression (Figure 6 B).

The *in vivo* localization was investigated by monitoring PI4Kβ1 fused to an N-terminal mCherry tag and *in vivo* fluorescence analyzed by whole-mount immunostaining. The immunostaining against mCherry-PI4Kβ1 expressed in the *pi4kβ1 pi4kβ2* double mutant showed mCherry-PI4Kβ1 at the cell plate from early to late cytokinesis and concentrated at the leading edges of the cell plate (Figure 6 C). Cytokinesis is the final step of cell division that separates a mother cell into two daughter cells. Unlike yeast and animal cells, where a contractile actin-myosin ring pulls in the plasma membrane, forming a cleavage furrow, cells in higher plants make a new membrane independently of the plasma membrane by homotypic fusion of vesicles.

During plant cytokinesis a specific membrane compartment for cell division called the cell plate is formed. In early telophase, the cell plate starts forming between the phragmoplast. The phragmoplast is a complex array of actin filaments and microtubules that provides guidance to membrane trafficking events delivering and recycling membrane vesicles to and from the expanding cell plate.

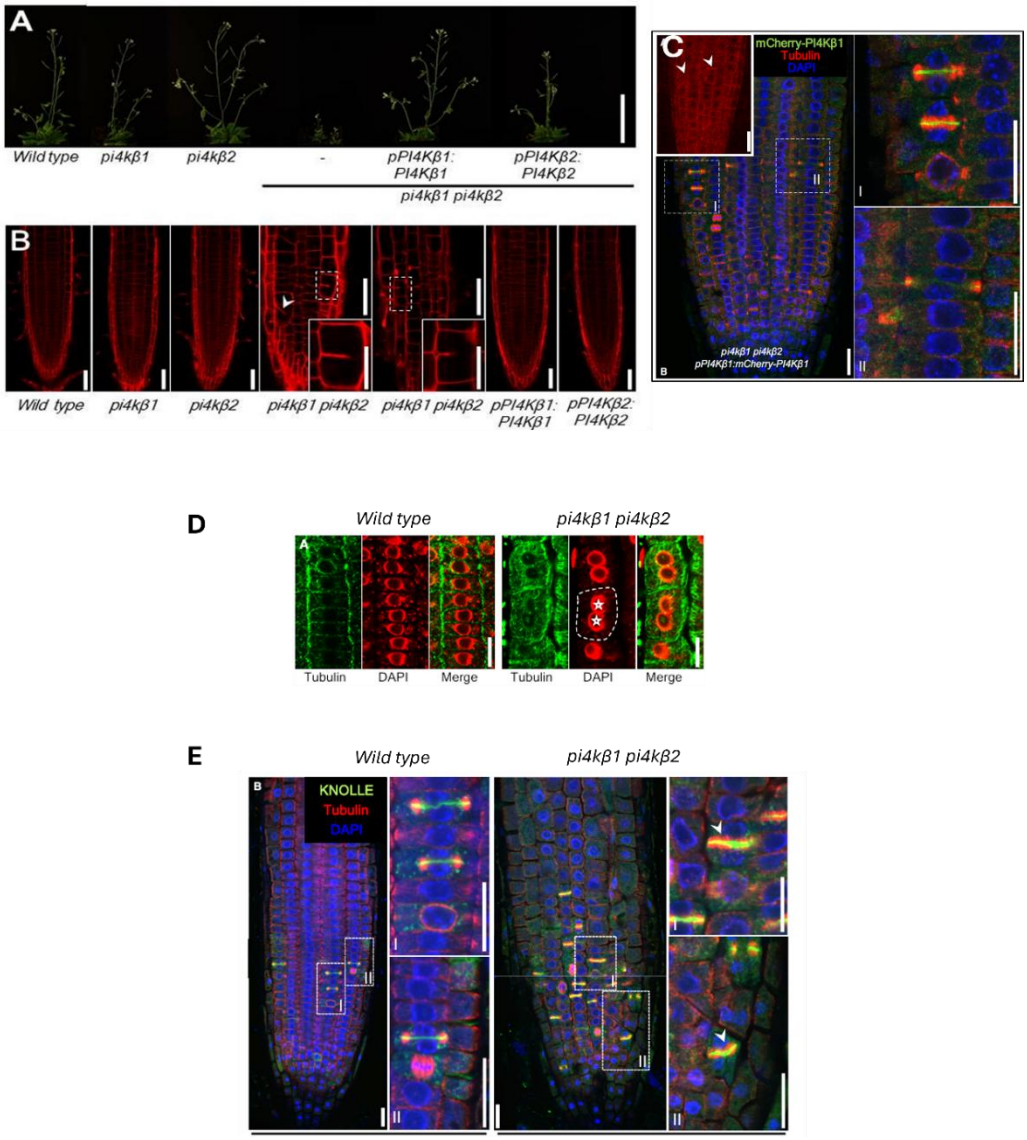

Figure 6. Dwarf phenotype and cytokinetic defects of the *Arabidopsis pi4kβ1 pi4kβ2* double mutant. A. The growth phenotype of the pi4kβ1 pi4kβ2 double mutant can be complemented by ectopic expression of PI4Kβ1 or PI4Kβ2. The plants shown are one-month-old. Bar, 10 cm. **B.** Propidium iodide (PI) staining of five-day-old roots illustrate the tissue patterning defect of the *pi4kβ1 pi4kβ2* double mutant and its complementation by ectopic expression of pPI4Kβ variants. **C.** *In vivo* localization of mCherry-PI4Kβ1 expressed from the pPI4Kβ1 promoter in root tips of 5-day-old complemented *pi4kβ1 pi4kβ2* plants. The subcellular distribution of mCherry-PI4Kβ1 was imaged using a Zeiss LSM880 in Airyscan Virtual Pinhole (VP) mode. Arrowheads, nascent cell plates decorated by mCherry PI4Kβ1. Scale bar, 20 µm. Figure taken from (Lin et al., 2019). **D**. Immunostaining of meristem cells of five-day-old wild type and *pi4kβ1 pi4kβ2* double mutant plants, using an anti-tubulin (green) antibody and DAPI staining (red). Asterisks indicate nuclei in multinucleated cells. Phenotypes are reminiscent of phenotypes observed also in *Arabidopsis mpk4* mutants (Beck et al., 2011; Lin et al., 2019). Bars, 10 µm. **E**. Whole-mount immunostaining of five-day-old seedlings of wild type or *pi4kβ1 pi4kβ2* double mutants, using anti-KNOLLE (green) and anti-tubulin (red) antibodies, and DAPI staining (blue). (I), (II), magnifications of areas highlighted in the overview images, as indicated. The images are representative for >15 independently grown plants. Arrowheads, solid phragmoplasts with immature cell plates in the *pi4kβ1 pi4kβ2* double mutant. Bars, 20 µm. Figure taken from (Lin et al., 2019).

During this process, the phragmoplast expands radially outward around the growing cell plate, transiting from a solid to a ring-like structure (Jürgens, 2005). The transition of the phragmoplast from a solid to a ring-like array drives vesicles delivered along phragmoplast microtubules from the center towards the leading edges of the cell plate (Müller & Jürgens, 2016).

Importantly, phenotypes and the observed stabilization of phragmoplast microtubules in the *pi4kβ1 pi4kβ2* double mutant resembled phenotypes previously observed for the *Arabidopsis mpk4* mutant like multiple nuclei and aberrant phragmoplasts (Figure 6 D-E) (Lin et al., 2019). Subsequent analyses revealed physical and genetic interactions of MPK4 with PI4Kβ1 (Lin et al., 2019) and as other published work identified PI4Kβ1 as a target for MPK4-mediated phosphorylation, it became an imminent question, how biochemical features of the PI4Kβ1 might change upon phosphorylation by MPK4 or possibly also other MAPKs, such as MPK6 (Lin et al., 2019; Murata et al., 2013).

Despite the recent findings to understand the molecular mechanisms that delineate the roles of PI4Kβ1 and PtdIns4P in the control of somatic cytokinesis in *Arabidopsis*, the biochemical features of the PI4Kβ1 remained unknown. To close this gap, it was the main goal of this thesis to biochemically understand the functions of the regulatory and catalytic domains of PI4Kβ1, how PI4Kβ1 is regulated by its substrate and product, and what are the effects of upstream kinases on PI4Kβ1 function.

1.5. PI4Kβ1 domain structure

PI4Kβ1 contains putative conserved domains also present in PI 4-kinases of animal and yeast origin. The N-terminal LKU domain, NH domain and a C- terminus catalytic domain are conserved within animals and yeasts. *Arabidopsis* PI4Kβ1 additionally possesses a plant-specific partially charged (PPC) domain of 318 amino acids (Lou et al., 2006; Xue et al., 1999b). The domain structures of different type III PI 4-kinases are illustrated in Figure 7.

The LKU domain of PI4Kβ1

In mammals, the LKU domain is conserved in type III PI-4Kinases of both the α and β families in PI4K230 and PI4K92 protein homologues, respectively, but its function remains unclear (T. Balla, 1998; Gehrmann & Heilmeyer, 1998).

In 2014, a mammalian PI4KIIIα mutant was generated lacking the LKU domain and the data reported a reduction in catalytic activity, using *in vitro* lipid kinase activity assays. The data

allowed to better understand the functional roles of the specific domains of the PI4KIIIα, which is an essential host factor for hepatitis C virus replication (Harak et al., 2014).

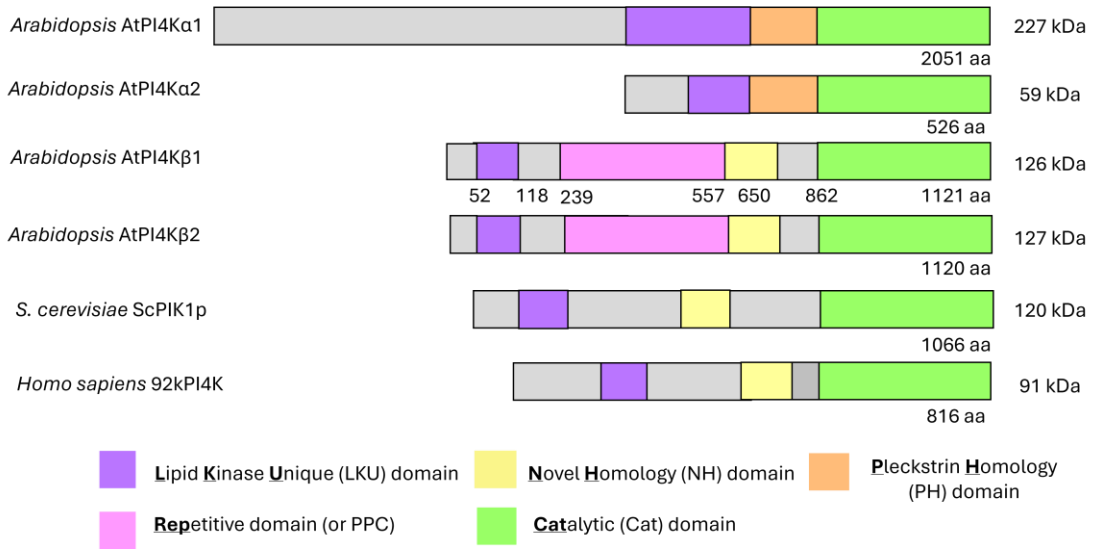

Figure 7. Protein domains present in Type III PI4-Kinases across eukaryotes. Schematic representation of different domains in protein homologues of PI4Kβ1 from *Arabidopsis*, existing in yeasts and mammals. The isoform AtPI4Kα, is also included here for comparison purposes. Numbers indicate amino acid positions. Accession numbers are as follows: AtPI4Kα1: At1G49340; AtPI4Kα2: At1g51040; AtPI4Kβ1: At5g64070; AtPI4Kβ2: At5g09350; ScPik1p: J8Q366; PI4K92: Q9UBF8. Figure designed here based on previous reports (Mueller-Roeber & Pical, 2002; Stevenson-Paulik et al., 2003; Xue et al., 1999b).

In the yeast *Saccharomyces cerevisiae*, the LKU from Pik1p (a protein homologue of PI4Kβ1 from *Arabidopsis*) was found to interact with frequenin 1 (Frq1; plant homologue AtCBL1) a Ca^{2+}-binding protein, and this interaction increased Pik1p activity by 3 -5-fold *in vitro*. The data indicated that Frq1 might enhance the efficiency of exocytotic-vesicle formation. The authors suggested that Frq1 may provide a feedback mechanism in which Ca^{2+}-signals can stimulate recruitment of PtdIns $(4,5)P_2$ at appropriate locations by promoting recruitment and activation of a PI 4-kinase at those sites (Hendricks et al., 1999a).

In plants, the LKU- PI4Kβ1 from *Arabidopsis* is only 20-37% identical in amino acid sequence to other PI 4-kinases and was found to interact with the Ca^{2+} sensor protein AtCBL1 through its NH_2 terminus. These findings propose a recruitment of PI4Kβ1 and AtCBL1 by the Rab GTPase, RabA4b, also localized in TGN-like compartments (Preuss et al., 2006). The recruitment of PI4Kβ1 might result in localized PI 4-Kinase activity and enrichment of PtdIns4P on these compartments. Subsequently, promoting the recruitment of PtdIns4P binding domain proteins or stimulating the delivery of PtdIns4P to tip-localized plasma membrane domains via fusion of RabA4b labeled secretory

compartments might be relevant to control physiological effects of PI4Kβ1 on polar tip growth in *Arabidopsis* (Preuss et al., 2006).

The PPC domain of PI4Kβ1

The PPC, which is sometimes also called repetitive domain, in PI4Kβ was first reported by (Xue et al., 1999a) and it was found to be specific to PI4Kβ1 orthologs from plants. Later, the PPC domain from *Oryza sativa* and *Arabidopsis thaliana* was functionally characterized. It was found that the repetitive domain contains a highly charged repetitive segment which is a unique domain only found in the β isoform. The PPC region of *Arabidopsis* PI4Kβ1 is 300 amino acids in length and harbors 11 repeats and 14 repeats in OsPI4K2, each containing a repeated 20-aa motif. The PPC domain consists of 46% charged amino acid residues, of which 25% are acidic (glutamate and aspartate) and 21% are basic (lysine, arginine, and histidine), with a highly conserved inner core sequence of hydrophobic/positively charged/hydrophobic amino acids.

By using a modified yeast based "Sequence of Membrane-Targeting Detection" (SMET) system together with transient expression of GFP fused to an isolated PPC in onion epidermal cells, the PPC domain was proposed to be responsible for membrane targeting of PI4Kβ1. Moreover, recombinant PPC, expressed in *E. coli* exhibited binding to phosphatidic acid (PA), PtdIns and PtdIns4P, but not phosphatidylcholine (PC), PtdIns5P, or PtdIns(4,5)P_2 using *in vitro* fat blots, suggesting a potential mechanism for regulating sub-cellular localization and lipid binding in cellular membranes (Lou et al., 2006).

Even though the PPC domain in PI4Kβ is plant specific, it is not the only repetitive domain found in lipid kinases. For instance, PI4P 5-kinases of *Arabidopsis* subfamily B (isoforms PIP5K1 – PIP5K9) contain a membrane occupation and recognition nexus (MORN) domain characterized by the presence of MORN-repeats, that is unique to plants. MORN-repeats are present in proteins from both animals and plants and are thought to mediate protein membrane contacts (Mueller-Roeber & Pical, 2002). For example, mammalian junctophilins are protein components of the junctional complexed present between the plasma membrane and the endoplasmic reticulum, and these proteins contain eight MORN motifs mediating plasma membrane targeting. However, whether the MORN domain of *Arabidopsis* PI4P 5-kinases have a role in the subcellular localization of these proteins is currently not known (Mueller-Roeber & Pical, 2002; Sajko et al., 2020).

PI4Kα1 and PI4Kβ1 from *Arabidopsis* contain different lipid-binding domains with possible similar functions. PI4Kα1 contains a PI-binding domain known as a PH domain believed to bind the reaction product, PtdIns4P. Binding of PtdIns4P reduced AtPI4Kα1 activity *in vitro*

by 70% (Stevenson et al., 1998). By contrast, increased specific activity of recombinant PI4Kβ1 protein was observed in the presence of PtdIns4P (Stevenson-Paulik et al., 2003). While PI4Kβ1 does not contain a PH domain, the PPC domain has been shown to bind PtdIns-monophosphates (Lou et al., 2006) and lipid binding to the PPC domain might serve a regulatory function in controlling PI4Kβ1 membrane recruitment and/or catalytic activity.

The NH domain of PI4Kβ1

The NH domain of PI4Kβ1 is specific to PI4Kβ- isoforms in yeasts, animals and plants (Xue et al., 1999a). Using a yeast two-hybrid system, it was found that the NH domain of *Arabidopsis* PI4Kβ1 interacted with the constitutively active form of *Arabidopsis* RabA4b (GTP bound) (Preuss et al., 2006). To our knowledge, no additional data has been reported to further understand the function of the NH domain, so its role in the regulation of PI4Kβ1 regulation remains unclear.

The Catalytic domain of PI4Kβ1

The catalytic domain is highly conserved across present PI 4-Kinases from various eukaryotes, and the catalytic domain of *Arabidopsis* PI4Kβ1 shares 43-57% identity with that of other PI 4-Kinases. The annotated catalytic domain of *Arabidopsis* PI4Kβ1 is located between residues 835-1106 and is responsible for catalyzing the phosphorylation of the substrate PtdIns to produce PtdIns4P (Xue et al., 1999b). The active site of kinases contains structural elements critical for catalysis that have been structurally well-characterized in enzymes of mammalian or yeast origin, but are only annotated in plants.

In kinases of mammalian origin, the catalytic core contains a widely conserved annotated region, the glycine-rich loop (or G-loop) characterized by a consensus GxGxxG sequence. The corresponding annotated G- loop region of *Arabidopsis* PI4Kβ1 is located between residues 841-847 (Data Base UniProt). The G-loop functions as a nucleotide-positioning motif to anchor ATP in the optimal orientation for catalysis and phosphor-transfer, and to protect the bound nucleotide from the solvent. In the G- loop triad, the second and third glycine residues flank residues that can be targets for phosphorylation by protein kinases (Steinberg, 2018).

Another conserved feature of the generic kinase catalytic region is the activation loop. In kinases of animal origin, the activation loop is usually 20-30 residues in length. The annotated activation loop of *Arabidopsis* PI4Kβ1 is located between residues 988-1012 (Data Base UniProt) and contains a conserved DFG motif (usually Asp-Phe-Gly) and extends to an APE motif (usually Ala-Pro-Glu). In active kinase structures, the activation

loop forms a cleft that binds the substrate and specifically interacts with the conserved HRD motif (usually His-Arg-Asp) which lies in the catalytic region of the protein. In an active conformation of the enzyme, the aspartic acid in the DFG motif of the activation loop binds to a magnesium ion that interacts directly with an oxygen atom of the ATP. By contrast, in an inactive conformation, the activation loop blocks substrate access, rendering the kinase catalytically inactive (Modi & Dunbrack, 2019).

The catalytic region containing a typical HRD (histidine-arginine-aspartate) motif is found in most protein kinases and lipid kinases and is suggested to perform functions in catalysis and stabilization of the active conformation of the kinase domain. In the catalytic region, the aspartate in the HRD motif is proposed to be a catalytic base, deprotonating the hydroxyl group from the tyrosine to catalyze a nucleophilic attack on the γ-phosphate of the ATP co-substrate as part of the phosphoryl transfer reaction. Aspartate acts as a proton acceptor late in the reaction and may help stabilize the inactive state through an interaction with the unphosphorylated tyrosine in the activation loop (Kanev et al., 2019; Strong et al., 2011).

The C-terminal tail of PI4Kβ1

To date, the C-terminus tail has not been annotated in the UniProt data base as a functional region or domain of PI4Kβ1. So far, Uniprot data base does not include this c-terminus tail as a functional region, but it is located right at the end of the C-terminus side of the protein, downstream the catalytic domain. Even though to our knowledge no information has been reported regarding the importance of a C-terminal tail in PI4-kinases, a research published in 2012 found that a C-terminal tail present in the catalytic subunit (p110α) of the class I PI 3-Kinase from human is important for membrane interaction. Class I PI 3-kinases are not known to be encoded in plant genomes and can phosphorylate PtdIns(4,5)P_2 in the D-3 position to form PtdIns(3,4,5)P_3, a lipid not found in plants. The biochemical analysis of the human class I PI 3-kinase states that the lipid binding sites in the kinase domain consist of the polybasic activation loop and hydrophobic elements in the C-terminal tail (Hon et al., 2012). The activation loop facilitates the electrostatic attraction to anionic lipids, and positions the head group of the PtdIns(4,5)P_2 substrate relative to the bound ATP for optimal phosphoryl transfer. Because the ATP binding pocket is depressed in the kinase domain, partial membrane penetration by the C-terminal region would facilitate the ATP γ-phosphate to come closer to the inositol ring of PtdIns(4,5)P_2. In addition, the removal of C-terminal tail from the catalytic domain completely abolished the binding to anionic lipids, suggesting an essential role for lipid binding. The results indicate that there can be two lipid-binding sites close at the kinase

domain, one is in the polybasic activation loop with electrostatic properties, and the other in the C-terminal region of hydrophobic nature (Hon et al., 2012) So far, due to the structural differences between enzymes, it remains unclear whether such information can be transferred to *Arabidopsis* PI4Kβ1.

Overall, even though some protein domains are widely conserved between enzymes of different eukaryotic origin, and one is plant-specific, we can judge the possible functions of annotated domains of *Arabidopsis* PI4Kβ1 reported in UniProt by observing the data reported for mammals, yeasts and plants. However, the regulation mechanisms of this enzyme by its substrate and product and the specific regions involved in lipid binding remains unknown.

1.6. Protein modelling

One way to anticipate protein structure similarities is by superimposing experimentally-determined or proposed protein structures in three-dimensional space. Only the best alignment for the structures will reveal shared structural or functional motifs between the superimposed structures. A classical approach to superimposition is to use computer-aided approximations to translate and rotate the structures with the aim of minimizing the root-mean-square-deviation of the structures (RMSD). The RMSD indicates the average of the coordinate differences of the corresponding atoms in the structures. Once the minimal possible RMSD is reached, the best superimposition of the structures may provide information about the similarity of the structures (D. Wu & Wu, 2010).

A further powerful tool to study protein structure-related questions is the use of molecular dynamics simulations (MD). MD is used to predict the behavior of atoms in a biological system and track the time evolution of interacting atoms based on Newtonian laws of motion. The relevance of MD in the protein field relies on the fact that biomolecules are under dynamic states of motion which are important for the function of proteins. For MD analysis, it is routine to first simulate dynamic features of proteins with amino acid residues surrounded by water and salt, using different computer-aided platforms like GROMACS, AMBER, vCHARMM, NAMD and others (Abraham et al., 2015; Brooks et al., 1982; Phillips et al., 2020; Salomon-Ferrer et al., 2013). Then, the output results can be visualized by external software like VMD, Chimera or Pymol. However, because an accurate simulation requires proper parameters to study the physical system, a force field is used to describe a physical system. A force field is a set of mathematical expressions and parameters to describe the inter-molecular and intra- molecular forces. The CHARMM (Chemistry at HARvard Macromolecular Mechanics) (Brooks et al., 1982) force field

designed to study lipids is used for simulating lipid bilayers and membrane proteins, and the current CHARMM36 lipid force field is especially parameterized for lipids. The biggest advantage of MD is its ability to vary *in vitro* and *in vivo* conditions like pH, water and ions, salt or ionic concentrations, cellular components or the composition of a lipid bilayer (Figure 8). Therefore, it is essential to combine simulations with experimental data to validate and enhance the accuracy of experimental results (Sinha et al., 2022).

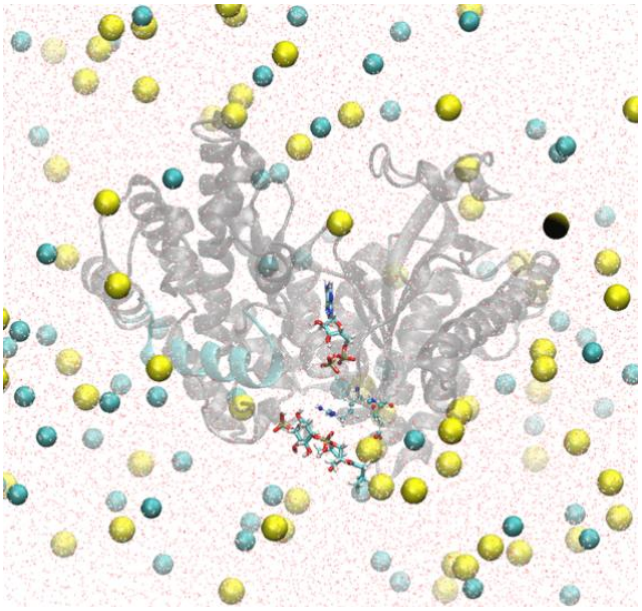

Figure 8. Schematic representation of a molecular dynamics simulation of a protein in a force field. The system is solved in TIP3P water (blue) with NaCl (yellow). The protein model interacts with ADP as a cofactor and with a PI4P (PtdIns4P) substrate model in the TIP3 water box and is neutralized with NaCl. MD was run for 1 ns (Figure obtained in this thesis).

1.7. Enzyme kinetics

Enzymes are the molecular machines of life, because they enable an immense range of biochemical reactions to manifest metabolism, signal transduction, and cell regulation and development in all organisms. At the biochemical level, understanding enzyme kinetics is crucial for elucidating the defining rates at which enzymes catalyze biochemical reactions in a cell, and which factors influence them. Moreover, the study of enzyme kinetics can be important for the industrial use of enzymes, such as in drug development, biofuel production, or food processing (Choi et al., 2017).

Enzyme kinetics describe the different steps representing the molecular interactions among substrates, inhibitors, products, and enzymes. The basic enzyme catalysis reaction scheme describes the conversion of a substrate **S** into a product **P**. The chemical

equilibrium is dictated by the laws of thermodynamics and depends on the ratio of forward and reverse reaction rates (*S→P* and *P→S*, respectively):

Where: **S**: Substrate; **P:** Product; **E**: enzyme.

The enzyme accelerates the conversion of **S** to **P** by the same factor in one direction as it does in the reverse direction, therefore the equilibrium is invariable (Yon-Kahn & Hervé, 2010). For the reaction to take place, the substrate must first be converted to a higher energy state, called the transition state. The energy required for a chemical reaction to occur to reach the transition state is the activation energy and limits the rate of the reaction. If the reactant molecules do not have enough energy to overcome the activation energy barrier, the reaction will not take place. Therefore, the higher the activation energy, the slower the reaction rate, or *vice versa*, the lower the activation energy the faster the reaction rate (Cooper & Hausman, 2007).

Molecules in solution must, thus, first react and go through an unstable transition, called the activated state, **A** (or transition state). The difference in potential energy between the activated state and the initial state is termed the experimental activation energy, **EE** (Yon-Kahn & Hervé, 2010). Activation of molecules results from the collision between molecules, once they react together. The theory of Eyring (Eyring, 1935) assumes statistical equilibrium between the number of molecules in an activated state and those in the initial state and the reaction rate is determined by the number of activated molecules that cross a certain critical region, which represents the peak of the energy barrier (Figure 9).

Enzymes act principally by reducing the activation energy, thus increasing the rates of reaction. The substrate binds at the active site of the enzyme and the enzyme-catalyzed mechanism comprises two reversible elementary steps: 1). The binding of a substrate (S) to a free enzyme (E) to form an enzyme-substrate complex (ES), and 2) the formation of the product, the dissolution of the ES complex, and regeneration of the active enzyme, as shown in Figure 10 A (Cooper & Hausman, 2007).

At the phenomenological level, which can often be experimentally monitored, enzymatic reactions display four different phases (Figure 10B). The pre-steady state phase (a) where the initial ES complex molecules are formed lasts often only less than one second until the

concentration of this intermediate states reaches a constant value (or steady state phase) (Yon-Kahn & Hervé, 2010).

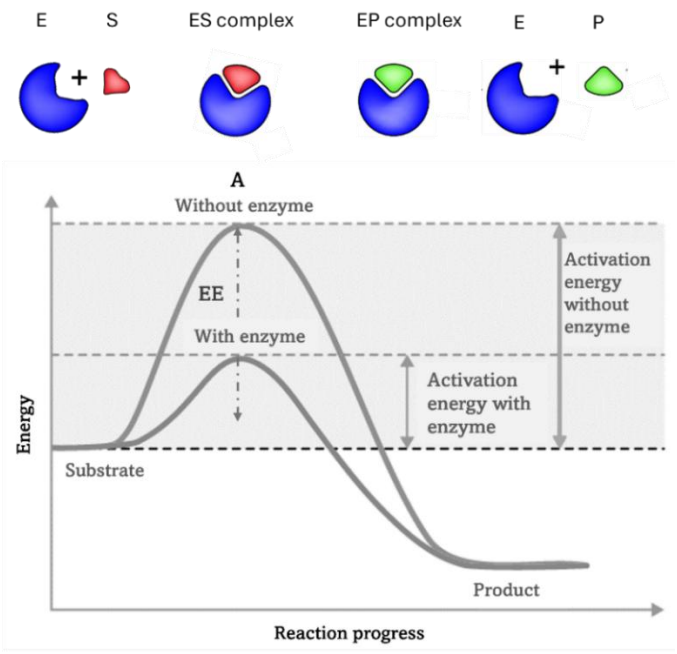

Figure 9. Reaction coordinate diagram for the conversion of a substrate S to a product P. Because the final energy state of P is lower than that of S, the reaction proceeds from left to right. The graph shows the relationship between energy and reaction progress. First, the substrate must pass through a higher energy transition state. The energy required to reach this transition state (the activation energy), is the amount of energy needed for the reaction to progress and determines the rate at which the reaction proceeds. In the presence of an enzyme the activation energy is lowered, and the reaction proceeds at faster rates, compared to the reaction without enzyme. E: Enzyme (blue); S: Substrate (red); ES: Enzyme substrate complex; EP: Enzyme-product complex; P: product (green). A. Activated state; EE: Experimental activation energy. Arrhenius law: activation energies originally described by (Arrhenius, 1889). Illustration modified from (Atkins & De Paula, 2006).

During the steady state phase (b), the rate of product P formation is constant. According to the Michaelis-Menten theory (which will be explained in more detail below), the concentration of the enzyme-substrate complex (ES) remains constant under these conditions. In the subsequent phase of inhibition by the reaction products (c), the concentrations of the reaction products become relevant and the reverse reaction occurs at detectable levels. However, if the equilibrium constant is large and the reaction happens in favor of the formation of the product P, the reverse reaction may be insignificant. At the end of the kinetics, the equilibrium phase (d) is reached, where the concentrations of consumed substrate and formed product will become constants (Yon-Kahn & Hervé, 2010).

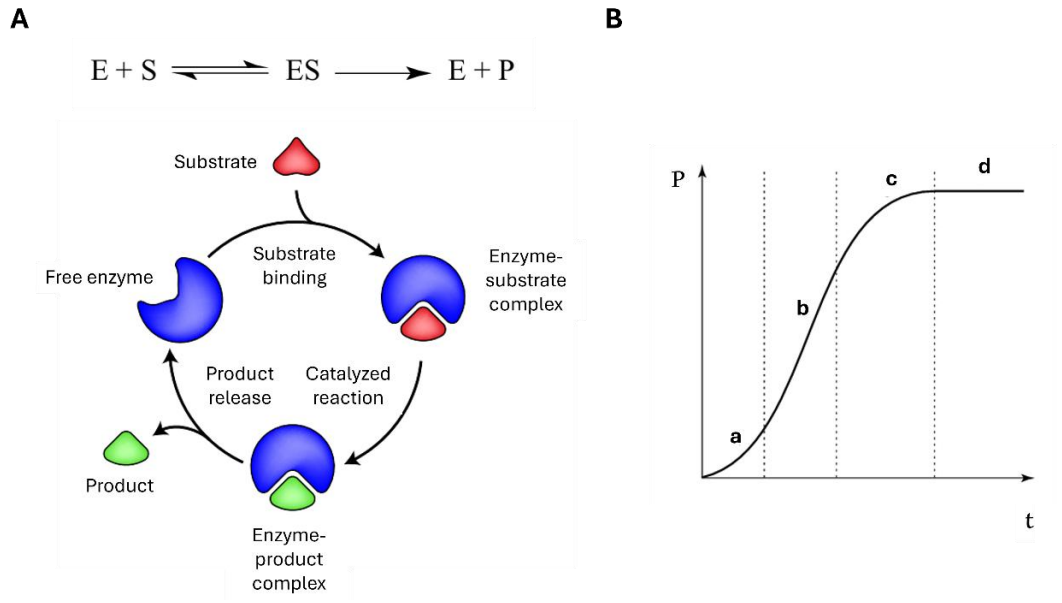

Figure 10. Representation of substrate binding to the active site of an enzyme. A. Free enzymes bind first to their substrate and catalyze the reaction. Then, an enzyme-substrate complex is formed, during which the transition state is stabilized by the enzyme facilitating the conversion of the bound substrate into a product. Ultimately, the enzyme-product complex dissociates and releases the free product, making the enzyme ready for the next catalysis. **B.** Kinetics of the appearance of the reaction products as a function of time. (a) pre-steady state phase (b) steady state phase (c) phase of inhibition by the products (d) equilibrium phase. Diagram A taken from (Harvard, 2018).

1.7.1. Non-allosteric regulation of catalysis (Michaelis-Menten Equation)

One of the most widely used equations to describe enzyme kinetics and to estimate kinetic parameters from reaction progress curves is the Michaelis-Menten (M-M) equation (Figure 11). In the 19th century Michaelis and Menten found that the invertase splits sucrose into glucose and fructose, and the optical rotation was measured by a polarimeter (Michaelis & Menten, 1913). However, this approach only works if there is a large concentration of substrate **S** compared to the enzyme **E**, and if the chance of an enzyme to encounter its substrate is not impaired by factors other than the concentrations of **E** and **S**. The Michaelis-Menten-model explains the dependency of enzyme-catalyzed reaction rate on the concentration of the substrate by two kinetic parameters, the catalytic constant k_{cat} and the Michaelis-Menten constant, K_m. The k_{cat} explains the maximum rate of the reaction at saturating substrate concentrations and the K_m represents the substrate concentration at which the reaction rate is half of V_{max} . The maximum rate of the reaction V_{max} reached when the active sites of the enzyme are saturated by the substrate (Choi et al., 2017; Michaelis & Menten, 1913).

$$v = \frac{(V_{\max}\, x\, [S])}{(K_m + [S])}$$

Equation 1

$$\frac{1}{v} = \frac{K_m}{V_{\max}}\frac{1}{[S]} + \frac{1}{V_{\max}}$$

Equation 2

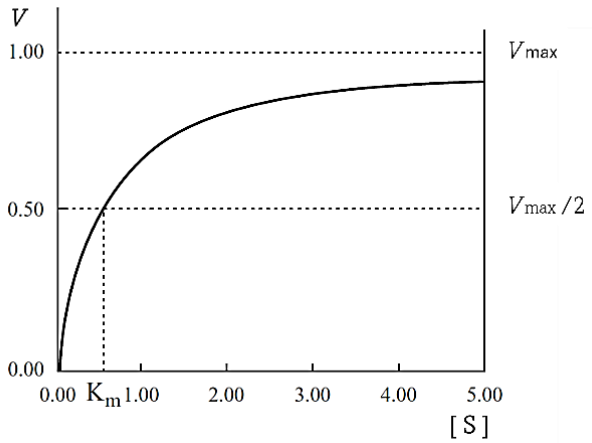

Figure 11. Michaelis-Menten equation and kinetic curve for enzyme reactions. Equation 1 describes the non-linear Michaelis-Menten equation and Equation 2 describes the linearized form, the Lineweaver–Burk equation. Where $\boldsymbol{V}$ is the initial velocity, $\boldsymbol{V_{max}}$ is maximum velocity when all the active sites of the enzyme are occupied by the substrate, [$\boldsymbol{S}$] is substrate concentration and $\boldsymbol{K_m}$ is the Michaelis–Menten constant. Michaelis-Menten kinetics graph, showing the velocity ($\boldsymbol{V}$) of a typical enzyme-catalyzed reaction versus substrate concentration [$\boldsymbol{S}$]. The kinetic parameters, $\boldsymbol{V_{max}}$ and $\boldsymbol{K_m}$ are graphically depicted. Equation 1 taken from (Michaelis & Menten, 1913), and kinetic curve taken from (Yon-Kahn & Hervé, 2010).

During a reaction that follows Michaelis-Menten-kinetics, initially a pre-steady state or quasi-steady state occurs, which involves the formation of the reaction product for a very short time, characterized by a slow increase in the abundance of enzyme-substrate complexes, which then rises quickly, producing an initial curvature in a reaction progress curve. Subsequently, the steady state is reached, and the **ES** complex concentration remains constant, due to the same degree of formation and breakdown of their intermediate forms. This state is characterized by a linear increase in product formation. The last assumption suggests that the model should be performed under conditions of rapid equilibrium, where the enzyme-substrate **ES** complex is in equilibrium with the free enzyme **E** and free substrate **S** (Yon-Kahn & Hervé, 2010).

One of the most common methods to estimate kinetic parameters of the M-M equation is the Lineweaver-Burk plot, which is a linearization method used for transforming the original non-linear M-M equation into a linear one, subsequently the data is fitted by a linear regression (Figure 11; Equation 2). However, the data do not generally satisfy the assumptions of a linear regression that assumes that the data points around the line follow a Gaussian distribution. Therefore, fitting the kinetic data to nonlinear equations based on numerical integration of rate equations without linearization, remains the best way to calculate the kinetic parameters (Y. S. Cho & Lim, 2018).

1.7.2. Allosteric regulation of catalysis (Hill equation)

While the enzyme kinetics of many enzymes can be investigated using the M-M equation, some enzymes exhibit kinetic properties, where the reaction rate is influenced by further parameters not considered in M-M theory. The apparent kinetic behavior of such enzymes then does not display hyperbolic kinetics but rather shows sigmoidal kinetics. This sigmoidal binding response was originally observed in 1910 by Archibald Vivian Hill, who described the cooperative kinetics of O_2 binding to hemoglobin. The mathematical explanation of this cooperativity was termed the Hill coefficient (Gesztelyi et al., 2012; Hill, 1913).

The degree of cooperativity in an enzyme-catalyzed “sigmoidal” reaction is determined by the Hill equation, which is used to estimate the cooperative interaction between two binding molecules. The mode of catalysis is considered to be “cooperative” if the binding of a first ligand to the enzyme changes the binding affinity for a second ligand (Somvanshi & Venkatesh, 2013). The degree of cooperativity is determined by the Hill equation (Figure 12):

$$Y = \left(\frac{I^{\eta_H}}{K_{0.5}^{\eta_H} + I^{\eta_H}} \right)$$

Equation 3

$$ln\left(\frac{Y}{1-Y}\right) = \eta_H \, ln \, I - \eta_H \ln K_{0.5}$$

Equation 4

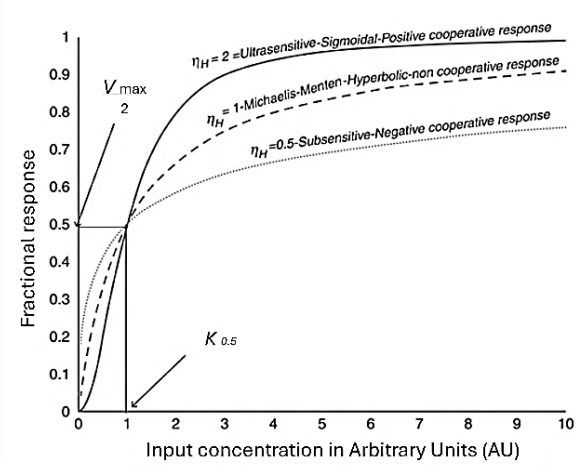

Figure 12.Hill equation and sigmoidal kinetic profile for enzyme reactions. Equation 3 describes the Hill equation and Equation 4 describes the linearized form. Where $\boldsymbol{Y}$ is velocity, [$\boldsymbol{I}$] is the substrate concentration, $\boldsymbol{n_H}$ is the Hill coefficient and $\boldsymbol{K_{0.5}}$ is the half-saturation constant. Sigmoidal kinetics curves for different values of Hill coefficient, showing the fractional response or velocity ($\boldsymbol{Y}$) of an enzyme-catalyzed reaction versus substrate input concentration [$\boldsymbol{I}$]. The kinetic parameter $\boldsymbol{K_{0.5}}$ is graphically depicted. Equation 3 and Equation 4 as well as the illustration originally described by Hill in 1910, but adapted in (Somvanshi & Venkatesh, 2013).

The allosteric regulation of the enzyme occurs upon binding of one ligand (or effector) to an allosteric site that is different from the active site, eliciting a conformational change in the protein. Effectors that enhance the protein's activity are called allosteric activators and mediate positive cooperativity. A positive cooperativity occurs when the binding of a ligand increases the enzyme affinity, increasing the probability of binding to another ligand. By contrast, allosteric inhibition or negative cooperativity occurs when the affinity for other ligands is reduced after an allosteric effector´s binding (Cornish-Bowden, 2014).

1.7.3. Radioisotope substrates in enzyme kinetics

The gold standard method for determining protein and lipid phosphorylation is the labeling of substrates with [γ-^{32}P] ATP *in vitro.* This method possesses a high sensitivity and specificity and can be used not only to study lipid kinase activity but also to investigate protein phosphorylation (Aponte et al., 2009). While concerns about the experimental handling of radioactive substances and the cost and environmental impact of their disposal have led to the use of non-radioactive methods to measure, e.g., protein kinase activities (Hastie et al., 2006), these procedures are time-consuming, and the fluorescence methods are subject to interferences from intrinsically fluorescent compounds or due to precipitated compounds (Janzen, 2002; Seethala & Menzel, 1997; Vedvik et al., 2004).

In this thesis, radiolabeling was employed to monitor *in vitro* lipid phosphorylation and *in vitro* protein phosphorylation, due to its high sensitivity, direct and quantitative measurement by using a phosphoimager, the simplicity and accuracy of the assays for kinetic reactions. Lipid kinase or protein kinase activities can be quantified by measuring the amount of incorporated radiolabeled [γ-^{32}P] ATP *in vitro* into a substrate as a function of time. The activity is usually expressed as a 'Unit', which is defined as the conversion of 1 µmol (or mmol) of phosphate into the lipid or protein substrate in 1 min. The specific activity is defined as units of activity per µg (or mg) of protein used in the assay (Hastie et al., 2006). In this thesis, kinetic analysis according to radiolabeling assays was used to describe the so-far-uncharacterized kinetic behavior of recombinant PI4Kβ1 protein *in vitro*. Moreover, kinetic analysis was used to describe the effects of protein phosphorylation on recombinant PI4Kβ1, elucidating how protein kinases acting upstream of PI4Kβ1 may impact on PI4Kβ1 function and PtdIns4P formation in *Arabidopsis*. As a background for this second aspect, the following paragraphs will outline the links of PI4Kβ1 to other signaling pathways in more detail.

1.8. Integration of plant PI metabolism with other signaling pathways

PIs are constantly formed and degraded with a high rate of turnover to reach a dynamic equilibrium that is subject to change according to intrinsic or environmental cues (M. Heilmann & Heilmann, 2024). Therefore, plants contain a network of enzymes that regulate the dynamic formation and degradation of PIs. When plants are exposed to environmental stresses, the PI network responds with quick, transient or localized signaling events mediated by PIs. For example, when plants are exposed to wounding or salt, the levels of PtdIns (4,5)P_2 change transiently. Also, plants exhibiting gravitropic curvature or exposed to auxin or salicylic acid show a transient change in PI formation (I. Heilmann, 2016). However, the transcription of only few relevant genes is induced upon perception of environmental stresses, while most transcripts for key enzymes of PI metabolism remain unchanged in abundance. Transcriptomic studies demonstrate that transcriptional regulation may not be a major factor for PI changes upon exposure to stresses, indicating that the control of PI dynamics is controlled by post-translational modifications of key enzymes, such as phosphorylation (Zimmermann et al., 2004).

A compendium table reported by (I. Heilmann, 2016), shows evidence of the different roles that PI signaling system plays in *Arabidopsis thaliana.* PIs participate in signalling pathways that regulate cytoskeletal structures, pollen tube growth, cell division, plant growth, membrane dynamics, clathrin-mediated endocytosis and other key roles involved in plant development. In consequence, the genetic perturbation of PI signaling components results in distinct phenotypes that affect important aspects of plant development (I. Heilmann, 2016). For example, different plant phenotypes resulted from genetic perturbation of PI-synthases, (Löfke et al., 2008), PI4Kβ1/PI4Kβ2 (Preuss et al., 2006) and PIP5K4, PIP5K5 or PIP5K6 (Ischebeck et al., 2008; König et al., 2007; Kusano et al., 2008; Sousa et al., 2008; Stenzel et al., 2008, 2012).

In addition, (Hempel et al., 2017) described an interconnection between MAPK-signalling with the PI-signalling pathway. The authors hypothesized that if there is a functional cooperativity in the regulation of the PI4P 5-kinase, PIP5K6, by MAPK, PIP5K6 activity would be reduced in tobacco pollen tubes. Subsequently, the link between MAPKs and PIP5K6 regulation was confirmed in the context of pathogen defense signalling in *Arabidopsis* (Menzel et al., 2019). Another study reported a functional link between the Pik1p in yeasts and a GTPase-dependent signaling pathway to control secretion of cargoes that require recycling mediated by early endosomes (EE) (Sciorra et al., 2005). The authors suggested a mechanistic involvement of Pik1p with Golgi-associated proteins, including the Ypt31p Rab-GTPase to regulate protein trafficking through the secretory pathway.

Interplay of PI4Kβ1 with Rab GTPase pathways was also reported for *Arabidopsis* (Preuss et al., 2006), suggesting regulation of membrane trafficking by the recruitment of cytosolic effector proteins to specific subcellular compartments involving Rab GTPases. Moreover, PI4Kβ1 binds specific PIs and controls the secretory pathway during polarized root hair expansion (Preuss et al., 2006). PI4Kβ1 and its product PtdIns4P are involved in controlling membrane trafficking pathways by unknown mechanisms, influencing the abundance of proteins (Tejos et al., 2014). PtdIns4P was reported to bind to the *Arabidopsis* EXOCYST subunit (AtEXO70A1) and also to Patellin 3 (PATL3), which is involved in exocytosis and has a key role in controlling the behaviour of secretory vesicles (Wu et al., 2017).

Interplay between the MAPK-signaling through the so-called NACK-PQR-pathway and PI4Kβ1 was observed by (Lin et al., 2019) in the context of somatic cytokinesis in *Arabidopsis*. As already described above, Lin and coauthors found that PtdIns4P formed by PI4Kβ1, and MPK4 acting in the *Arabidopsis* equivalent of the tobacco NACK-PQR pathway, are both implicated in cytoskeletal regulation and microtubule rearrangements during somatic cytokinesis in root cells. MPK4 was first found to phosphorylate MAP65-3

and control the turnover of MTs during cytokinesis (Kosetsu et al., 2010). Later, it was demonstrated that PI4Kβ1 and MPK4 jointly regulate the microtubule-associated protein 65-3 (MAP65-3) and act in the same pathway to synergistically control phragmoplast dynamics during cell plate formation in somatic cytokinesis (Lin et al., 2019).

As the regulatory link between MAPKs and enzymes of *Arabidopsis* PI metabolism, including PI4Kβ1 (Hempel et al., 2017; Lin et al., 2019), is highly relevant for this thesis, the following chapters will explore the functional role of MAPKs cascades in plants.

1.9. Mitogen-activated protein kinase (MAPK) cascades in plants

Mitogen-activated protein kinase (MAPK) cascades are highly conserved signaling pathways with important roles in the control of growth, development, and defense response in all eukaryotes, including plants. MAPK cascades consist of MAPK kinase kinases (MAPKKKs/MEKKs), MAPK kinases (MAPKKs/MKKs/MEKs), and MAPKs/MPKs, which act as hierarchical cascades to efficiently amplify specific stimuli from plasma membrane receptors to different downstream responses (Jiang et al., 2022; Sun & Zhang, 2022). In general, extracellular or endogenous signals activate MAPKKKs, which phosphorylate and activate the conserved phosphorylation S/T-X_{3-5}-S/T motifs of downstream MAPKKs, and then, the activated MAPKKs phosphorylate and activate the subsequent MAPKs at their T-X-Y activation motif and transfer the signal into the nucleus. Therefore, highly ordered protein–protein interactions are the basis of MAPK-mediated signal transduction (Jiang et al., 2022).

The *Arabidopsis* genome encodes 60 putative MAPKKKs, 10 MAPKKs, and 20 MAPKs. MAP Kinases belong to a large family of serine/threonine kinases which are activated by dual phosphorylation on threonine and tyrosine residues (MAPK Group, 2002). The 20 MAPKs represent a family divided in four subfamilies (A–D) according to their characteristics and phylogenetic relationships:

- ✓ Group A (MPK3/**MPK6**/MPK10) contain a TEY or TQY motif.
- ✓ Group B (**MPK4**/MPK5/MPK11/MPK12/MPK13) with TEY, MEY, TVY, and TEC motifs
- ✓ Group C (MPK1/MPK2/MPK7/MPK14) has a TEY motif
- ✓ Group D (MPK8/MPK9/MPK15/MPK16/MPK17/MPK18/MPK19/MPK20) contains a TDY motif (Jiang et al., 2022).

By contrast, in mammals at least 14 MAPKKKs, 7 MAPKKs, and 12 MAPKs have been identified, indicating a more complex situation in plant MAPKs cascades compared to mammals. In the MAPKs family the most extensively studied groups are the extracellular signal-regulated kinases 1/2 (ERK1/2), c-Jun amino (N)-terminal kinases 1/2/3 (JNK1/2/3) and p38 isoforms (α, β, γ, and δ) (Zhang et al., 2002).

MAPKs generally interact through their common docking interaction site: The C-terminal region of MAPKs contains a widely conserved common docking (CD) site, which acts as a docking site (D-site) both for upstream MAPKKs and for substrate proteins. The D-site contains two hydrophobic residues that mediate the specificity of MAPK-protein interactions. Moreover, all MAPKs have hydrophobic pockets which form a docking groove and allow their interaction with linear (LxLxL/I) binding features in their substrate proteins (Jiang et al., 2022).

MAPK cascades are involved in various signal transduction pathways in plants. For example, in *Arabidopsis* the OXI1 (oxidative stress inducible 1)-MPK3/6 signaling pathway is activated by active oxygen species (AOS) treatment, which links oxidative burst signals to diverse downstream responses (Rentel et al., 2004). In *Arabidopsis*, the impairment of components comprising the downstream of YODA (ANP1-MKK4/6 and MPK3/6, activated by pathogen-associated molecular patterns (PAMPs), leads to more pronounced plant phenotypes, indicating that events like stomatal development, embryonic development and developmental defects in primary roots are regulated by the YODA pathway (Figure 13) (Smékalová et al., 2014a).

Recent studies have found that MKK3 and MPK6 act as negative regulators of jasmonic acid (JA) signaling (Takahashi et al., 2007) and MPK4 is involved in the regulation of the equilibrium between the salicylic acid and JA/Ethylene-related defense response (Brodersen et al., 2006). In addition, two MAPKs cascade pathways are involved in plant responses to biotic stress. For instance, two conserved pathways are involved in the detection of pathogen invasion, MEKK1–MKK4/5–MAPK3/6–WRKY22/29 and MEKK1–MKK1/2–MPK4 (Droillard et al., 2004) and are activated by bacterial flagellin Flg22 (Asai et al., 2002).

Additionally, MAPKs cascades are involved in mediating plant responses to abiotic stresses like MEKK1–MKK2–MPK4/MPK6, where MKK2 is activated by MEKK1 induced by cold and salt stress in *Arabidopsis* protoplasts (Teige et al., 2004). In tobacco, the NACK-PQR cascade associated with regulation of cell division processes, localizes in the nucleus and during cytokinesis at the phragmoplast and consists of three main kinases: the protein

kinase 1 (MAPKKK-NPK1) – (MAPKK- NQK1/MEK1) – (MAPK-NRK1/MPK1). In this case, NPK1 phosphorylates NQK1 by binding to two microtubule kinesin-like proteins NACK1 (NPK1-activating kinesin-like protein 1), and NACK2, which control cell plate formation. In *Arabidopsis*, three kinases ANP2/ANP3, orthologous genes of tobacco NPK1, are involved in cell division processes together with downstream ANQ1/MKK6 and MPK4 (Figure 13). This cascade controls microtubule remodeling during cell plate formation and the phragmoplast dynamics and plays an essential role in the structural organization of mitosis through reversible phosphorylation of MAP65 (Jiang et al., 2022).

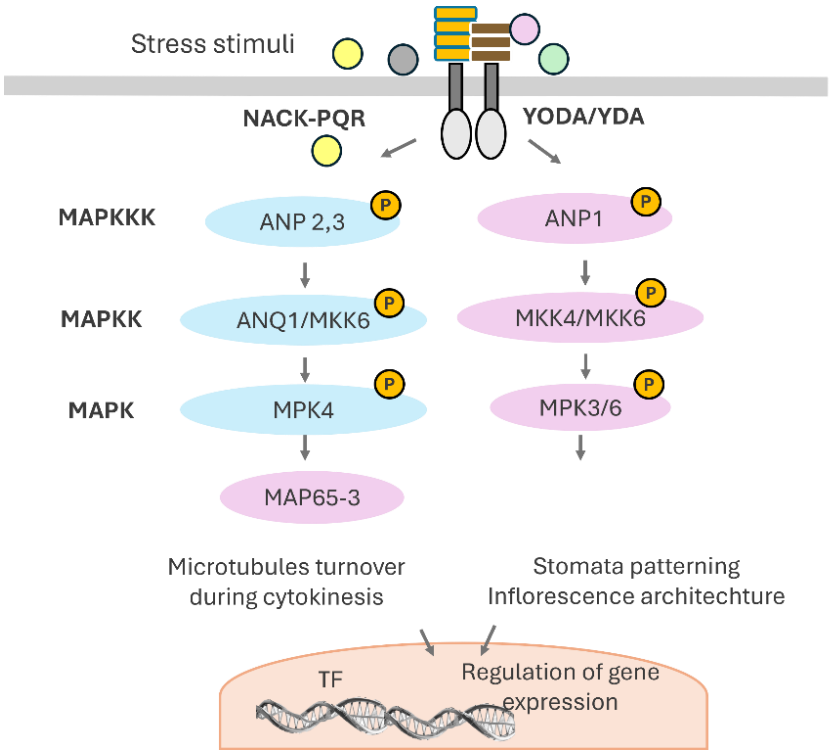

Figure 13. The MAPK pathways that control plant cytokinesis and stomata patterning. Components of the NACK-PQR pathway (left) and the YDA (YODA) signalling pathway (right) are involved in different developmental processes including cytokinesis, stomata patterning and inflorescence architecture. Picture made here based in (Musielak & Bayer, 2014; Sasabe & Machida, 2012; Soyano et al., 2003).

Once MAPKs are activated, they phosphorylate their substrate proteins in Ser/Thre residues that are followed by a Pro-residue to regulate several cellular events by transducing extracellular signals to intracellular responses (Cargnello & Roux, 2011). Current evidence shows that MAPKs also target PI-kinases and PI4P 5-kinases for phosphorylation, thus influencing PI-dependent cellular processes.

1.10. Evidence for MAPK-mediated phosphorylation of PI4Kβ1

Recent findings found that two essential MAPKs that play a role in regulation of camalexin biosynthesis, defense gene activation, stomatal development, inflorescence architecture and cytokinesis, can phosphorylate PI-kinases and PI4P 5-kinases in *Arabidopsis.* MPK4 was found initially in supplementary data to weakly phosphorylate PI4Kβ1 *in vitro* (Latrasse et al., 2017). Later, Lin et al., 2019 not only confirmed this phosphorylation event by using *in vitro* phosphorylation assays with recombinant purified proteins, but also demonstrated that MPK4 and PI4Kβ1 interact physically by using yeast-two-hybrid and co-immunoprecipitation assays and genetically by mutant epistasis analysis (Lin et al., 2019).

Wang et al.,2020 revealed that *Arabidopsis* PI4Kβ1 is also a target for other upstream protein kinases, including MPK6 (Mitogen-activated protein kinase 6), SnRK2.6 (sucrose non-fermenting-1-related protein kinase 2.6), SnRK2.4 and OXI1 (serine/threonine kinase). By using *in vivo* protein extracts obtained from *Arabidopsis* plants exposed to different environmental stresses (salt stress, cold, flg22, abscisic acid ABA and H_2O_2), as substrate pools for *in vitro* kinase reactions, these published results provide valuable information about the functions of protein kinases in controlling cellular activities and help to better understand the response of plants to biotic and abiotic stresses (Wang et al., 2020).

Together, these reports clearly indicate that there is interplay between PI4Kβ1 and the upstream MPK4 and MPK6, suggesting that these players act in a common pathway to regulate downstream processes like cell plate formation during cytokinesis. To understand this interplay at the molecular level, in this thesis *in vitro* experiments were performed to elucidate the effects of MAPK-mediated phosphorylation on the kinetic behaviour of recombinant PI4Kβ1. We envision that these biochemical data will serve as a basis to better understand the effects of MAPK-PI4Kβ1 interactions in the cellular and developmental context *in planta*.

1.11. Aims and Objectives

The aim of this thesis is dedicated to elucidate the biochemical features of PI4Kβ1 and its regulation by MAPK-mediated phosphorylation. Different experimental approaches were combined to address biochemical features of enriched recombinant PI4Kβ1, including the expression of *Arabidopsis* PI4Kβ1 and various substitution or deletion variants in different *E. coli* systems, protein enrichment by affinity chromatography, radioactive *in vitro* lipid kinase assays and *in vitro* protein kinase assays, protein-lipid binding assays, and molecular dynamic simulations. The specific goals of this thesis were:

1) to determine kinetic parameters of recombinant purified PI4Kβ1 upon PtdIns substrate and ATP co-substrate binding
2) to describe the mode by which PI4Kβ1 associates with membranes enriched in PIs with the aid of molecular dynamic simulations
3) to determine kinetic parameters of recombinant PI4Kβ1 variants upon PtdIns substrate binding
4) to determine target sites for MAPK-mediated phosphorylation of PI4Kβ1
5) to identify the functional effects of MAPK mediated phosphorylation on PI4Kβ1 activity and kinetics

2. Results

At the onset of this research, it was known that *Arabidopsis pi4kβ1 pi4kβ2* double mutants displays defects in cytokinesis (Kang et al., 2011; Preuss et al., 2006) that resembled defects also displayed by an *mpk4* mutant (Beck et al., 2011). Further experiments conducted by Lin et al., 2019, demonstrated that PI4Kβ1 and MPK4 interacted physically and genetically, and that PI4Kβ1 was a substrate for phosphorylation by MPK4, as had also been shown in other studies (Wang et al., 2020). These previous studies raised an interest in analyzing the biochemical features of PI4Kβ1 and how such features might be impacted by phosphorylation. This thesis aimed to biochemically characterize the regulation of recombinantly expressed MBP-PI4Kβ1 by PIs and by upstream phosphorylation to elucidate the kinetic mechanisms that might help to better understand how membrane trafficking events that govern cytokinesis are controlled by this essential plant kinase in *Arabidopsis.*

2.1. Recombinant expression and purification of MBP-PI4Kβ1

For biochemical characterization of the wild type PI4Kβ1 from *Arabidopsis,* a maltose-binding protein (MBP) was fused as an N-terminal tag. This was done to enhance the solubility of the large membrane-associated PI4Kβ1 protein. Proteins were recombinantly expressed in *E. coli* BL21 (DE3) and purified by affinity chromatography using the ÄKTA purification system (See Section 4.15.2). Upon induction of expression, cells were harvested, lysed and ultracentrifuged to obtain the supernatant containing the soluble proteins. The supernatant was loaded on an SDS-PAGE and proteins were detected by Western Blot. Once the size of the full-length, truncated and substitution variants was confirmed, the supernatant was used for enrichment on Dextrin Sepharose resin and proteins were eluted using 10 mM maltose. All MBP-PI4Kβ1 protein variants used in this thesis were purified using the same protocol and eluted in the same buffer to ensure proteins are comparable during kinetic characterization.

The enrichment of wild type MBP-PI4Kβ1 is illustrated in Figure 14. The corresponding enrichment of further truncated or substitution variants of PI4Kβ1 is shown in Appendix Figure 34. A control was run in parallel in the SDS-PAGE, by loading the soluble fraction obtained after transforming *E. coli* cells with an empty pMalc5G plasmid, expressing only

the MBP-tag alone. However, shorter truncated variants of the MBP-PI4Kβ1, were observed in all the overexpressed MBP-PI4Kβ1, possibly due to incomplete protein synthesis and/or proteolytic cleavage (Bernier et al., 2018).

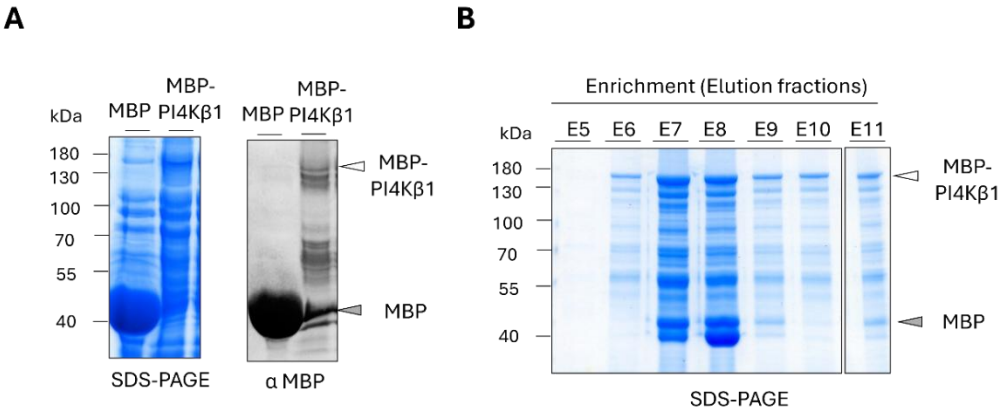

Figure 14. Enrichment of MBP-PI4Kβ1. A. The expression of MBP-PI4Kβ1 in the soluble fraction was confirmed by SDS-PAGE gel, then immunodetected using a primary antibody against MBP and a secondary antibody against IgG with an alkaline phosphatase (AP) conjugate for colorimetric detection. MBP: Control, including soluble fraction obtained after expression of empty pMalc5G plasmid. **B.** The soluble fraction was used for enrichment and different elution fractions were collected (E5-E11). The full-length MBP-PI4Kβ1 fusion protein is indicated by a white arrowhead. Protein sizes were determined according to the PageRuler™ Pre-stained Protein Ladder. The expected molecular size of full-length MBP-PI4Kβ1 was 168 kDa. This picture is representative for the other enrichment procedures for the PI4Kβ1 variants.

Once enough purity of the recombinantly expressed MBP-PI4Kβ1 was achieved, we used radioactive *in vitro* lipid kinase reactions to test whether the fusion protein was catalytically active and to assess the reaction conditions for linear substrate conversion.

2.2. Reaction progress curve: estimation of linear range

Enzyme activities are affected by factors like the concentration of the enzyme, the concentrations of substrates, temperature, pH or the presence of inhibitors in the reaction. Therefore, it is important to operate in the linear range of the reaction to ensure there are no limiting factors during the assay. For this reason, we first determined the linearity of the enzyme and substrate concentrations for a radioactive *in vitro* lipid kinase assay. The *in vitro* lipid kinase assay is a multi-step procedure where – in brief - the recombinant MBP-PI4Kβ1 protein is first incubated with radiolabeled [γ-^{32}P] ATP and PtdIns substrate. After incubation, lipids are extracted from the reaction mix, separated by thin-layer chromatography, and analyzed by phosphorimaging for the abundance of

radiolabeled PtdIns4P. When a constant concentration of the recombinantly purified MBP-PI4Kβ1 was incubated for 30 min with increasing concentrations of PtdIns substrate, the reaction rate increased linearly by 5-fold. Similarly, when a constant concentration of the lipid PtdIns was incubated for 30 min with increasing concentrations of MBP-PI4Kβ1 the reaction rate increased linearly by 2-fold (Figure 15). To determine the molar concentration of radiolabeled [γ-^{32}P] ATP incorporated into PtdIns by MBP-PI4Kβ1, a standard curve was generated by plotting the phosphorimager signals corresponding to each concentration of [γ-^{32}P] ATP. The calibration curve was fitted to the straight-line equation $y = mx + b$ and the $slope = m$ and $b = y - intercept$ were used to calculate the unknown lipid kinase activities (Appendix Figure 35).

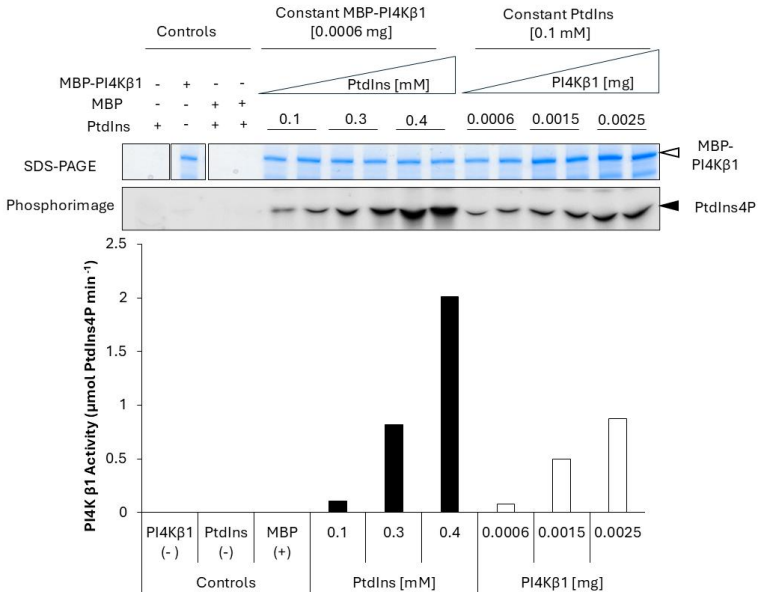

Figure 15.Estimation of linear range for different PtdIns or MBP-PI4Kβ1 concentrations. The SDS-PAGE shows the MBP- PI4Kβ1 (white arrow) concentration used for each assay. The phosphorimage of TLC plate shows the product of the kinase reaction PtdIns4P (black arrow). The black bars show the PI4Kβ1 activity estimated by increasing PtdIns concentrations and the white bars shows the PI4Kβ1 activity estimated by increasing the enzyme concentration. This calibration experiment was only performed twice. The data represents the mean of the experiment. No statistics were performed. The error is approximately 10%.

Once the appropriate linear concentrations for the MBP-PI4Kβ1 and PtdIns were determined, a reaction progress curve was performed at constant concentrations of PI4Kβ1 (0.009 mg) and PtdIns (0.3 mM), and the reaction rate was monitored every 10 min over a total time of 110 min (Figure 16) to estimate the linear time-range of the reaction. The time-course curve shows a plateau phase after 80 min indicating substrate depletion or the presence of inhibitors that may limit enzyme activity. The linear time-region was found between (at least) 0-30 min, therefore a reaction time of 15 min was selected for further kinetic assays.

The identity of the radiolabeled lipid product was confirmed as PtdIns4P by comparing Rf values of the unknown lipid samples with the migration of unlabeled *bona fide* lipid standards by TLC analysis (Appendix Figure 36). Once the linear range for the *in vitro* lipid kinase reactions was found, kinetic characterization assays were performed for MBP-PI4Kβ1.

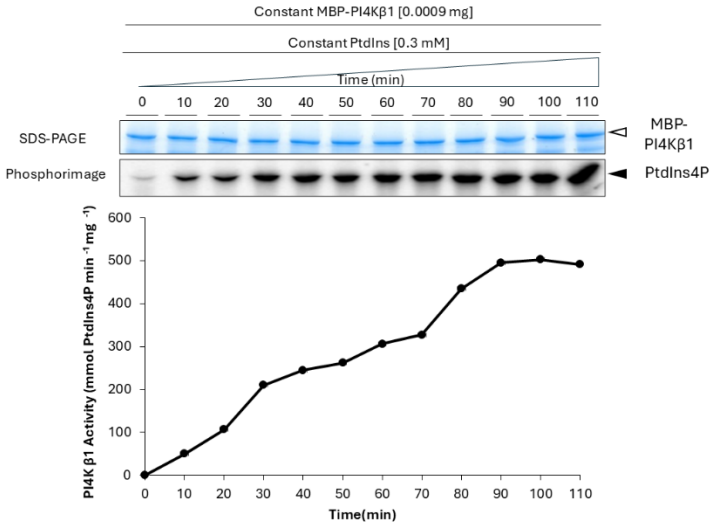

Figure 16.Time-course activity for MBP-PI4Kβ1. Monitoring of MBP-PI4Kβ1 activity progression over time. SDS-PAGE shows equal concentrations of MBP-PI4Kβ1 used for each sample point (white arrow). The phosphorimage of the TLC plate shows the product of the kinase reaction PtdIns4P (black arrow), increasing over time. The assay was performed using constant PtdIns [0.3 Mm] and MBP-PI4Kβ1 [0.009 mg] concentrations over a total period of 110 minutes. This calibration experiment was only performed twice. The data represents the mean of the experiment. No statistics were performed. The error is approximately 10%.

2.3. MBP-PI4Kβ1 shows positive allosteric cooperativity upon product binding

Kinetic characterization of full-length MBP-PI4Kβ1 was carried out using the recombinantly enzyme expressed in *E. coli* and purified by affinity chromatography as described above. Kinetic *in vitro* lipid phosphorylation assays were performed in the linear range under the steady-state kinetic conditions and the reaction rate was determined during the early phase of the reaction at 15 min of incubation. Kinetics assays were performed using a discontinuous assay “end point”, where the amount of product formed was measured at a fixed period of time, here 15 min.

MBP-PI4Kβ1 displayed pronounced sigmoidal reaction kinetics, when the initial reaction velocity of PtdIns4P formation was plotted as a function of increasing PtdIns substrate

concentrations (Figure 17 A). Non-sigmoidal reaction kinetics were evident by the hyperbolic behavior obtained by plotting the initial velocity of PtdIns4P formation as a function of increasing ATP substrate concentrations (Figure 17 B). Equal concentrations of MBP-PI4Kβ1 used for each reaction point were confirmed by SDS-PAGE analysis (see Appendix Figure 38).

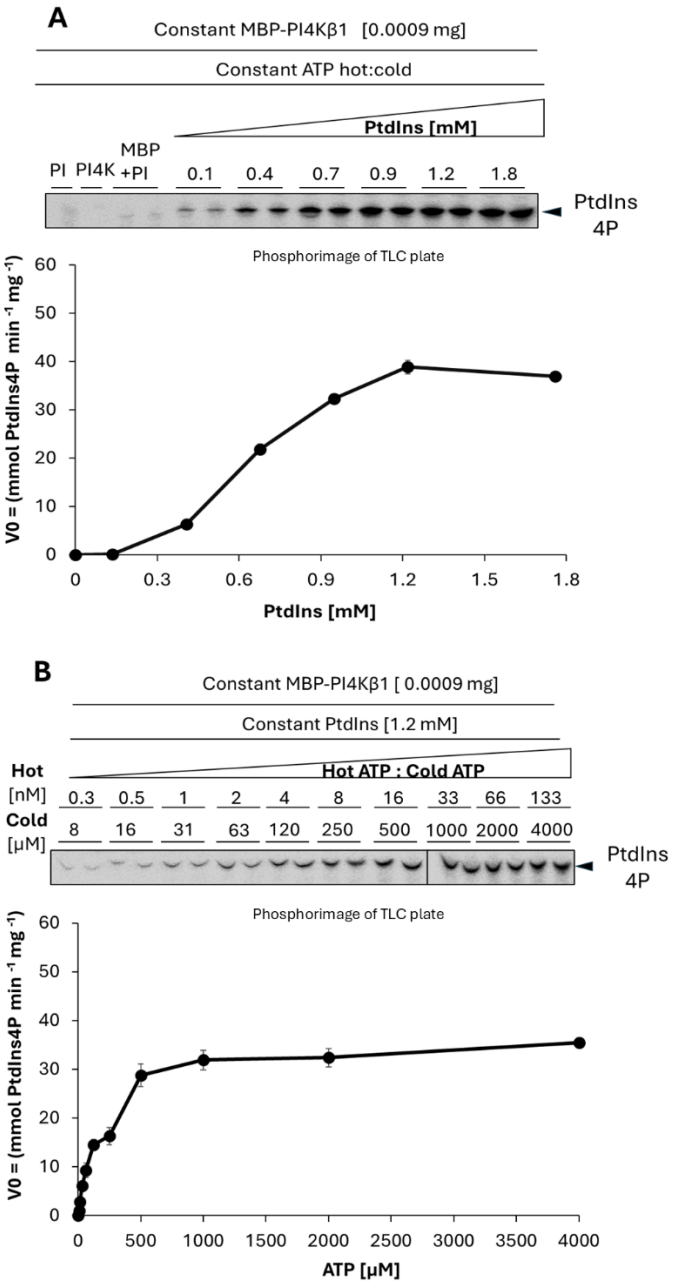

Figure 17. Kinetic characterization of MBP-PI4Kβ1 for PtdIns and ATP substrates. Black arrow shows the product of the reaction (PtdIns4P) resolved by TLC plate and the radioactive lipid was detected by phosphorimaging. Radioactive PtdIns4P was quantified in Image Quant by densitometry using the calibration curve for radiolabeled [γ-^{32}P] ATP and initial velocity obtained. **A.** Sigmoidal reaction kinetics for the wild type MBP-PI4Kβ1 was obtained by plotting the initial velocity as a function of increasing PtdIns concentrations. **B.** A non-sigmoidal, hyperbolic reaction kinetics was obtained by plotting the initial velocity as a function of increasing ATP concentrations. The data represents the mean of six data points ± standard error.

The sigmoidal kinetic profile for the reaction with increasing PtdIns concentrations indicates allosteric regulation, where the binding of a ligand at one site on the protein influences substrate conversion in the catalytic site (Somvanshi & Venkatesh, 2013). Due to cooperative binding of two or more ligands at different sites of the enzyme, the observed kinetics cannot be interpreted easily by the Michaelis–Menten equation, and therefore the Hill equation was employed to estimate the kinetic parameters. Logarithmic transformation of the kinetic data was applied to enable the use of the linear form of the Hill equation described by (Endrenyi et al., 1975) where the Hill coefficient (η_H) was obtained by the slope and the half-saturating constant ($K_{0.5}$) by calculating the inverse of the natural logarithm (ln) of the X-intercept (See equation in section 4.17.8; Equation 3). For the sigmoidal kinetics obtained at increasing lipid concentrations, an $\eta_H = 3.6$ was calculated, indicating a high degree of positive cooperativity in the binding sites of the enzyme, where the initial binding of the ligand enhances the binding of the forthcoming ligands on the enzyme. The experimental half-saturating constant was $K_{0.5}$ = 0.6 mM at PtdIns saturating concentrations (Figure 18 A). This value indicates the affinity of the enzyme towards the substrate, where at a PtdIns concentration of 0.6 mM half of the active sites of the PI4Kβ1 were occupied with the PtdIns substrate.

The kinetic constants for the non-sigmoidal hyperbolic curve at increasing ATP concentrations were calculated according to the linear form of the Michaelis-Menten equation, the Lineweaver Burk-Plot. The enzyme displayed a negative cooperativity for the co-substrate ATP, indicating that the binding of one ATP molecule decreases the affinity of the enzyme for the next molecule. The Michaelis-constant was $K_m = 219\ \mu\text{M}$ when ATP concentrations were increased, suggesting that at an ATP concentration of 219 µM half of the active sites of the PI4Kβ1 were occupied with the ATP substrate. The K_m was obtained by multiplying $m\ x\ V_{max}$ and the V_{max} was calculated by dividing $1\ /\ b$ ($V_{max} = 38.1$ mmol PtdIns4P min^{-1} mg^{-1}) (Figure 18 B).

2.4. Regulatory domains are required for proper PI4Kβ1 activity

Based on the sigmoidal kinetics, it was next addressed whether the sigmoidal response observed for MBP-PI4Kβ1 was caused by allosteric binding of a ligand to the N-terminal regulatory domains of PI4Kβ1. This experiment was motivated by the previous report that the PPC domain binds to PtdIns-monophosphates (Lou et al., 2006). A truncated variant

of MBP-PI4Kβ1 was expressed in *E. coli* and enriched that lacked the N-terminal regulatory domains and consisted only of the catalytic domain.

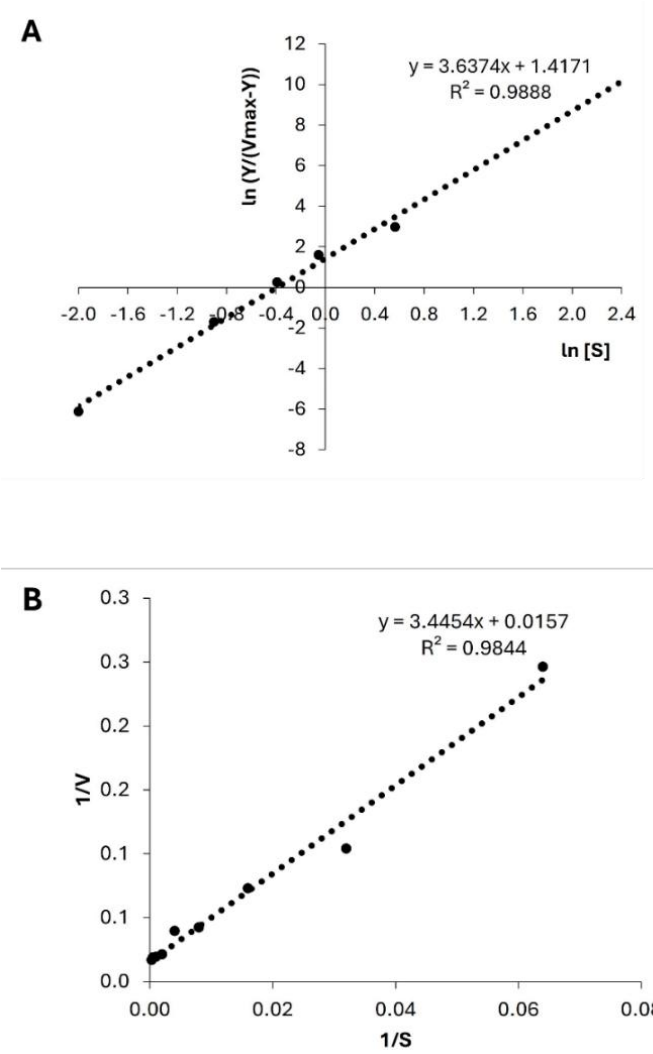

Figure 18. Estimation of kinetic parameters for MBP-PI4Kβ1. A. Linearized Hill plot for the PI4Kβ1 sigmoidal kinetics at increasing PtdIns substrate concentrations, showing the slope $\boldsymbol{m = 3.63}$, and the x$-\boldsymbol{intercept} - \boldsymbol{n\ Log\ Kd = -0.4}$. The $\boldsymbol{LN}$ of -0.4 retrieved the $\boldsymbol{K_{0.5} = 0.6\ mM}$. **B.** Lineweaver Burk plot for the PI4Kβ1 hyperbolic non-sigmoidal kinetics at increasing ATP substrate concentrations, showing the slope $\boldsymbol{m = 3.44}$ and $\boldsymbol{V_{max} = 38.1\ mmol}$ PtdIns4P min $^{-1}$ mg^{-1} and $\boldsymbol{K_m = 219\ \mu M}$

Kinetic characterization of the truncated MBP-PI4Kβ1$_{806\text{-}1121}$ was performed by obtaining the initial velocities while increasing the PtdIns concentrations. We hypothesized that a non-sigmoidal, hyperbolic response was going to be obtained after the removal of the regulatory domains. Surprisingly, the catalytic domain exhibited very low activity ($V_{max} = 275$ µmol PtdIns4P min^{-1} mg^{-1} for MBP-PI4Kβ1$_{806\text{-}1121}$, compared to wild type MBP-PI4Kβ1 with $V_{max} = 39$ mmol PtdIns4P min^{-1} mg^{-1}), which was only detectable by phosphorimaging after overnight exposure. While the kinetic pattern was indeed shifted

from sigmoidal to a hyperbolic curve, due to difficulties in reliably detecting the radioactive PtdIns4P in both repetitions, this kinetic experiment must be further confirmed (Appendix Figure 37). The data indicates that the N-terminal regulatory domains of PI4Kβ1 are essential for catalytic activity. To further address this aspect, and before further kinetic experiments, it was attempted to better understand the relative positioning of the PI4Kβ1 protein to its substrate membrane by using molecular modeling.

2.5. A 3D structural model of the PI4Kβ1-membrane interaction

The crystal structure of *Arabidopsis* PI4Kβ1 has not been solved to date, but the protein shares similarities in sequence and structure with other PI4-kinases and PI3-kinases of human origin that have been better characterized. Due to the availability of published structural studies of the human PI3Kα in complex with PtdIns(4,5)P_2 and ATP (Maheshwari et al., 2017a) in the Alphafill database (Hekkelman et al., 2023) 3D structures of human PI3Kα (UniProt: 4ovv) and PI3Kγ (UniProt:1E8X) were superimposed with a model of PI4Kβ1 from *Arabidopsis* and their similarity was evaluated (Appendix Figure 40 A-C) in cooperation with the group of Prof. Dr. Panagiotis Kastritis (MLU). Sequence alignment shows that the PI3Kα shares 336 identical and 543 similar residues with *Arabidopsis* PI4Kβ1, corresponding to a degree of sequence identity of 25.4 % and sequence similarity of 41.1 %, respectively. Human PI3Kγ shares 345 identical and 553 similar residues with *Arabidopsis* PI4Kβ1, corresponding to 25.5% identity and 40.9 % similarity, respectively. Similarities and differences in sequence and domain structures between the proteins used for the structural modelling are illustrated in Figure 19**.**

An Alpha Fold (AF) model for PI4Kβ1 represented only a partial protein after super-positioning, and the following residues were included into the final model: F46-A143; N541-E641; E835-D1103 or E835-L1121. The partial model for *Arabidopsis* PI4Kβ1 shows the conservation of several residues across the different domains (Figure 20 A). The LKU, NH and catalytic (Catal) domains are known to be conserved across eukaryotes, whereas the PPC (repetitive domain) is plant specific and has no equivalent in the human template proteins (Xue et al., 1999a). The partial model revealed the positioning of key features of the kinase domain, including the glycine-rich loop (G-loop), the catalytic loop and activation loop, which have been well characterized for human protein kinases (Walker et al., 1999) and are annotated in the protein data base Uniprot.

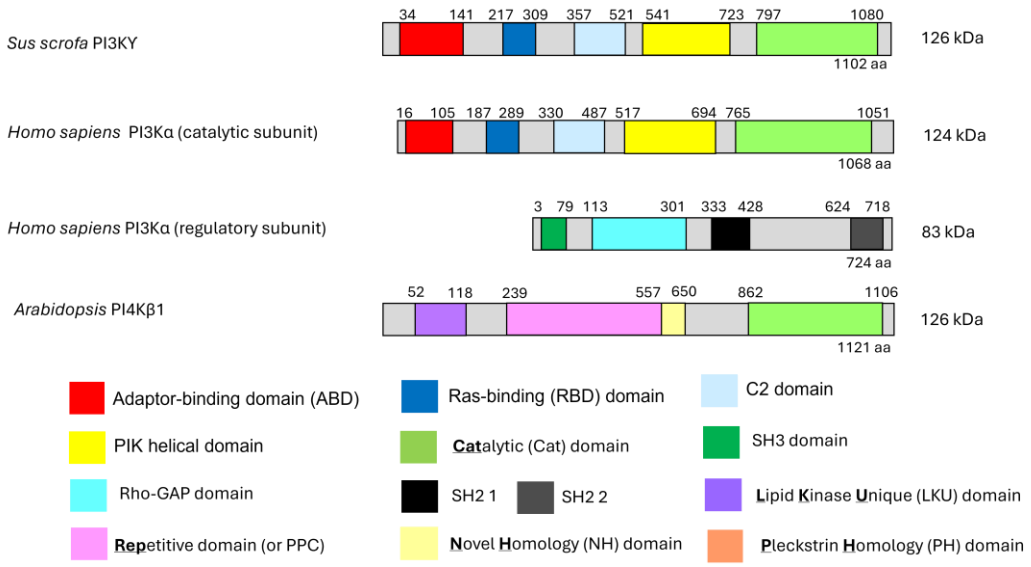

Figure 19. Protein domains present in PI3-Kinase α and PI3-Kinase ϒ in mammals and *Arabidopsis* PI4Kβ1. Schematic representation of different domains in PI3-Kinases from pig (*Sus scrofa*) and human (*Homo sapiens*) used for superimposition with *Arabidopsis* PI4Kβ1. Uniprot reference numbers are as follows: PI3KY: 1E8X; PI3Kα catalytic and regulatory subunits: 4OVV.

The partial model of *Arabidopsis* PI4Kβ1 shows the enzyme orienting a catalytic groove towards the model membrane surface holding the substrate lipid head groups, which protrude into the catalytic groove, bringing the lipid head group in position for phosphotransfer from the bound ATP (Figure 20).

This orientation is in accordance with data on the membrane-association of other PI 4-kinases of human origin. Interestingly, the model also revealed a C-terminal helical tail region of 18 residues in length that appears well conserved across PI-kinases from different eukaryotes. This C-terminal helix (to our knowledge) has not previously been described as a conserved element of PI-kinases, and it shares 8 identical and 12 similar residues (42.1 and 63.1% respectively), with the homologous human PI4KβIII and 7 identical and 10 similar residues (36.8% and 52.6% respectively) with the homologous PIK1p from *Saccharomyces cerevisiae.* The C- terminal helix contains 6 hydrophobic (33.3%), 4 aromatic (22.2%), 3 basic (16.6%), 3 neutral (16.6%), 1 acidic (5.5%) and 1 aliphatic (5.5%) residue. The partial model of PI4Kβ1 suggests that the C-terminal tail may be in close proximity to the reaction product, PtdIns4P (designated in Figure 20 A as “PIP4P”) at the membrane (Figure 20 A). Additionally, the Leucine in position 1117 appears as a key residue predicted to mediate interaction with the substrate PtdIns (occupancy: 35.3%) and the product PtdIns4P (occupancy: 12.3 %). The arginine in position 626 was predicted to be a crucial residue for interaction with PtdIns (occupancy: 40.9%) and PtdIns4P (35.1%) (Appendix Figure 41).

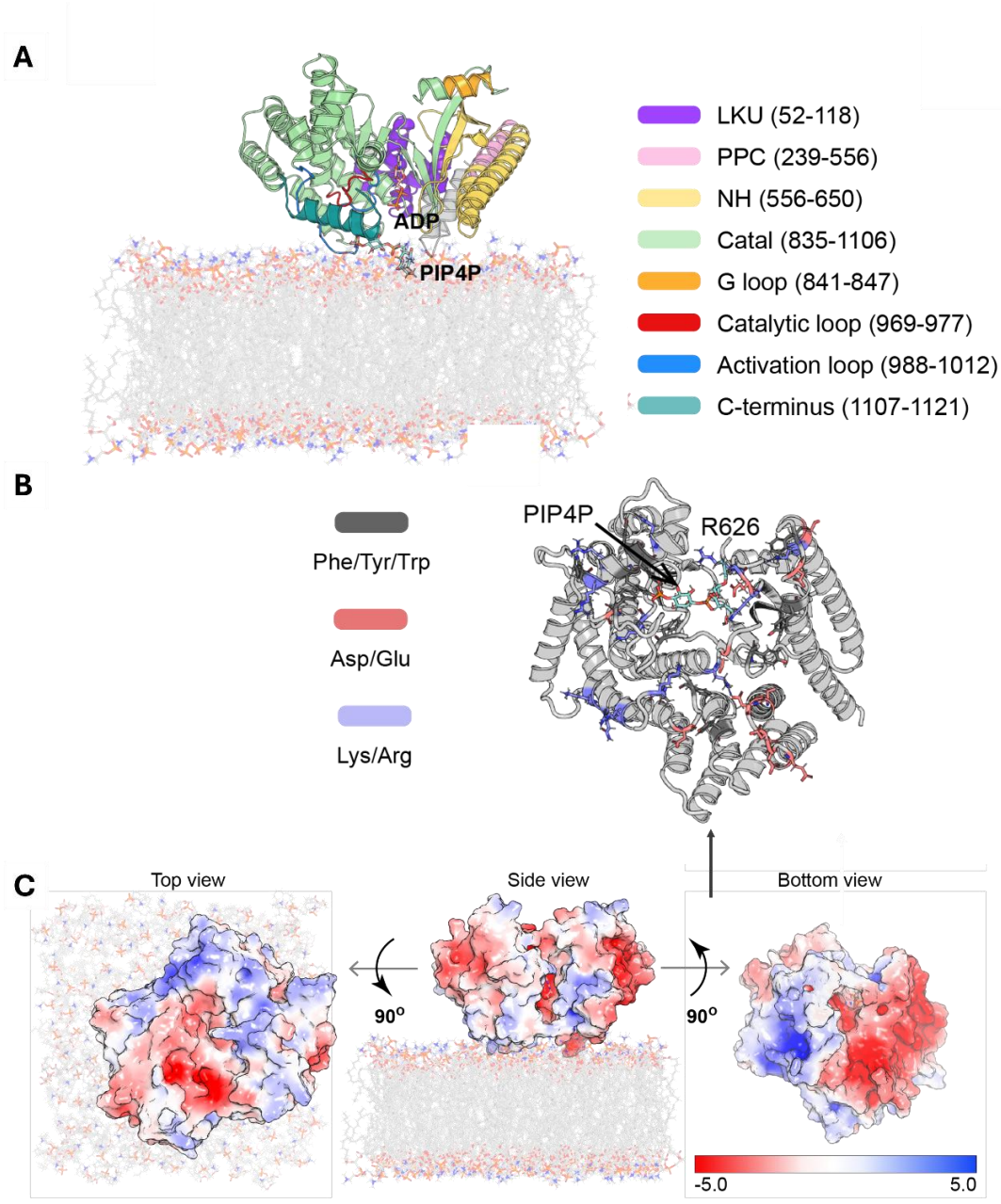

Figure 20. AlphaFold-based model of partial PI4Kβ1 with PIP4P and ADP. A. Color coded according to protein domains. **B**. Key electrostatic residues that may interact with the membrane within 10 Å of the protein-membrane interface. **C.** PI4Kβ1 protein surface color coded according to electrostatic potential (APBS Electrostatics Plugin of PyMoL). Top view, side view, and bottom view, as indicated. The model membrane used was calculated by CHARMM-GUI with a lipid composition of DMPC/DOPC/DMPI/DMPI-4P (20:20:1:1). DMPC, dimyristoyl-PtdCho; DOPC, dioleoyl-PtdCho; DMPI, dimyristoyl-PtdIns; DMPI-4P, dimyristoyl-PtdIns4P; PIP4P, PtdIns4P. The model was obtained in cooperation with Dr. Marija Sorokina and Prof. Dr. Panagiotis Kastritis (MLU).

The partial model of *Arabidopsis* PI4Kβ1 model contained a total of 487 residues with 63 acidic Asp/Glu (12.9%), 53 basic Lys/Arg (10.8%) and 54 hydrophobic aromatic Phe/Tyr/Trp (11%) that regulate the electrostatic properties of the enzyme (Figure 20 B). The electrostatic potential surface of PI4Kβ1 is colored in blue (Lys/Arg) for positive charges

and in red (Asp/Glu) for negative charges in the top, side and bottom views (Figure 20 C). Interestingly, the bottom view shows that the area predicted to interact with the membrane consists in a majority of acidic residues (right side) but also basic residues (left side). Based on a similar finding in the mechanism used by a human type II PIPKβ to bind its target membranes (Rao et al., 1998), our results may indicate, that *Arabidopsis* PI4Kβ1 can electrostatically interact with negatively charged anionic substrate lipids through basic residues at the protein-membrane interface, but that also acid/aromatic residues may participate in protein-membrane association.

Based on the partial alpha-fold model of PI4Kβ1, MD simulations were performed to obtain an approximate impression of molecular forces between the molecules involved, in particular between protein residues of the active site and the substrate PtdIns, the product PtdIns4P, and the co-substrate, ATP. The MD shows that the C-terminal tail of PI4Kβ1 might be involved in the interaction of PI4Kβ1 with the reaction product, PtdIns4P, which interacts through hydrogen bonding between its D-4 phosphate and residues of the C-terminal helix (Figure 21 A-B).

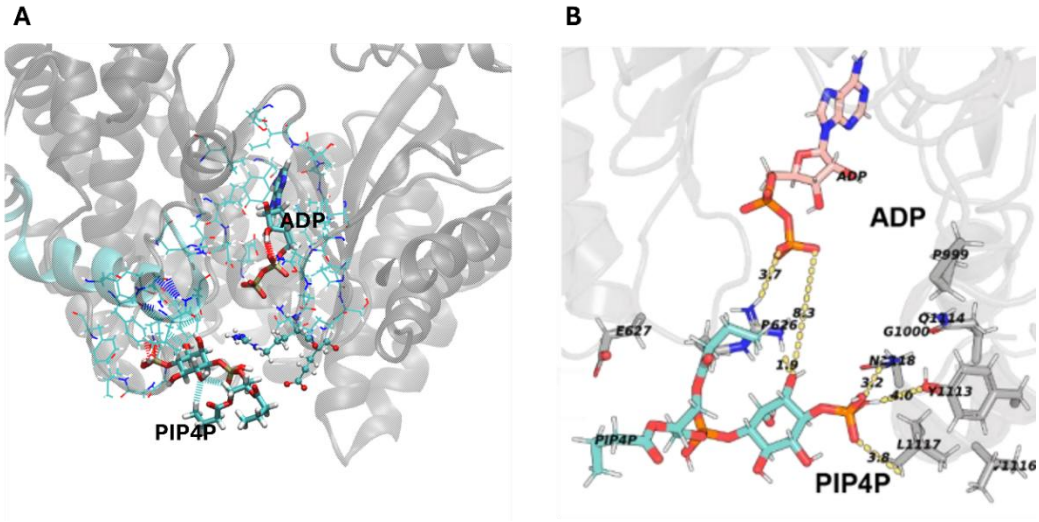

Figure 21. Molecular dynamics simulations for PI4Kβ1 in complex with ADP and PIP4P. MD: 1,000,000 fs == 1.0 ns (ca. 1 ns per 1 day). **A.** Full-Length PI4Kβ1 (F46-A143; N541-E641; E835-L1121). **B.** PI4Kβ1-C-terminus-deletion (F46-A143; N541-E641; E835-D1103). PIP4P here represents PtdIns4P. The model was obtained in cooperation with Dr. Marija Sorokina and Prof. Dr. Panagiotis Kastritis (MLU).

The stability of the protein model relative to its conformation can be determined by the deviations obtained in the root mean square deviation (RMSD) during the course of the MD-simulation. The RMSD value was calculated for 1 ns in order to evaluate the stability of PI4Kβ1 in comparison to a deduced truncated PI4Kβ1-variant lacking the C-terminal helix. The RMSD plots show that the trajectory map for the PI4Kβ1 protein was maintained at a level of 2.0 Å in a complex with the substrate PtdIns after 1 ns, but the structure

showed a steady increase above 2.0 Å in complex with the product PtdIns4P. This behavior suggests a higher stability of the enzyme when it is bound to PtdIns than to PtdIns4P, due to a lower RMSD value (Appendix Figure 40 D-I). In other words, PI4Kβ1 may display a tendency for conformational change when it is bound to its reaction product, PtdIns4P, possibly related to product release.

By contrast, when the equivalent analysis was performed for the PI4Kβ1-variant lacking the C-terminal tail helix, there was a steep increase at the beginning of the MD-simulation and a more stable trajectory for substrate and product binding than was observed for the intact PI4Kβ1 model, suggesting a structural conformational change in the protein after deletion of the helix. The deletion also seemed to increase the stability of the protein, due to a more stable trajectory (Figure 40 D-I), suggesting that a conformational change related to product release might not occur when the C-terminal helix is missing. Together, the modeling data suggested a previously unknown contribution of the C-terminal helix to catalysis and served as a basis for further *in vitro* experiments.

Based on the findings from the MD-simulations, we specifically asked whether deletion of the C-terminal helix or alanine-substitutions of leucine 1117 or arginine 626 had an impact on the performance of the PI4Kβ1 enzyme *in vitro*. Therefore, the respective PI4Kβ1-variants were generated in *E. coli* and enriched and subjected to kinetic characterization.

2.6. Kinetic characterization of MBP-PI4Kβ1 variants deleted or substituted in its C-terminal helix

Based on the *in silico* modeling of PI4Kβ1, *in vitro* experiments were performed to elucidate the relevance of the predicted catalytic contribution of the C-terminal helix in the PI4Kβ1-protein. To determine whether the helix was relevant for catalysis, a C-terminally truncated variant PI4Kβ1$_{1107\text{-}1121}$ was generated. Moreover, alanine substitution variants PI4Kβ1 L1117A and PI4Kβ1 R626A were generated. All PI4Kβ1-variants were expressed as MBP-fusion in *E. coli* and enriched as before, and were then subjected to kinetic analysis in *in vitro* lipid phosphorylation assays. Equal concentrations of MBP-PI4Kβ1 used for each reaction point were confirmed by SDS-PAGE analysis (see Appendix Figure 38 and Figure 39).

Intriguingly, the deletion of the 18-residue C-terminal helix of PI4Kβ1 abolished lipid kinase activity (almost undetectable $V_0 = 1.2$ mmol PtdIns4P min^{-1} mg^{-1}) (Figure 22 A),

indicating that the C-terminal helix is necessary for catalysis, either for substrate binding or for product release, or – alternatively – that it was essential for protein integrity.

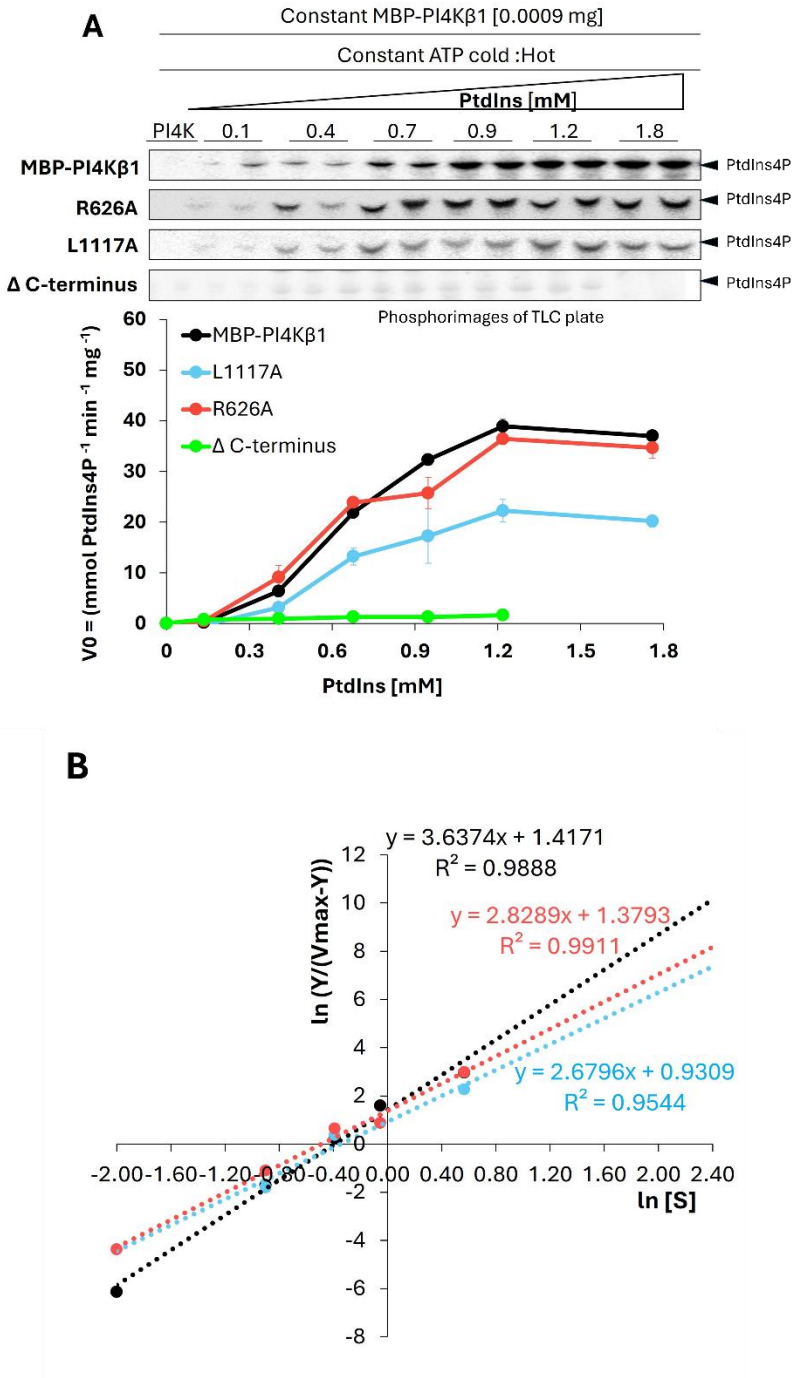

Figure 22. Kinetic characterization of PI4Kβ1- variants deleted or substituted in the C-terminal helix. **A.** Phosphorimage after *in vitro* lipid phosphorylation assays employing radiolabeling, using recombinant variants of PI4Kβ1. WT, Wild type MBP-PI4Kβ1; MBP-PI4Kβ1 R626A; L1117, MBP-PI4Kβ1 L1117A; Δ C-terminus, MBP-PI4Kβ1$_{1107-1121}$. Black arrow heads show the product of the reaction (PtdIns4P) as resolved by TLC. Sigmoidal reaction kinetics were obtained upon incubation with increasing PtdIns concentrations for MBP-PI4Kβ1 L1117A, and for MBP- PI4Kβ1 R626A and for the Δ C-terminus deleted variant. The data represents the mean of four data points ± standard error. **B.** Linearized Hill plot for the substitution variants of PI4Kβ1 at increasing PtdIns substrate concentrations, showing the Hill coefficients (slopes). The corresponding data is given in Table 1.

Table 1. Kinetic constants of MBP-PI4Kβ1- variants deleted or substituted in the C-terminal helix estimated from Hill plot.

Protein variant	η_H	$K_{0.5}$
MBP-PI4Kβ1	3.63	0.67 mM
MBP-PI4Kβ1-R626A	2.82	0.61 mM
MBP-PI4Kβ1-L1117A	2.67	0.68 mM
MBP-PI4Kβ1-Δ C-terminus	-	-

To more subtly analyze the effects of the C-terminal helix on the function of PI4Kβ1, individual residues suggested by the MD-simulations to interact with the substrate or the product were substituted for alanines. Both MBP-PI4Kβ1 L1117A and MBP-PI4Kβ1 R626A displayed sigmoidal kinetics as already seen for the MBP-PI4Kβ1 (Figure 17 A) when the initial reaction velocity was plotted as a function of increasing PtdIns substrate concentrations (Figure 22 A). Kinetic constants were calculated using the linear form of the Hill equation as described above (Figure 22 B; see section 4.17.8; Equation 4).

While MBP-PI4Kβ1 R626A showed a similar V_{max} compared to the wild type MBP-PI4Kβ1 (36 mmol PtdIns4P min^{-1} mg^{-1} vs. 39 mmol PtdIns4P min^{-1} mg^{-1}, respectively), MBP-PI4Kβ1 L1117A displayed a substantially lower V_{max} compared to the wild type (22 mmol PtdIns4P min^{-1} mg^{-1} vs 39 mmol PtdIns4P min^{-1} mg^{-1}, respectively). However, the $K_{0.5}$ did not significantly change, neither in MBP-PI4Kβ1 R626A ($K_{0.5} = 0.61\ mM$) nor in MBP-PI4Kβ1 L1117A ($K_{0.5} = 0.68\ mM$) compared to wild type MBP-PI4Kβ1 ($K_{0.5} = 0.67\ mM$).

Overall, the kinetic analysis of MBP-PI4Kβ1 and its variants indicates allosteric regulation through a component present in the reaction. As it is known that PI4Kβ1 can bind PtdIns-monophosphates through its PPC region (Lou et al., 2006), we conclude that PI4Kβ1 is likely displaying cooperative activation by its reaction product, PtdIns4P. This interpretation is in line with previously reported activating effects of PtdIns4P on PI4Kβ1 (Stevenson-Paulik et al., 2004). Based on structural modeling and MD-simulation combined with experimental data, furthermore a contribution of a C-terminal helix of PI4Kβ1 can be proposed.

In addition to the allosteric regulation of PI4Kβ1 by its product, PtdIns4P, it was next addressed how PI4Kβ1 might be regulated by upstream protein kinases.

2.7. MBP-PI4Kβ1 protein is phosphorylated *in vitro* by the protein kinases, MPK4, MPK6, SnRK2.6 and CPK11

Arabidopsis PI4Kβ1 was first reported as a target for MPK4 (Mitogen-activated protein kinase 4) upon flagellin 22 treatment in supplementary data (Latrasse et al., 2017) and later confirmed by targeted *in vitro* protein phosphorylation assays using recombinantly expressed proteins (Lin et al., 2019).

Additionally, an important phosphoproteomic study found PI4Kβ1 as a target for the protein kinases, MPK6 (Mitogen-activated protein kinase 6) and SnRK2.6 (sucrose non-fermenting-1-related protein kinase 2.6) in *in vivo Arabidopsis* phosphopeptide analyses (Wang et al., 2020). While no phosphorylation studies have been reported for CPK11 (calcium-dependent protein kinase 11)-mediated phosphorylation of PI4Kβ1, the N-terminal domain of PI4Kβ1 is known to interact with the calcineurin B–like protein (AtCBL1), a Ca^{2+}sensor protein, suggesting a role of Ca^{2+} binding proteins in the regulation of PI4Kβ1 (Preuss et al., 2006). Therefore, due to the availability of enriched CPK11 in our research group (kindly provided by Johanna N.), effects of CPK11 on PI4Kβ1 were also tested in this thesis.

Experiments were performed to test the phosphorylation of enriched recombinant MBP-PI4Kβ1 protein by other recombinantly expressed and purified protein kinases, including MPK4, MPK6, SnRK2.6, and CPK11. The protein kinases were expressed as fusion proteins to hexa-histidine-tags ($_{6x}$His), and the MPK-variants were additionally modified by amino acid substitutions to represent their constitutive active (CA) states or – as controls – their kinase-dead (KD) states (see section 4.12.1). CA-$_{6x}$His-MPK4, CA-$_{6x}$His-MPK6, $_{6x}$His-SnRK2.6 and $_{6x}$His-CPK11 were expressed as fusions to N-terminal $_{6x}$His-tags in different *E. coli* strains (see section 4.12.2) and enriched by affinity chromatography (see section 4.15.1). The quality of the enriched recombinant fusion proteins is illustrated in Appendix Figure 42. The recombinantly expressed and enriched proteins were used for either non-radioactive (γ-S-ATP) or radioactive (labeled [γ ^{32}P]-ATP) *in vitro* protein phosphorylation tests against MBP- PI4Kβ1 protein as a substrate, or against control substrates, such as casein (Cas) or myelin basic protein (MyBP) (see section 4.18).

First, a time-course of *in vitro* phosphorylation assay was performed using radiolabeled [γ-^{32}P]-ATP to estimate the linear time-range of the reaction (Figure 23).

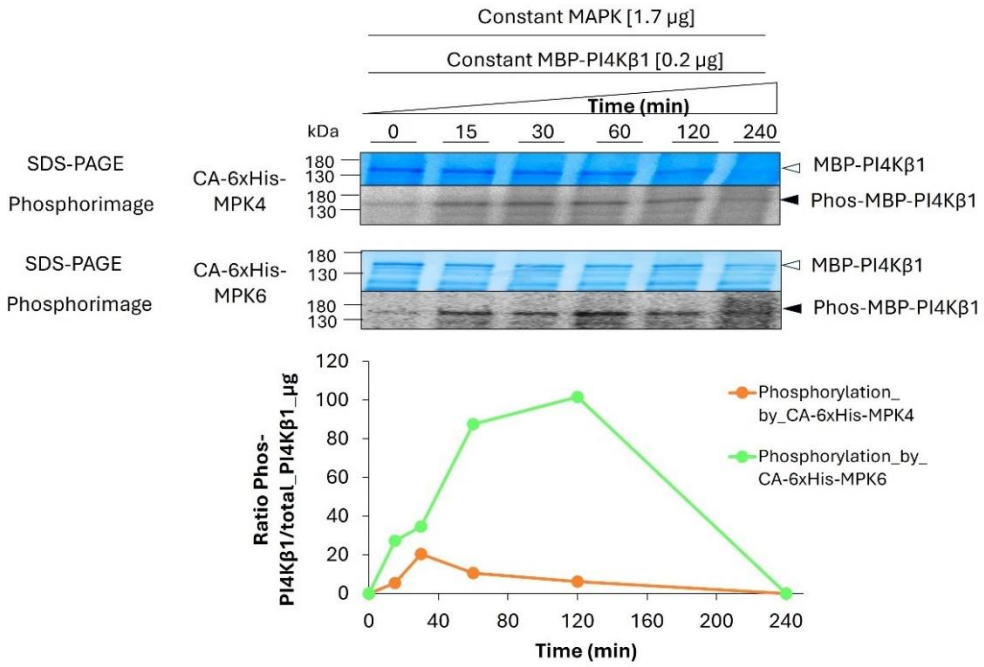

Figure 23. Time-course *in vitro* protein phosphorylation assay of MBP-PI4Kβ1 by upstream CA-$_{6x}$His-MPK4 or CA-$_{6x}$His-MPK6. The phosphorylation of enriched recombinant MBP-PI4Kβ1 protein by potential upstream protein kinases, CA-$_{6x}$His-MPK4 or CA-$_{6x}$His-MPK6, was tested in *in vitro* protein phosphorylation assays**.** Proteins were incubated in the presence of [γ ^{32}P]ATP for radiolabeling, extracted and separated by SDS-PAGE. Dried SDS-PAGE gels were then analyzed by phosphorimaging. Assays were performed using constant concentrations of both the MBP-PI4Kβ1 [0.2 µg] substrate and of the upstream kinases CA-$_{6x}$His-MPK4 and CA-$_{6x}$His-MPK6 [1.7 µg]. Protein phosphorylation was monitored over a total period of 240 minutes. A representative phosphorimage is shown below the SDS-PAGE gels for CA-$_{6x}$His-MPK4 or CA-$_{6x}$His-MPK6, as indicated**.** White arrow heads (MBP-PI4Kβ1); black arrow heads, Phosphorylated MBP-PI4Kβ1. The graph represents the ratio of phosphorylated MBP-PI4Kβ1 protein to the MBP-PI4Kβ1 input in µg protein at each time point. Protein amounts were estimated by densitometry on Coomassie-stained SDS-PAGE gels, using BSA as a known standard. Radioactive phosphorylated PI4Kβ1 was quantified in ImageQuant by densitometry using the calibration curve for radiolabeled [γ-^{32}P] ATP. Protein sizes were determined according to the PageRuler™ Prestained Protein Ladder. The expected molecular size for the MBP-PI4Kβ1 fusion proteinis 168 kDa. The assay was performed one time, no statistics were performed.

The time-course phosphorylation of MBP-PI4Kβ1 by CA-$_{6x}$His-MPK4 exhibited a light increase from 0-30 min, but a constant decrease from 30-240 min, indicating that after 30 min of kinase reaction, a limiting factor affected the phosphorylation of the substrate protein by CA-$_{6x}$His-MPK4. By contrast, a steep increase in phosphorylation of MBP-PI4Kβ1 was observed from 0-60 min of incubation when phosphorylation by CA-$_{6x}$His-MPK6 was tested, reaching a plateau from 60-120 min, and declining again from 120-240 min, suggesting a limiting factor was present after 60 min of incubation. As noticed in the SDS-PAGE for both assays, even though protein concentrations were carefully estimated, we perceived a reduction in the protein concentration at the end of the assays, possibly due

to protein degradation after long incubation times. Hence, we chose 15 min as a reaction time for all further *in vitro* protein phosphorylation assays.

Based on the initial experiments for calibration, further radioactive *in vitro* protein phosphorylation assays using radiolabeled [γ-^{32}P] ATP were performed to analyze in more detail whether MBP-PI4Kβ1 is a target for phosphorylation by upstream CA-$_{6x}$His-MPK4, CA-$_{6x}$His-MPK6, $_{6x}$His-SnRK2.6 or $_{6x}$His-CPK11 (Figure 24 A-D). These experiments confirm the previously published analyses (Latrasse et al., 2017; Lin et al., 2019; Wang et al., 2020) by targeted in *vitro* experiments and also demonstrate for the first time phosphorylation of MBP-PI4Kβ1 by CPK11. Under the identical conditions (with the exception of 0.55 mM Ca^{2+} added for CPK11), phosphorylation of MBP-PI4Kβ1 was stronger upon incubation with CA-$_{6x}$His-MPK6 or $_{6x}$His-CPK11 and substantially weaker upon incubation with CA-$_{6x}$His-MPK4 or $_{6x}$His-SnRK2.6 (Figure 24 E).

For the two MAPKS, CA-$_{6x}$His-MPK4 and CA-$_{6x}$His-MPK6 phosphorylation of MBP-PI4Kβ1 was also tested by a non-radioactive *in vitro* phosphorylation assays using γS-ATP and immunodetection, verifying that MBP-PI4Kβ1 is a target for phosphorylation by both CA-$_{6x}$His-MPK4 and CA-$_{6x}$His-MPK6 (Figure 25).

Even though it was verified that MBP-PI4Kβ1 is a target for phosphorylation by all four upstream protein kinases tested, further experiments were focused on the regulation of MBP-PI4Kβ1 by MAPKs, because previous findings in our research group evidenced a regulatory link between MAPK (M. Heilmann & Heilmann, 2022; Hempel et al., 2017; Lin et al., 2019; Menzel et al., 2019) with specific regard to PI4Kβ1, understanding the complex regulation of PI4Kβ1 by MAPKs might facilitate our comprehension about the functional interplay of these proteins during somatic cytokinesis in *Arabidopsis* in future experiments.

To characterize the phosphorylation of MBP-PI4Kβ1 by the MAPKs, MPK4 or MPK6, in more detail, we next analyzed putative phosphosites targeted by upstream MPK4 and MPK6 in at the PI4Kβ1 protein by phosphoproteomics.

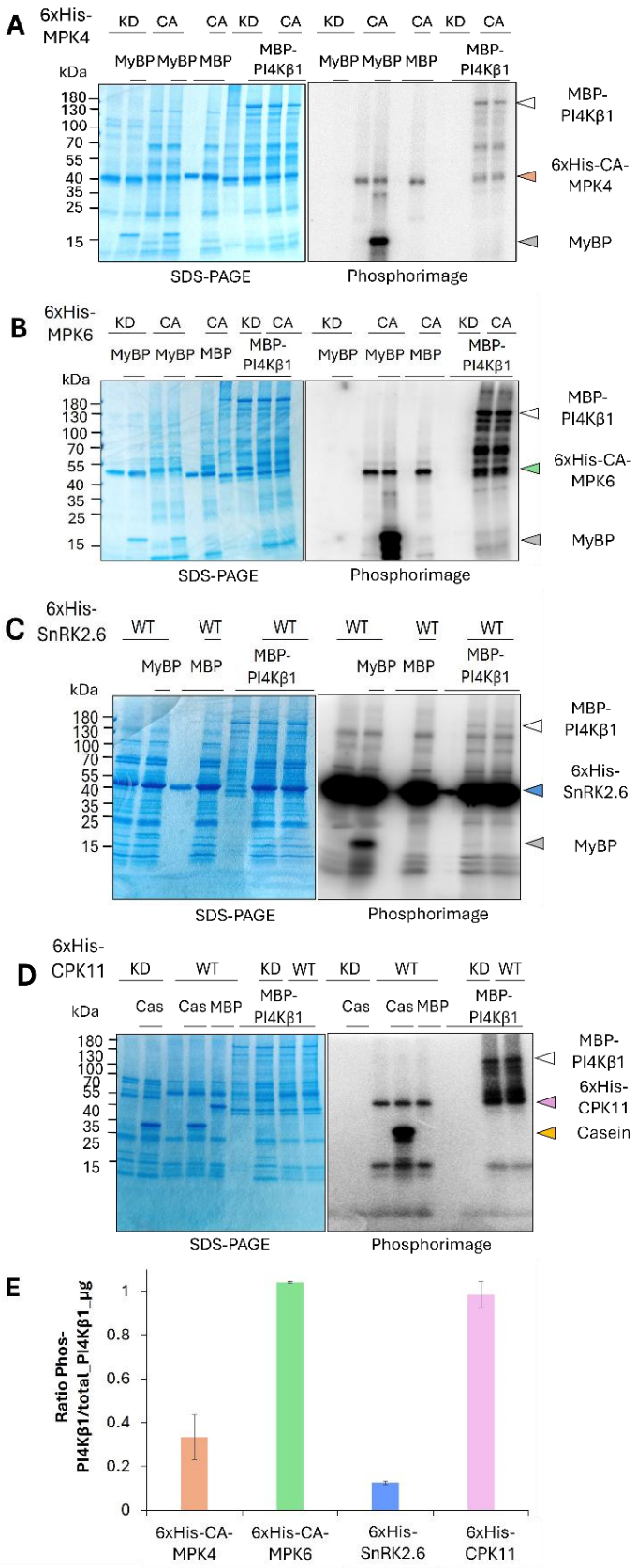

Figure 24. Enriched recombinant MBP-PI4Kβ1 protein is phosphorylated *in vitro* by recombinant protein kinases, CA-$_{6x}$His-MPK4, CA-$_{6x}$His-MPK6, $_{6x}$His-SnRK2.6 or $_{6x}$His-CPK11. The phosphorylation of enriched recombinant MBP-PI4Kβ1 protein by various protein kinase candidates was tested in *in vitro* protein phosphorylation assays. Proteins

were incubated in the presence of [γ- ^{32}P]ATP for radiolabeling, extracted and separated by SDS-PAGE. Dried SDS-PAGE gels were then analyzed by phosphorimaging. Assays were incubated for 15 min using constant concentrations of both the MBP-PI4Kβ1 [0.2 µg] substrate and of the upstream protein kinases (CA-$_{6x}$His-MPK4 PI4Kβ1 [1.7 µg], CA-$_{6x}$His-MPK6 [1.7 µg], $_{6x}$His-SnRK2.6 [2.5 µg] or $_{6x}$His-CPK11 [1.5 µg]. **A.** Phosphorylation of MBP-PI4Kβ1 by constitutively active (CA)- $_{6x}$His-MPK4, with the respective controls Kinase-Dead (KD)-$_{6x}$His-MPK4, Maltose Binding Protein (MBP), Myelin Basic Protein (MyBP). White arrowhead, MBP-PI4Kβ1; orange arrow head, MPK4; grey arrow head, MyBP. **B.** Phosphorylation of MBP-PI4Kβ1 by CA-$_{6x}$His-MPK6, with the respective controls KD-$_{6x}$His-MPK6; MBP; and MyBP. Green arrowhead, MPK6; grey arrow head, MyBP. **C.** Phosphorylation of MBP-PI4Kβ1 by $_{6x}$His-SnRK2.6, with the respective controls, MBP and MyBP. Blue arrowhead, WT-SnRK2.6; gray arrow head, MyBP. **D.** Phosphorylation of MBP-PI4Kβ1 by $_{6x}$His-CPK11 in the presence of 50 mM Ca^{2+}, with respective controls, KD-$_{6x}$His-CPK11, MBP and Casein (Cas). Pink arrow heads, CPK11; yellow arrow heads, Cas. **E.** Bar graph showing the ratios of phosphorylated (Phos) MBP-PI4Kβ1 against the total MBP-PI4Kβ1 protein loaded in the gel in µg. Protein amounts were estimated by densitometry on Coomassie-stained SDS-PAGE gels, using BSA as a known standard. Radioactive phosphorylated PI4Kβ1 was quantified in ImageQuant by densitometry using the calibration curve for radiolabeled [γ-^{32}P] ATP. Protein sizes were determined according to the PageRuler™ Prestained Protein Ladder. The expected molecular sizes for the proteins used were as follows, MBP- PI4Kβ1, 168 kDa; CA-$_{6x}$His-MPK4, 42 kDa; KD-$_{6x}$His-MPK4, 42 kDa; CA-$_{6x}$His-MPK6, 48 kDa; KD-$_{6x}$His-MPK6, 48 kDa; $_{6x}$His-SnRK2.6, 41 kDa; $_{6x}$His-CPK11, 55 kDa; KD-$_{6x}$His-CPK11, 55 kDa; MyBP, 18.5 kDa; Cas, 26 kDa; MBP, 42 kDa. MAPKs and SnRK2.6. The data represents the mean of four data points ± standard deviation.

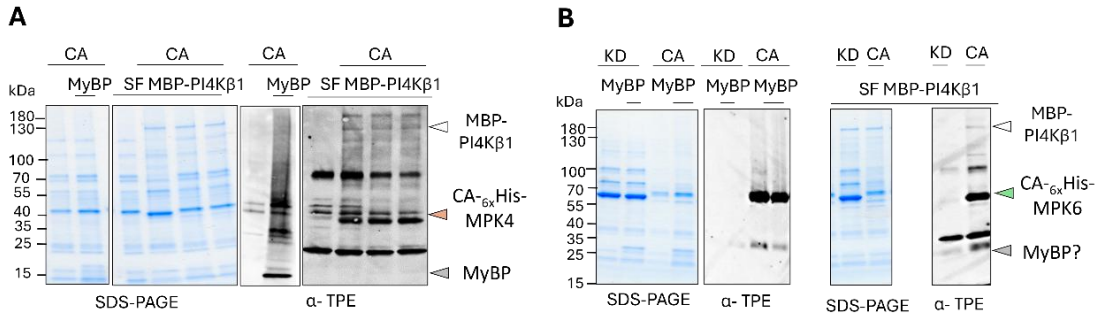

Figure 25. Phosphorylation of enriched recombinant MBP- PI4Kβ1 protein by CA-$_{6x}$His-MPK4 or CA-$_{6x}$His-MPK6 by an alternative, non-radioactive *in vitro* phosphorylation test using [γS-ATP]. The phosphorylation of expressed recombinant MBP-PI4Kβ1 protein (in soluble fraction (SF)), by CA-$_{6x}$His-MPK4 or CA-$_{6x}$His-MPK6 was tested by non-radioactive *in vitro* protein phosphorylation assays. Proteins were incubated in the presence of [γS-ATP] for labeling, extracted and separated by SDS-PAGE. Phosphorylated proteins were detected using a primary antibody against the thiophosphate ester (α-TPE) and a secondary antibody fused to horse-radish peroxidase (HRP). HRP activity was detected by enhanced chemiluminescence. **A**. Phosphorylation of MBP-PI4Kβ1 [0.2 µg] by CA-$_{6x}$His-MPK4 [1 µg], with Myelin Basic Protein (MyBP) as a control. White arrow head, MBP-PI4Kβ1; orange arrow head, MPK4; gray arrow heads, MyBP. **B.** Phosphorylation of MBP-PI4Kβ1 [0.2 µg] by CA-$_{6x}$His-MPK6 [0.9 µg], with the respective controls KD-$_{6x}$His-MPK6, MBP and MyBP. Green arrow head, MPK6; gray arrow head, MyBP.

2.8. Mass spectrometric phosphopeptide analysis suggests numerous phosphosites mainly in the PPC domain of MBP-PI4Kβ1 in addition to published phosphosites

In cooperation with the MLU core facilty proteomic mass spectrometry (Dr. Matthew Fuszard and Dr. Dirk Dobritzsch), mass spectrometry (MS) analysis was used to identify phosphorylated residues in enriched recombinant MBP-PI4Kβ1 protein upon incubation with either CA-$_{6x}$His-MPK4 or with CA-$_{6x}$His-MPK6. In the first step, *in vitro* phosphorylation assays were performed by incubating the recombinantly expressed and enriched MBP-PI4Kβ1 protein with either CA-$_{6x}$His-MPK4 or CA-$_{6x}$His-MPK6 in the presence of cold ATP, instead of radiolabeled ATP as described in Section 4.18.1. Upon incubation, proteins were then resolved by SDS-PAGE, stained with Coomassie-blue. The protein band corresponding to MBP-PI4Kβ1 was excised and digested by trypsin (see section 4.19). A representative SDS-PAGE gel used to excise the corresponding bands can be seen in Appendix Figure 43. The extracted peptides were analyzed by LC-MS-MS in cooperation with Dr. Dirk Dobritzsch and Dr. Matt Fuszard (MLU Core Facility Proteomic Mass Spectrometry). The overall peptide sequence coverage for MBP-PI4Kβ1 varied between 40-50% (Appendix Figure 44). The phosphopeptide sequences, putative target residues and the probabilities of post-translational modifications (PTM) can be seen in Appendix Table 14.

In total, 11 and 18 putative PI4Kβ1 phosphopeptides were found upon incubation with MPK4 or with MPK6 respectively. Interestingly, most of the phosphosites were located in the plant-specific PPC-domain, and only some phosphosites were differentially targeted by MPK4 and MPK6 (Figure 26). It is possible that the identification of candidate phosphosites mainly in the PPC is related to a possible role in the control of targeting at the PI4Kβ1 protein to membranes (Lou et al., 2006). As expected, MAPKs preferentially phosphorylated the MBP-PI4Kβ1 substrate in Ser/Thr-Pro target motifs (S/TP). However, other serines not directly followed by a proline were also identified as putative target sites, raising questions about the specificity of MAPK-mediated phosphorylation under the *in vitro* conditions used.

Additionally, a putative phosphosite S642 targeted by CA-$_{6x}$His-MPK6 was localized in the NH domain of MBP-PI4Kβ1. The NH domain is known to interact with RabA4b GTPase and selectively recruits PI4Kβ1 to tip-localized membranes in root hairs, possibly suggesting a role of this phosphosite in membrane recruitment to specific subcellular compartments (Preuss et al., 2006).

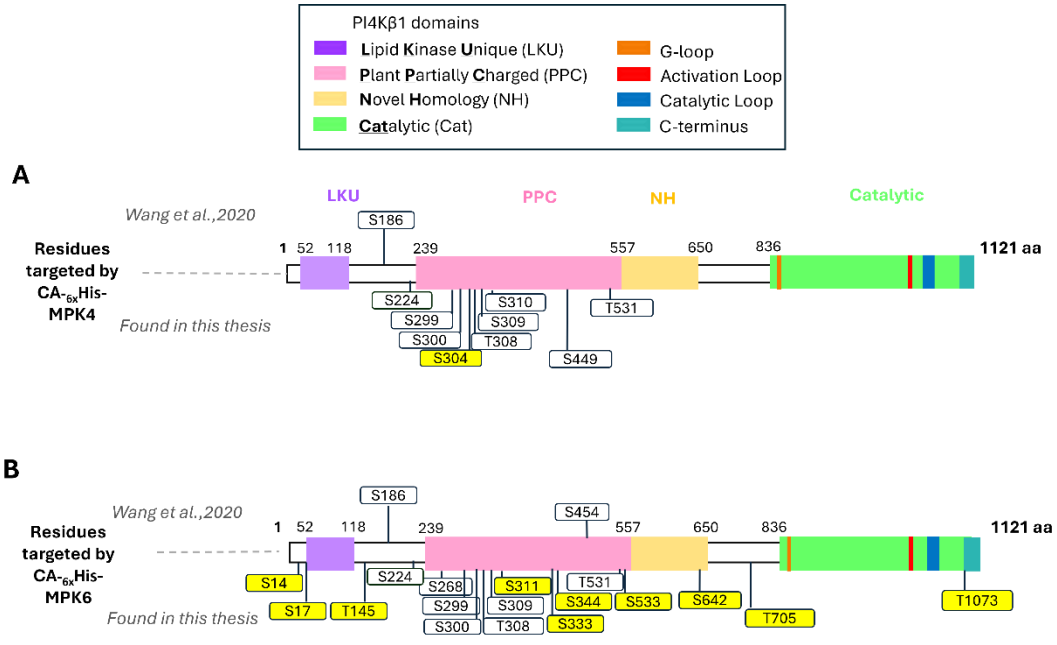

Figure 26 .Putative phosphosites identified by MS in MBP-PI4Kβ1 after *in vitro* phosphorylation by upstream MAPKs. Schematic representation of PI4Kβ1 domain structure, with domains and regions colored. **A.** Distribution of putative phosphosites identified in MBP-PI4Kβ1 targeted by CA-$_{6x}$His-MPK4. **B.** Distribution of putative phosphosites targeted in MBP-PI4Kβ1 by CA-$_{6x}$His-MPK6. Residues highlighted above show sites reported by previous phosphoproteomic analysis (Wang et al., 2020). Residues highlighted below indicate sites identified by our MS analysis. Colored yellow boxes indicate differential sites identified for each MAPK. The MS analysis was supported by Dr. Dirk Dobritzsch in the MLU Core Facility Proteomic Mass Spectrometry. The assay was repeated 3 times with reproducible results.

On the other hand, the putative phosphosites T705 and T1073 located near the catalytic domain and in the C-terminal region, respectively, might play a role in the regulation of catalytic activity of PI4Kβ1. Overall, while one could speculate about one or the other site, the MS analysis provided such a large number of candidate phosphosites that it appeared reasonable to assume a high false discovery rate. Therefore, to validate or narrow down list of putative phosphosites found by MS analysis, we next performed peptide microarray analyses.

2.9. Peptide microarrays analysis revealed new phosphosites on *Arabidopsis* PI4Kβ1

Peptide arrays allow the identification of phosphorylation sites on synthetic target protein substrates (Schutkowski et al., 2005). To identify phosphosites on PI4Kβ1 targeted by upstream MAPKs, peptide oligomers resembling the whole PI4Kβ1 sequence were synthesized and immobilized via flexible linkers on glass slides in the High-Density PepStar

microarray format by a commercial partner (JPT) (Figure 27 A). Peptide arrays were incubated with either CA-$_{6x}$His-MPK4 or with CA-$_{6x}$His-MPK6 in the presence of [γ-^{33}P]ATP, and after washing steps phosphorylated peptides were detected on the arrays by phosphorimaging .

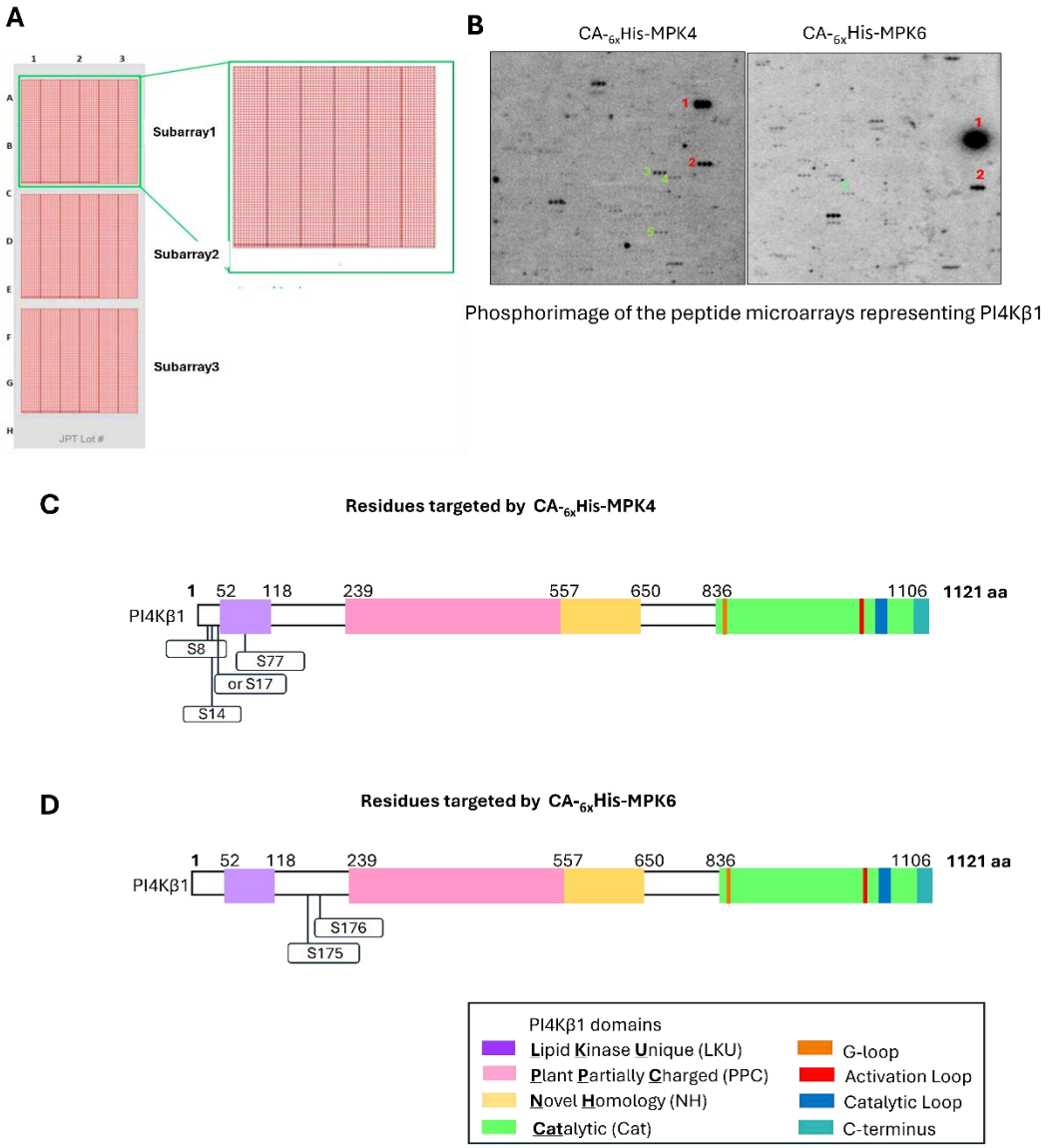

Figure 27. Peptide microarrays with immobilized peptides of PI4Kβ1 phosphorylated by upstream CA-$_{6x}$His-MPK4 or CA-$_{6x}$His-MPK6. Profiling of CA-$_{6x}$His-MPK4 and CA-$_{6x}$His-MPK6 by using peptide microarrays (JPT peptide technologies; Inc. Berlin, Germany) displaying synthetic peptides representing the PI4Kβ1 protein sequence (30 fmol/peptide). **A.** Design of microarrays consisting of a glass slide printed in 3 identical subarrays, each subarray is divided in 16 individual blocks and each spot on the microarray represents a single individual peptide. The array contains linear 13-15 mer peptides with a shift of 2-mer and an overlap of 11-mer. Peptides are chemoselectively linked via the N-terminus to the microarray surface. **B.** Representative peptide blot of PI4Kβ1 (residues 1-1121 aa) spotted in triplicates. The arrays were incubated with 5 µg of CA-$_{6x}$His-MPK4 or CA-$_{6x}$His-MPK6 and radiolabeled [γ-^{33}P] ATP and phosphorylated peptides were detected by phosphorimaging. Control peptides were included in the array (Red numbers 1,2). Exposure time 7days. Three peptides were phosphorylated by CA-$_{6x}$His-MPK4 (green numbers 3,4,5) and one peptide was phosphorylated by CA-$_{6x}$His-MPK6 (green number 3). **C.** Schematic

representation of the full-length PI4Kβ1, domains and regions colored accordingly. Phosphorylated sites targeted by CA-$_{6x}$His-MPK4 are depicted. **D.** Schematic representation of the full-length PI4Kβ1, domains and regions colored accordingly. Phosphorylated sites targeted by CA-$_{6x}$His-MPK6 are depicted. The assay was repeated two times.

The incubation resulted in peptide phosphorylation, but only 3 and 1 peptide sequences were found to be phosphorylated by CA-$_{6x}$His-MPK4 or with CA-$_{6x}$His-MPK6, respectively (Figure 27 B-E). The phosphopeptide sequences can be seen in Appendix Table 15.Despite the high purity levels (>80%) of the upstream kinases and the experimental verification of MAPK activity used for this assay, unfortunately few phosphorylated peptides were obtained and none of the sites found here could confirm the ones reported previously by others (Wang et al., 2020) nor by MS analysis (Hendricks et al., 1999; Preuss et al., 2006).

The few sequences found to be phosphorylated in both assays, indicate that the upstream kinases could not effectively phosphorylate the synthetic peptides representing PI4Kβ1, possibly due to the linear structure of the peptides displayed in the planar surface and the absence of a natively folded protein. It is possible that residues involved in phosphorylation at the target kinase only come together and are available upon protein folding, making it difficult for upstream kinases to phosphorylate peptide substrates. Additionally, it is known that phosphorylation motifs in the substrate, possibly absent here, are relevant for MAPKs to guide kinase-substrate recognition (Chen et al., 2011).

The data so far left us with a large number of candidate phosphosites to study, posing the problem of how to prioritize further experiments. To better understand the effect of the phosphorylation on the PI4Kβ1 function, we selected phosphorylation sites in PI4Kβ1 containing the classical motif for MAPKs phosphorylation, the S/T-P motif. Due to the availability of published phosphorylation sites reported for PI4Kβ1 by upstream MPK6 in a previous and non-targeted *Arabidopsis* phosphoproteomic analysis (Wang et al., 2020), we prioritized the sites S186 and S454 (both followed by a proline) as potential target sites and performed site-directed mutagenesis to elucidate their effects on PI4Kβ1 function.

2.10. MBP-PI4Kβ1 S186 S454 substitution variants display reduced phosphorylation by CA-$_{6x}$His-MPK4 or CA-$_{6x}$His-MPK6

The data so far suggested that MBP-PI4Kβ1 is a target for phosphorylation by CA-$_{6x}$His-MPK4 or CA-$_{6x}$His-MPK6 at different target sites, which remained still undefined. To validate whether the positions S186 and S454 in PI4Kβ1 are relevant target sites for phosphorylation by upstream MAPKs, site directed-mutagenesis was performed to substitute these serines to either alanines (aiming to generate a non-polar phospho-ablation variant), or to aspartic acid (aiming to generate a negatively charged phospho-mimetic variant). In either case (A or D variants), the substituted residues can no longer serve as targets for phosphorylation by a protein kinase.

In vitro protein phosphorylation assays were performed using MBP-PI4Kβ1 or the substituted variants MBP-PI4Kβ1 S186A/D; MBP-PI4Kβ1 S454A/D; or the double substituted variants MBP-PI4Kβ1 S186A S454A or MBP-PI4Kβ1 S186D S454D as substrates. Equal concentrations of single and double MBP-AtPI4Kβ1 [0.2 µg] substitution variants were incubated with constant concentrations of either CA-$_{6X}$HIS-MPK4 [1.7 µg] or CA-$_{6X}$HIS-MPK6 [1.7 µg] and radiolabeled [γ-^{32}P]ATP (See section 4.18.1), proteins were separated by SDS-PAGE, and phosphorylated proteins were detected by phosphorimaging. The results indicate a clearly reduced degree of phosphorylation in all single and – more prominently – also in the double MBP-PI4Kβ1 substitution variants upon incubation with CA-$_{6X}$HIS-MPK4. The MBP-PI4Kβ1 S186A-S454A or MBP-PI4Kβ1 S186D-S454D variants displayed a significant reduction in phosphorylation of 57 % and 60% respectively, compared to the degree of phosphorylation observed in the parental MBP-PI4Kβ1 protein (Figure 28 A, C). Similarly, phosphorylation also decreased in single and double PI4Kβ1 substitution variants upon incubation with CA-$_{6X}$HIS-MPK6. In these experiments, the S454A, S186D, S186A-S454A and S186D-S454D substitution variants displayed a significant reduction in phosphorylation of 55 %, 70%, 71% and 86 %, respectively, compared to the degree of phosphorylation observed in the parental MBP-PI4Kβ1 protein (Figure 28 B, C). This *in vitro* data confirm that serines in the positions 186 and 454 are important phosphosites targeted by both upstream MAPKs and together can account for more than 80% of the total phosphorylation mediated by the upstream kinases. However, a remaining 20-40% of phosphorylation was still observed even in the MBP-PI4Kβ1 double substitution variants, suggesting that there are further relevant phosphosites, possibly among the canditates identified in our MS or peptide array experiments. Alternatively, it is possible that in the absence of certain target sites in the double substitution variants

the upstream protein kinases may randomly carry out off-target phosphorylations, as has previously been observed for MPK6 (Hempel et al., 2017).

Based on the results so far, the residues S186 and S454 appeared as relevant phosphorylation sites targeted by MPK4 and MPK6, accounting for >80% of phosphorylation mediated by these protein kinases in the PI4Kβ1. Therefore, S186 and S454 appeared as ideal sites for the characterization of effects of MPK4-mediated or MPK6-mediated phosphorylation on the function of the PI4Kβ1 enzyme. To evaluate this, it was next tested whether phosphorylation by MAPKs influenced the catalytic activity and/or kinetic behavior of enriched recombinant MBP-PI4Kβ1 protein.

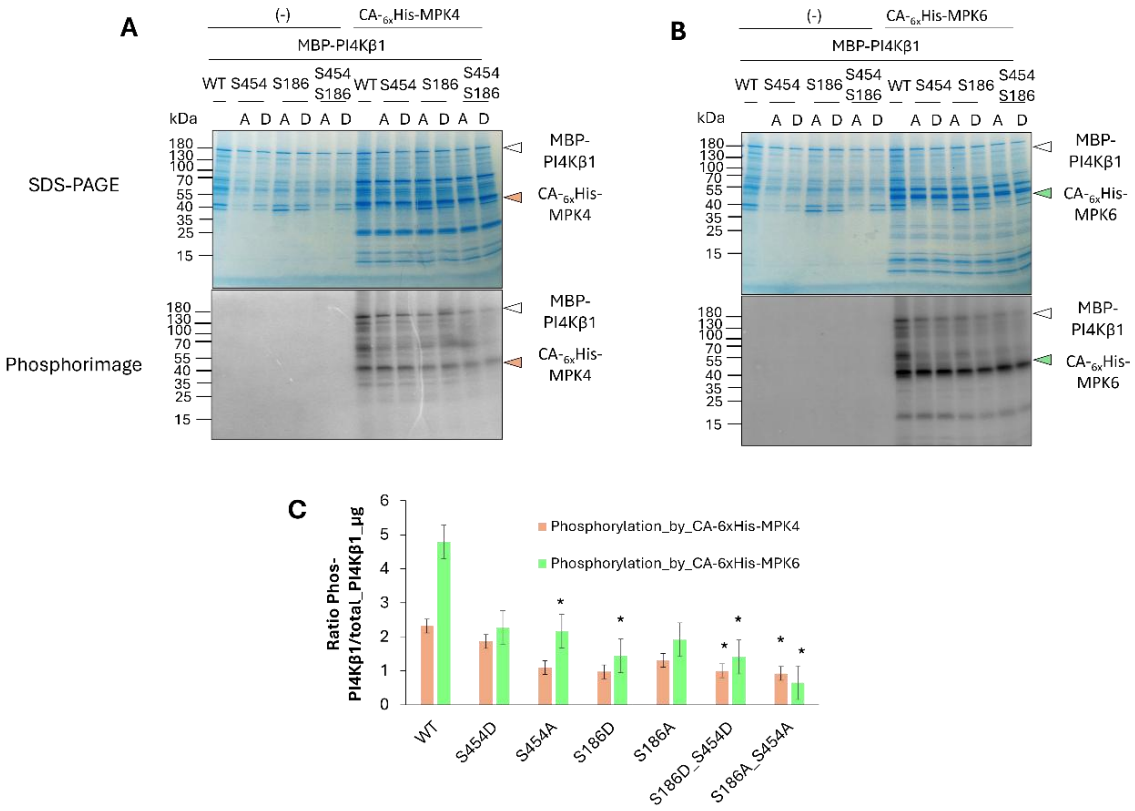

Figure 28. *In vitro* phosphorylation of single and double PI4Kβ1 substitution variants by CA-6xHis-MPK4 or CA-6xHis-MPK6. *In vitro* protein phosphorylation assays were performed by incubating MBP-PI4Kβ1 substitution variants with each MAPK in the presence of γ[^{32}P]ATP. The phosphorylation reactions were stopped after 15 min, proteins were separated by SDS-PAGE and phosphorylated proteins in dried gels were visualized by phosphorimaging. **A.** Phosphorylation of MBP-PI4Kβ1 substitution variants by CA-$_{6x}$His-MPK4. White arrow head, MBP-PI4Kβ1; orange arrow head, MPK4. **B.** Phosphorylation of MBP-PI4Kβ1 substitution variants by CA-$_{6x}$His-MPK6. **C.** Ratios of phosphorylated (Phos) MBP-PI4Kβ1 signal against the total µg MBP-PI4Kβ1 in the assay. Protein quantification was performed in ImageQuant by densitometry using BSA as a known standard. Radioactive phosphorylated PI4Kβ1 was quantified in ImageQuant by densitometry using the calibration curve for radiolabeled γ[^{32}P] ATP. Protein sizes were determined according to the PageRuler™ Prestained Protein Ladder. The expected molecular sizes were MBP-PI4Kβ1 substitution variants, 168 kDa; CA-$_{6x}$His-MPK4, 42 kDa; CA-$_{6x}$His-MPK6, 48 kDa.

The experiment was performed three times with similar results. The data represents the mean of three data points ± standard error (*) Asterisk indicates significant differences according to ANOVA ($P \leq 0.05$) compared to the WT.

2.11. Regulation of PI4Kβ1 function by MAPK-mediated phosphorylation

To assess whether MAPK-mediated phosphorylation influenced the catalytic activity of MBP-PI4Kβ1 *in vitro* experiments were performed in which enriched recombinant MBP-PI4Kβ1 protein was pre-incubated for 15 min with CA-$_{6x}$His-MPK4 or with CA-$_{6x}$His-MPK6, and then the lipid kinase activity of MBP-PI4Kβ1 was assessed against its substrate, PtdIns. To test whether the pre-incubation with the MAPKs would grossly alter the reactive behavior of MBP-PI4Kβ1, it was first confirmed that a lipid kinase reaction time of 15 min would still yield substrate conversion in the linear phase of the reaction (Appendix Figure 45).

The time-course activity of MBP-WT-PI4Kβ1 pre-phosphorylated by upstream CA-$_{6x}$His-MPK4 and CA-$_{6x}$His-MPK6 exhibited a linear increase from 0-40 min and a constant activity until the end of the reaction. Therefore, 15 min pre-phosphorylation of the target kinase by the corresponding MAPK and 15 min as the reaction time for the *in vitro* lipid kinase assays were chosen to evaluate the effect of phosphorylation on kinase activity.

To investigate the effects of the pre-phosphorylation in more detail, enriched recombinant MBP-PI4Kβ1 or the MBP-PI4Kβ1 variants carrying S/A or S/D substitutions in positions S186 and/or S454 were pre-incubated together for 15 min with cold ATP (See section 4.21.1), to allow phosphorylation by the upstream CA-$_{6x}$His-MAPKs in the presence of cold ATP. Subsequently, the lipid substrate PtdIns and [γ-^{32}P]ATP were added to the reaction and the lipid kinase reaction was allowed to proceed for 15 min. Reactions were stopped, lipids were extracted, resolved by TLC, and the catalytic activity of MBP-PI4Kβ1 the substitution variants was determined by phosphorimaging. For all kinase reactions the same buffer conditions were used. For comparison purposes equal protein concentrations were used and carefully estimated by densitometry on SDS-PAGE gels (data not shown), using BSA as a standard. Control samples were mock-treated, not including the MAPKs in the reaction.

The catalytic activity of MBP-PI4Kβ1 was significantly reduced by approx. 19 % or 37 % upon pre-phosphorylation by CA-$_{6x}$His-MPK4 or CA-$_{6x}$His-MPK6, respectively (Figure 29 A). This finding is in line with the stronger degree of phosphorylation observed upon incubation of MBP-PI4Kβ1 with CA-$_{6x}$His-MPK6 than with CA-$_{6x}$His-MPK4 (Figure 28).

Secondly, we assessed the effects of the two key residues serine 186 and serine 454 in controlling MBP-PI4Kβ1 activity. Under the conditions used, MBP-PI4Kβ1 S186D and MBP-PI4Kβ1 S186A displayed a differential effect on activity, with S186D exhibiting a light increase of 6 % and S186A a significant decline by 57 % of the activity determined for wild type MBP-PI4Kβ1. By contrast, other single or double substitutions in MBP-PI4Kβ1 S454D, MBP-PI4Kβ1 S454A, MBP-PI4Kβ1 S186D S454D, or MBP-PI4Kβ1 S186A S454A all showed significantly decreased catalytic activity (Figure 29 B).

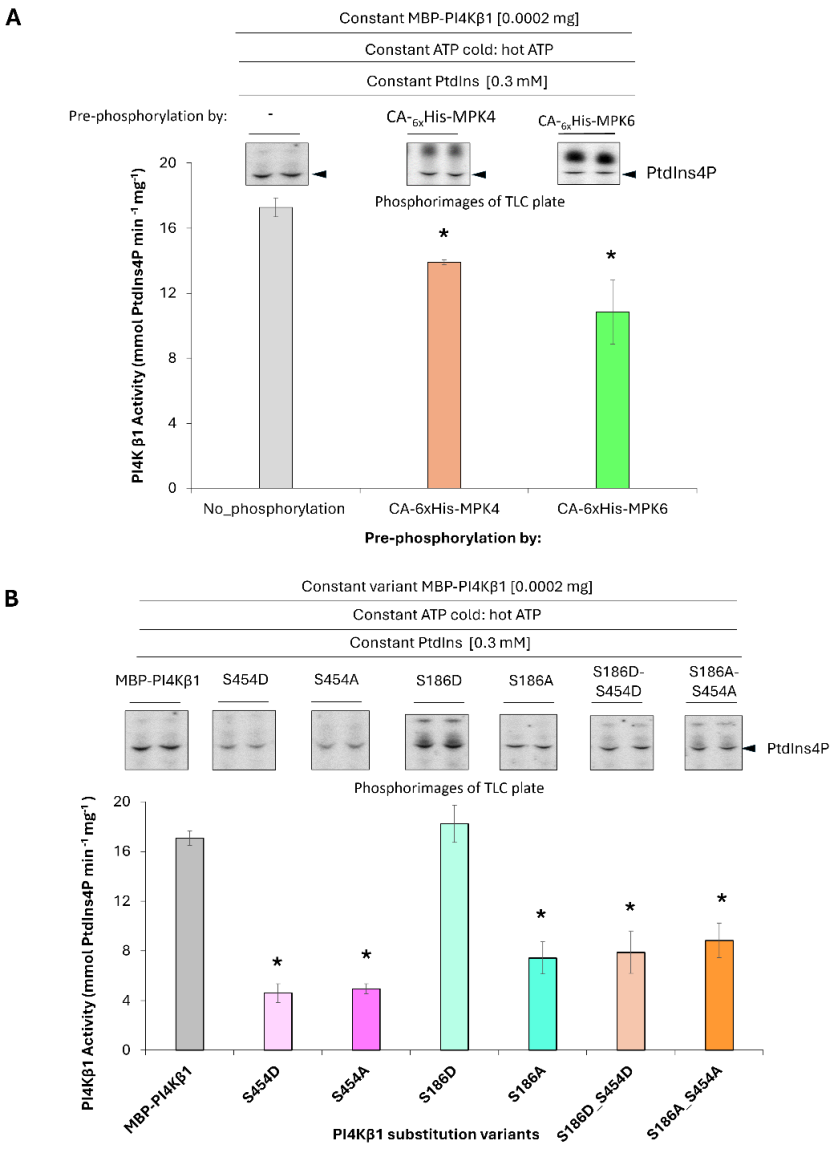

Figure 29. Catalytic activity of MBP-PI4Kβ1 upon MAPK-mediated phosphorylation or in MBP-PI4Kβ1 substitution variants. The lipid kinase activity of recombinant MBP-PI4Kβ1 against PtdIns was assessed upon pre-incubation with MAPKs, or in MBP-PI4Kβ1 substitution variants carrying A or D substitutions in residues S186 or S454 previously found to represent relevant MAPK-phosphorylation target sites. The products of the lipid kinase reaction are indicated by a black arrow head (PtdIns4P). **A.** Effect of CA-$_{6x}$His-MPK4 (orange bars) or CA-$_{6x}$His-MPK6 (green bars) phosphorylation on MBP-PI4Kβ1 activity. **B.** Effect of single and double amino acid substitutions on MBP-PI4Kβ1 activity. Equal protein concentrations were used, according to SDS-PAGE-analysis with BSA as a reference

(not shown). The data represents the mean of six data points ± standard deviation. (*) Asterisk indicates significant differences with the control group according to ANOVA ($P \leq 0.05$). The experiment was performed three times with similar results.

Based on these findings, it appears that reversible phosphorylation of PI4Kβ1 by MAPKs might be a part of controlling the activation or inactivation of PI4Kβ1 activity, possibly contributing to controlling the abundance of PtdIns4P in relevant membrane compartments. The residue S454 is located in the PPC domain, which mediates lipid/membrane binding (Lou et al., 2006), and consequently a phosphorylation of this residue might interfere or promote lipid binding features of the PPC domain.

The MBP-PI4Kβ1 substitution S186D may mimick a phosphorylated form of MBP-PI4Kβ1 and compared to MBP-PI4Kβ1 S186 might represent a more active state of the MBP-PI4Kβ1, as indicated by the higher catalytic activity of MBP-PI4Kβ1 S186D compared to MBP-PI4Kβ1 S186A (Figure 29 B). The introduction of aspartic acid to mimic the negative charge of the phosphate group possibly induces a conformational change, facilitating the binding to the substrate PtdIns and leading to an increase in activity.

While the analysis of effects of pre-phosphorylation of MBP-PI4Kβ1 and the analysis of the MBP-PI4Kβ1 substitution variants revealed a possible effect on catalytic function of the MBP-PI4Kβ1 protein, the design of the assays shown in Figure 29 allows no conclusions about the kinetic behavior of the protein. Therefore, a more detailed study of MBP-PI4Kβ1 kinetics was performed, using the MBP-PI4Kβ1 substitution variants.

2.12. Kinetic characterization of MBP-PI4Kβ1 substitution variants

Kinetic characterization of the different phospho-mimetic and phospho-ablation variants of MBP-PI4Kβ1 can provide insights into the allosteric regulation of the enzyme. As was recently reported by (Lin et al., 2019), PI4Kβ1 displays functional interplay with MPK4 to mediate phragmoplast organization during cytokinesis of *Arabidopsis* root cells (Lin et al., 2019). In the same study, it is also shown that recombinant MBP-PI4Kβ1 protein can be phosphorylated *in vitro* by recombinant MPK4 (Lin et al., 2019). However, so far the targeted residues and their effects on catalysis remained unclear. Therefore, we explored the roles of MBP-PI4Kβ1 S186 and MBP-PI4Kβ1 S454 on enzyme kinetics as previously for MBP-PI4Kβ1 (see Figure 17 and Figure 22).

MBP-PI4Kβ1 and its substitution variants MBP-PI4Kβ1 S186A or S186D, MBP-PI4Kβ1 S454A or D, or the double substitution variants MBP-PI4Kβ1 S186A S454A or S186D S454D were analyzed for catalytic activity under identical and non-limiting reaction conditions in the presence of increasing concentrations of the substrate lipid, PtdIns (Figure 30). Equal concentrations of MBP-PI4Kβ1 and substitution variants used for each reaction point were confirmed by SDS-PAGE analysis (see Appendix 38). The results show that all MBP-PI4Kβ1 substitution variants displayed sigmoid reaction kinetics and, thus, were all allosterically regulated after binding to the lipid PtdIns, as already seen for the MBP-PI4Kβ1 protein (see Figure 17 and Figure 22). This validates the sigmoidal response observed for MBP-PI4Kβ1, confirming that allosteric regulation modulates catalysis by MBP-PI4Kβ1.

Interestingly, the MBP-PI4Kβ1 substitutions in position S186D and 186A, exhibited a differential kinetic response. The kinetic analysis reveals that MBP-PI4Kβ1 S186D exhibited an activation, which was even more pronounced than observed in the previous activity assays (see Figure 29 B), suggesting that the introduction of a negative charge in position 186 results in an increased reaction rate of the enzyme (Figure 30 A). This activation was evident after calculating its kinetic constants, exhibiting a substantial higher affinity towards its substrate ($K_{0.5}$= 0.37 mM) compared to the parental MBP-PI4Kβ1 enzyme ($K_{0.5}$= 0.67). By contrast, MBP-PI4Kβ1 S186A displayed a reduced catalytic rate, indicating that this substitution impeded catalysis. The inactivation of MBP-PI4Kβ1 S186A was accompanied by an unchanged affinity for PtdIns substrate compared to the parental MBP-PI4Kβ1 enzyme (both at $K_{0.5}$= 0.67) (Figure 30 B and Table 2). The data indicate that phosphorylation of PI4Kβ1 in position S186 might control substrate affinity and results in increased production of PtdIns4P. This *in vitro* pattern might corroborate previous findings by (Lin et al., 2019), where an *in vivo* activation of mCherry-PI4Kβ1 by MPK4-YFP was suggested in cytokinetic roots PtdIns4P where MPK4-YFP fluorescence was observed at the cell plate earlier than a reported for PtdIns4P, suggesting that formation of PtdIns4P might have been stimulated by MPK4 (Lin et al., 2019).

By contrast, the substitution variants MBP-PI4Kβ1 S454D and S454A both demonstrated similar kinetic behaviour compared to MBP-PI4Kβ1 ($K_{0.5}$= 0.52 mM, $K_{0.5}$= 0.55 mM, $K_{0.5}$= 0.67 mM, respectively) (see Table 2), without a significant difference between the two substitution variants (Figure 30). However, the double substitution variants again displayed a differential effect that was similar to that of the MBP-PI4Kβ1 S186A vs. MBP-PI4Kβ1 S186D variants, observed by a higher reaction rate in the phospho-mimic variant and lower in the phospho-ablation variant for position S186 compared to MBP-PI4Kβ1, suggesting that the substitution by aspartic acid in position S186 might mimic a

phosphorylated form of PI4Kβ1. The substitutions MBP-PI4Kβ1 S186D S454D or MBP-PI4Kβ1 S186A S454A, revealed also similar substrate affinities as the parental MBP-PI4Kβ1 protein ($K_{0.5}$= 0.61 mM, $K_{0.5}$= 0.61 mM, $K_{0.5}$= 0.67 mM, respectively) (Figure 30 A-B and Table 2).

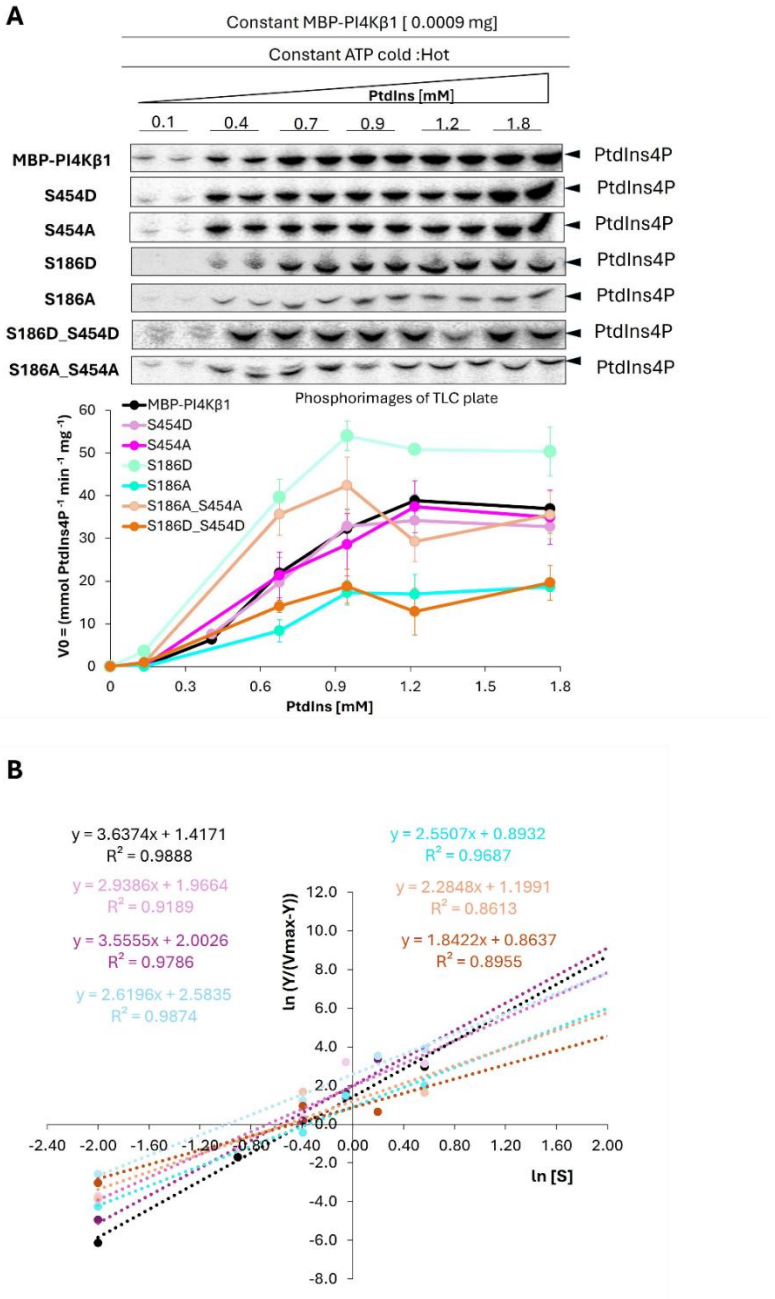

Figure 30. Kinetic characterization of phosphomimicry and phosphoablation MBP-PI4Kβ1 variants against PtdIns. **A.** Sigmoidal reaction kinetics was obtained for all recombinantly expressed and enriched MBP-PI4Kβ1 substitution variants by plotting the initial velocity as a function of increasing PtdIns concentrations. Black arrow shows the product of the reaction (PtdIns4P) resolved by TLC plate and the radioactive lipid was detected by phosphorimaging using a phosphoimager. Radioactive phosphorylated PtdIns was quantified in Image Quant by densitometry using the calibration curve for radiolabeled [γ-^{32}P] ATP. The data represents the mean of four data points ± standard error. **B.** Linearized Hill plot for the substitution variants of MBP-PI4Kβ1 at increasing PtdIns substrate concentrations.

Kinetic characterization of the different phospho-mimetic and phospho-ablation PI4Kβ1 variants was also assessed by using increasing concentrations of the substrate ATP, while keeping protein amounts and PtdIns substrate concentrations constant. As for the parental MBP-PI4Kβ1 protein, non-sigmoidal reaction kinetics were observed in all cases, following a hyperbolic behavior similar to Michaelis-Menten (Figure 31).

Table 2. Kinetic constants of MBP- PI4Kβ1 substitution variants estimated from Hill plot.

Protein variant	η_H	$K_{0.5}$
MBP-PI4Kβ1	3.63	0.67 mM
MBP-PI4Kβ1-S454D	2.93	0.52 mM
MBP-PI4Kβ1-S454A	3.55	0.55 mM
MBP-PI4Kβ1-S186D	2.61	0.37 mM
MBP-PI4Kβ1-S186A	2.55	0.67 mM
MBP-PI4Kβ1-S186D-S454D	2.28	0.61 mM
MBP-PI4Kβ1-S186A-S454A	1.84	0.61 mM

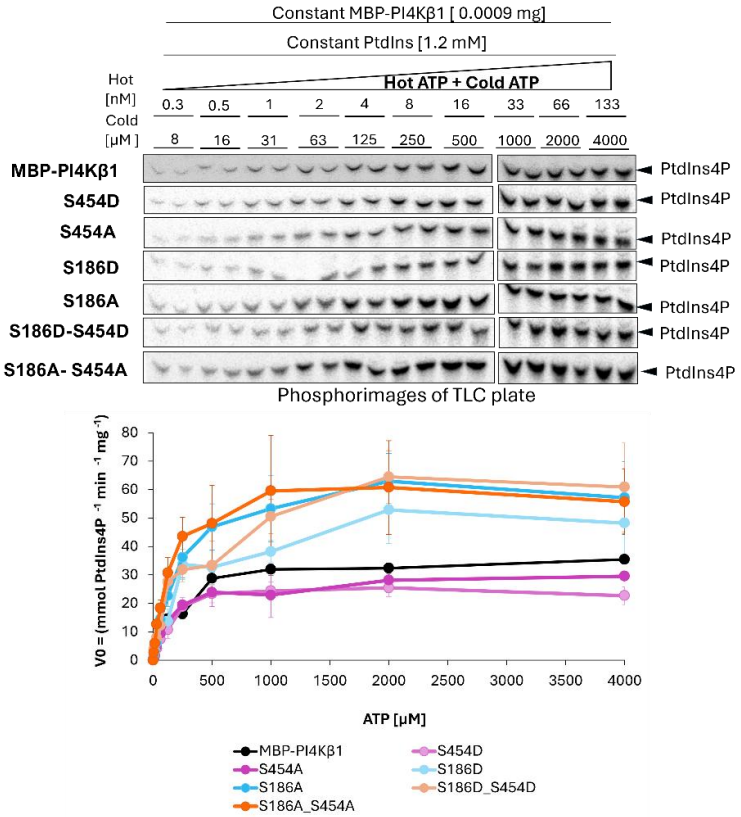

Figure 31. Kinetic characterization of phosphomimicry and phosphoablation PI4Kβ1 variants against ATP. Hyperbolic reaction kinetics was obtained for all recombinantly expressed and enriched MBP-PI4Kβ1 substitution variants by plotting the initial velocity as a function of increasing ATP concentrations. Black arrow shows the product of the reaction (PtdIns4P) resolved by TLC and the radioactive lipid was detected by phosphorimaging. Radioactive

PtdIns4P was quantified in Image Quant by densitometry using the calibration curve for radiolabeled [γ- ^{32}P] ATP. The data represents the mean of four data points ± standard error.

It should be noted that these experiments were performed with protein elution fractions that were not as pure as those for the kinetic assays against increasing concentrations of PtdIns substrate shown above.

Based on the *in vitro* kinetic characterization of all recombinantly expressed MBP-PI4Kβ1 substitution variants, it appears that different residues targeted by upstream MAPKs plays a differential role in the regulation of PI4Kβ1 activity to modulate the production of PtdIns4P. To further investigate the contribution of PI4Kβ1 position S454, which is located in the PPC-domain of PI4Kβ1 and this domain is believed to target the protein to the membrane (Lou et al., 2006), we asked if the phosphor-mimetic S454D or the phosphor-ablation S454A variants showed a reduced capability to bind lipids.

2.13. Recombinant MBP-PI4Kβ1 binds PIs

To better understand how PIs might regulate AtPI4Kβ1 functionality, the direct binding of recombinant MBP-PI4Kβ1 to PIs was investigated by *in vitro* lipid overlay assays. To analyze protein-lipid interactions, equal concentrations of recombinantly expressed and enriched *Arabidopsis* MBP-PI4Kβ1 and substitution variants were incubated with membranes spotted with different phospholipids (Figure 32 A-B).

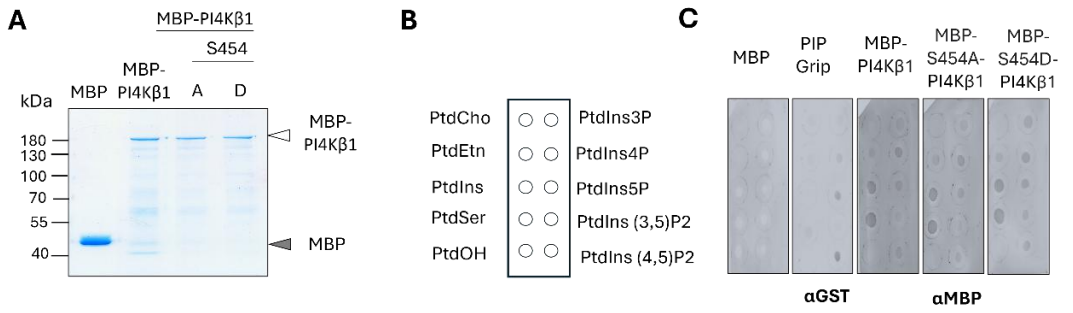

Figure 32. Lipid interaction studies of PI4Kβ1 with PIs. The lipid binding of purified recombinant MBP-WT-PI4Kβ1, MBP-S454A-PI4Kβ1 and MBP-S454D-PI4Kβ1 was assessed by lipid overlay assays. **A**. SDS-PAGE gel showing equal protein concentrations used for lipid-binding analysis. The evaluated samples included a negative control (MBP), a positive control (PIP Grip), MBP-PI4Kβ1 and substitution variants. MBP-PI4Kβ1 (white arrow), Maltose Binding Protein (MBP) (grey arrow). **B**. Schematic representation of self-casted lipid blots. First, several PIs present in plants (PtdIns3P, PtdIns4P, PtdIns5P, PtdIns(3,5)P_2, PtdIns(4,5)P_2 were spotted, followed by further phospholipids Phosphatidylcholine (PtdCho), Phosphatidylethanolamine (PtdEth), phosphatidylinositol (PtdIns), phosphatidylserine (PtdSer) and Phosphatidic acid (PtdOH) **C.** Lipid overlay assays with enriched MBP, PIP Grip, MBP-PI4Kβ1 MBP-S454A-PI4Kβ1 and MBP-S454D-PI4Kβ1 protein fractions. Interactions were visualized by using a primary antibody against MBP (or GST for positive control) and a secondary antibody against IgG with an AP conjugate for colorimetric detection. The experiment was repeated twice with similar results.

The *in vitro* data show that all recombinant proteins displayed binding to anionic phopsholipids, including PtdIns3P, PtdIns4P, PtdIns5P, PtdSer or PtdOH. A commercial positive "PIP-Grip" control intended to bind PtdIns(4,5)P_2 displayed the expected binding in addition to (weaker) binding to PtdIns4P and PtdIns5P. MBP used as a negative control did not display any lipid binding capabilities. No differences in lipid binding were observed between MBP-PI4Kβ1 and its substitution variants, MBP-PI4Kβ1 S454A or MBP-PI4Kβ1 S454D (Figure 32 C). Lipid binding tests using commercially available PIP strips additionally validated the binding to PtdIns monophosphates (Appendix Figure 46). The data on *Arabidopsis* MBP-PI4Kβ1 and its variants is partially consistent with information previously reported by (Lou et al., 2006), where the PPC-domain of a PI4Kβ derived from rice selectively bound PtdIns4P, PtdIns and PtdOH but not PtdCho, PtdIns5P or PtdIns(4,5)P_2. In the context of our characterization of possible effects of protein phosphorylation in PI4Kβ1-position S454, the results do not provide evidence for a role of S454 in lipid binding or in targeting the kinase to certain subcellular membrane compartments. The regulatory effects of specific phosphosites in PI4Kβ1 related to lipid binding, thus, appear to be more complex and will require further tests.

3. Discussion

Phosphatidylinositol 4-kinase β1 (PI4Kβ1) is a key enzyme of plant phosphoinositide biosynthesis at endosomal membranes, where it mediates the ATP-dependent conversion of PtdIns to PtdIns4P. Here, so far unexplored biochemical features of purified recombinant MBP-PI4Kβ1 protein produced in *E. coli* BL21 (DE3) were addressed.

3.1. Kinetic analysis of MBP-PI4Kβ1 suggests positive allosteric cooperativity upon product binding.

Most previous kinetic studies for phosphoinositide kinases have been reported for enzymes of human origin (Beeton et al., 2000; Chung & Fleming, 1995; Kunz et al., 2000; Maheshwari et al., 2017b; Zhao et al., 2000) and some for enzymes from yeast (Nickels et al., 1992). In comparison to the corresponding plant enzymes, as far as they exist, these other enzymes are functionally divergent and catalyze reactions that are in part not known for plants, e.g. the D-4-phosphorylation of PtdIns3P or the D5-phosphorylation of PtdIns(4,5)P_2. To our knowledge, only one other study investigated the kinetic properties of plant phosphoinositide kinases, namely of the PI4P 5-kinases, PIP5K1 and PIP5K10 from *Arabidopsis* (Perera et al., 2005). In that study, either kinase was expressed as a fusion to a glutathione S-transferase (GST) tag and expressed in *Spodoptera frugiperda* (Sf9) insect cells or in *E. coli* to perform kinetic analysis using the purified enzyme. The data showed that PIP5K10 had a similar K_m but an approx. 10-fold lower V_{max} than PIP5K1. The results also revealed that both *Arabidopsis* enzymes displayed 200-fold or 20-fold, respectively, lower K_m / V_{max} compared to the human PI4P 5-kinase, PIP5K1α, possibly explaining the relatively low abundance of PtdIns (4,5)P_2 in plants (Perera et al., 2005). The data shown by (Perera et al., 2005) illustrate that enzymes of PI metabolism can differ massively in their biochemical properties, including substrate affinities or the maximal catalytic rates of substrate conversion.

The kinetic properties of PI4Kβ1 have not been elucidated to date, largely due to the fact that PI4Kβ1 is a membrane-associated protein, imposing difficulties during expression and purification. Therefore, to overcome some of the solubility issues encountered with smaller fusion-tags, in this study PI4Kβ1 was fused to MBP, a well-known solubility tag. The MBP-PI4Kβ1 fusion protein obtained from *E. coli* expression was catalytically active

and displayed interesting biochemical features. Kinetic analysis revealed sigmoid reaction kinetics suggestive of a positive cooperativity upon allosteric binding of a ligand. As the enzyme assay contained only three likely ligands, PtdIns substrate, ATP co-substrate, and PtdIns4P product, it can be assumed that the cooperative effect in the reaction kinetics was exerted by the binding by one or more of these partners. Kinetic analysis against increasing concentrations of ATP did not show any sigmoid kinetics, ruling out an effect of ATP. As it was previously reported that PI4Kβ1 can allosterically bind PtdIns-monophosphates, including PtdIns4P, through its PPC domain, a likely explanation for the sigmoidal kinetics is a cooperative effect of product binding. Results presented in this thesis demonstrate this positive cooperativity, suggesting that the binding of the product at allosteric sites that are physically distinct from the PtdIns-binding active site, may elicit a conformational change in the PI4Kβ1 protein, increasing the affinity of the enzyme towards the substrate in the active site and (Somvanshi & Venkatesh, 2013). The hill coefficient of 3.6 obtained for the MBP-PI4Kβ1 protein indicates that the protein contains 3 or more binding sites for the allosteric effector, likely for PtdIns4P, that act together to promote catalysis.

The classical works of Hill on the human hemoglobin binding to O_2, revealed a Hill coefficient of 2.8 - 3.4 depending on the conditions of measurement (Hill, 1913; Holt & Ackers, 2009). In 1975, glucokinases obtained from liver of mammals and amphibians also exhibited sigmoidal kinetics in the presence of glucose, with a hill coefficient of 1.5 and a $K_{0.5}$ of 1.5 - 8.5 mM. The sigmoidal behavior of glucokinase is believed to be an adaptative process to increase the efficiency of the liver uptake of glucose at the variable concentrations in the blood, that may result from variations in the diet (Niemeyer et al., 1975).

As sigmoidal kinetics have not previously been reported for other phosphoinositide kinases, there is currently no reference enzyme for direct comparison. We hypothesize that the allosteric regulation occurs through the binding of PtdIns4P to the regulatory PPC domain of PI4Kβ1, which was originally reported by (Lou et al., 2006). This notion is consistent with other published data (Stevenson-Paulik et al., 2003) who observed an increase in the specific activity of recombinant PI4Kβ1 protein upon exogenous addition of PtdIns4P, suggesting an activation of the enzyme upon binding to the product. These published results are consistent with the cooperative kinetics observed here. The observed sigmoidicity could be explained because at lower substrate concentrations the initial velocity is slow due to the lack of product in the reaction, but as the reaction

progresses, more PtdIns4P is formed which will then activate the enzyme, leading to a sudden increase in the initial velocity.

The affinity of the enzyme towards its substrate is measured by estimation of the $K_{m,}$ termed in the Hill equation as $K_{0.5.}$ Based on the experimental data in this thesis, a $K_{0.5.}$ of 0.6 mM was determined for MBP-PI4Kβ1, indicating that the enzyme require a rather large amount of PtdIns substrate before it reaches its maximal velocity (V_{max}= 39 mmol PtdIns4P $min^{-1}mg^{-1}$). While there have been no kinetic data on *Arabidopsis* PI 4-kinases so far, data reported for PIP5K1 from *Arabidopsis* showed a higher affinity towards its substrate PtdIns4P ($K_m = 69\ \mu M$) and a lower V_{max} 600 pmol PIP_2 min^{-1} mg^{-1} (Perera et al., 2005) compared to values determined here for MBP-PI4Kβ1 from *Arabidopsis*. By comparison, a human type II PI 4-kinase that has been shown to account for up to 95% of the total PI 4-kinase activity in cells exhibited a $K_{m,}$ value for PtdIns of 167 µM, suggesting a substantially higher affinity (Chung & Fleming, 1995) than was determined here for MBP-PI4Kβ1 (Figure 18). Another type II PI 4-kinase from yeast also revealed a higher $K_{m,}$ value of 0.013 mol fraction for PtdIns and also a lower $V_{max} = 2.2$ µmol PtdIns4P min^{-1} mg^{-1} (Nickels et al., 1992) compared to MBP-PI4Kβ1. It is important to note that a discontinuous method "end point" analysis was used here to estimate the kinetic parameters, which is less precise than a continuous method where the product is measured without set intervals over time. However, even the discontinuous method allowed us to get a first insight of the approximate kinetic parameters for the PI4Kβ1 to better understand its regulation *in vitro.*

The high maximum velocity observed for MBP-PI4Kβ1 (Figure 17) might explain why the PtdIns4P is the most abundant phosphoinositide, making up approximately 80% of the plant global PI pool (Munnik & Nielsen, 2011; Vermeer et al., 2009b). In *Arabidopsis* root hairs, PtdIns4P accumulates massively at the plasma membrane and PI4Kα1 has been suggested to produce this PtdIns4P pool (Noack et al., 2022; Simon et al., 2016). By contrast, PtdIns4P is less abundant at the TGN/EE of vegetative cells, and due to its TGN/EE-localization PI4Kβ1 is believed to synthesize this pool (Noack et al., 2022; Preuss et al., 2006). The reported global PtdIns4P concentrations for *Arabidopsis* plasma membrane roots and *Oryza sativa* shoots (≈ 2 nM mg^{-1} PM protein (Yang et al., 2021) and ≈ 80 nmol min^{-1} $DW^{-1,}$ respectively, (Li et al., 2017)), are lower than might be required for the catalytic velocities obtained here (V_{max}= 39 mmol PtdIns4P $min^{-1}mg^{-1}$ for MBP-PI4Kβ1). However, it is important to note that within the plasma membrane, PtdIns4P and PtdIns(4,5)P_2 can distribute asymmetrically and form highly enriched membrane nanodomains with diameters smaller than 1 µm (Fratini et al., 2021; Furt et al., 2010; M. Heilmann & Heilmann, 2024). Such narrow spots with substantially higher concentrations

of PIs may also occur at the TGN/EE, possibly consistent with the high catalytic velocities obtained for PI4Kβ1 (Furt et al., 2010).

While no direct comparison can be made based on the data reported for PI 4-kinases from human or yeast, due to their classification as enzymes of the type II subfamily and their different subcellular localization at the plasma membrane, the published results still indicate that different kinetic regulation mechanisms for PI 4-kinases may be involved in regulating different cellular processes. For instance, human and yeast PI 4-kinases lack the regulatory PPC domain present in PI4Kβ1 from *Arabidopsis*, leading to a non-sigmoidal Michaelis-Menten behavior instead of a sigmoidal cooperative kinetic profiles as observed here, due to the presence of allosteric binding sites in the regulatory domain PPC in PI4Kβ1 from *Arabidopsis*. A possible regulation mechanism for the PI4Kβ1 from *Arabidopsis* might partially rely on the "mnemonical mechanism" proposed previously by (Storer & Cornish-Bowden, 1977) for glucokinases. The mnemonical mechanism is based on the fact that the enzyme can "memorize" the active conformation after catalysis and will eventually "forget" later. The glucokinase exists in three different conformations open, super-open and closed-open. In the absence of glucose, the glucokinase enzyme remains in a super-open conformation, once glucose binds to the super-open conformation the enzyme undergoes a slow conformational change to an open form, and then the catalysis occurs by converting to the closed form in the presence of ATP. Once the reaction ends, the enzyme changes back to an open conformation to enable the release of the product. A large portion of the enzyme remains in an open conformation for some time in case that another glucose binds to the protein, otherwise it will slowly come back to the super-open form, meaning that it has two catalytic cycles a "slow cycle" and a "fast cycle". At low glucose concentrations, glucokinase uses the slow cycle, represented by a low-affinity structure because the super-open form is more stable than the other conformations when glucose is not present. By contrast, when the glucose concentration rises, glucokinase alternatively uses a fast cycle with a high-affinity structure. Considering an equivalent mnemonical mechanism, PI4Kβ1 may also take three different conformations, and a shift between "slow" and "fast" cycles might depend on the presence of the PtdIns4P product of the reaction, which also serves as an allosteric/cooperative activator mediating activation of the enzyme as the reaction progresses (Kamata et al., 2004).

Overall, our results demonstrated a $K_m = 219\ \mu M$ for MBP-PI4Kβ1 against ATP, which is lower to values reported for human type II PI4-Kinase ($K_m = 260\ \mu M$) and for yeast PI 4-kinase ($K_m = 360\ \mu M$). This indicates a higher affinity of PI4Kβ1 towards the substrate ATP compared to humans and mammals. In this context, it is important to note that MBP-

PI4Kβ1 exhibited non-sigmoidal hyperbolic kinetics as a function of increasing concentrations of the co-substrate, ATP. In addition, at the highest ATP concentrations tested the curve showed a slight increase in velocity, possibly suggesting that the enzyme forms either dimers, trimers or oligomeric states due to the distinct active sites present on the oligomer. So far, the oligomeric state of the PI4Kβ1 is not known, but it was previously reported that *Arabidopsis* PI4Kα forms a heterotetrameric complex with No Pollen Germination (NPG), EFR3 of Plants (EFOP) and hyccin-containing (HYC) in plasma membrane nanodomains (Noack et al., 2022). The authors also discussed that PI4Kα1 might naturally form homodimers, based on an animal report where PI4KαIII dimerizes at the plasma membrane (Lees et al., 2017). This observation allows several important conclusions, i) that binding of ATP might occur only at one binding site of the enzyme and ii) that despite of its technical challenges the multi-step lipid phosphorylation assay is suitable to still reveal sigmoid or non-sigmoid kinetics even at low substrate concentrations and ensuing low reaction rates.

3.2. Regulatory domains are required for catalysis by MBP-PI4Kβ1.

To test whether the sigmoidal reaction behavior obtained for MBP-PI4Kβ1 against increasing substrate concentrations was due to PtdIns4P and the presence of putative allosteric sites located in the regulatory domains in the N-terminal half of the enzyme, we removed the disordered regions connecting the N-terminal domains (LKU, PPC and NH). Interestingly the catalytic domain including 30 additional N-terminal residues, displayed only very low activity (Appendix Figure 37). A similar behavior was seen in a human type III PtdIns 4-kinase PI4K230 expressed in sf9 insect cells *in vitro*. For this enzyme, removal of N-terminal protein regions resulted in an inactivation, possibly suggesting that a coordination between the N-terminal domains and the catalytic region of the protein are required for establishing the catalytic core region (Gehrmann et al., 1999). Additionally, the sigmoidal kinetic function initially seen for full-length MBP-PI4Kβ1 was shifted to a hyperbolic response upon deletion of N-terminal protein domains. These results might explain the role of the regulatory domains in the control of PI4Kβ1-mediated catalysis by enabling the binding to the reaction product, PtdIns4P, which in turn influences the binding affinity of the enzyme towards the substrate.

3.3. 3D structural modeling suggests a model of PI4Kβ1-membrane interaction.

While it is known that *Arabidopsis* PI4Kβ1 associates with the TGN (Preuss et al., 2006), it was not clear at the biochemical level how the enzyme is oriented towards its target membranes, and so far there have been no studies on the structural features of PI4Kβ1 from plants. After superimposing an AlphaFld 3D model of *Arabidopsis* PI4Kβ1 with structural models for human PI3Ks and estimating the electrostatic potential surface of the enzyme governed by the number of acid, basic and neutral residues, the orientation of the protein towards a membrane bilayer was elucidated. Interestingly, a C-terminal helix of PI4Kβ1 was found to be essential for interactions with both the substrate PtdIns and the reaction product PtdIns4P, which are present as lipids in the membrane (Figure 22). A similar finding was reported by (Hon et al., 2012), after crystallization and structure determination of a Class I PI 3-Kinase from humans. The authors found that upon removal of the C-terminal helix the protein no longer exhibit any detectable binding to anionic lipids, establishing the C-terminal alpha helix as a key disordered region required for lipid binding. Considering the work by Hon *et al.* and the findings in this thesis, we hypothesize that the catalytic domain of *Arabidopsis* PI4Kβ1 displays complex interactions with lipids through at least two lipid-binding sites, a polybasic activation loop of electrostatic nature, and a C-terminal tail of hydrophobic nature. The activation loop might first facilitate the electrostatic attraction of anionic lipids and may position the head group of the PtdIns substrate relative to bound ATP for phosphoryl transfer. As the ATP binding pocket is depressed in the catalytic domain of the PI4Kβ1 model, partial membrane penetration by the C-terminal helix region might additionally facilitate the ATP γ-phosphate to come closer to the inositol ring of the PtdIns substrate (Hon et al., 2012).

Further postulates might be deduced from the protein model of *Arabidopsis* PI4Kβ1 (Figure 20)**.** By observing the electrostatic surface potential in the bottom view (i. e. the membrane interface) of PI4Kβ1, the protein surface area interacting with the membrane consists of both acidic residues (Figure 20C, right side) but also basic residues (Figure 20C, left side), suggesting that the protein can electrostatically interact through basic residues with negatively charged anionic lipids in the membrane, such as PtdIns4P, PtdOH or PtdSer, but also through the acid/aromatic to mediate membrane association through other interactions. A similar study for a human type II PIPKβ found that the basic region of the enzyme is targeted to the plasma membrane through electrostatic interactions to bind the acidic head groups of anionic lipids (Rao et al., 1998). Moreover, an electrostatic switch

mechanism was proposed to explain the membrane association of human PI4P 5-kinases, depending on the charge of the membrane. The authors suggest that the loss of charge in the membrane by phospholipases or phosphatases promote the detachment of the kinase, while a synthesis of anionic lipids in the membrane will progressively induce the recruitment of the kinase to the membrane (Fairn et al., 2009).

The electrostatic properties of the membrane were recently proposed to be associated with the anionic lipid, PtdIns4P, which accumulates in the membranes to facilitate the interaction with polybasic regions of proteins. However, PtdIns4P distributes differentially in cells of yeasts, mammals or plants. In yeast, the major PtdIns4P pool is produced by Pik1p at the TGN and only a minor pool is produced by stt4p at the plasma membrane (Audhya et al., 2000; Audhya & Emr, 2002). Similarly, in animals, PI4KIIIα is responsible for synthesizing a minor pool of PtdIns4P at the plasma membrane, and its isoform PI4KIIIβ is in charge of producing the major pool at the Golgi/TGN and in endosomes. Contrarily, in plants, PtdIns4P is highly concentrated at the plasma membrane where it is synthesized by PI4KIIIα (Noack et al., 2022) whereas the pool of PtdIns4P produced by PI4Kβ1 at the TGN is far less abundant (Lin et al., 2019; Simon et al., 2014; Vermeer et al., 2009b). Everything considered, the modeling approach suggests that *Arabidopsis* PI4Kβ1 might electrostatically interact with negatively charged membranes, thereby contributing to the localization of proteins containing polybasic domains. Nevertheless, these interactions strongly depend on variations in lipid composition, cytosolic environment like ion influx and protein modifications like phosphorylation events.

3.4. The contribution of the C-terminal helix and of residues L1117 and R626 to the kinetic features of MBP-PI4Kβ1

The MD simulations performed as part of the structural modeling of PI4Kβ1 revealed that an arginine in position 626 in the NH domain of PI4Kβ1 might form hydrogen bonds with the lipid substrate, with the co-substrate ATP, and with the reaction product, PtdIns4P. Interestingly, arginine and other positively charged residues have previously been proposed to stabilize the phosphoryl transfer transition states by coordinating the transferred phosphoryl group. The positively charged side chain of an arginine in the alkaline phosphatase was previously found to form hydrogen bonds with the negatively charged non-bridging oxygens, providing stabilization to the phosphoryl transfer transition state (O'Brien et al., 2008; O'Brien & Herschlag, 1999). Another residue identified in the

MD simulations was the leucine in position 1117 in the C-terminal tail of at the PI4Kβ1 protein. In the MD simulations, L1117 formed hydrogen bonds with both the lipid substrate, PtdIns, and with the reaction product, PtdIns4P. The leucine residue has a hydrophobic nature and its presence in a protein may improve interactions with lipids. Surface-exposed leucine residues have a high hydrophobic side chain density, providing a large surface for interactions with lipid tails, suggesting that leucine might impact hydropathy, with possible structural consequences in α-helices and β-sheets of proteins (Baumann & Zerbe, 2024). This could explain in our data why this leucine in the enzyme showed the higher occupancy percentage or number of interactions with the substrate/product obtained during MD (Figure 21).

Even though, R626 and L1117 are thought to be essential for the binding of PI4Kβ1 to its substrate, its co-substrate and for product binding according to MD, our experimental *in vitro* data revealed that their substitution to alanine did not affect the binding affinity towards the substrate (Figure 22). By contrast, an alanine substitution in L1117 negatively impacted the maximal velocity of the PI4Kβ1 enzyme. In addition, a sigmoidal kinetic pattern was also obtained for the MBP-PI4Kβ1 L1117A substitution variant upon increasing substrate concentrations as already seen for the parental MBP-PI4Kβ1 protein, validating the allosteric regulation of PI4Kβ1 (Figure 22).

An essential contribution of the C-terminal helix to PI4Kβ1-mediated catalysis can be deduced from the analysis of the C-terminal deletion variant, MBP-PI4Kβ1$_{1107\text{-}1121}$. The deletion of the C-terminal helix abolished enzyme activity, indicating that this helix, not considered as part of the catalytic domain according to UniProt data base, is essential for either substrate binding or for product release. A similar finding was reported for a human class II PI 3-kinase, where the deletion of a C-terminal region abolished the binding to anionic lipids and was assumed to be important for protein-membrane interaction (Hon et al., 2012).

Overall, the control of catalytic behaviour of PI4Kβ1 appears complex, based on the differential effects of substrate availability and allosteric product binding. Beyond these effects, it was known at the beginning of this thesis that PI4Kβ1 is a target for phosphorylation by upstream MAPKs. Therefore, a substantial part of this thesis was dedicated to elucidate the effects of protein phosphorylation on the biochemical behavior of PI4Kβ1.

3.5. MPK4, MPK6, SnRK2.6 and CPK11 phosphorylate MBP-PI4Kβ1 *in vitro*

Protein phosphorylation is a common and reversible post-translational modification (PTM) that involves the addition of a phosphate group to an amino acid side chain of a target protein. The most frequent phosphorylated amino acid residues in eukaryotic cells are serine, threonine, and tyrosine (Newcombe et al., 2022).

It was previously reported that PI4Kβ1 is a target for upstream phosphorylation by different kinases using *in vitro* phosphorylation or phosphoproteomic analysis. MPK4 was first reported to phosphorylate PI4Kβ1 *in vitro* in supplemental data (Latrasse et al., 2017), which was later validated by (Lin et al., 2019) using recombinant purified proteins. Our research further confirmed the phosphorylation of MBP-PI4Kβ1 by using an upstream constitutively active MPK4, that contained substitutions in the conserved TXY motif in the amino acid positions D198G/E202A. *In vivo* MPK4 is usually activated by a MAPK cascade that starts with the activation of MAPKKK (ANP2/3), subsequently activating downstream MAPKK(MKK6), which would finally activate a MAPK (MPK4) (Jiang et al., 2022). Due to the availability of the CA-$_{6x}$-His- MPK4, this variant was used for phosphorylation assays in this thesis. As a negative control, a kinase-dead MPK4 variant was used that contained a K71R substitution in the ATP binding site. Assays performed in this thesis confirmed the known autophosphorylation of CA-MPK4 as well as the phosphorylation of its target, MBP-PI4Kβ1 (Figure 24 A,E). The data are consistent with, previous reports that *Arabidopsis mpk4* mutants show defects in mitosis and cytokinesis (Beck et al., 2011; Lin et al., 2019) that are similar to defects found in *Arabidopsis pi4Kβ1 pi4Kβ2* mutants, indicating that both proteins not only interact and exhibit a functional interplay to regulate cytokinesis at the cell plate, but also that these cellular processes are controlled by phosphorylation events.

A global phosphoproteomic analysis on *Arabidopsis* showed that PI4Kβ1 is a target for phosphorylation by the protein kinases, MPK6 and SnRK2.6 (Wang et al., 2020). In this study, peptides were collected from *Arabidopsis* plants overexpressing different protein kinases. The plants had been exposed to different environmental stresses such as salt stress, cold, receptor stimulation, the phytohormone abscisic acid (ABA) or H_2O_2 and then subjected to MS-based phosphopeptide analysis. Our *in vitro* phosphorylation results using recombinantly purified proteins could successfully confirm that the constitutively active MPK6 phosphorylates enriched recombinant MBP-PI4Kβ1 protein (Figure 24 B, C).

In plants, MPK6, is mainly activated by a MAPK cascade that starts with the activation of MAPKKK (MEKK1), subsequently activating downstream MAPKK (MKK4/6), which would end in the downstream activation of the MAPKK (MPK6) (Droillard et al., 2004). Due to the availability of the CA-$_{6x}$His-MPK6, containing substitutions in the conserved TXY motif in the amino acid positions D218G/E222A, with our collaboration partner (Dr. Justin Lee, Leibniz Institute of Plant Biochemistry (IPB) Halle), the CA-$_{6x}$His-MPK6 variant was used for phosphorylation assays in this thesis. Our *in vitro* phosphorylation assays using CA-$_{6x}$His-MPK6 demonstrated phosphorylation of enriched recombinant MBP-PI4Kβ1 protein (Figure 24 B). As a negative control for the phosphorylation reaction, again a kinase-dead variant of MPK6 was used, which contained a K92R substitution in the ATP binding site. As MPK6 was found to be localized at the phragmoplast and pre-prophase bands and is believed to play a role in determination of the cell division plane due to single *mpk6* mutant plants exhibiting cytokinetic defects like multinucleated cells, it might be possible that an interplay between MPK6 and PI4Kβ1 is important to regulate cell plate formation during cytokinesis (Smékalová et al., 2014a).

In our *in vitro* phosphorylation assays, the protein kinase, SnRK2.6, also weakly phosphorylated enriched recombinant MBP-PI4Kβ1. Protein SnRKs form three groups classified as SnRK1, SnRK2 and SnRK3 according to their sequence similarity and domain structure. SnRK2.6 is part of the SnRK2 family. The SnRK2 family consists of 10 members divided in three classes according to their activation in presence of ABA. The SnRK2 family is activated by osmotic and salt stress, controls sugar metabolism and is involved in the ABA signal transduction pathway (Hrabak et al., 2003). Because it was already reported that SnRK2.6 exhibits a strong autophosphorylation, indicative of strong phosphoryl transfer activity, this isoform was expressed, purified and used for our assays (Maszkowska et al., 2021). *In vitro*, $_{6x}$His-SnRK2.6 displayed strong autophosphorylation and also phosphorylated enriched recombinant MBP-PI4Kβ1 protein (Figure 24 C,E). Moreover, (Wang et al., 2020) suggested that S785/T786 located in the catalytic domain are target phosphorylation sites in PI4Kβ1. Because SnRK2s can phosphorylate regulatory-associated protein of TOR (RAPTOR) and inactivate target of rapamycin complex (TORC), a negative regulator of autophagy, it has been proposed that autophagy may be activated in a SnRK2.6-dependent manner, allowing plants to adapt to nutrient-limiting environmental conditions (Agbemafle et al., 2023). Together with these previous reports, we might hypothesize that when plants are exposed to nutrient limitation, ABA accumulates, which possibly activates SnRK2.6 to phosphorylate downstream effectors, including PI4Kβ1. Such phosphorylation events might be involved in controlling autophagy in *Arabidopsis*. However, this is largely speculative at this point, and the functional interplay between

these two proteins remains unknown. With our focus on the effects of MAPKs on PI4Kβ1, the analysis of SnRK2.6 was not further attempted in this thesis.

Another protein kinase candidate tested in this thesis as a potential upstream regulator of PI4Kβ1 is CPK11. The selection of CPK11 was motivated by previous results demonstrating that CPK11 can phosphorylate the *Arabidopsis* PI4P 5-kinase, PIP5K6 (Hempel, 2015), which is an enzyme that acts in close functional proximity to PI4Kβ1 (Ischebeck, Vu, et al., 2010). Considering these previous findings and the fact that PI4Kβ1 was previously found to interact with a calcium sensor protein (AtCBL1) (Preuss et al., 2006), the positive phosphorylation of enriched recombinant PI4Kβ1 protein by CPK11 (Figure 24 D,E) suggests an interconnection between the PI-signaling system and calcium signalling to control secretion and vesicle trafficking in *Arabidopsis*. However, with our focus on the effects of MAPKs on PI4Kβ1, the analysis of CPK11 was not further attempted in this thesis.

3.6. MPK4 and MPK6 target S186 and S454 as the two main phosphosites in PI4Kβ1

At the onset of this thesis, it was found that PI4Kβ1 S186 is a site phosphorylated by an unknown upstream kinase, and that PI4Kβ1 S454 is a phosphosite likely targeted by MPK6 (Wang et al., 2020). Both of these residues are followed in the PI4Kβ1 sequence by prolines, and S/TP is the preferred phosphorylation motif (S/TP) for MAPKs. Therefore, in this thesis, single and double substitution variants for PI4Kβ1 were generated in which S186 and/or S454 were substituted by alanines (A) or alternatively for aspartate (D) residues. The A or D substitutions were chosen in accordance with previous reports to possibly simulate non-phosphorylated (A) or phosphorylated (D) forms of the PI4Kβ1 protein. Please note that alternative substitutions would have been possible or even advisable, such as glutamate instead of aspartate, as glutamate more closely resembles a phospho-serine residue (Newcombe et al., 2022). However, in previous studies aspartate substitutions have been shown to be effective (Newcombe et al., 2022). None of the substituted residues can serve as phosphorylation sites in the PI4Kβ1 protein, and *in vitro* protein phosphorylation assays using recombinantly purified proteins revealed that the single and double substitution variants for S186 and S454 exhibited a gradual decrease upon CA-$_{6x}$His-MPK4 and CA-$_{6x}$His-MPK6 phosphorylation, with the double mutants showing a reduction in the degree of *in vitro* phosphorylation of 60 and 86 % respectively (Figure 28). The data indicate that these residues, that were selected based on published

phosphoproteomics analyses, are in fact key sites targeted in the PI4Kβ1 protein by both MPK4 and MPK6.

Further attempts to delineate additional phosphosites by MS analysis in cooperation with the MLU Core Facilty Proteomic Mass Spectrometry of by using peptide arrays did not yield interpretable results (Figure 26). Phosphorylation assays were initially performed in a batch solution by incubating CA-$_{6x}$His-MPK4 or CA-$_{6x}$His-MPK6 with MBP-PI4Kβ1 in the presence of cold ATP for 30 min at room temperature. However, possibly due to the low concentrations of enriched MBP-PI4Kβ1 substrate protein, the assay was largely not successful, and the proteins could often not be reliably detected. Therefore, a second approach was used, where a phosphorylation assay was performed, subsequently the protein mixture was separated by SDS-PAGE and the corresponding target protein range was excised, extracted and the gel bands subjected to in-gel digestion, followed by MS analysis. While this approach resulted in a coverage of the PI4Kβ1 sequence between 40-50%, the results obtained by LC/MS/MS indicated numerous phosphosites, mostly distributed in the N-terminal portion of the protein, focusing in the disordered regions around the LKU domain and in the PPC domain. The majority of the potential phosphosites were found in the PPC domain, possibly indicating a role of the phosphorylation by MAPKs in the targeting of the enzyme to the membranes (Figure 26). However, the published sites S186 and S454 were not determined in our MS analysis, possibly due to different fragmentation mode used in our measurements. Unfortunately, the residue S186 (located in the MBP-PI4Kβ1 sequence in the position 582) was not covered by the MS approach, but the S454 (located in the MBP-PI4Kβ1 sequence in the position 851) was covered. During MS/MS experiments, specific fragments of peptides may form, depending on the peptide sequence. In our study, the Higher-energy collisional dissociation (HCD) fragmentation mode was used, whereas (Wang et al., 2020) utilized a collision induced dissociation (CID) mode for their analysis. The HCD fragmentation is considered the most efficient fragmentation method for cross-link phosphopeptides analysis. HCD has a higher energy and shorter activation time than the CID and generates abundant informative ions in the low-mass region like the characteristic α2 ion, the β2 ion pair, y1 and y2 ions and immonium ions, facilitating the analysis of phosphorylation events in target proteins. By contrast, CID produces mainly β- and y-ions and has the major disadvantage that in the fragment ions less than one-third of the precursor ions m/z are lost in the MS/MS spectra, known as “the one-third effect” (Shao et al., 2014).

While from a technical perspective it seems that we used the best fragmentation mode for our phosphopeptide analysis, it is worth to consider other factors like efficiency of the

method used for phosphopeptide enrichment, the use of alternative enzymes for peptide digestion, or the use of an alternative data acquisition mode for the mass spectrometer, like data dependent acquisition (DDA) or data-independent acquisition (DIA). DDA selectively fragments the peptide ions with higher intensities (making some more abundant) and ions further fragmented in the second stage of the tandem mass spectrometry, leading to the omission of less abundant but probably critical peptides. By contrast, DIA fragments all ions within a pre-defined selected m/z range, then all the precursors within this mass range are fragmented, ensuring an extensive coverage and enabling the detection of low-abundance peptides that DDA might miss (Van der Laan et al., 2020).

The alternative approach using peptide microarrays also resulted in only few peptide sequences of PI4Kβ1 phosphorylated by CA-$_{6x}$His-MPK4 or CA-$_{6x}$His-MPK6 (Figure 27), and none of these residues were found in our MS spectrometry analysis, and also not in the list of published phosphosites, raising questions about the reliability of the results obtained using this method. The residues found here were mostly located near the LKU-domain. Since it is known that the LKU-domain of *Arabidopsis* PI4Kβ1 interacts with the calcium sensor protein AtCBL1 (Preuss et al., 2006) and that in yeast binding of PIK1P to frequenin increased PIK1P activity (Hendricks et al., 1999), this data might indicate that phosphorylation in disordered regions around the LKU might impact the PI4Kβ1 activity. It is also believed that the MAPKs might require well-defined motifs that possibly only come together upon protein folding and are absent in the linear peptide structure displayed on the glass support of the microarrays, possibly making it difficult for the MAPKs to phosphorylate peptide substrates (Chen et al., 2011).

3.7. Phosphorylation by MPK4 or MPK6 can influence catalytic function of MBP-PI4Kβ1.

With a focus on the main phosphosites, PI4Kβ1 S186 and PI4Kβ1 S454, the effects of these phosphorylation events on the catalytic function of MBP-PI4Kβ1 was studied. So far, effects of phosphorylation of PI4Kβ1 had not been elucidated, and the kinetic analysis established in this thesis provided an experimental framework to address how PI4Kβ1 kinetics might change upon phosphorylation. Hempel and co-authors (Hempel et al., 2017), have previously shown that phosphorylation of the PI4P 5-kinase, PIP5K6, by upstream MPK6 results in an approx. 60 % reduction of PIP5K6 catalytic activity, but no

kinetic analyses were performed for that enzyme. Similarly, we also found by radioactive *in vitro* lipid kinase assays that phosphorylation by CA-$_{6x}$His-MPK4 or CA-$_{6x}$His-MPK6 significantly reduced PI4Kβ1 activity (Figure 29 A). The inhibitory effects of phosphorylation observed here on PI4Kβ1 function appear to be consistent with the regulation of a human type II PIPKβ, where its localization and activity is regulated by phosphorylation via an electrostatic switch model. This model proposed that the presence of negative charges by phosphorylation residues on the protein, mediates dissociation of the protein from the membrane enriched with anionic lipids, interfering with substrate access (Fairn et al., 2009).

As at least two distinct phosphorylation sites, S186 and S454, in the PI4Kβ1 protein were targeted by the MAPKs used, the observed inhibitory effect of *in vitro* phosphorylation of MBP-PI4Kβ1 will likely represent a sum-outcome of the combined phosphorylation. The contribution of the individual sites was addressed by analyzing PI4Kβ1 substitution variants, in which phosphomimicking (S-D-substitutions) or phosphoablation (S-A-substitutions) was attempted. We are aware that these substitutions do not fully "simulate" the phosphorylated or non-phosphorylated states of the enzyme, due to the differences in the charge and/or structure of the respective side-chains to those of phospho-serine or serine, respectively. The activity of non-phosphorylated single A or D substitutions for S454 or of S186 S454 double substitutions MBP-PI4Kβ1 was substantially decreased. This observation suggests that catalytic activity can be altered by substituting serines in specific positions, and that these positions are important for catalysis. By contrast, an individual D-substitution in position S186 of the PI4Kβ1-protein resulted in a slight increase in activity, whereas an A-substitution in the same position reduced catalytic activity of the respective MBP-PI4Kβ1 variant (Figure 29 B). The differential effect on MBP-PI4Kβ1 activity suggests that the presence of a negative surface charge introduced in this position might activate catalytic activity. All the data considered, it might be possible that phosphorylation on position S186 might impact PI4Kβ1 catalysis, through a conformational change that might increase the production of PtdIns4P. This hypothesis is supported by the subsequent kinetic analysis of the MBP-PI4Kβ1 substitution variants, which enables more detailed conclusions about the effects of introducing negative surface charges at critical positions of the protein.

The results on the relative catalytic activities determined by end-product determination indicated differences in catalytic behavior of MBP-PI4Kβ1 substitution variants compared to their parental MBP-PI4Kβ1 enzyme. However, these analyses represented only one set of reaction conditions and do not allow conclusions about important parameters to

describe MBP-PI4Kβ1 catalysis. By contrast, kinetic analysis of the parental MBP-PI4Kβ1 protein indicated that the enzyme is allosterically regulated, likely by the product of the reaction, PtdIns4P, resulting in a positive cooperative effect on catalysis. Therefore, kinetic characterization of six substitution variants (MBP-PI4Kβ1 S186A/D; MBP-PI4Kβ1 S454 A/D; MBP-PI4Kβ1 S186A S454A; or MBP-PI4Kβ1 S186D S454D) was performed to elucidate whether the introduction of negative surface charges in relevant phosphosites exerted an effect on substrate affinity or catalytic performance.

The kinetic analysis of the substitution variants of MBP-PI4Kβ1 indicates that all variants retained sigmoidal kinetics, suggesting that allosteric regulation was still present. While the MBP-PI4Kβ1 S454A or MBP-PI4Kβ1 S454D variants did not display major differences in their kinetic behavior compared to the parental MBP-PI4Kβ1 enzyme (Figure 30). The substitution variants MBP-PI4Kβ1 S186A and MBP-PI4Kβ1 S186D differed substantially and differentially from the control. The MBP-PI4Kβ1 S186D substitution variant displayed an increased V_{max} and a decreased $K_{0.5}$ value, indicating an activation of catalytic rate and increase affinity for the substrate, PtdIns. By contrast, the MBP-PI4Kβ1 S186A substitution variant displayed reduced V_{max} and an unaltered $K_{0.5}$. Together, these observations suggest that the introduction of a negative aspartate charge at position S186 (and possibly also a phosphorylation event at that site) might activate the enzyme and promote catalysis. This notion is confirmed by the kinetic behavior of the double substitution variants, MBP-PI4Kβ1 S186D S454D, which also displayed the activation shown by the MBP-PI4Kβ1 186D single substitution; whereas MBP-PI4Kβ1 S186A S454A exhibited kinetic behaviour similar to the MBP-PI4Kβ1 S186A single substitution variant (Figure 30). In essence, the kinetic analyses show an activation of the enzyme upon introduction of a negative charge at position S186, regardless of further substitutions. This observation brings light to a possible regulation mechanism of PI4Kβ1 upon phosphorylation. We hypothesize that the substitution of serine 186 by aspartic acid, mimics the phosphorylation of PI4Kβ1, leading to a conformational change on the protein that results in an increase in both the affinity towards its substrate and in the catalytic rate of the enzyme. Conversely, the S186A substitution resulted in an inactivation of the MBP-PI4Kβ1 S186A protein, notably with the same substrate affinity as the parental MBP-PI4Kβ1 protein. The data is consistent with *in vivo* data previously reported in *Arabidopsis* roots by (Lin et al., 2019) where it was suggested that mCherry-PI4Kβ1 is activated by MPK4-YFP at the nascent cell plate, according to the dynamics of a fluorescent reporter for PtdIns4P, indicating a role for MAPK-phosphorylation in the activation of the enzyme PI4Kβ1.

One of the most common mechanisms by which proteins can be modified is by phosphorylation, however the determination of the functional roles of specific phosphorylated residues is not well understood in most cases. Structural information was particularly limited in this project, due to the lack of nuclear magnetic resonance (NMR) and X-ray crystallography studies that would help to determine the structure of *Arabidopsis* PI4Kβ1. Therefore, the MD simulations used here, uncovered conserved domains and regions widely conserved in eukaryotes and provided additional information about the orientation of the enzyme towards the membrane. The MD simulations also suggested further amino acid residues involved in catalysis. However, with all these benefits, the model did not prove instructive for interpreting the contribution of the proposed phosphosites, as S186 and S454 were not included in the final model. Residue S186 is situated in a disordered region consisting of flexible linkers and loops in a non-conserved protein region, whereas residue S454 is situated in a region of the PPC which was also non-conserved and therefore not included in the model. While, thus, we cannot draw conclusions about possible activation mechanisms involving the phosphorylation in residue 186 of PI4Kβ1, based on the modeling, we can nevertheless speculate according to other published work how this activation could be happening. It is reasonable to assume that phosphorylation of PI4Kβ1 in position S186 might induce a conformational change largely driven by an electrostatic perturbation induced by the negatively charged phosphate group. At physiological pH, the phosphate group carries a −2 charge, while the site of phosphorylation (serine) is neutral before phosphorylation. Once phosphorylation occurs, modified residues gain chemical properties, including a double negative charge of −2 under physiological conditions (pKa of the phosphorylated amino acid is ≈ 6) (Groban et al., 2006). The presence of a negative charge on the surface of the protein might induce a change in hydrophobicity in the surrounding phosphosites, which results from electrostatic properties of the protein, for instance the net charge per residue, the distribution of charged side-chain contacts, or the isoelectric point. Phosphorylation events can also perturb contacts between basic and acid residues on the protein surface, resulting in a reduction or increase of repulsion or attraction (Polyansky & Zagrovic, 2012). This might explain the activation effect seen on MBP-PI4Kβ1 S186D upon introduction of the surface charge. It could be that the introduction of this negative charge on the surface of the protein alters the electrostatic proteins of the enzyme, inducing a conformational change to a more open conformation upon binding to the product (Srivastava et al., 2022).

A conformational change and impact on protein function was also observed when PPIases (prolyl *cis/trans* isomerases) like cyclophilins or parvulins catalyzed the cis-to-trans isomerization of prolyl peptide bonds (Schiene et al., 1998). In *Arabidopsis*, 14 cyclophilins-

like proteins have been reported to be involved in protein folding and plant development. For example, the cyclophilin TLP40 located in the thylakoid regulates the activity of a D1 phosphatase (Romano et al., 2004). Also, a human parvulin-like PPIase Pin2 recognizes substrates in a phosphorylation-dependent prolyl isomerization manner. When the Ser/Thr-Pro-containing peptides are phosphorylated, the cis to trans isomerization rate is 8-fold lower than that of the non-phosphorylated. Interestingly, Schutkowski et al., 1998 discussed that phosphorylation of Ser/Thr-Pro motifs regulates peptide dynamics by changing the tertiary structure of polypeptides and impact protein function. Structural changes occur because phosphorylation alters the electrostatic nature of proteins after the introduction of a negative charge, modulating the thermodynamic equilibrium and catalyzing protein folding of the phosphorylated substrate (Schutkowski et al., 1998). These findings might explain why the introduction of a negatively charged phosphate group in the S186 may have induced a conformational change that impacted the PI4Kβ1 function. While enzyme-facilitated prolyl-cis/trans-isomerization might, thus, have a role *in vivo*, effects of phosphorylation/phosphomimicry on catalysis of MBP-PI4Kβ1 variants were observed using purified recombinant enzymes tested *in vitro* in the absence of an cyclophilin-like isomerase.

In humans it was observed that phosphorylation triggers regional conformational changes of the CypD (Cyclophilin D) protein itself, by reducing and enhancing the local flexibility of the protein at distinct regions, a behavior explained by a “seesaw” model of flexibility. This model explains that when the enzyme is substrate-free the protein is much more flexible and major changes occur in distinct regions. Substrate binding leads to a reduced flexibility in those regions, which is compensated by the major fluctuations at the binding sites of the substrate (Kumutima et al., 2022). Thus, conformational changes following phosphorylation can regulate catalytic activity, protein interaction and subcellular location by themselves (Lu et al., 2022).

In contrast to the situation for MBP-PI4Kβ1 S186, so far no clear effect was observed for the substitution variants MBP-PI4Kβ1 S454A or MBP-PI4Kβ1 S454D. Residue S454 is located in the PPC domain of the PI4Kβ1 protein, which is implicated in mediating membrane association through binding to anionic lipids (Lou et al., 2006). While experiments in this thesis could verify the binding to anionic lipids (Figure 32), there was no detectable effect of the S454A or S454D substitutions on lipid binding analyzed by lipid overlay assays, even upon the introduction of a negative surface charge in MBP-PI4Kβ1 S454D. However, lipid overlay assays are based on the immunodetection of proteins bound to lipid-containing membranes, and it is possible that the quantitative resolution of

this method is not suitable to detect more subtle differences in lipid binding that might have been present. Future experiments should, therefore, resort to more quantitative means of analysis, such as microscale thermophoresis (MST) (Jerabek-Willemsen et al., 2014).

Overall, for the interpretation of the effects of substitution variants, it is important to consider further complexity. Direct effects of a surface charge introduced might be accompanied by additional, secondary effects. For instance, it is possible that the conformational change in the PI4Kβ1 protein by an S186 phosphorylation might enable further phosphorylation by the same of other protein kinase(s) that further modify the catalytic behavior of the enzyme. While we currently have only limited data on this notion, a set of preliminary experiments was performed where the MBP-PI4Kβ1 A or D substitution variants were first subjected to *in vitro* phosphorylation by CA-$_{6x}$His-MPK4 or CA-$_{6x}$His-MPK6 and then analyzed for their catalytic activity in end-product determinations (see Appendix Figure 47). Interestingly, these experiments showed differences in the effects of protein phosphorylation on catalytic activity, and especially the MBP-PI4Kβ1 S186D variant, again, displayed higher catalytic activity upon phosphorylation by CA-$_{6x}$His-MPK4 or CA-$_{6x}$His-MPK6 than the corresponding MBP-PI4Kβ1 S186A variant or the parental MBP-PI4Kβ1 enzyme (Appendix Figure 47). However, while it is tempting to speculate, these preliminary results should be viewed with caution, because several effects are overlayed (the substitutions and further phosphorylation events), and because no kinetic analyses were performed. If there are additional effects of phosphorylation even in the MBP-PI4Kβ1 substitution variants, these effects might be due to additional phosphosites that were not considered for analysis in this thesis. Considering a conformational change in the substitution variants, it is possible that additional phosphosites might become more prominent in these enzyme variants. Candidate sites for such additional phosphorylation might be among those that were determined by LC/MS/MS (Figure 26) or even by the peptide microarray analysis (Figure 27).

In sum, the data presented in this thesis provide first insights into the biochemical regulation of *Arabidopsis* PI4Kβ1 at the enzyme level. The enzyme is allosterically regulated, likely by cooperative product binding, and is subject to phosphorylation by upstream protein kinases, including the important MAPKs, MPK4 and MPK6. Phosphorylation by the MAPKs occurs mainly at two sites, S186 and S454. An activation of PI4Kβ1 by MAPK-mediated phosphorylation in S186 is consistent with previous cell biological data that demonstrate synergistic function, e.g. of MPK4 with PI4Kβ1 in controlling phragmoplast dynamics during cytokinesis of *Arabidopsis* root cells. Based on

the results presented in this thesis, and by using the PI4Kβ1 substitution variants characterized therein, it will now be possible to address the effects of MAPK-mediated phosphorylation of PI4Kβ1 *in vivo* and to hopefully better understand the regulatory interplay of MAPKs and PI metabolism in a meaningful developmental context also *in planta*.

4. Materials and Methods

4.1. Equipment and devices

The equipment and devices used for this thesis are listed in Table 3

Table 3. **Equipment and devices**.

Equipment and devices	Company
ÄKTA pure ™/ ÄKTA prime plus ™ FPLC	Cytiva Lifesciences, Stockholm, Sweden
New Brunswick Innova 44 Incubator Shaker	Eppendorf AG, Hamburg, Germany
Centrifuges 5424 R, 5810 R	Eppendorf AG, Hamburg, Germany
Optimal L-90K – Ultracentrifuge	Beckman Coulter, California, USA
Sonifier W.250D	Branson Ultrasonics, Connecticut, USA
Slab gel dryer 4050 D	UniEquip, Munich, Germany
Reacti-Therm™ Heating and Stirring Modules	ThermoScientific, Henningsdorf, Germany
Agarose gel chambers MINI	Cti, Idstein, Germany
Gel Detection System Gel iX Imager	INTAS, Göttingen Germany
Imaging system Fusion solo S	Vilber Lourmat GmbH, Eberhardzell, Germany
Gel Detection System Quantum ST4 3026-WL	Vilber Lourmat Deutschland GmbH, Eberhardzell, Germany
TAdvanced Thermocycler	Biometra, Göttingen, Germany
Ultrospec 2100 pro UV/Vis Spectrometer	Biochrom, Cambridge, UK
Nanodrop 2000 spectrophotometer	Thermo Fisher Scientific, Schwerte, Germany
Mini vertical protein electrophoresis unit SE250	Hoefer Pharmacia Biotech Inc., San Francisco, CA, USA
Mini-PROTEAN® Tetra Vertical Blotting Chamber	BioRad Laboratories GmbH, Munich, Germany
Fusion Solo S	Vilber Lourmat Deutschland GmbH, Eberhardzell, Germany
Branson ultrasonic cleaner - Model B12	Branson, Emerson Electric, Dietzenbach-Steinberg, Germany
Amersham™ Typhoon™ Biomolecular Imager	Cytiva Lifesciences, Stockholm, Sweden
FUJI Imaging Plate Screen BAS-IP SR 2040E	Cytiva Lifesciences, Stockholm, Sweden
FUJIFILM BAS Imaging plate eraser	Cytiva Lifesciences, Stockholm, Sweden

4.2. Chemicals

Chemicals used are listed in Table 4. All other chemicals used but not specifically included were supplied by the companies Sigma-Aldrich/Merck (Munich/Darmstadt, Germany), Carl Roth GmbH (Karlsruhe, Germany) or AppliChem (Darmstadt, Germany).

Table 4.Chemicals used in this project.

Chemical	Company
Albumin Fraction V (BSA)	Sigma-Aldrich, Munich, Germany
Ammonium thiocyanate	Carl Roth, Karlsruhe, Germany
[gamma-P32] ATP, 10 mCi/ml; 6000 Ci/mmol (SRP-501)	Hartmann Analytics
[gamma-P33] ATP, 10 mCi/ml;3000 Ci/mmol (SCF-301)	Hartmann Analytics
ATP Solution [10 mM] and [100 mM]	Thermo Fisher Scientific, Schwerte, Germany
ATP- gamma- S (138911)	Abcam, Cambridge, UK
Biozym LE Agarose	Biozym Scientific GmbH, Hessisch Oldendorf, Germany
Bovine Serum Albumin Fatty Acid-free	Sigma-Aldrich, Munich, Germany
Bradford reagent, 5x concentrate	SERVA Electrophoresis GmbH, Heidelberg, Germany
Bromophenol blue	Sigma-Aldrich, Munich, Germany
Chlorophorm	Sigma-Aldrich, Munich, Germany
cOmplete ™ , EDTA-free tablets Protease Inhibitor Cocktail	Sigma-Aldrich, Munich, Germany
Dimethylsulfoxid (DMSO)	Sigma-Aldrich, Munich, Germany
1,4-Dithiothreitol (DTT)	Carl Roth, Karlsruhe, Germany
Ethylenediaminetetraacetic acid (EDTA)	Sigma-Aldrich, Munich, Germany
Glycerol	Sigma-Aldrich, Munich, Germany
Guanidiniumthiocyanate	Carl Roth, Karlsruhe, Germany
HisPur™ Ni-NTA Resin	Thermo Fisher Scientific, Schwerte, Germany
Imodazole	Sigma-Aldrich, Munich, Germany
Isopropyl β-D-1-thiogalactopyranoside (IPTG), dioxane free	Thermo Fisher Scientific, Schwerte, Germany
Imidazole ACS reagent	Sigma-Aldrich, Munich, Germany
L-Rhamnose Monohydrat	Carl Roth, Karlsruhe, Germany
L-(+)-Arabinose	Carl Roth, Karlsruhe, Germany
2-Mercaptoethanol	Carl Roth, Karlsruhe, Germany
MIDORI Green Advance	NIPPON Genetics EUROPE GmbH, Düren, Germany
Orange G	Sigma-Aldrich, Munich, Germany
p-Nitrotetrazolium blue chloride (NBT)	Carl Roth, Karlsruhe, Germany
p-Nitrobenzyl mesylate (PNBM)	Abcam, Cambridge, UK
Phenol solution, saturated with 0.1 M citrate buffer, pH 4.3	Sigma-Aldrich, Munich, Germany
Inhibitor Cocktail Tablets	Sigma-Aldrich, Munich, Germany
Quick Coomassie® Stain	SERVA Electrophoresis GmbH, Heidelberg, Germany
Rotiphorese® Gel 30 (37,5:1)	Carl Roth, Karlsruhe, Germany
Skim milk powder for blotting	SERVA Electrophoresis GmbH, Heidelberg, Germany
Sodium acetate solution	Carl Roth, Karlsruhe, Germany
Sodium Dodecyl Sulfate (SDS)	Sigma-Aldrich, Munich, Germany

Sodium Chloride	Sigma-Aldrich, Munich, Germany
Tris(hydroxymethyl)aminomethane (TRIS)	Sigma-Aldrich, Munich, Germany
N,N,N´,N´-Tetramethyl-ethylenediamine (TEMED)	Sigma-Aldrich, Munich, Germany
Xylene cyanol	Sigma-Aldrich, Munich, Germany

4.3. Antibiotics and selection of bacteria

All antibiotics used here are specified in Table 5.

Table 5. Antibiotics used

Antibiotic	Stock solution	Final Concentration	Company
Carnebicilin disodium	100 mg/mL	100 µg/mL	Duchefa, Haarlem, Netherlands
Kanamycin monosulfate	50 mg/mL	50 µg/mL	Duchefa, Haarlem, Netherlands
Chloramphenicol	25 mg/mL	25 µg/mL	Duchefa, Haarlem, Netherlands

4.4. Phospholipids

All phospholipids used here were obtained from Avanti Polar Lipids Inc. (Merck, Darmstadt, Germany) and are shown Table 6.

Table 6. Phospholipids used in this project.

Phospholipids *(Kinase Assay)*	**Product No.**	**Stock solution**	**Working Solution**
PtdIns (PI) Soy	840044C	10 mg/mL	12 µg; 0.2 mM
Brain PI (4)P	840045	1 mg/mL	5 µg (Used as standard)
Brain PI (4,5)P2	840046	1 mg/mL	5 µg (Used as standard)
Phospholipids *(Enzyme Kinetics)*	**Product No.**	**Stock solution**	**Working Solution**
PtdIns (PI) Soy	840044C	10 mg/mL	6 µg; 0.1 mM
			18 µg; 0.4 mM
			30 µg; 0.7 mM
			42 µg; 0.9 mM
			54 µg; 1.2 mM
			78 µg; 1.8 mM
Phospholipids - Lipid Binding Assays	**Product No.**	**Stock solution**	**Working Solution**
18:1 PtdCho	850375P	10 mg/mL	3 µg
18:1 PtdEtn	850725P	10 mg/mL	3 µg

18:1 PtdIns	850149P	10 mg/mL	3 µg
18:1 PtdSer	840035P	10 mg/mL	3 µg
18:1 PtdOH	840875P	10 mg/mL	3 µg
18:1 PtdIns3P	850150P	1 mg/mL	3 µg
18:1 PtdIns4P	850151P	1 mg/mL	3 µg
18:1 PtdIns(5)P	850152P	1 mg/mL	3 µg
PtdIns(3,5)P2	850154P	1 mg/mL	3 µg
PtdIns(4,5)P2	850155P	1 mg/mL	3 µg

4.5. Consumables and kits

Used kits and single-use material are listed in Table 7.

Table 7.Consumables and kits

Consumable	**Company**
Amersham™ Protran®, Nitrocellulose membrane 0.45 µm	GE Healthcare GmbH, Solingen, Germany
Filter paper 550 g/m^2	Whatman (GE Healthcare), Maidstone, UK
Filtropur S 0.22 µm (filter for syringes)	Sarstedt, Nürnbrecht, Germany
Bottle-Top Vacuum Filtration Systems, PVDF	VWR, Darmstadt, Germany
Pierce ™ Centrifuge Columns 5 ml	Thermo Fisher Scientific, Schwerte, Germany
PIP Strips (#P-6001)	Echelon Biosciences Inc., MoBiTec, Göttingen, Germany
Protein LoBind Tube 2.0 mL	Eppendorf AG, Hamburg, Germany
SERVAGel™ TG PRIMETM 4 – 20 %(12 sample wells)	SERVA Electrophoresis GmbH, Heidelberg, Germany
Glass Pasteur pipettes, 2 ml, 150 mm, Tip length: 60 mm	Carl Roth, Karlsruhe, Germany
TLC plates Silica, 20 x20 cm; 60 Å pore diameter	Sigma-Aldrich, Munich, Germany
MBPTrap™ HP x 5 mL – Purification column	Cytiva Lifesciences, Stockholm, Sweden
HisTrap HP™ HP x 5 mL - Purification column	Cytiva Lifesciences, Stockholm, Sweden
HiTrap® Desalting column x 5 mL	Cytiva Lifesciences, Stockholm, Sweden
PD MiniTrap G-25	Cytiva Lifesciences, Stockholm, Sweden
Micropeptide array	JPT peptide technologies Inc. (Berlin, Germany)
Kit	**Company**
GeneJET™ Plasmid Miniprep Kit	Thermo Fisher Scientific, Schwerte, Germany
Hi Yield® Plasmid Mini DNA Isolation Kit	SLG, Munich, Germany
GeneJET™ Gel Extraction Kit	Thermo Fisher Scientific, Schwerte, Germany

Gateaway™ LR Clonase™ II Enzyme-Mix	Thermo Fisher Scientific, Schwerte, Germany

4.6. Enzymes, proteins, peptides and molecular size markers

Restriction enzymes BamHI and NotI were obtained from New England Biolabs Inc. (Frankfurt, Germany). Other used enzymes, proteins, peptides and molecular size markers and their suppliers are listed in Table 8.

Table 8.Enzymes, proteins, peptides and molecular size markers

Enzymes	**Company**
Lysozyme (chicken egg white) min. 100 000 units/mg, cryst	SERVA Electrophoresis GmbH, Heidelberg, Germany
Phusion® High Fidelity DNA-Polymerase	New England Biolabs Inc., Frankfurt, Germany
DpnI	New England Biolabs Inc., Frankfurt, Germany
Proteins	**Company**
PtdIns (4,5)P2 Grip (#G-4501)	Echelon Biosciences Inc., MoBiTec, Göttingen, Germany
Myelin Basic Protein, dephosphorylated 5mg/mL (Bovine) (31314)	Active motif, Waterloo, Belgium
Molecular size marker	**Company**
GeneRuler ™ 1 kb DNA Ladder	Thermo Fisher Scientific, Schwerte, Germany
PageRulerTM Prestained Protein Ladder, 10 to 180 kDa	Thermo Fisher Scientific, Schwerte, Germany
PageRulerTM Unstained Protein Ladder,10 to 200 kDa	Thermo Fisher Scientific, Schwerte, Germany

4.7. Microorganisms

Microorganisms used for plasmid amplification and cloning are described in Table 9. and those used for heterologous expression of plant proteins are described in Table 10.

Table 9.Microorganisms used for plasmid amplification and cloning

Microorganism	Genotype	Description	Company
Escherichia coli (E. coli) strain NEB5α	fhuA2 Δ(argF-lacZ)U169 phoA glnV44 Φ80 Δ(lacZ)M15 gyrA96 recA1 relA1 endA1 thi-1 hsdR17	Chemically competent *E. coli* is a derivative of DH5α. It yields high-quality plasmid DNA due to the absence of nonspecific endonuclease I (endA1) and keeps plasmids stable due to low levels of homologous recombination (recA1)	New England Biolabs Inc., Frankfurt, Germany

Escherichia coli (*E. coli)* strain DB 3.1	F- gyrA462 endA1 glnV44 Δ(sr1- recA) mcrB mrr hsdS20(rB-, mB-) ara14 galK2 lacY1 proA2rpsL20(Smr) xyl5 Δleu mtl1	Chemically competent *E. coli* cells contain the gyrA462 allele which gives resistance to the toxic effects of the ccdB gene	Thermo Fisher Sci-entific, Dreieich, Germany

Table 10. Microorganisms used for recombinant protein expression

Microorganism	Genotype	Description	Company
Escherichia coli (*E. coli*) strain BL21 (DE3)	fhuA2 [lon] ompTgal(λ DE3) [dcm] ΔhsdSλ DE3 = λ sBamHIoΔEcoRI-B int::(lacI::PlacUV5::T7gene1) i21 Δnin5	Chemically competent *E. coli* cells suitable for protein expression. B strain does not contain Lon and OmpT proteases. It contains the λ DE3 prophage, which carries the gene for T7 RNA polymerase under the control of a *lacUV5* promoter, allowing the expression of T7 RNA polymerase under IPTG induction.	Thermo Fisher Sci-entific, Schwerte, Germany
Escherichia coli (*E. coli*) strain BL21 AI	F- ompT hsdSB (rB-mB-) gal dcm araB::T7RNAPtetA	Chemically Competent *E. coli* cells designed for tight regulation and strong expression of toxic proteins. B strain does not contain Lon and OmpT proteases. It contains a chromosomal insertion of a cassette containing the T7 RNA polymerase into the *ara*B locus of the araBAD operon, allowing the expression of T7 RNA polymerase under the control of the arabinose-inducible *ara*BAD promoter.	Thermo Fisher Sci-entific, Schwerte, Germany
Escherichia coli (*E. coli*) strain KRX	[F´, traD36, ΔompP, proA+B+, lacIq, Δ(lacZ)M15] ΔompT, endA1, recA1, gyrA96 (Nalr), thi-1, hsdR17 (rk–, mk+), e14– (McrA–), relA1, supE44, Δ(lac-proAB), Δ(rhaBAD)::T7 RNA polymerase.	Chemically competent *E. coli* cells designed for efficient transformation and tightly controlled protein expression. K strain contains a chromosomal copy of the T7 RNA polymerase under the control of by a rhamnose-inducible promoter (*rha*BAD) to provide strong control of the proteins expressed using T7 promoter.	Collaboration with Justin Lee (Available as glycerol stock)

4.8. Culture media

All culture media were autoclaved for 20 min at 121°C. Luria Bertani (LB) liquid media was used for the heterologous expression of all proteins studied in this thesis. The media contained yeast extract 0.5 % (w/v), tryptone 1 % (w/v) and NaCl 0.5 % (w/v). For solid media, 1.5 % (w/v) micro agar was added.

4.9. Vectors used in this thesis

All vectors used in this thesis for heterologous protein expression and cloning are described in Table 11.

Table 11.Vectors used for recombinant *E. coli* expression and cloning

Vector	Antibiotic resistance	Description	Provided by
PMAL-c5G	Ampicilin (Amp^R)	Bacterial expression vector for cytoplasmic expression of Maltose Binding Protein (MBP) fusions, where the protein of interest can be cleaved from MBP with a specific protease Genenase I in the cleavage site. Inducible under IPTG-tac promoter. Contains a multiple cloning site (MCS) for insertion of foreign DNA. MBP fusions include an N-terminal signal sequence	Dr. Mareike Heilmann, Dept. of Plant Biochemistry, MLU
PGEX4T-1	Ampicilin (Amp^R)	Bacterial expression vector for expression of Gluthanione S- transferase (GST) fusions with a thrombin site, where the protein of interest can be cleaved from GST with a protease factor Xa in the cleavage site. Inducible under IPTG-tac promoter. Contains a multiple cloning site (MCS) for insertion of foreign DNA. GST fusions include an N-terminal signal sequence	Dr. Mareike Heilmann, Dept. of Plant Biochemistry, MLU
PDEST17	Ampicilin (Amp^R) Chloramphenicol (Cm^R)	Gateway® destination vector for inducible expression of N-terminally 6xHis-tagged proteins in bacterial cells. This vector is used for LR recombination reaction between donor vector with attL sites containing the gene of interest and the destination vector containing attR sites. In between the two attR sites there is a a CmR gene for counterselection and ccdB gene (encodes for a bacterial toxin that act on DNA gyrase) for negative selection. Amp^R for selection on *E. coli.* Inducible under IPTG-T7 promoter His fusions. Include an N-terminal signal sequence.	Dr. Justin Lee, Leibniz Institute of Plant Biochemistry (IPB) Halle
$pDONR^{TM}$ 221	Kanamycin (Kan^R) Chloramphenicol	Gateway® donor vector for BP recombination reaction between the donor vector with attP sites and attB PCR product. It contains a Cm^R gene for counterselection and ccdB gene (encodes for a	Dr. Mareike Heilmann, Dept. of

(Cm^R)	bacterial toxin that act on DNA gyrase). Kan^R for selection on *E. coli*	Plant Biochemistry, MLU

4.10. DNA, RNA and cDNA manipulation

4.10.1. RNA isolation from *Arabidopsis*

Total RNA was isolated from *Arabidopsis* mature leaves and siliques using the TRIzol-method. The plant material was frozen in liquid nitrogen and homogenized using mortar and pestle. Throughout the grinding process, the sample was covered with liquid nitrogen and the pestle was pressed down against the mortar to grind the sample until a powdery texture was obtained. The sample was mixed with 1 mL TRIzol solution containing 38 % (v/v) Roti-Phenol (Roth, Karlsruhe, Germany), 0.8 M guanidinium thiocyanate, 0.4 M ammonium thiocyanate, 0.1 M sodium acetate pH 5.0, 5 % (v/v) glycerol (see Table 4). Samples were incubated for 10 min at room temperature, until thawed, transferred to RNase-free 2 mL-reaction tubes and centrifuged at 15,870 x g for 10 min at 4°C to sediment debris. The soluble fraction was transferred to a new 1.5 mL tube. 200 µL chloroform was added and the mixture was hand-shaken for 15 s and incubated 2-3 min at RT. Then, centrifuged for 15 min at 15,870 x g at 4°C to facilitate phase separation. The upper phase was transferred to a new 1.5 mL tube and RNA was precipitated with ½ volume of 2-propanol and ½ volume of high-salt precipitation buffer (0.8 M sodium citrate, 1.2 M NaCl), inverted and incubated at RT for 10 min. Pellet RNA was obtained by centrifuging at 15,870 x g and 4°C for 15 min and supernatant was removed. The RNA precipitate forming a gel-like pellet, was washed two times with 900 µL 75 % (v/v) ethanol and centrifuged at 15,870 x g and 4°C for 5 min. Redundant ethanol was discarded and tubes were transferred to the ice and air-dried at RT for 10 min. Dried RNA was dissolved in 10-20 µL RNAse-free ddH_2O and stored at -80 °C until use for cDNA synthesis.

4.10.2. cDNA synthesis

Complementary DNA (cDNA) was synthesized from the RNA-template through reverse transcription. For cDNA synthesis 1-5 µg total RNA were used and the synthesis was performed using RevertAid H Minus First Strand cDNA Synthesis Kit (#K1632, Thermo Fisher Scientific, Schwerte, Germany) according to the manufacturer´s instructions. cDNA was stored at -20 °C until further use.

4.10.3. Determination of DNA and RNA concentrations

DNA or RNA concentrations were photometrically determined at 260 nm using a NanoDrop2000 photometer (VWR International, Darmstadt, Germany). The quality of DNA and RNA was estimated according to the ratio of absorbance at 260/280 nm, where a ratio of ~1.8 and ~2.0 was accepted as "pure" for DNA and RNA, respectively. The absorbance ratio 260/230 nm was used as a secondary measure for nucleic acid purity, where a ratio between the range of ~2.0-2.2 was considered as "pure". If the ratio was lower in either case, it indicated the presence of protein, phenol or other contaminants like EDTA and carbohydrates that absorb strongly at 230 nm or near 280 nm.

4.10.4. Separation of DNA and RNA by agarose gel electrophoresis

DNA and RNA were electrophoretically separated according to their size in 1 % (w/v) agarose gels. The gels were prepared by melting agarose in a microwave oven in 1x Tris-Acetate-EDTA buffer (TAE buffer) (40 mM Tris, 20 mM glacial acetic acid, 1 mM EDTA). 500 mL agarose gel were cooled down to 50-60°C and 20 µL of non-carcinogenic dye MIDORI Green Advance (Nippon Genetics EUROPE, Düren, Germany) were added to detect DNA and RNA. The samples were mixed with 5x DNA-loading dye (60 % (v/v) glycerol, 0.4 % (w/v) Orange G, 0.03 % (w/v) bromophenol blue, 0.03 % (w/v) xylene cyanol (Sigma-Aldrich, Munich, Germany) and loaded into the gels. A GeneRuler^{TM} 1 kb DNA Ladder (Thermo Fisher Scientific, Schwerte, Germany) was used to estimate the size of the DNA fragments. The electrophoresis was performed in 1x TAE running buffer at 130 to 175 V until the negatively charged DNA migrated to the positively charged electrode (anode). Once the yellow dye of the DNA loading buffer reached the bottom of the gel, the gel was placed in the Detection System Quantum ST4 (Vilber Lourmat Deutschland GmbH, Eberhardzell, Germany) and nucleic acids were visualized when irradiated by UV light. UV wavelength excited the fluorophore bound to DNA and emitted green fluorescence at 530 nm allowing the detection of DNA and RNA in agarose gels.

4.11. Molecular Biology Methods

4.11.1. Polymerase chain reaction (PCR) for DNA amplification

To amplify a cDNA sequence of interest from a cDNA mixture the PCR technique was used. PCR experiments were carried out according to the instructions provided by Phusion®

High-Fidelity PCR Kit (New England Biolabs Inc., Frankfurt, Germany). In brief, PCR reactions were performed in a TAdvanced thermocycler (Biometra, Göttingen, Germany), in a 50 µL reaction volume and contained following components: ~ 20 ng of template DNA, 2 µM of each oligonucleotide primer, 100 µM of dNTPs, 1 X Phusion HF reaction buffer and 1 U of High fidelity Phusion DNA polymerase and mixed thoroughly (New England Biolabs Inc., Frankfurt, Germany). Primers used for restriction enzyme cloning contained restriction sites to the 5' end of both PCR primers and 4 additional bases were added between the recognition site and the 5' end of the primer to provide enough DNA for the restriction enzyme to bind the recognition site and cut efficiently. In contrast, primers used for Gateaway cloning contained attB sites sites to the 5' end of both PCR primers. Primers used here are listed in (See Appendix Table 16). The reaction underwent the following thermal cycling steps: denaturation (98 °C, 1 min or 2 min for mutagenesis PCR), annealing (~ 60 °C, 30 s), extension (72 °C, 1 min/1000 bp), and a final extension step (72 °C, 10 min). PCR products were separated by agarose gel electrophoresis as described above (See Section 4.10.4) and then extracted from agarose gels.

4.11.2. Extraction of DNA from agarose gels

The GeneJET^{TM} Gel Extraction Kit (#K0692, Thermo Fisher Scientific, Schwerte, Germany) was used for extraction and purification of vectors and insert DNA from agarose gels. All purification steps were carried out at room temperature and centrifuged at 12000 x g. First, the gel slice containing the DNA fragment was excised and placed in a 1.5 mL Eppendorf tube. Then the binding buffer was added in a 1:1 ratio (v/v) and the gel mixture incubated at 50-60°C until gel slice was completely dissolved. The DNA was loaded into the silica spin purification column, washed with washing buffer, and the DNA was eluted with 20-30 µL elution buffer. Purified insert was used for restriction enzyme digestion.

4.11.3. DNA Restriction

All restriction enzymes used here (BamHI, NotI, SalI) (New England Biolabs Inc., Frankfurt, Germany) produced sticky ends after digestion and were used to cut inserts and vectors containing the respective restriction site. Reactions were performed as described in New England Biolabs Inc. (Frankfurt, Germany) in a 50 µL volume containing 1 x CutSmart buffer, 20 U restriction enzyme, ~1 µg insert DNA or vector DNA and incubated at 37°C for 2 hours for insert DNA and overnight for vector DNA. The restriction reactions were stopped by incubating the samples for 20 min at 80°C. The vector DNA used here was isolated as described in Section 4.11.8, then separated by DNA gel electrophoresis (see section4.10.4) and finally purified (See section 4.11.2). The purified digested insert DNA was used for DNA ligation.

4.11.4. Ligation

For ligation of insert DNA into the digested vector, T4 DNA ligase (New England Biolabs Inc., Frankfurt, Germany) was used to catalyze the formation of covalent phosphodiester bond formation of the two DNA fragments. In short, a reaction mixture of 20 µL total volume was prepared according to manufacturer's protocol: 2 µL T4 DNA Ligase Buffer (10X), 1 µL Vector DNA, 3 µL insert DNA and 1 µL T4 DNA ligase. The reaction contained a molar ratio of 3:1 insert:vector and was incubated at RT for1-2 h. The reaction was heat inactivated at 65 °C for 10 min and the whole reaction mixture was used for transformation into chemo-competent *E. coli* NEB5α (See section 4.11.7)

4.11.5. Gateway cloning

Gateway®cloning based on site specific recombination reaction between different attachment sites was used to insert the cDNA encoding for the constitutively inactive (KD) MPK4 into a final pDEST™17 expression vector. For this purpose, Gateway™ BP Clonase™ II enzyme mix (Thermo Fisher Scientific, Schwerte, Germany) was used first to catalyze the *in vitro* recombination of PCR product (with att B1-B2 sites) into an entry vector pDONR™221 (with att P1-P2 sites) to generate an entry clone. For this, 1 µL PCR product, 1 µL pDONR™221, 8 µL 1X TE buffer (10 mM Tris-HCl, pH 8.0, 1 mM EDTA) and 1 µL BP clonase II enzyme mix were mixed. The reactions were incubated overnight under mix at 25°C. Reaction was terminated by 1 µL proteinase K and incubation at 37°C for 10 min. The mixture was used for transformation into *E. coli* NEB5α5, for plasmid amplification and selection of the Kanamycin resistant entry-clones.

Afterwards similarly, Gateway™ LR Clonase™ II enzyme mix (Thermo Fisher Scientific, Schwerte, Germany) was used to catalyze the *in vitro* recombination of the entry-clone obtained in the previous step (with att L1-L2 sites) and the PDEST17 destination vector (with att R1-R2 sites) to generate an expression clone. For this, 1 µL MPK4-pDONR™221, 1 µL pDEST™17, 8 µL 1X TE buffer (10 mM Tris-HCl, pH 8.0, 1 mM EDTA) and 1 µL LR clonase II enzyme mix were mixed. The reactions were incubated overnight under mix at 25°C. Reaction was terminated by 1 µL proteinase K and incubation at 37°C for 10 min. The mixture was used for transformation into *E. coli* NEB5α5, for plasmid amplification, selection of the Ampicilin resistant expression-clone and verified by sequencing (See 4.11.10). The sequencing verified PDEST17+MPK4 was subsequently used for site-directed mutagenesis (See Section 4.11.11) to obtain the KD-MPK4 using the corresponding primers (Appendix Table 18)

4.11.6. Preparation of chemo-competent *E. coli* cells

Chemically competent cells were prepared using cold salt washes to disrupt the cell membrane and prepare the bacteria to take up foreign DNA or make them "competent". For this purpose, a pre-culture containing 20 mL LB medium was inoculated with 200 µL of *E. coli* cells (New England Biolabs Inc., Frankfurt, Germany) and grown overnight at 30°C and 180 rpm in a shaker incubator (New Brunswick Innova 44, Eppendorf AG, Hamburg, Germany). Then, 5 mL pre-culture was inoculated into 500 mL LB medium and grown until to O.D. 600 reached 0.4-0.6. The cells were aliquoted into 50 ml reaction tubes, then incubated on ice for 10 min and centrifuged at 3,320 x g and 4°C for 10 min. Pellet cells were resuspended in 100 ml TBF buffer (10 mM HEPES pH 6.7;pH adjusted with KOH, 15 mM $CaCl_2$ x 2 H2O, 250 mM KCl, 55 mM $MnCl_2$), incubated for 10 min on ice and centrifuged at 3,320 x g and 4°C for 10 min. The pellet was resuspended in 4 mL of cold TFB, mixed with 3.75 mL of dimethyl sulfoxide DMSO (a final concentration of 7 % (v/v) incubated on ice for 10 min. 200 µL aliquots were prepared in 1.5 mL Eppendorf tubes, frozen in liquid nitrogen and stored at -80°C until use for transformation.

4.11.7. Transformation of chemo-competent *E. coli*

For plasmid amplification, foreign DNA was introduced into the *E. coli* NEB5α competent cells by heat shock transformation. In brief, 100 µL of chemically competent *E. coli* cells were mixed with 20 µL Ligation-DNA mixture (or gateaway DNA-mixture) and incubated on ice for 30 min. Then, heat shock was performed in a thermal block at 42 °C for 1 min. During heat shock the sudden increase in temperature creates pores in the plasma membrane of the bacteria allowing the vector DNA to enter the bacterial cell. Later, 900 µL of LB medium were added and cells were incubated at 37°C for 1 h. For transformation, cells were centrifuged 20s at 10.000 rpm and pelleted cells were resuspended in 100 µL LB media, plated on LB solid plates containing the corresponding antibiotics and incubated overnight at 37°C. A single colony was used for plasmid amplification and isolation.

For retransformations and plasmid amplification, similarly 100 µL of chemically competent *E. coli* NEB5α cells were mixed with 1 µL plasmid-DNA. For protein overexpression 100 µL of chemically competent *E. coli* BL21(DE3) and *E. coli* BL21(AI) were mixed with 1 µL plasmid-DNA. A single colony was used to inoculate protein overexpression cultures (See section 4.12.2).

4.11.8. Plasmid amplification and isolation from *E. coli*

For plasmid amplification, a single colony of transformed *E. coli* NEB5α was inoculated in a 5 mL LB medium containing the appropriate antibiotic and grown overnight at 37°C and

180 rpm. Cells were collected by centrifugation for 1 min at 10.000 rpm and plasmids were extracted following the standard protocol recommended by the GeneJET Plasmid Miniprep Kit (Thermo Fisher Scientific). In brief, cells were mixed with the resuspension solution to remove RNA from samples, then resuspended in lysis solution to release plasmid DNA through SDS-alkaline lysis and later neutralized to create appropriate conditions for binding of plasmid DNA to the silica spin columns. Subsequently, cell debris are pelleted by centrifugation and the supernatant containing the plasmid DNA is loaded in the spin column. Finally, the DNA bound to the column is washed and eluted with elution buffer. Plasmid DNA concentrations and quality were determined as described above (See 4.10.3). The plasmids extracted were used for restriction enzyme cloning (See 4.11.3), ligation purposes (See 4.11.4) or re-transformation (see 4.11.7).

4.11.9. Confirmation of ligation reaction

Resistant *E. coli* NEB5α colonies grown on solid LB medium plates after the ligation reaction, were grown as described in Section 4.11.8 and plasmids extracted and verified by digestion with the appropriate restriction enzymes. The digestion reaction mixture contained a total volume of 25 µL and was performed as described in Section 4.11.3. The reaction mixture containing the DNA was separated by gel electrophoresis (See 4.10.4), the size of DNA fragments was verified, and DNA plasmids were sequenced.

4.11.10. DNA Sequencing

To confirm the exact sequence of the cloned inserts, DNA samples were analyzed by sequencing. For sequencing, 5 µL of plasmid DNA containing ~ 30-100 ng/µL DNA were mixed with 5 µL of 5 µM oligonucleotides in a total volume of 10 µL. The oligonucleotides used for this purpose are available in Appendix Table 17. The nucleotide sequence of each DNA plasmid was determined by sanger sequencing in GENEWIZ “from azenta life sciences” (Leipzig, Germany). The sequence was visualized in a chromatogram using Chromas software (version 2.6.6, Technelysium Pty Ltd, South Brisbane, Australia), the data was exported in FASTA format, and the sequence was aligned to the reference sequence obtained in TAIR database (Carnegie Institution, Stanford, CA and National Center for Genome Resources, Santa Fe, USA) using the online tool Multalin (Appendix Table 21). Correct clones in expression vectors were subsequently used for heterologous expression in *E. coli* (See section4.12)

4.11.11. Site-directed mutagenesis

Site-directed mutagenesis was used to substitute single bases in cDNA sequences, which led to substitution of target amino acids in the expressed protein. The introduction of the

site-directed mutation was performed by single-primer PCR reactions, where forward and reverse complementary primers contained the corresponding mutated bases in the center of both primers (Edelheit et al., 2009). In short, the protocol was performed as described by Edelheit *et al*., 2009 and included 5 main steps: 1) Two separate PCR reactions were performed as described in Section 4.11.1 but using as template ~ 500 ng of plasmid-DNA containing the cDNA insert (plasmid already sequenced). One reaction contained the forward primer and the other contained the reverse primer. 2) The two separate PCR products were combined in a 0.5 mL tube and cooled down gradually from 95°C to 37°C (95°C for 5 min; 90°C for 1min; 80°C for 1 min; 70°C for 30s; 60°C for 30s; 50°C for 30s; 40°C for 30s; 37°C on hold) to denature the newly synthesized mutated DNA from the plasmid template DNA and reanneal the complementary DNA. Later, the methylated (parental DNA) was digested overnight at 37°C with 20 U of DpnI (New England Biolabs Inc., Frankfurt, Germany) and the reaction stopped at 80°C for 20 min. 20-30 µL of the digested reaction mixture was used for transformation of the reannealed mutated plasmids into *E. coli* as described in Section 4.11.7. The mutated DNA-plasmids were amplified, isolated and the DNA substitutions verified by sequencing (See Section 4.11.10).

4.12. Heterologous expression of plant proteins in *E. coli*

4.12.1. Constructs for heterologous protein expression

For heterologous expression of the recombinant enzyme used in this thesis in *E. coli*, restriction enzyme cloning was used to clone the cDNA for full-length PI4Kβ1, for the C-terminal-deletion of PI4Kβ1, or for the catalytic domain of PI4Kβ1 into the pMAL-c5G vector (see section4.9, Table 11.) to fuse the Maltose Binding Protein (MBP) affinity tag using NotI and BamHI restriction sites (see Appendix Table 16). The substitution variants of PI4Kβ1 (S186A; S186D; S454A; S454D; S186A-S454A; S186D-S454D; L1117A; R626A) were obtained using the sequencing-verified pMAL-c5G+WT-PI4Kβ1 vector as a template for the PCR reaction and site-directed mutagenesis was performed as described above (See Section 4.11.11).

The cDNA clones encoding the constitutively-active (CA) $_{6x}$His-MPK4, CA-$_{6x}$His-MPK6, or kinase-dead MPK6 were obtained by Dr. Justin Lee (Leibniz Institute of Plant Biochemistry (IPB) Halle) and were introduced into the PDEST17 vector fused to $_{6x}$His affinity tag using Gateaway recombinational cloning. The constitutively active variants of MPK4 and MPK6 contained substitutions in the conserved TXY motif in the amino acid positions

D198G/E202A and D218G/E222A, respectively (Berriri et al., 2012). The kinase-dead MPK4 and MPK6 contained substitutions in V69A/K92R and K92R, respectively (Bethke et al., 2009) The cDNA sequences of all MAPK variants were confirmed by sequencing using vector-specific primers for the PDEST17 vector, binding to the T7 promoter (see appendix Table 17).

To enable comparable phosphorylation results, all MAPK-variants contained the same affinity His-tag, therefore the kinase-dead MPK4 originally obtained with a GST-tag, was re-cloned in this thesis to add a $_{6x}$His-tag to the kinase-dead MPK4. For that the cDNA of wild type MPK4 was cloned into the PDEST17 vector (see section 4.11.5) and then subjected to site-directed mutagenesis to again obtain the kinase-dead variant, as described above (se section 4.11.11). All vectors used in this thesis are described in Table 11. and cloning techniques were performed according to section 4.11

4.12.2. Culture conditions for the recombinant expression of MBP-tagged proteins or 6xHis-tagged proteins in *E. coli*

MBP-PI4Kβ1: The following culture conditions were used for the expression of MBP-PI4Kβ1, the truncated variants of PI4Kβ1, or for the substitution variants of PI4Kβ1. Briefly, a pre-culture (inoculum) was prepared by inoculating a single colony of transformed *E. coli* BL21 (DE3) into 30 mL LB medium and incubated overnight at 30 °C in a shaker incubator (New Brunswick Innova 44, Eppendorf AG, Hamburg, Germany). Two mL from the pre-culture were used to inoculate 200 mL LB media overexpression culture in a 1 L baffled flask (or 8 mL pre-culture for 800 mL LB media for ÄKTA enrichment) and grown at 37°C and shaking at 100 rpm until an optical density O.D.600 0.6-0.8. LB media contained carbenicillin and 0.2% glucose. *E. coli* cultures were cooled down in the cold room (5°C) for 20 min and protein expression was induced by 0.5 mM isopropyl β-D-1-thiogalactopyranoside (IPTG) and grown for approximately 48 h at 15°C shaking at 100 rpm. The cultures were harvested in 250 mL reaction tubes and the cells were sedimented at 3220 x g at 4°C. Cell sediments were resuspended in 30 mL media and transferred to a 50 mL tube and again sedimented at 3220 x g. The remaining media was discarded, the wet cell sediment was weighed, and cells were frozen in liquid nitrogen and stored at -80°C until cell lysis. As a control, *E. coli* expressing MBP alone was prepared accordingly. A catalytically inactive MBP-K864-PI4Kβ1-$_{5x}$His was already available in the group and was

expressed under the same conditions and used as a negative control for lipid kinase assays (Ischebeck, Vu, et al., 2010).

The following culture conditions were used for all the $_{6x}$His-tagged MAPKs with variation in the *E. coli* strain used due to the availability the proteins during the collaboration with Dr. Justin Lee.

CA-$_{6x}$His-MPK4: Due to the high toxicity of CA-MPK4 when overexpressed in other *E. coli* strains and the ensuing reduced cell growth of such strains, we used *E. coli* BL21 AI, which contained a tightly regulated araBAD promoter and allowed a controlled expression of the protein. In brief, a pre-culture (inoculum) was prepared by inoculating a single colony of transformed *E. coli* BL21 (AI) into 30 mL LB medium and incubated overnight at 30 °C and shaking at 180 rpm. One mL of the pre-culture was used to inoculate 200 mL LB media overexpression culture in a 1 L baffled flask and grown at 37 °C, shaking 100 rpm until an optical density O.D.600 0.6-0.8. *E. coli* cultures were cooled down in the cold room (5°C) for 20 min. Protein expression was induced by 0.2% L-Arabinose and grown overnight at 20°C and shaking at 100 rpm. The cultures were harvested in 250 mL tubes and centrifuged at 3220 x g at 4 °C. The pelleted cells were resuspended in 30 mL media, transferred to a 50 mL tube and sedimented by centrifugation at 3220 x g (Centrifuge 5810 R, Eppendorf AG, Hamburg, Germany). The remaining media was discarded, the wet cell sediment was weighed, and cells were frozen in liquid nitrogen and stored at -80°C until cell lysis. Pre-cultures were also harvested and used for lysis and enrichment, since *E. coli* cells showed leaky protein expression, even using BL21 (AI) cells as a host.

CA-$_{6x}$His-MPK6: Solid LB media plates with colonies containing the CA-$_{6x}$His -MPK6 expressed in *E. coli* KRX cells (Table 3) were provided by Dr. Justin Lee (Leibniz Institute of Plant Biochemistry (IPB) Halle). For this study, glycerol stocks were prepared and stored at -80 °C until use for heterologous expression of CA-$_{6x}$His -MPK6. *E. coli* KRX cells contain a tightly regulated rhaPBAD promoter and allow a controlled expression of the protein. In brief, a pre-culture (incoculum) was prepared by inoculating 50 µL of the glycerol stock into 30 mL LB medium and incubated overnight at 30 °C and shaking at 180 rpm. One mL from the pre-culture was used to inoculate 200 mL LB media overexpression culture in a 1 L baffled flask (or 8 mL pre-culture for 800 mL LB media for ÄKTA enrichment) and grown at 37°C and shaking at 100 rpm until an optical density O.D.600 0.6-0.8. *E. coli* cultures were cooled down in the cold room (5 °C) for 20 min and protein expression was induced by 0.2% L-Rhamnose and let *E. coli* cultures grown overnight at 20°C and 100 rpm. The cultures were harvested in 250 mL tubes and centrifuged at 3220 x g at 4 °C. The cell sediments were resuspended in 30 mL media and transferred to a 50 mL tube and

centrifuged at 3220 x g. The remaining media was discarded, the wet cell sediment was weighed, and cells were frozen in liquid nitrogen and stored at -80 °C until cell lysis.

KD-$_{6x}$His-MPK4, KD-$_{6x}$His-MPK6 and $_{6x}$His-SnRK2.6: The constitutively inactive protein kinase-variants were expressed in *E. coli* BL21 (DE3). In brief, a pre-culture (inoculum) was prepared by inoculating a single colony of transformed *E. coli* BL21 (AI) into 30 mL LB medium and incubated overnight at 30°C and shaking at 180 rpm. One mL from the pre-culture were used to inoculate 200 mL LB media overexpression culture in a 1 L baffled flask and grown at 37°C and shaking at 100 rpm until an optical density O.D.600 0.6-0.8. *E. coli* cultures were cooled down in the cold room (5 °C) for 20 min and protein expression was induced by 1 mM IPTG and cultures were grown over night at 20°C and shaking at 100 rpm. The cultures were harvested in 250 mL tubes and cells were sedimented at 3220 x g at 4°C. The pelleted cells were resuspended in 30 mL media and transferred to a 50 mL tube and centrifuged at 3220 x g. The remaining media was discarded, the wet cell sediment was weighed, and cells were frozen in liquid nitrogen and stored at -80 °C until cell lysis. Pre-cultures were also harvested and used for lysis, since *E. coli* cells showed leaky protein expression, even using BL21 (DE3) cells as a host.

4.12.3. Chemical cell lysis

The pelleted *E. coli* cells were thawed, and 5 mL of lysis buffer was added for each 1 g of cells. The lysis buffer contained Tris HCl 20 mM pH 7.4, 2 mg/mL of lysozyme, 5 mM of DTT, 100 mM NaCL and 1x Protease inhibitor (cOmplete™, EDTA-free Protease Inhibitor Cocktail, Roche, Merck), 10 % (v/v) glycerol and 0.3 % (v/v) triton X-100. Cells were resuspended in lysis buffer and incubated on ice for 30 min, and then cells were sonicated.

For enrichment, pelleted *E. coli* cells were thawed, and 5 mL of equilibration buffer for enrichment (See section4.15.2) were added for every 1 g of cells. Cells were resuspended and 0.3 % (v/v) triton x-100, 1 mM DTT and 1 tablet of EDTA-free Protease Inhibitor Cocktail was added, and then cells were sonicated.

4.12.4. Physical cell lysis by ultrasound sonication

Samples were sonicated on ice with a total of 8000 Joules of energy in 4 cycles of 2.000 J, for 5 minutes, 2 sec ON, 2 sec OFF using the Bransonic B12 Ultrasonics Sonifier (tip probe ¼ ") (Branson, Emerson Electric, Dietzenbach-Steinberg, Germany). The cell lysates were centrifuged at 20,800 x g and 4 °C for 10 min, and the soluble protein fraction was retained for enrichment.

For enrichment, samples were sonicated using the Sonifier W.250D (tip probe ¼ ") (Branson Ultrasonics, Connecticut, USA) with pre-defined program no. 13 with a total sonification time of 1 min, amplitude 40 %, pulse 10 s, pause 40 s, quantity 6x and a total program time of 5 min 30 s. The cell lysates were ultracentrifuged (Optimal L-90K – Ultracentrifuge, Beckman Coulter, California, USA) at 20,800 x g and 8 °C for 30 min, and the soluble protein fraction was retained for enrichment.

4.13. Separation of proteins by sodium dodecyl sulfate polyacrylamide gel electrophoresis (SDS-PAGE)

Protein samples were separated in an SDS-PAGE gel based on their molecular weight under reducing conditions according to Laemmli(Laemmli, 1970). Briefly, samples were mixed with 4 x Laemmli sample buffer (250 mM Tris-HCl pH 6.8, 8 % (w/v) SDS, 0.04 % (w/v) bromophenol blue, 40 % (v/v) glycerol, 400 mM dithiothreitol (DTT) (see chemicals Table 4) and loaded into self-casted SDS Gel (8% resolving gel for PI4Kβ1 or 12% for MAPKs (see Appendix Table 19) or into a pre-casted 4–20 % SDS gradient gel (SERVA Gel^{TM} TG PRIME^{TM}, SERVA Electrophoresis GmbH, Heidelberg, Germany). Gels were run at a constant 30 mA (self-cast) or 70 mA (pre-cast) in SDS running buffer (0.3 % (w/v) Tris, 1.44 % (w/v), glycine, 0.1 % (w/v) SDS) in a SE250 Electrophorese Chamber (Hoefer Pharmacia Biotech Inc., San Francisco, CA, USA) until the dye bromophenol blue of the Laemmli sample buffer reached the bottom of the gel. Pre-stained PageRuler^{TM} was used as a protein ladder (10 to 180 kDa) (Thermo Fisher Scientific, Schwerte, Germany). Gels were stained with Quick Coomassie® Stain (SERVA Electrophoresis GmbH, Heidelberg, Germany) or used for immunodetection (western blot).

4.14. Immunodetection of proteins (Western blot)

For immunodetection, proteins separated in an SDS-PAGE gel were transferred to a nitrocellulose membrane according to the method of Towbin and coworkers (Towbin et al., 1979) in transfer buffer (0.582 % (w/v) Tris, 0.293 % (w/v), glycine, 0.375 % (w/v) SDS, 20 % (v/v) methanol) using a wet blotting system (Mini-PROTEAN® Tetra System Blotting Chamber (BioRad Laboratories GmbH, Munich, Germany) for 75 min at constant 60 V and 400 mA. The blotting membranes were blocked for 30 min at room temperature in 3 % (w/v) milk powder in 1x TBS buffer (50 mM Tris-HCl pH 7.5, 150 mM NaCl) under shaking.

The membranes were incubated for 1 h at RT or overnight at 4°C with the primary antibody solution diluted according to manufacturer's instructions. The membranes were washed three times for 10 min with 1x TBS and then incubated with the respective secondary antibody diluted according to manufacturer's instructions for 1 h at room temperature (Table 12). Subsequently, they were washed three times with 1x TBS buffer and once in Alkaline Phosphatase (AP) buffer (100 mM Tris-HCl, pH 9.5, 100 mM NaCl, 5 mM $MgCl_2$) each for 10 min or three times with 1x TBS buffer for HRP detection.

For colorimetric detection of AP activity, a detection solution containing AP buffer, 0.175 mg/mL X-phosphat or BCIP: 5-Bromo-4-chloro-3-indolyl phosphate; 50 mg/ml stock solution in ddH_2O (Carl Roth, Karlsruhe, Germany) and 0.338 mg/mL Nitro Blue Tetrazolium (NBT) (75 mg/ml stock solution in 70 % (v/v) dimethylformamide) (Carl Roth, Karlsruhe, Germany) were added to the membrane and incubated for approximately 10 min. For chemiluminescence detection with Horseradish peroxidase (HRP), detection was performed with SuperSignal™ West Femto Maximum Sensitivity Substrate (Thermo Fisher Scientific, Schwerte, Germany) in a Fusion Solo S (Vilber Lourmat GmbH, Eberhardzell, Germany) using the FusionCapt Advance Solo 7 (version 17.01) software.

Table 12. Primary and secondary antibodies

Primary antibody	**Buffer**	**Supplier**
Anti-GST	3% Milk in TBS buffer	(Ref:27-4577-01) Merck, Darmstadt, Germany.
Anti-MBP	3% Milk in TBS buffer	(Ref:E8032) New England Biolab Inc, Frankfurt, Germany
Anti-His_5	1% BSA in TBS buffer	(Ref:34660) Qiagen, Hilden, Germany
Anti- Thiophosphate ester	5% Milk in TBS buffer	(Ref:SD2020) Thermo-Fisher Scientific Invi-trogen, Schwerte, Germany
Secondary antibody	**Buffer**	**Supplier**
Anti-**Goat** IgG Alkaline Phosphatase Conjugated	3% Milk in TBS buffer	(Ref: A4187) Merck Darmstadt, Germany
Anti-**Mouse** IgG Alkaline phosphatase	3% Milk in TBS buffer	(Ref: A3562) Merck Darmstadt, Germany
Anti-**Rabbit** IgG HRP (Horsadish peroxidase) Conjugated	5% Milk in TBS buffer	(Ref: A6154) Merck Darmstadt, Germany

4.15. Enrichment of plant proteins by affinity chromatography

To enrich the proteins of interest, affinity chromatography was used to immobilize the tagged-protein in solution (mobile phase) to the solid support/resin (solid phase), then washed to remove other proteins, and finally the bound protein of interest was eluted from the resin to obtain the “enriched” protein fraction. The protein enrichment, thus, involved four main principal steps 1) Equilibration, 2) Sample loading, 3) Washing, 4) Elution.

4.15.1. Small scale protein enrichment

For the enrichment of CA-$_{6x}$His-MPK4, CA-$_{6x}$His-MPK4 or CA-$_{6x}$His-MPK6, 5 mL Pierce™ Centrifuge spin columns and HisPur™ Ni-NTA Resin (Thermo Fisher Scientific, Schwerte, Germany) were used. Briefly, 200 µL of resin were washed three times with 2 mL equilibration buffer (25 mM Tris HCl, pH 7.4, 75 mM NaCl, 10 mM imidazole) in a 15 mL falcon tube and centrifuged at 400 x g for 1 min at 4°C. Then, two mL of soluble fraction were incubated with the equilibrated resin for 1 h at room temperature in a vertical tube rotator and centrifuged. The flow-through was discarded, and the resins were washed three times with 2 mL washing buffer (50 mM Tris HCL, pH 7.4, 75 mM NaCl and 50 mM imidazole) (see chemicals Table 4). Finally, the bound proteins were recovered by adding 200 µL elution buffer (50 mM Tris HCl, 500 mM NaCl and 200 mM imidazole) and incubating for 10 min. Four elution fractions were collected, the flow-through was kept, and enriched proteins were checked by SDS-PAGE (see section4.13). Imidazole was removed by size exclusion chromatography on PD MiniTrap G-25 (Cytiva Lifesciences, Stockholm, Sweden) using a desalting buffer (20 mM Tris-HCl, pH 7.4, 500 Na Cl, glycerol 5 % (v/v)), according to the manufacturer’s "spin protocol".

4.15.2. Large scale protein enrichment

For larger-scale enrichment, an ÄKTA pure chromatography system (Cytiva Lifesciences, Stockholm, Sweden) equipped with a UV monitor with fixed 260nm/280 nm wavelengths was used to purify the proteins by affinity chromatography. Prior to use, all buffers were filtered on a 0.22 µm membrane Mixed Cellulose Ester filter (MCE) and degassed using a vacuum pump (Bottle-Top Vacuum Filtration Systems). The ÄKTA-system was always flushed with degassed ddH_2O, and pumps were also washed and purged before use to remove any residual air from the pump heads.

- **MBP-tagged proteins** - To enrich MBP-tagge proteins, a 5 mL MBPTrap HP and 50 mL Superloop™ (Cytiva Lifesciences, Stockholm, Sweden) were used. For equilibration a total volume of 5 CV (column volumes) of equilibration buffer (20 mM Tris-HCl, pH 7.4, 100 mM NaCl, 1 % (v/v) glycerol) was used. Then, 20 mL of the soluble fraction was injected through the injection valve using the superloop under a constant flow of 2 mL/min. Later, the column was washed with 5 CV equilibration buffer and the bound MBP-tagged protein was recovered by adding elution buffer (20 mM Tris-HCl, pH 7.4, 100 mM NaCl, 1 mM DTT, 1 % (v/v) glycerol and 10 mM maltose) in a 100% linear gradient. Approximately 20 elution fractions of 1 mL each, were collected in the fraction collector, and the proteins in each fraction were analyzed by SDS-PAGE. Finally, fractions were aliquoted, frozen in liquid nitrogen and stored at -80 °C.

- **His-tagged proteins** - His-tagged proteins were enriched on a 5 mL HisTrap HP and 50 mL Superloop™ (Cytiva Lifesciences, Stockholm, Sweden) were used. In brief, to strip off the nickel ions in the column and recharge it with new nickel ions, 5 CV of stripping buffer (50 mM EDTA, 0.5 M NaCl, 20 mM Na_2HPO_4) were added to the column at flow rate 3 mL/min and then 2.5 mL of nickel sulfate ($NiSO_4$ 0.1 M) was manually added via the injection valve with a 5 mL syringe (capillary loop must be connected) to recharge the column. Finally, washing buffer (50 mM Tris-HCl, pH 7.4, 75 mM, NaCl, 30 mM imidazole) was added to remove unbound nickel ions, and the column was stored in binding buffer for immediate use or in 20 % (v/v) ethanol for further use.

For equilibration, a total volume of 5 CV of equilibration buffer (25 mM Tris-HCl, pH 7.4, 75 mM NaCl, 20 mM imidazole) was applied. Then, 20 mL of the soluble fraction were injected through the injection valve using the superloop under a constant flow of 2 mL/min. Later, the column was washed with 5 CV washing buffer (50 mM Tris-HCl, pH 7.4, 75 mM NaCl, 30 mM imidazole), and the bound His-tagged proteins were recovered by adding elution buffer (50 mM Tris-HCl, pH 7.4, 500 mM NaCl, 500 mM imidazole) in a 100 % linear gradient. Approximately 20 elution fractions of 1 mL each were collected, and protein purity was analyzed by SDS-PAGE. Fractions were aliquoted, frozen in liquid nitrogen and stored at -80 °C.

To remove imidazole from the eluted fractions, a 5mL HiTrap desalting column was installed and the appropriate method selected in the UNICORN™ 7 control software. A volume of 2.5 mL of desalting buffer (20 mM tris pH 7.5, 0.5 M NaCl, 5 % Glycerol) was injected via a syringe to equilibrate the column (for this the capillary loop must be connected). The next method was selected to manually load the eluted protein in the injection valve, the eluted fractions were collected, and protein purity was analyzed by SDS-PAGE. Columns were regenerated using 5 CV of ddH_2O, NaCl 1.5 M, NaOH 0.5 M, ddH_2O and were stored in 20 % (v/v) ethanol.

4.16. Determination of protein concentrations

- Bradford assay: This colorimetric assay is based on the binding of the Coomassie Brilliant Blue G-250 dye to basic and aromatic amino acids residues in the protein and was used to determine unknown protein concentrations (Bradford, 1976). For this purpose, 10 µL of protein samples with unknown concentration were mixed with 990 µl of 1X Bradford reagent (5x Bradford reagent, SERVA Electrophoresis GmbH, Heidelberg, Germany) and incubated for 10 min at room temperature. Absorption was measured at 595 nm in a UV/VIS spectrometer (Ultrospec 2100 pro, Biochrom, Cambridge, United Kingdom). Relative protein concentrations were calculated using a standard curve from a bovine serum albumin (BSA)(Sigma-Aldrich, Munich, Germany). A calibration curve was generated according to SERVA Electrophoresis GmbH protocol (SERVA Electrophoresis GmbH, 2024).

- Densitometry: Protein concentrations were alternatively determined by using densitometry in SDS-PAGE gel, where BSA was used as external standard of known concentration. A BSA stock solution of 2 mg/mL was prepared and subsequently a working solution of 0.23 µg/µL BSA. Briefly, 5 serial dilutions 1:1 were prepared (0.23, 0.12, 0.06, 0.03, 0.014, 0.007 µg/µL) and 10 µL from each dilution were mixed 5 µL Laemmli buffer and run on SDS-PAGE gel. Densitometric analysis was performed in Image J software by calculating the peak area for each known BSA concentration and the intensities were used for estimation of unknown protein concentrations.

  For estimation of unknown protein concentrations not only the molecular weight of the BSA 66 kDa was considered but also the molarity (Equation 5). Since the

proteins of interest $_{6x}$His-MPK4, $_{6x}$His-MPK6 and MBP-PI4Kβ1 (42 kDa, 48 kDa and 168 kDa, respectively) have different molecular weights compared to the BSA, the appropriate standard BSA concentration with a comparable molarity to the proteins of interest was chosen (See Equation 6 for PI4Kβ1 and Equation 7 for MAPKs). Then, 10 µL from each protein sample were mixed 5 µL Laemmli buffer and run on SDS-PAGE gel (see section 4.13).

$$BSA\ [\mu M\ or\ \mu mol/L] = \left(\frac{BSA\ [\mu g]}{BSA\ Molarity\ [66.500\ \mu mol/\mu L]}\right) x10^6$$

Equation 5

$$Unknown\ PI4K\beta 1\ [\mu g/\mu L] = \left(\frac{\left(\frac{Band\ intensity\ PI4K\beta 1\ x\ BSA\ [0.6\ \mu g]}{BSA\ Band\ intensity}\right)}{Volume\ loaded\ in\ SDS-PAGE\ [\mu L]}\right)$$

Equation 6

$$Unkown\ MAPKs\ [\mu g/\mu L] = \left(\frac{\left(\frac{Band\ intensity\ MAPK\ x\ BSA\ [1.2\ \mu g]}{BSA\ Band\ intensity}\right)}{Volume\ loaded\ in\ SDS-PAGE\ [\mu L]}\right)$$

Equation 7

Where:

BSA [µg]: Is the concentration of BSA in [µg] used for the SDS-PAGE.

BSA Molarity: Is the molarity of BSA expressed in µmol/ µL.

Band Intensity PI4Kβ1: Is the band intensity obtained by densitometric analysis from the SDS-PAGE.

BSA [0.6 µg]: Is the concentration of BSA used to calculate unknown concentrations of PI4Kβ1.

BSA [1.2 µg]: Is the concentration of BSA used to calculate unknown concentrations of MAPKs.

Volume loaded in SDS-PAGE: Total volume loaded on the SDS-PAGE gel in µL (here 10 µL)

4.17. *In vitro* lipid kinase assay for PI4Kβ1 activity

4.17.1. Estimation of PI4Kβ1 lipid kinase activity *in vitro*

For estimation of the total lipid kinase activity for MBP-WT-PI4Kβ1, substitution variants or truncated variants, a 50 µL reaction mixture was prepared : 20 µL of lipid buffer (10 µL

75 mM $MgCl_2$, 1 µL 50 mM Na-Molybdate, 1 µL 50 mM ATP, 1 µL 10 µCi γ[^{32}P]ATP, 2 µL of 30 mM Tris, pH 7.2, and 5 µL of PtdIns/Triton x-100 mixed micelles containing 12 µg or 0.3 mM Soy PtdIns, was mixed with 30 µL of protein solution (0.0002 mg enriched PI4Kβ1 and 30 mM Tris HCl pH 7.2, 10 mM $MgCl_2$, 0.1 mM EDTA, DTT 1 mM). PtdIns/Triton x-100 micelles were prepared by evaporating 1.2 µL of a 10 mg/mL soybean PtdIns stock solution (Avanti Polar Lipids Inc., Merck, Darmstadt, Germany) and then solubilized in 5 µL of 2% triton x-100. The mixture was sonicated in ice bath for 10 min and added to the lipid reaction mixture. The reaction was incubated at RT for 15 min and stopped by adding chloroform: methanol (v/v 1:2). Lipids were extracted, separated in a TLC plate and analyzed by phosphorimaging (Section 4.17.4)

4.17.2. Lipid extraction and thin layer chromatography (TLC)

Lipids were extracted using a biphasic solvent mixture 2:1 (v/v) of chloroform/methanol as originally established by Folch *et al*., 1956 (Folch et al., 1957). For this purpose, 1.5 mL of chloroform:methanol (1:2, v/v), 500 µl of 2.4 M hydrochloride acid solution and 250 µL of 0.5 M EDTA, pH 8.0 were added in a glass tube to the reaction solution and mixed. The suspension was mixed and 500 µL of chloroform were added to the test tube and the sample mixed again. When two different phases were visible, the lower (organic) phase containing the lipids was transferred to a new glass tube. The remaining sample was re-extracted by adding 500 µL of chloroform, mixed and the lower phase was combined with the previously extracted chloroform layers.

The chloroform was evaporated under streaming air for 45 min in a Reacti-Therm™ module (ThermoScientific, Henningsdorf, Germany), the dried lipids were resuspended in 20 µL chloroform and spotted 2 cm above the bottom end of a TLC plate (TLC plate Silica, 20 x20 cm; 60 Å pore diameter, Sigma-Aldrich, Munich, Germany). Before running the TLC plate, the developing chamber was equilibrated (Saturated) with 100 mL of the mobile phase containing Chloroform/methanol/ammonium hydroxide/H_2O 86:76:6:16 (v/v/v/v) and Whatman® paper, to allow the uniform distribution of the solvent. Then, the TLC plate was developed for 45-50min, air-dried, covered in plastic wrap and lipids were detected by phosphorimaging (See Section 4.17.4)

4.17.3. Calibration curve of radiolabeled γ[^{32}P]ATP

To estimate the concentrations of γ [^{32}P]ATP (Hot ATP) incorporated into PtdIns or phosphorylated proteins, we performed 25 serial dilutions in duplicates in a ratio 1:1 in 1.5 mL reaction tubes. For this purpose, 1 µL of hot ATP stock solution (Ref: SRP-501; specific activity: 6000 Ci/mmol; radioactive concentration: 10 µCi/µL; molarity: 1.67 µM)

was mixed with 1 µL ddH_2O. Subsequently, 1 µL was spotted in duplicates on a TLC plate, and immediately a phosphor-imaging screen was exposed for 25 min. The screens were scanned and the intensities of each spot corresponding to the different concentrations of hot ATP were collected.

The highest hot ATP final concentrations of the dilution series (33, 16, 8, 4, 2, 1, 0.5, 0.26, 0.13 , 0.07, 0.03,0.02,0.01 and 0.004 nM) exhibited intensities above the intensity values obtained in our lipid sample. However, the lowest concentrations (2034, 1017, 508, 254, 127, 63, 31, 15 and 7.9 fM) showed intensity values falling in the range of our phosphorylated lipid samples. Therefore, a calibration curve was built by plotting the intensity values versus the lowest nine ATP concentrations used for calibration. Data points were fitted by linear regression analysis, and the slope (m) and the intercept of the linear relations with the Y-axis (b) were used to estimate molar lipid kinase activities (Appendix Figure 35).

4.17.4. Quantification of phosphorylated lipids by phosphorimaging .

The TLC plate was placed in a phosphor screen cassette with a phosphor-imaging screen on top and exposed for 25 min. The screens were scanned with an Amersham™ Typhoon™ Biomolecular Imager (Cytiva Lifesciences, Stockholm, Sweden) (PTM sensitivity of 4000 V; pixel size 100 µm) and visualized by phosphorimaging. The radioactive intensities were analyzed using ImageQuantTL software V10.1 (Cytiva Lifesciences, Stockholm, Sweden) (see Appendix Table 20). In brief, the phosphorimage-file was opened, vertical lanes were created automatically, the background subtracted by using the rolling ball method (radius 6), band peaks were manually selected and volume values (intensity) under the peak of the lipid samples were compared to the standard curve to determine the concentration of γ[^{32}P]ATP incorporated into PtdIns or the specific activity, expressed here in mmol PtdIns4P min^{-1} mg^{-1} as indicated below.

4.17.5. Determination of PI4Kβ1 activity for Initial velocity (V_0) for PI4Kβ1

One unit (U) of enzyme was defined as the amount of enzyme [mg] that catalyzes the incorporation of 1 mmol of phosphate into the substrate PtdIns in 1 minute. The amount of product produced per unit time at the start of the reaction is called the initial velocity V_0. Since it was determined here that 15 min was the time point at the beginning of the linear range, all the reactions were stopped at 15 min. The specific activity for the initial velocity (V_0) was expressed in 1 mmol PtdIns4P min^{-1} mg^{-1} and was calculated according to the following Equation 8:

$$V_0 = \left(\frac{\left(\frac{Intensity\ PtdIns4P - b}{m} \right)}{Time\ (\min)\ x\ Reaction\ volume\ (L)\ x\ Protein\ [mg]} \right) x\ 10^{-12}$$

Equation 8

Where:

Intensity PtdIns4P: Is the signal intensity obtained by phosphorimaging of the product of the reaction in the TLC plate

b: is the y-intercept of the line, obtained here in the calibration curve (See Appendix Figure 35)

m: m is the slope of the line, obtained here in the calibration curve (See Appendix Figure 35)

Time: Is the total time of the kinase reaction in minutes

Reaction volume: Is the total reaction volume in Liters

Protein: Is the total PI4Kβ1 concentration used for the assay in [mg]

10^{-12} : Exponential expression used to convert fM units (calibration curve) to mmol/mg.

4.17.6. Confirmation of lipid Identity and Lipid Integrity

The identity of the lipid product, phosphatidylinositol 4-phosphate (PtdIns4P) (sometimes also referred as PIP4P) was assessed by TLC-analysis comparing the relative migration of bona fide standard lipids (PtdIns, PtdIns4P or PtdIns(4,5)P_2) with that of the radiolabeled lipid product. For this purpose, the standard lipids and unknown lipid samples were resolved on the same TLC plates, i.e. under identical conditions. In brief, 5 µL of each 1 mg/mL lipid standard stock solution and 20 µL of unknown radiolabeled lipids previously extracted and solubilized in chloroform were loaded at the bottom of the TLC plate and run for 50 min as described in Section 4.17.2. To visualize the separated lipids, the TLC plate was cut in two parts, the side containing the standard lipids was submerged for 10 s in a 10 % (w/w) CuSO4, 8 % (w/w) H_3PO_4 solution, air-dried and heated at 180 °C on a heating plate until the standards became visible as charred bands. The radioactive part of the TLC plate visualized by phosphorimaging (Section 4.17.4).

4.17.7. Reaction progress curve: estimation of linear range

To characterize the lipid kinase activity of MBP-WT-PI4Kβ1 we used radiolabeled [γ-^{32}P] ATP in a kinase reaction containing the lipid kinase and the PtdIns, as initially described for lipid kinases (M. H. Cho & Boss, 1995). Initially, a 50 µL reaction mixture was prepared in glass tubes, containing 20 µL of lipid buffer (10 µL 75 mM $MgCl_2$, 1 µL 50 mM Na-Molybdate, 1 µL 50 mM ATP, 1 µL 10 µCi γ [^{32}P]ATP, 2 µL of 30 mM Tris, pH 7.2, and 5 µL of PtdIns/Triton-x100-mixed micelles containing different soybean PtdIns concentrations) was mixed with 30 µL of protein solution (containing different PI4Kβ1 concentrations and

30 mM Tris, pH 7.2)(see below). PtdIns/Triton-100-micelles were prepared before use by evaporating 0.6 µL (or more depending on the desired concentrations) of a 10 mg/mL soy bean PtdIns stock solution (Avanti Polar Lipids Inc., Merck, Darmstadt, Germany). The dried PtdIns was solubilized in 5 µL of 2 % (v/v) Triton x-100 in ddH_2O. The mixture was sonicated on ice for 10 min and then added to the lipid reaction mixture.

To ensure that the kinase reaction was monitored in the linear range, we tested three different PtdIns concentrations (0.1, 0.3 and 0.4 mM) against a constant 0.0005 mg PI4Kβ1 and 1 mM ATP, or three different PI4Kβ1 protein concentrations (0.0006, 0.0015 and 0.0025 mg) against a constant 0.1 mM PtdIns and 1 mM ATP. A ratio of 1:1 for cold and hot radiolabeled [γ-^{32}P]-ATP was used. Reactions were incubated at room temperature for 1h, and were stopped by adding chloroform:methanol (1:2, v/v). Lipids were extracted (see section 4.17.2), separated by TLC and analyzed by phosphorimaging (Section 4.17.4).

Once the linear range for the protein and lipid concentrations was determined, a reaction progress curve was obtained where the reaction was stopped at different time points (0, 10, 20, 30, 40, 50, 60, 70, 80, 90 min), using constant 0.0009 mg PI4Kβ1, 0.3 mM PtdIns and 1 mM ATP. The kinase reactions were incubated at room temperature and stopped by adding chloroform:methanol (1:2, v/v). Lipids were extracted, separated by TLC and analyzed by phosphorimaging (see Sections 4.17.2 and 4.17.4)

4.17.8. Estimation of kinetic parameters of MBP-PI4Kβ1

A discontinuous method (also called endpoint") was used to measure the amount of product (PtdIns4P) formed during the kinase reaction over a fixed period of time, 15 min (linear range estimated in Section 4.17.7). For the estimation of kinetic parameters (V_{max} and K_m / $K_{0.5}$) increasing concentrations of PtdIns were used with a constant ATP concentration of 1 mM and a constant PI4Kβ1 protein amount of 0.0009 mg per assay. The molarity concentrations of PtdIns Soy used in the assays were calculated according to Equation 9 and Equation 10.

$$PtdIns\ [\mu M\ or\ \mu mol/L] = \left(\frac{PtdIns\ Soy\ [\mu g/\mu L]\ x\ Volume\ [\mu L]}{Molarity\ PtdIns\ Soy\ [\mu g/\mu mol]\ x\ Reaction\ volume\ [\mu L]}\right) x\ 10^6$$

Equation 9

$$PtdIns\ [mM\ or\ mmol/L\ ] =\ PtdIns\ [\mu M]\ x\ 10^{-3}$$

Equation 10

Where:

PtdIns Soy: Is the concentration of the stock solution in [µg/µL]

Volume: Is the volume taken from the stock solution and evaporated in [µL].

Molarity PtdIns Soy: is the molarity of the PtdIns Soy in [µg/ µmol]

Reaction volume: Is the total kinase reaction volume in [µL]

10^6 : Exponential expression used to convert µmol/µL to µmol/L.

10^{-3} : Exponential expression used to convert µM to mM

Alternatively, to determine the affinity for the co-substrate, ATP, increasing ATP concentrations were tested with constant saturating concentrations of 1.2 mM PtdIns and a constant PI4Kβ1 protein amount of 0.0009 mg per assay. The final molarity concentrations in the kinase reaction, of radiolabeled ATP (Equation 11), cold ATP (Equation 12), total ATP (Equation 13), ratio of ATP hot:cold (Equation 14) and calculation of molarity for hot ATP (Equation 15), are shown below:

$$Cf\ Hot\ ATP\ [nM\ or\ nmol/L] = \left(\frac{Ci\ [\mu M]\ x\ Volume\ [L]}{Reaction\ volume\ [L]}\right) x10^3$$

Equation 11

$$Cf\ Cold\ ATP\ [\mu M\ or\ \mu mol/L] = \left(\frac{Ci\ [mM] x\ Volume\ [L]}{Reaction\ volume\ [L]}\right) x\ 10^3$$

Equation 12

$$Total\ ATP\ [\mu M\ o\ \mu mol/L] = Hot\ ATP\ [nM]\ x10^{-3} + Cold\ ATP\ [\mu M]$$

Equation 13

$$Ratio\ Factor\ [Cold: Hot]\ ATP = \frac{Cold\ ATP\ [1000\ \mu M]}{Hot\ ATP\ [0.0333\ \mu M]}$$

Equation 14

$$Hot\ ATP\ [\mu M\ o\ \mu mol/L] = \left(\frac{Radioactive\ Concentration\ [mCi/mL]}{Specific\ Activity\ [Ci/mmol]}\right) x\ 10^{-3}$$

Equation 15

Where:

Cf: Final concentration of hot ATP in [nM] or cold ATP in [µM] in the kinase reaction

Ci: Initial concentration of hot ATP in [µM] or cold ATP in [mM]

Volume: Is the volume taken from the ATP stock solution

Reaction volume: Is the total kinase reaction volume in [µL]

10^3: Exponential expression to convert [µM] to [nM] of hot ATP and [mM] to [µM] of cold ATP.

Radioactive concentration: Provided by Hartmann analytics ref. [SRP-501]

Specific activity: Provided by Hartmann analytics ref. [SRP-501]

10^{-3}: Exponential expression to convert [mM] to [µM] of hot ATP

Concentrations and volumes used for both saturation curves are shown in Table 13 (Section "*Molarity PI"). Lower concentrations of hot and cold ATP were obtained by serial dilutions 1:1. PtdIns/Triton x-100 micelles were prepared as described above.

The reaction was incubated at RT for 15 min and stopped by adding chloroform: methanol (v/v 1:2). Lipids were extracted, separated on a TLC plate (Section 4.17.2), and analyzed by phosphorimaging (Section 4.17.4)

The sigmoidal response curve is typically represented by the Hill equation given below:

$$Y = \left(\frac{I^{\eta_H}}{K_{0.5}^{\eta_H} + I^{\eta_H}}\right)$$

Equation 3

Where *Y* = output response; *I* = input concentration. n^H = Hill coefficient and $K_{0.5}$= half-saturation constant

The Hill coefficient characterizes the degree of cooperativity, where the initial binding of a ligand to the enzyme enhances the binding of the next ligand. The measure of cooperativity can be quantified based on the steepness of the curve (Goldbeter & Dupont, 1990; Somvanshi & Venkatesh, 2013) A Hill coefficient, that is nH < 1, indicates negative cooperativity where binding of one ligand decreases the affinity for the binding of the next ligand. A Hill coefficient nH > 1 leads to a sigmoidal response. The stronger the co-operativity the stronger the sigmoidicity of the kinetic binding curve (Goldbeter & Dupont, 1990).

Table 13. Concentrations of PI and ATP used for estimation of kinetic parameters**.**

Lipid Soy PI				Cold ATP			Hot [γ-^{32}P]-ATP			Final [µM] Cold + Hot ATP
PI Stock [µg/µl]	Volume from stock (µL)	PI [µg]	*Molarity [mM]	Cold ATP Stock [mM]	Volume from stock (µL)	*Molarity [µM]	Hot ATP Stock [µM]	Volume from stock (µL)	*Molarity [µM]	
	14.4	144	3.2	50	4	4000	1.67	4	0.1333	4000
	12.6	126	2.8	50	2	2000	1.67	2	0.0667	2000
	9.0	90	2.0	50	1	1000	1.67	1	0.0333	1000
	7.8	78	1.8	25	1	500	0.83	1	0.0167	500
	5.4	54	1.2	13	1	250	0.42	1	0.0083	250
	4.2	42	0.9	6	1	125	0.21	1	0.0042	125
	3.1	31	0.7	3	1	63	0.10	1	0.0021	63
	1.9	19	0.4	1.6	1	31	0.05	1	0.0010	31
10	0.6	6	0.1	0.8	1	16	0.03	1	0.0005	16
				0.4	1	8	0.01	1	0.0003	8

*Molarity concentrations for PI (PtdIns) and ATP are expressed as final concentration in a final reaction volume of 50 µL

The half saturation constant quantifies the substrate concentration at which half of the active sites of the enzyme are occupied by the ligands (Somvanshi & Venkatesh, 2013)

The estimation of Hill kinetic parameters can be obtained by linearizing the equation as indicated below (Endrenyi et al., 1975; Somvanshi & Venkatesh, 2013):

$$ln\left(\frac{Y}{1-Y}\right) = \eta_H \, ln \, I - \eta_H \ln K_{0.5}$$

Equation 4

Where *ln* = Natural logarithm; Y = output response ; n^H = Hill coefficient; *I* = input concentration. and $K_{0.5}$= half-saturation constant

Then, by plotting the left part of the equation on the Y-axis, against the natural logarithm of I ($ln\ I$) on the X-axis, we can calculate the Hill coefficient as the slope of the curve and the intercept of Y-axis can be used to estimate the half-saturation constant ($K_{0.5}$) (Coval, 1970; Endrenyi et al., 1975; Somvanshi & Venkatesh, 2013).

4.18. *In vitro* protein phosphorylation assays

4.18.1. Radioactive *in vitro* protein phosphorylation assay

Initially, a time- course *in vitro* radioactive phosphorylation was performed to test whether the reaction conditions would indicate the linear range of phosphorylation, in principle to ensure that ATP was not limiting and that there were no inhibitors that could impair the reaction. In brief, the reactions were performed in 30 µL reaction buffer containing 30 mM Tris HCl pH 7.5, 10 mM $MgCl_2$, 0.1 mM EDTA, DTT 1 mM and 0.75 µL of 10 µCi/µL γ[^{32}P]ATP and 0.15 µL of 10 mM of cold ATP. Initially, soluble fractions containing MBP- PI4Kβ1 and enriched CA-$_{6x}$His-MPK4 or CA-$_{6x}$His-MPK6 were used in a ratio of 9:1 (w/w, 1.7 µg vs. 0.2 µg) for the protein kinase reactions. The reactions were incubated for 0, 10, 20, 30, 40, 50, 60, or 70 min at room temperature and stopped by adding 1 x Laemmli buffer. The protein samples were separated on pre-cast SDS-PAGE gels (SERVA Gel^{TM} TG PRIME^{TM}, SERVA Electrophoresis GmbH, Heidelberg, Germany) and the gels were stained over night as described in section 4.13. The gels were dried at 80 °C using a gel dryer 4050 D (UniEquip, Munich, Germany) connected to a vacuum pump. The dried gels containing radiolabeled phosphorylated proteins were placed in a phosphor screen cassette with a phosphor screen over the gel and exposed for 2 h. The screens were scanned with an Amersham™ Typhoon™ Biomolecular Imager (Cytiva Lifesciences, Stockholm, Sweden). The radioactive signal intensities were analyzed using ImageQuantTL software (Cytiva Lifesciences, Stockholm, Sweden) (Section 4.17.4)

Once the conditions for the linear range of the phosphorylation reactions were found, further *in vitro* protein phosphorylation assays were performed as described above, only that reactions were incubated for only 20 min at room temperature.

For MS-based phosphopeptide analysis, the same *in vitro* phosphorylation reactions were performed but using only cold ATP instead of radiolabeled ATP, and reactions were incubated at 23°C for 30 min.

4.18.2. Non-radioactive *in vitro* phosphorylation assay

Similarly, following the method by Allen et al., 2007 non-radioactive protein phosphorylation tests were performed in 20 µL reaction buffer as described above, but instead of radiolabel containing 1 mM γS-ATP (Sigma Aldrich, Munich, Germany), which is used by the upstream kinase to thiophosphorylate its substrate (Allen et al., 2007). Reactions were incubated at 30 °C for 30 min and stopped by adding 20 mM EDTA, pH 8.0. Then, an alkylation reaction was performed by adding 2.5 mM p-nitrobenzyl mesylate

(PNBM) (Abcam, Cambridge, United Kingdom) to convert the thiophosphate groups to thiophosphate esters on the modified protein, which can then be detected by the α-Thiophosphate ester-specific antibody. Samples were mixed, incubated for 1-2 h at room temperature or over night and stopped by adding 1x Laemmli buffer. Samples were loaded on pre-cast SDS-PAGE Gels (SERVA Gel™ TG PRIME™, SERVA Electrophoresis GmbH, Heidelberg, Germany) and proteins were separated (See Section 4.13) and the thiophosphorylated proteins detected by Western blotting and a chemiluminescent detection, as described above (see Section 4.14)

4.19. Identification of phosphorylation sites on MBP-PI4Kβ1 by Mass Spectrometry

Mass spectrometry experiments were performed in cooperation with Dr. Dirk Dobritzsch and Dr. Matthew Fuszard from the MLU Core Facility Proteomic Mass Spectrometry. In brief, to determine phosphorylation sites in target proteins, *in vitro* phosphorylation reactions were performed using cold ATP (see Section 4.18.1), then separated by SDS-PAGE, stained with Coomassie blue and bands corresponding to MBP-PI4Kβ1 were excised. Excised bands were reduced, alkylated, digested with trypsin, and the tryptic peptides were extracted with extraction buffer (1:2 (v/v) 5% formic acid/acetonitrile (ACN)). Subsequently, buffers and contaminants that interfere with downstream MS were removed by using Pierce® C18 Tips following by the Universal solid-phase protein preparation (USP^3). Samples were analyzed using MALDI-MS Orbitrap Fusion Lumos Tribrid Mass Spectrometer (Fisher Scientific, Schwerte) and phosphorylated proteins were identified using the software Proteome Discoverer Version 2.5 (see Appendix Table 20). The key experimental steps are described in more detail in the following paragraphs.

4.19.1. In-gel reduction, alkylation, tryptic digestion

The in-gel digestion protocol used for this thesis was initially described by (Shevchenko et al., 1996) and later optimized to obtain higher yields of tryptic peptides (Shevchenko et al., 2007). In brief, *in vitro* phosphorylation assays were first performed as described in Section4.18.1. A control was included incubating MBP-PI4Kβ1 alone, without any upstream protein kinase present. Proteins were separated by SDS-PAGE, the protein gels were stained for 2 h using fresh Coomassie blue dye and washed three times for 2 h with ddH_2O. The protein gels were transferred into a plastic bag, bands corresponding to MBP-PI4Kβ1 were excised with a clean scalpel (cubes ca. 1 x 1 mm) and placed in LoBind

reaction tubes (Eppendorf, Hamburg, Germany). Subsequently gel pieces were incubated with ammonium bicarbonate/ACN (1:1, v/v). Then, ACN was added until pieces became white and shrinked. ACN was removed, and trypsin buffer (13 ng μL^{-1} 1 trypsin in 10 mM ammonium bicarbonate containing 10% (v/v) ACN) added to completely cover the dry gel pieces and the mixture was incubated for 120 min on ice. During this step, the endopeptidase trypsin cleaves at the C-terminal position after the basic amino acids arginine and lysine. Later, ammonium bicarbonate buffer (10 mM DTT in 100 mM ammonium bicarbonate) was added and samples were incubated over night at 37 °C. Tubes were chilled at room temperature, gel pieces spined down using a microcentrifuge, and 1.5 mL aliquots were collected from the supernatants.

4.19.2. Extraction of digested peptides for LC MS/MS analysis

To extract the tryptic peptides from the digest reactions, extraction buffer was added (1:2 - v/v of 5 % (v/w) formic acid/ACN) and samples were incubated for 15 min at 37 °C in a shaker. Supernatants were collected into a 250 µl PCR tube and dried in a vacuum centrifuge. For LC MS/MS analysis, 0.1 % (v/v) trifluoroacetic acid (TFA) was added, the reaction mixed and incubated for 2–5 min in a sonication bath and sedimented for 15 min (9,408 x g.). A 10 µL aliquot was then used for MS analysis. The remaining samples was dried down in a vacuum centrifuge and stored at 20 °C.

4.19.3. Sample preparation: USP^3 using Pierce® C18 Tips

Sample preparation is essential to remove several contaminants, such as lipids, nucleic acids, or detergents present in samples that can interfere with enzymatic digestion and MS analysis. Here, the USP^3 method was used for protein sample preparation, as described before (Dagley et al., 2019; Hughes et al., 2019).

Pierce reversed-phase C18 Tips were used to remove interfering contaminants and obtain peptides in MS-compatible solutions, enabling the acquisition of high-quality spectra. The method described by thermo Scientific (reference: 87781) was followed. In brief, samples were adjusted to 0.1-1.0% TFA using 2.5% TFA. Then, the tip was equilibrated by aspirating 10 µL of 50% ACN in water and then discarding the solvent. The step was repeated once. 10 µL of sample was taken into the C18 tip. The tip was rinses by aspirating 10 µL of 0.1% TFA/5% ACN and the solvent was discarded. This step was repeated once. Samples were eluted according to the analysis desired: for MALDI-TOF 2-10µL of 0.1% TFA was aspirated in 50-95% ACN elution solution with or without matrix and dispensed directly onto a MALDI plate. For LC/MS or LC/MS/MS, 2-10µL of 0.1% formic acid or 0.1% acetic acid was

aspirated in a 50-95% ACN or methanol and dispensed into an autosampler vial or well plate.

In brief, commercially available magnetic beads were freshly prepared by rinsing with MiliQ waters at a stock concentration of 20 µg/µL (Sera-Mag Speed beads GE Healthcare). Then, 4 µL of the beads were used per 50 µL (or 200 µL) of protein. Beads were added to all samples along with a final ACN concentration of 70 % and incubated for 20 min at room temperature. Samples were placed in a magnetic rack and ACN was removed by evaporation.

4.19.4. MS spectrometry analysis for phosphopeptides

A liquid chromatography (LC) system UltiMate 3000 UHPLC coupled to the Orbitrap Exploris ™ 480 Mass Spectrometer (MS) (Thermo Scientific, Dreireich, Germany) was used here. Tryptic peptides were analyzed with a data dependent acquisition (DDA) scan strategy with inclusion list to specifically select and isolate MBP-PI4Kβ1-derived phosphopeptides for MS/MS peptide sequencing. The LC system was equipped with a Trap Column C18 (300 µm x 5 mm) and an analytical waters ACQUITZ UPLC column M-class peptide BEH C18 (130 0 Å, 75 µm x 250 mm). A 70 minute run was executed with 60 min gradient as follows: 10min 3% B, 10-51 min 3% to 25% B, 51-55 min 25%-50% B, 55-57 min 50-80% B, 57-59 min 80% B, 60- 70 min 3% (A:Water and B: ACN).

MS/MS spectra were used to search the “The Arabidopsis Information Resource (TAIR10) database (ftp://ftp.arabidopsis.org)” for PI4Kβ1 sequences with the Proteome discoverer 2.5 integrated with a tool IMP-ptmRS to localize the modification sites within peptide sequences obtained after the fragmentation technique HCD. High field asymmetric waveform ion mobility spectrometry (FAIMS) ion mobility was set at -35 CV. The MS scan “Scan MasterScan” contained a orbitrap resolution of 120000, scan range (m/z) set at 350-1450 and a positive polarity. The MS/MS “Scan ddMSnScan” contained a resolution of 30000, a HCD collision energy of 31% and a isolation window (m/z) of 1.4. The measurements and data analysis was performed by Dr. Mattew Fuszard (MLU Core Facility Proteomic Mass Spectrometry).

4.20. Identification of phosphorylation sites on PI4Kβ1 by Peptide Microarrays

In order to find phosphorylation sites in PI4Kβ1 that are targeted by the CA-$_{6x}$His-MPK4 or by CA-$_{6x}$His-MPK6, Custom PepStar™ Peptide Microarrays (JPT peptide technologies Inc,

Berlin, Germany) were used. The microarrays, consisted of a collection of 13-mer oligopeptide sequences that were immobilized on glass slides, with a shift of two amino acids and an overlap of 11-mers, covering the full amino acid sequence of the PI4Kβ1 sequence. The glass slides contained the spotted peptide arrays as three identical sub-arrays, each one subdivided in 16 individual block with triplicate spots representing a single individual peptide. A schematic representation of the method can be seen below (Figure 33).

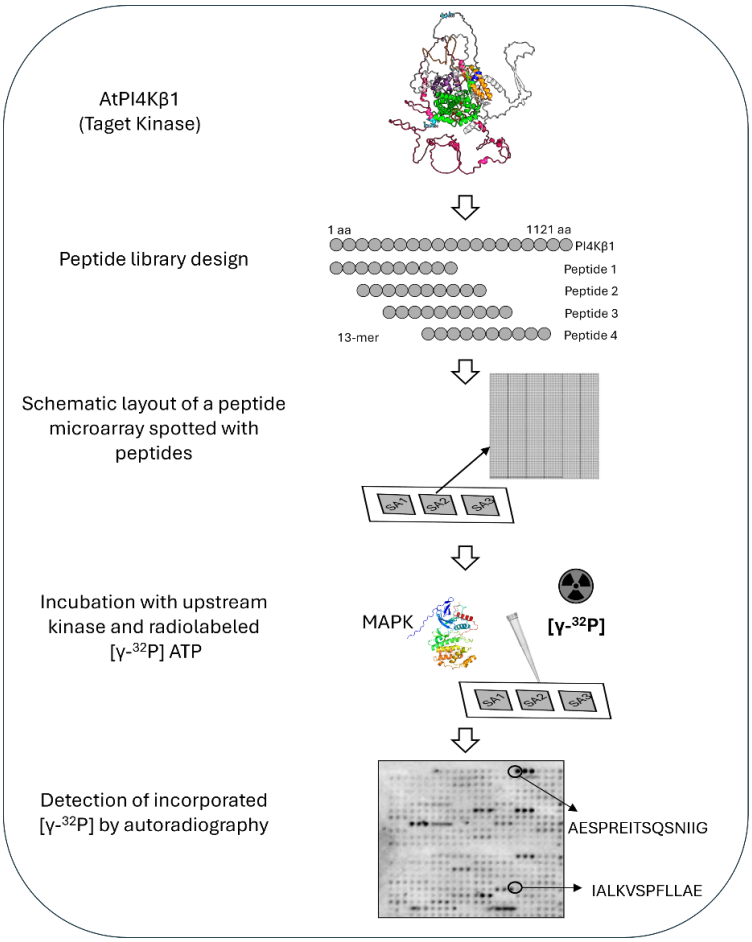

Figure 33.Schematic representation of a protein kinase assay using peptide microarrays. Peptide collections representing the PI4Kβ1 protein were spotted in triplicates on glass slides, followed by the incubation with a purified upstream MAPK under specific reaction conditions. The radiation emitted by each individual spot, indicates peptide phosphorylation which is detected by phosphorimaging using Amersham™ Typhoon™ Biomolecular Imager.

For this purpose, a microarray-chip-sandwich was assembled by placing the PepStar™ slide on the bottom (peptides facing upwards) and a blank glass slide on top. The two slides were separated by spacers. In brief, a 400 µL kinase reaction containing 0.5 µL of 10 mM cold ATP, 40 µL 10x Protein Kinase (PK) NEB buffer (500 mM Tris-HCl, pH 7.5, 100 mM $MgCl_2$, 1 mM EDTA, 20 mM DTT, 0.1% (w/v) Brij 35), 200 µL of γ [^{33}P] ATP 10 µCi/µL, 40 µg

of CA-$_{6x}$His-MPK6 and 2% BSA were placed into the reaction chamber formed by the two slides. The microarrays were incubated for 2 h at 30 °C and the reaction was stopped by quickly submerging the slides 5 times in 2 % (w/v) of phosphoric acid. Slides were submerged 5 times in dd H_2O and the process was repeated 3 times with fresh water. Subsequently, the slides were submerged 5 times in 100 % methanol and left to dry under a fume hood for 30-60 min. Finally, a phosphor-imaging screen was exposed on the peptide microarray overnight. The screens were scanned with an Amersham™ Typhoon™ Biomolecular Imager (Cytiva Lifesciences, Stockholm, Sweden).

4.21. Effect of protein phosphorylation on PI4Kβ1 function

4.21.1. Effect of *in vitro* MAPKs phosphorylation on lipid PI4Kβ1 activity

To test for effects of protein phosphorylation on the catalytic activity of the enriched MBP-PI4Kβ1 protein, three phospho-mimetic (MBP-PI4Kβ1 S186D; MBP-PI4Kβ1 S454D; MBP-PI4Kβ1 S186D S454D) and three phospho-ablation variants (MBP-PI4Kβ1 S186A; MBP-PI4Kβ1 S454A; MBP-PI4Kβ1 S186A S454A), *in vitro* lipid kinase activity assays were performed (see section4.17), but in this case using PI4Kβ1 variants pre-phosphorylated by upstream CA-$_{6x}$His-MPK4 or CA-$_{6x}$His-MPK6. The pre-phosphorylation was achieved by incubating the MBP-PI4Kβ1 variants with the MAPK-variants for 20 min at room temperature in 30 µL of protein solution containing 0.2 µg enriched PI4Kβ1, 1.8 µg enriched MAPK, 30 mM Tris-HCl, pH 7.2, 10 mM $MgCl_2$, 0.1 mM EDTA, 1 mM DTT and 50 µM cold ATP. After this pre-incubation, 20 µL of lipid buffer (see section 4.17.1) was added to the pre-phosphorylation reaction and the mixture incubated for 15 min at room temperature. The reaction was stopped, lipids extracted, separated by TLC plate and analyzed by phosphorimaging (see sections 4.17.2 and 4.17.4)

4.21.2. Effects of amino acid substitutions on MBP-PI4Kβ1-lipid interactions

In vitro lipid overlay assays were performed to assess protein-lipid interactions of MBP-PI4Kβ1 variants. For this purpose, a nitrocellulose membrane (5.5 x 2.8 cm) was prepared, and 10 equally distributed pencil circle spots were marked. Then, 3 µg of PtdCho, PtdEtn, PtdIns, PtdSer, PtdOH, PtdIns3P, PtdIns4P, PtdIns5P, PtdIns(3,5)P_2, or PtdIns(4,5)P_2 were spotted on the membrane. All lipids were obtained from Avanti Polar Lipids Inc. (Merck, Darmstadt, Germany).The membranes were dried at room temperature for 20 min in the dark and were then blocked with 7 mL of blocking buffer (3% (w/v) fatty acid-free BSA

dissolved in 1x TBS-T, 0.1 % (v/v) Tween) for 30 min at room temperature. The blocking solution was discarded and the lipid-protein-binding solutions containing 0.5 µg/mL of enriched proteins of interest were prepared in 3 % (w/v) fatty acid-free BSA dissolved in 1 x TBS buffer. The membranes were incubated shaking with the protein-binding solutions for 2 h (or overnight at 4°C). The fat blot was washed 3x for 10 min with 1x TBS buffer and incubated for 2 h at room temperature with 7 mL of primary antibody solution containing 3 % (w/v) fatty acid-free BSA in 1x TBS. Subsequently, the solution was discarded, the membrane washed 3x and incubated for 1 h at room temperature with 7 mL of secondary antibody solution containing 3 % (w/v) fatty acid-free BSA in 1x TBS (Table 12). The blot was washed 3x and finally incubated with 10 mL of the AP colorimetric solution (See section 4.14)

Alternatively, lipid overlay assays were also performed using commercial "PIP strips" (#P-6001, Echelon Biosciences Inc., MoBiTec, Göttingen, Germany). PIP strips are available with 15 different lipids dotted on a nitrocellulose membrane containing 100 pmol of lipid per spot. In addition to the 10 lipids contained in the self-spotted blots described above, the commercial PIP strips also contained lyso-PtdOH, lyso-PtdCho, sphingosine 1-phosphate (S1P), PtdIns(3,4)P_2 and PtdIns(3,4,5)P_3. All buffers and protein binding solutions were prepared as described above and the test was performed according to manufacturing instructions. As a positive control for protein lipid binding, the commercial PIP grip PtdIns(4,5)P_2 Grip (#G-4501) (Echelon Biosciences Inc., MoBiTec, Göttingen, Germany) was used. Enriched MBP was used as negative control.

4.22. Alpha fold (AF) PI4Kβ1 structure: predicted domains

The Alpha Fold Protein Structure Data Base (Varadi et al., 2024) [https://alphafold.ebi.ac.uk/]) (see Appendix Table 21) was used to obtain a predicted structural model of *Arabidopsis* PI4Kβ1 and to analyze the confidence of the predicted model or per-residue model confidence score (pLDDT) (0-100). Where pLDDT > 90 is considered a very high confidence; 90 > pLDDT > 70 is high confidence; 70 > pLDDT > 50 is low confidence; pLDDT < 50 is very low confidence. Additionally, the Universal Protein Resource (UniProt) (UniProt: Q9FMJ0) (see Appendix Table 21) was also used to get information about domains, compositional bias, region and repeats of the PI4Kβ1 protein.

4.23. Modelling of AF PI4Kβ1 to predict protein orientation at the membrane.

Modelling of the Alpha Fold (AF) partial model for PI4Kβ1 was performed in collaboration with Prof. Dr. Panagiotis Kastritis (Kastritis Laboratory for Biolomolecular Research, MLU) and Marija Sorokina (Research Training Group RTG2467) the MLU.

4.23.1. Superposition of AF PI4Kβ1 with PI3K (mammals)

The superposition method in PyMol 2.5.7 was used to align and superimpose the 3D structures of two candidate proteins and evaluate their similarity (see Appendix Table 20). The Alpha Fold (AF) model for PI4Kβ1 was truncated after super-positioning with the structural model of human phosphatidylinositol 4,5-bisphosphate 3-kinase catalytic subunit gamma isoform (PI3K) (PI3Kα-CS, pdb 1E8X: https://www.rcsb.org/structure/1e8x; https://www.uniprot.org/uniprotkb/O02697/entry;) and PI3Kα (4ovv; https://www.rcsb.org/structure/4OVV). For the generation of the partial PI4Kβ1 model, the predicted local distance difference test (pLDDT) scores were considered, where the score (0-100) is a per-residue confidence score, with values greater than 90 indicating high confidence, and values below 50 indicating low confidence.

4.23.2. PtdIns, PtdInsP_2, or ATP/ADP modelling

As a template for the positioning of lipid substrates or products (PtdIns or PtdIns4P, here termed PIP4P), the complex of PI3Kα-CS (https://www.uniprot.org/uniprotkb/P42336/entry) and phosphatidylinositol 3-kinase regulatory subunit alpha (PI3Kα-RS) (https://www.uniprot.org/uniprotkb/P27986/entry) with diC4-PtdInsP_2 (PDB ID: 4OVV; https://www.rcsb.org/structure/4OVV) and PIP4P (resname: PI4; resid: 2001) were used. PtdIns (resname: PI0; resid: 2001) was created from diC4-PIP_2 (https://www.rcsb.org/ligand/PBU) by manually removing the phosphate groups from the C5 and C4 atoms. PtdIns4P was created from diC4-PtdInsP_2 (https://www.rcsb.org/ligand/PBU) by removing of the phosphate from the C5 atom. Parameter and topology files for PIP4P and PtdIns were created with CHARMM-GUI (Ligand Reader & Modeler). PI3Kα in complex with diC4-PIP2 (https://www.rcsb.org/structure/4OVV) (4OVV) was also used for comparison.

The ATP model was taken from the PI3K structure resolved with a bound ATP molecule (1e8x: https://www.rcsb.org/structure/1e8x).

The AF structure was superimposed with 1E8X. ADP was created from ATP by removing the vicinal phosphate-group. Parameter and topology files for ADP and ATP were created with CHARMM-GUI (Ligand Reader & Modeler)

4.23.3. Molecular dynamic (MD) simulations

For the MD simulations, four virtual systems were set up: two for full-length PI4Kβ1full and two for the C-terminally truncated PI4Kβ1$_{1107\text{-}1121.}$

PI4Kβ1-full (F46-A143; N541-E641; E835-L1121) and PI4Kβ1-no-C-term (F46-A143; N541-E641; E835-D1103)

1. Pi4Kβ1-full+PI4P+ADP
2. Pi4Kβ1-full+PI+ATP
3. Pi4Kβ1-no-C-term+PI4P+ADP
4. Pi4Kβ1-no-C-term+PI+ATP

Each system was solvated *in silico* in Transferable intermolecular potential with 3 points, TIP3P water with 0.15 M NaCl.

Two rounds of restricted relaxation for 0.1 ns each was run before 1 ns MD was started. On restricted atoms a force of 5 kcal mol-1 Å-2was applied.

1. 0.1 ns unrestricted solvent and H-atoms
2. 0.1 ns unrestricted solvent, sidechains, C-term (S1101-L1121), ADP/ATP, and PI4P/PI
3. 1 ns unrestricted MD simulation.

4.23.4. System set up

Active site refinement of the protein complex was performed using NAMD 2.13 for Linux-x86_64- multicore employing CHARMM36 force field (See Appendix Table 20). The force field topology and parameter files for the ligands (ADP and PI4P) were generated via Ligand Reader & Modeler of CHARMM-GUI with CGenFF v. 2.4. Analysis and visualisation were performed using VMD 1.9.3 for LINUXAMD64 and PyMol 2.5.7. The protein model (7,829 atoms) with ADP as a cofactor (39 atoms) and PI4P (67 atoms) was solvated in a water box of TIP3 water (127,974 atoms) and neutralized with 150 mM NaCl (153 atoms). The complete simulation setup comprised 136,162 atoms. All histidine residues were considered as HSD (protonated on delta carbon).

4.23.5. Minimization-relaxation cycles

Altogether two all-atom minimization-relaxation cycles were performed. During the first cycle water & ions environment, and hydrogens were allowed to relax, keeping the protein, ADP, and PI4P harmonically restrained at 5 kcal mol-1 Å -2 for 1000 minimization steps. Subsequently, the temperature was changed from 0 K to 310 K with an increment of 10 K relaxing the system for 1 ps for each increment (NVT ensemble). Additionally, the restrained system was relaxed for 0.1 ns at 310 K, 1.01325 bar. In the next step, previously relaxed system was minimized for further 1000 steps. During this step side chains, ADP, and PI4P, as well all hydrogens, water molecules, and ions were set free. Backbone of all protein chains were restrained at 5 kcal mol-1 Å -2. Thereafter, the restrained system was incrementally heated as described for the first cycle. Finally. The restrained system was relaxed for 0.1 ns at 310 K, 1.01325 bar.

Finally, an unrestricted MD simulation for 1 ns was performed. All described minimization-relaxation steps were performed with an integration timestep of 1 fs using periodic-boundary conditions. Long-range electrostatic interactions were treated with particle-mesh Ewald electrostatics with maximum grid spacing of 1 Å. Non-bonded van der Walls interactions and short-range electrostatic interactions were calculated with a cutoff of 12 Å and a switching distance of 10 Å. For the constant temperature control was used Langevin thermostat (310 K) with collision frequency of 1.0 ps-1. To enable temperature and pressure control, a Nose-Hoover Langevin barostat (1.01325 bar) was used. The trajectory file (.dcd) format was written very 0.005 ns.

4.23.6. RMSD and RMSF

Root Mean Square deviation (RMSD) was measured for all atoms of protein excluding cofactors and the lipid. Root Mean Square Fluctuation (RMSF) was measured for all Cα atoms of the protein. RMSD and RMSF were measured with standard protocols of VMD (VMD 1.9.3 for LINUXAMD64.

4.23.7. Hydrogen Bonds Analysis

Analysis of hydrogen bonds that occurs between AF truncated model PI4Kβ1 and ADP/ATP and PI/ATP during 1 ns in MD were tested with VMD 1.9.3 for LINUXAMD64. The following parameters were considered:

- Selection 1: protein
- Selection 2: resname ADP or resname PIP4P or resname ATP or resname PI
- Only polar atoms (N, O, S, F)
- Donor-Acceptor distance: 4.0 Å

- Angle cutoff (degrees): 120°
- Calculate detailed info for: residue pair
- Main: backbone
- Side: Side chain of a residue
-

4.24. Membrane modelling

The current membrane was modelled with CHARMM-GUI (Membrane Builder) with the following steps:

1. Align a vector (two atoms) along Z PROA Ser998 (362) Gly1001 (365)
2. Translate molecule along Z axis 25 Angstrom
3. Water along Z axis: 22.5
4. Ratios of lipid components DMPC/DOPC/DMPI: 20/20/1
5. Length of X and Y: 75 (initial guess)

5. Literature

Abraham, M. J., Murtola, T., Schulz, R., Páll, S., Smith, J. C., Hess, B., & Lindah, E. (2015). Gromacs: High performance molecular simulations through multi-level parallelism from laptops to supercomputers. *SoftwareX*, *1–2*, 19–25. https://doi.org/10.1016/j.softx.2015.06.001

Agbemafle, W., Wong, M. M., & Bassham, D. C. (2023). Transcriptional and post-translational regulation of plant autophagy. *Journal of Experimental Botany*, *74*(19), 6006–6022. https://doi.org/10.1093/jxb/erad211

Akhter, S., Uddin, M. N., Jeong, I. S., Kim, D. W., Liu, X. M., & Bahk, J. D. (2016). Role of Arabidopsis AtPI4Kγ3, a type II phosphoinositide 4-kinase, in abiotic stress responses and floral transition. *Plant Biotechnology Journal*, *14*(1), 215–230. https://doi.org/10.1111/pbi.12376

Alberts, B., Johnson, A., Lewis, J., Raff, M., Roberts, K., & Walter, P. (2002). *Molecular Biology of the Cell: The Compartmentalization of Cells*. Garland Science.

Allen, J. J., Li, M., Brinkworth, C. S., Paulson, J. L., Wang, D., Hübner, A., Chou, W. H., Davis, R. J., Burlingame, A. L., Messing, R. O., Katayama, C. D., Hedrick, S. M., & Shokat, K. M. (2007). A semisynthetic epitope for kinase substrates. *Nature Methods*, *4*(6), 511–516. https://doi.org/10.1038/nmeth1048

Aponte, A. M., Phillips, D., Harris, R. A., Blinova, K., French, S., Johnson, D. T., & Balaban, R. S. (2009). 32P Labeling of Protein Phosphorylation and Metabolite Association in the Mitochondria Matrix. *Methods in Enzymology*, *457*(B), 63–80. https://doi.org/10.1016/S0076-6879(09)05004-6

Arrhenius, S. (1889). *Über die Reaktionsgeschwindigkeit bei der Inversion von Rohrzucker durch Säuren*.

Asai, T., Tena, G., Plotnikova, J., Willmann, M. R., Chiu, W.-L., Gomez-Gomez2, L., Boller3, T., Ausubel, F. M., & Sheen, J. (2002). MAP kinase signalling cascade in Arabidopsis innate immunity. *Nature*, *415*. https://doi.org/https://doi.org/10.3389/fpls.2012.00169

Atkins, P., & De Paula, J. (2006). The temperature dependence of reaction rates. In *PhysicalChemistry* (8th ed.). Great Britain by Oxford University Press.

Balla, A., & Balla, T. (2006). Phosphatidylinositol 4-kinases: old enzymes with emerging functions. *Trends in Cell Biology*, *16*(7), 351–361. https://doi.org/10.1016/j.tcb.2006.05.003

Balla, T. (1998). Phosphatidylinositol 4-kinases. *Biochimica et Biophysica Acta*, *1436*, 69–85. https://doi.org/https://doi.org/10.1016/S0005-2760(98)00134-9

Bandman, V. (2011). *Mechanisms and Kinetics of Exocytosis and Endocytosis in Plant and in Yeast Cells*. Technischen Universität Darmstadt.

Baumann, C., & Zerbe, O. (2024). The role of leucine and isoleucine in tuning the hydropathy of class A GPCRs. *Proteins: Structure, Function and Bioinformatics*, *92*(1), 15–23. https://doi.org/10.1002/prot.26559

Beck, M., Komis, G., Ziemann, A., Menzel, D., & Samaj, J. (2011). Mitogen-activated protein kinase 4 is involved in the regulation of mitotic and cytokinetic microtubule transitions in Arabidopsis thaliana. *New Phytologist*, *189*(4), 1069–1083. https://doi.org/10.1111/j.1469-8137.2010.03565.x

Beeton, C., Chance, E., Foukas, L., & Shepherd, P. (2000). Comparison of the kinetic properties of the lipid- and protein-kinase activities of the p110α and p110β catalytic subunits of class-Ia phosphoinositide 3-kinases. *Biochem.J.*, *350*, 353–359.

Bernier, S. C., Morency, L. P., Najmanovich, R., & Salesse, C. (2018). Identification of an alternative translation initiation site in the sequence of the commonly used Glutathione S-Transferase tag. *Journal of Biotechnology*, *286*(September), 14–16. https://doi.org/10.1016/j.jbiotec.2018.09.003

Berriri, S., Garcia, A. V., dit Frey, N. F., Rozhon, W., Pateyron, S., Leonhardt, N., Montillet, J. L., Leung, J., Hirt, H., & Colcombet, J. (2012). Constitutively active mitogen-activated protein kinase versions reveal functions of Arabidopsis MPK4 in pathogen defense signaling. *Plant Cell*, *24*(10), 4281–4293. https://doi.org/10.1105/tpc.112.101253

Bethke, G., Unthan, T., Uhrig, J. F., Pö Schl, Y., Gust, A. A., Scheel, D., & Lee, J. (2009). Flg22 regulates the release of an ethylene response factor substrate from MAP kinase 6 in Arabidopsis thaliana via ethylene signaling. *PNAS May*, *12*, 8067–8072. https://doi.org/https://doi.org/10.1073/pnas.0810206106

Bradford, M. M. (1976). A Rapid and Sensitive Method for the Quantitation of Microgram Quantities of Protein Utilizing the Principle of Protein-Dye Binding. *ANALYTICAL BIOCHEMISTRY*, *72*, 248–254. https://doi.org/https://doi.org/10.1016/0003-2697(76)90527-3

Brodersen, P., Petersen, M., Nielsen, H. B., Zhu, S., Newman, M. A., Shokat, K. M., Rietz, S., Parker, J., & Mundy, J. (2006). Arabidopsis MAP kinase 4 regulates salicylic acid- and jasmonic acid/ethylene-dependent responses via EDS1 and PAD4. *Plant Journal*, *47*(4), 532–546. https://doi.org/10.1111/j.1365-313X.2006.02806.x

Brooks, B. R., Bruccoleri, R. E., Olafson, B. D., States, D. J., Swaminathan, ; S, & Karplus, M. (1982). *CHARMM: A Program for Macromolecular Energy, Minimization, and Dynamics Calculations*. https://doi.org/https://doi.org/10.1002/jcc.540040211

Cargnello, M., & Roux, P. P. (2011). Activation and Function of the MAPKs and Their Substrates, the MAPK-Activated Protein Kinases. *Microbiology and Molecular Biology Reviews*, *75*(1), 50–83. https://doi.org/10.1128/mmbr.00031-10

Chen, Y. C., Aguan, K., Yang, C. W., Wang, Y. T., Pal, N. R., & Chung, I. F. (2011). Discovery of protein Phosphorylation motifs through exploratory data analysis. *PLoS ONE*, *6*(5). https://doi.org/10.1371/journal.pone.0020025

Cho, M. H., & Boss, W. F. (1995). Transmembrane Signaling and Phosphoinositides. *Methods in Cell Biology*, *49*, 543–553.

Cho, Y. S., & Lim, H. S. (2018). Comparison of various estimation methods for the parameters of Michaelis-Menten equation based on in vitro elimination kinetic simulation data. *Transl Clin Pharmacol TCP*, *39*(1), 1–48. https://doi.org/10.12793/tcp.2018.26.1.xx

Choi, B., Rempala, G. A., & Kim, J. K. (2017). Beyond the Michaelis-Menten equation: Accurate and efficient estimation of enzyme kinetic parameters.

Scientific Reports, *7*(1), 1–11. https://doi.org/10.1038/s41598-017-17072-z

Chung, H., & Fleming, N. (1995). Regulation of phosphatidylinositol kinases by arachidonic acid in rat submandibular gland cells. *Pflugers Arch-Eur J Physiol*, *429*, 789–796. https://doi.org/10.1007/BF00374802

Cooper, G., & Hausman, R. (2007). *The cell: a molecular approach(4th_edition)* (4th ed., pp. 1–847). ASM Press.

Cornish-Bowden, A. (2014). Understanding allosteric and cooperative interactions in enzymes. *FEBS Journal*, *281*(2), 621–632. https://doi.org/10.1111/febs.12469

Coval, M. L. (1970). Analysis of Hill interaction coefficients and the invalidity of the Kwon and Brown equation. *Journal of Biological Chemistry*, *245*(23), 6335–6336. https://doi.org/10.1016/s0021-9258(18)62614-6

Dagley, L. F., Infusini, G., Larsen, R. H., Sandow, J. J., & Webb, A. I. (2019). Universal Solid-Phase Protein Preparation (USP3) for Bottom-up and Top-down Proteomics. *Journal of Proteome Research*, *18*(7), 2915–2924. https://doi.org/10.1021/acs.jproteome.9b00217

Droillard, M. J., Boudsocq, M., Barbier-Brygoo, H., & Laurière, C. (2004). Involvement of MPK4 in osmotic stress response pathways in cell suspensions and plantlets of Arabidopsis thaliana: Activation by hypoosmolarity and negative role in hyperosmolarity tolerance. *FEBS Letters*, *574*(1–3), 42–48. https://doi.org/10.1016/j.febslet.2004.08.001

Edelheit, O., Hanukoglu, A., & Hanukoglu, I. (2009). Simple and efficient site-directed mutagenesis using two single-primer reactions in parallel to generate mutants for protein structure-function studies. *BMC Biotechnology*, *9*. https://doi.org/10.1186/1472-6750-9-61

Endrenyi, L., Kwong, F. H. F., & Fajszi, C. (1975). Evaluation of Hill Slopes and Hill Coefficients when the Saturation Binding or Velocity is not Known. *European Journal of Biochemistry*, *51*(2), 317–328. https://doi.org/10.1111/j.1432-1033.1975.tb03931.x

Eyring, H. (1935). The activated complex in chemical reactions. *The Journal of Chemical Physics*, *3*(2), 63–71. https://doi.org/10.1063/1.1749604

Fairn, G. D., Ogata, K., Botelho, R. J., Stahl, P. D., Anderson, R. A., De Camilli, P., Meyer, T., Wodak, S., & Grinstein, S. (2009). An electrostatic switch displaces phosphatidylinositol phosphate kinases from the membrane during phagocytosis. *Journal of Cell Biology*, *187*(5), 701–714. https://doi.org/10.1083/jcb.200909025

Folch, J., Lees, M., & Sloane Stanley, G. H. (1957). A simple method for the isolation and purification of total lipides from animal tissues. *The Journal of Biological Chemistry*, *226*(1), 497–509. https://doi.org/10.1016/s0021-9258(18)64849-5

Fratini, M., Krishnamoorthy, P., Stenzel, I., Riechmann, M., Matzner, M., Bacia, K., Heilmann, M., & Heilmann, I. (2021). Plasma membrane nano-organization specifies phosphoinositide effects on Rho-GTPases and actin dynamics in tobacco pollen tubes. *Plant Cell*, *33*(3), 642–670. https://doi.org/10.1093/plcell/koaa035

Furt, F., König, S., Bessoule, J. J., Sargueil, F., Zallot, R., Stanislas, T., Noirot, E., Lherminier, J., Simon-Plas, F., Heilmann, I., & Mongrand, S. (2010). Polyphosphoinositides are enriched in plant membrane rafts and form microdomains in the plasma membrane. *Plant Physiology*, *152*(4), 2173–2187. https://doi.org/10.1104/pp.109.149823

Galvão, R. M., Kota, U., Soderblom, E. J., Goshe, M. B., & Boss, W. F. (2008). Characterization of a new family of protein kinases from Arabidopsis containing phosphoinositide 3/4-kinase and ubiquitin-like domains. *Biochemical Journal*, *409*(1), 117–127. https://doi.org/10.1042/BJ20070959

Gehrmann, T., & Heilmeyer, L. M. G. (1998). Phosphatidylinositol 4-kinases. *European Journal of Biochemistry*, *253*(2), 357–370. https://doi.org/10.1046/j.1432-1327.1998.2530357.x

Gehrmann, T., lya Gu lkan, H., Suer, S., Herberg, F. W., Balla, A., rgy Vereb, G., Mayr, G. W., & Heilmeyer Jr aY, L. M. (1999). Functional expression and characterization of a new human phosphatidylinositol 4-kinase PI4K230. *Biochemica et Biophysica Acta*, 341–356. https://doi.org/10.1016/s1388-1981(99)00029-3

Gerth, K., Lin, F., Menzel, W., Krishnamoorthy, P., Stenzel, I., Heilmann, M., & Heilmann, I. (2017). Guilt by Association: A Phenotype-Based View of the Plant Phosphoinositide Network. *Annu. Rev. Plant Biol*, *68*, 349–374. https://doi.org/10.1146/annurev-arplant-042916

Gesztelyi, R., Zsuga, J., Kemeny-Beke, A., Varga, B., Juhasz, B., & Tosaki, A. (2012). The Hill equation and the origin of quantitative pharmacology. *Archive for History of Exact Sciences*, *66*(4), 427–438. https://doi.org/10.1007/s00407-012-0098-5

Goldbeter, A., & Dupont, G. (1990). Allosteric regulation, cooperativity, and biochemical oscillations. *Biophysical Chemistry*, *37*, 341–353.

Gonorazky, G., Laxalt, A. M., Dekker, H. L., Rep, M., Munnik, T., Testerink, C., & de la Canal, L. (2012). Phosphatidylinositol 4-phosphate is associated to extracellular lipoproteic fractions and is detected in tomato apoplastic fluids. *Plant Biology*, *14*(1), 41–49. https://doi.org/10.1111/j.1438-8677.2011.00488.x

Groban, E. S., Narayanan, A., & Jacobson, M. P. (2006). Conformational changes in protein loops and helices induced by post-translational phosphorylation. *PLoS Computational Biology*, *2*(4), 238–250. https://doi.org/10.1371/journal.pcbi.0020032

Groves, J. T., & Kuriyan, J. (2010). Molecular mechanisms in signal transduction at the membrane. *Nature Structural and Molecular Biology*, *17*(6), 659–665. https://doi.org/10.1038/nsmb.1844

Harak, C., Radujkovic, D., Taveneau, C., Reiss, S., Klein, R., Bressanelli, S., & Lohmann, V. (2014). Mapping of Functional Domains of the Lipid Kinase Phosphatidylinositol 4-Kinase Type III Alpha Involved in Enzymatic Activity and Hepatitis C Virus Replication. *Journal of Virology*, *88*(17), 9909–9926. https://doi.org/10.1128/jvi.01063-14

Harvard, U. (2018). The Molecular Basis of Enzymatic Catalysis. In *LifeScences* (pp. 1–12). https://projects.iq.harvard.edu/files/lifesciences1abookv1/files/7_-_dna_structure_chemistry_revised_9-24-2018.pdf

Hastie, C. J., McLauchlan, H. J., & Cohen, P. (2006). Assay of protein kinases using radiolabeled ATP: A protocol. *Nature Protocols*, *1*(2), 968–971. https://doi.org/10.1038/nprot.2006.149

Heilmann, I. (2016). Phosphoinositide signaling in plant development. *Development (Cambridge)*, *143*(12), 2044–2055. https://doi.org/10.1242/dev.136432

Heilmann, M., & Heilmann, I. (2015). Plant phosphoinositides - Complex networks controlling growth and adaptation. In *Biochimica et Biophysica Acta - Molecular and Cell Biology of Lipids* (Vol. 1851, Issue 6, pp. 759–769). Elsevier B.V. https://doi.org/10.1016/j.bbalip.2014.09.018

Heilmann, M., & Heilmann, I. (2022). Regulators regulated: Different layers of control for plasma membrane phosphoinositides in plants. *Current Opinion in Plant Biology*, *67*. https://doi.org/10.1016/j.pbi.2022.102218

Heilmann, M., & Heilmann, I. (2024). Getting attached to membranes—How plant signaling networks employ PtdIns(4,5)P2. *Plant Physiology*. https://doi.org/10.1093/plphys/kiae393

Hekkelman, M. L., de Vries, I., Joosten, R. P., & Perrakis, A. (2023). AlphaFill: enriching AlphaFold models with ligands and cofactors. *Nature Methods*, *20*(2), 205–213. https://doi.org/10.1038/s41592-022-01685-y

Hempel, F. (2015). *New links for old pathways: Protein kinases that target PI4P 5-kinases with regulatory roles in polar tip growth in plants*. Martin-Luther-Universität Halle-Wittenberg.

Hempel, F., Stenzel, I., Heilmann, M., Krishnamoorthy, P., Menzel, W., Golbik, R., Helm, S., Dobritzsch, D., Baginsky, S., Lee, J., Hoehenwarter, W., & Heilmann, I. (2017). MAPKS influence pollen tube growth by controlling the formation of phosphatidylinositol 4,5-bisphosphate in an apical plasma membrane domain. *Plant Cell*, *29*(12), 3030–3050. https://doi.org/10.1105/tpc.17.00543

Hendricks, K. B., Wang, B. Q., Schnieders, E. A., & Thorner, J. (1999). Yeast homologue of neuronal frequenin is a regulator of phosphatidylinositol-4-OH kinase. *Nature Cell Biology*, *1*. https://doi.org/https://doi.org/10.1038/12058

Hill, A. V. (1913). *The combinations of haemoglobin with oxygen and with carbon monoxide I*. https://doi.org/https://doi.org/10.1042/bj0070471

Hirano, T., & Sato, M. (2019). Physiological Functions of Phosphoinositide-Modifying Enzymes and Their Interacting Proteins in Arabidopsis. *Adv. Exp. Med Biol-Protein Reviews*, 139–157. http://www.springer.com/series/14330

Holt, J. M., & Ackers, G. K. (2009). Chapter 7 The Hill Coefficient. Inadequate Resolution of Cooperativity in Human Hemoglobin. In *Methods in Enzymology* (Vol. 455, Issue A, pp. 193–212). Academic Press Inc. https://doi.org/10.1016/S0076-6879(08)04207-9

Hon, W. C., Berndt, A., & Williams, R. L. (2012). Regulation of lipid binding underlies the activation mechanism of class IA PI3-kinases. *Oncogene*, *31*(32), 3655–3666. https://doi.org/10.1038/onc.2011.532

Hrabak, E. M., Chan, C. W. M., Gribskov, M., Harper, J. F., Choi, J. H., Halford, N., Kudla, J., Luan, S., Nimmo, H. G., Sussman, M. R., Thomas, M., Walker-Simmons, K., Zhu, J. K., & Harmon, A. C. (2003). The Arabidopsis CDPK-SnRK superfamily of protein kinases. *Plant Physiology*, *132*(2), 666–680. https://doi.org/10.1104/pp.102.011999

Hughes, C. S., Moggridge, S., Müller, T., Sorensen, P. H., Morin, G. B., & Krijgsveld, J. (2019). Single-pot, solid-phase-enhanced sample preparation for proteomics experiments. *Nature Protocols*, *14*(1), 68–85. https://doi.org/10.1038/s41596-018-0082-x

Ischebeck, T., Seiler, S., & Heilmann, I. (2010). At the poles across kingdoms: Phosphoinositides and polar tip growth. *Protoplasma*, *240*(1), 13–31. https://doi.org/10.1007/s00709-009-0093-0

Ischebeck, T., Stenzel, I., & Heilmann, I. (2008). Type B phosphatidylinositol-4-phosphate 5-kinases mediate Arabidopsis and Nicotiana tabacum pollen tube growth by regulating apical pectin secretion. *Plant Cell*, *20*(12), 3312–3330. https://doi.org/10.1105/tpc.108.059568

Ischebeck, T., Vu, L. H., Jin, X., Stenzel, I., Löfke, C., & Heilmann, I. (2010). Functional cooperativity of enzymes of phosphoinositide conversion according to synergistic effects on pectin secretion in tobacco pollen tubes. *Molecular Plant*, *3*(5), 870–881. https://doi.org/10.1093/mp/ssq031

Jaillais, Y., Bayer, E., Bergmann, D. C., Botella, M. A., Boutté, Y., Bozkurt, T. O., Caillaud, M. C., Germain, V., Grossmann, G., Heilmann, I., Hemsley, P. A., Kirchhelle, C., Martinière, A., Miao, Y., Mongrand, S., Müller, S., Noack, L. C., Oda, Y., Ott, T., … Gronnier, J. (2024). Guidelines for naming and studying plasma membrane domains in plants. *Nature Plants*, 1172–1183. https://doi.org/10.1038/s41477-024-01742-8

Janzen, W. (2002). *Method sin molecular biology: High Throughput Screening* (Vol. 190). Humana Pressinc.

Jerabek-Willemsen, M., André, T., Wanner, R., Roth, H. M., Duhr, S., Baaske, P., & Breitsprecher, D. (2014). MicroScale Thermophoresis: Interaction analysis and beyond. *Journal of Molecular Structure*, *1077*, 101–113. https://doi.org/10.1016/j.molstruc.2014.03.009

Jiang, M., Zhang, Y., Li, P., Jian, J., Zhao, C., & Wen, G. (2022). Mitogen-Activated Protein Kinase and Substrate Identification in Plant Growth and Development. In *International Journal of Molecular Sciences* (Vol. 23, Issue 5). MDPI. https://doi.org/10.3390/ijms23052744

Jürgens, G. (2005). Plant cytokinesis: Fission by fusion. In *Trends in Cell Biology* (Vol. 15, Issue 5, pp. 277–283). Elsevier Ltd. https://doi.org/10.1016/j.tcb.2005.03.005

Kamata, K., Mitsuya, M., Nishimura, T., Eiki, J. I., & Nagata, Y. (2004). Structural basis for allosteric regulation of the monomeric allosteric enzyme human glucokinase. *Structure*, *12*(3), 429–438. https://doi.org/10.1016/j.str.2004.02.005

Kanev, G. K., de Graaf, C., de Esch, I. J. P., Leurs, R., Würdinger, T., Westerman, B. A., & Kooistra, A. J. (2019). The Landscape of Atypical and Eukaryotic Protein Kinases. In *Trends in Pharmacological Sciences* (Vol. 40, Issue 11, pp. 818–832). Elsevier Ltd. https://doi.org/10.1016/j.tips.2019.09.002

Kang, B. H., Nielsen, E., Preuss, M. L., Mastronarde, D., & Staehelin, L. A. (2011). Electron Tomography of RabA4b- and PI-4Kβ1-Labeled Trans Golgi Network Compartments in Arabidopsis. *Traffic*, *12*(3), 313–329. https://doi.org/10.1111/j.1600-0854.2010.01146.x

König, S., Mosblech, A., & Heilmann, I. (2007). Stress-inducible and constitutive phosphoinositide pools have distinctive fatty acid patterns in Arabidopsis

thaliana . *The FASEB Journal*, *21*(9), 1958–1967. https://doi.org/10.1096/fj.06-7887com

Kosetsu, K., Matsunaga, S., Nakagami, H., Colcombet, J., Sasabe, M., Soyano, T., Takahashi, Y., Hirt, H., & Machida, Y. (2010). The MAP kinase MPK4 Is required for cytokinesis in Arabidopsis thaliana. *Plant Cell*, *22*(11), 3778–3790. https://doi.org/10.1105/tpc.110.077164

Kumutima, J., Yao, X. Q., & Hamelberg, D. (2022). Post-translational Modifications of Cyclophilin D Fine-Tune Its Conformational Dynamics and Activity: Implications for Its Mitochondrial Function. *Journal of Physical Chemistry B*, *126*(51), 10844–10853. https://doi.org/10.1021/acs.jpcb.2c06208

Kunz, J., Wilson, M. P., Kisseleva, M., Hurley, J. H., Majerus, P. W., & Anderson, R. A. (2000). The Activation Loop of Phosphatidylinositol Phosphate Kinases Determines Signaling Specificity. *Biological Chemistry, and Molecular Biophysics*, *5*, 1–11. https://doi.org/10.1016/s1097-2765(00)80398-6

Kusano, H., Testerink, C., Vermeer, J. E. M., Tsuge, T., Shimada, H., Oka, A., Munnik, T., & Aoyama, T. (2008). The Arabidopsis phosphatidylinositol phosphate 5-kinase PIP5K3 is a key regulator of root hair tip growth. *Plant Cell*, *20*(2), 367–380. https://doi.org/10.1105/tpc.107.056119

Laemmli, U. (1970). Cleavage of structural Proteins during assembly of the had of Bactertiophage T4. *Nature*, *227*. https://doi.org/10.1038/227680a0

LaMontagne, E. D., & Heese, A. (2017). Trans-Golgi network/early endosome: a central sorting station for cargo proteins in plant immunity. *Current Opinion in Plant Biology*, *40*, 114–121. https://doi.org/10.1016/j.pbi.2017.08.012

Latrasse, D., Jégu, T., Li, H., de Zelicourt, A., Raynaud, C., Legras, S., Gust, A., Samajova, O., Veluchamy, A., Rayapuram, N., Ramirez-Prado, J. S., Kulikova, O., Colcombet, J., Bigeard, J., Genot, B., Bisseling, T., Benhamed, M., & Hirt, H. (2017). MAPK-triggered chromatin reprogramming by histone deacetylase in plant innate immunity. *Genome Biology*, *18*(1). https://doi.org/10.1186/s13059-017-1261-8

Laude, A. J., & Prior, I. A. (2004). Plasma membrane microdomains: Organization, function and trafficking (Review). In *Molecular Membrane Biology* (Vol. 21, Issue 3, pp. 193–205). https://doi.org/10.1080/09687680410001700517

Le Roy, C., & Wrana, J. L. (2005). Signaling and endocytosis: A team effort for cell migration. *Developmental Cell*, *9*(2), 167–168. https://doi.org/10.1016/j.devcel.2005.07.007

Lees, J. A., Zhang, Y., Oh, M. S., Schauder, C. M., Yu, X., Baskin, J. M., Dobbs, K., Notarangelo, L. D., De Camilli, P., Walz, T., & Reinisch, K. M. (2017). Architecture of the human PI4KIIIα lipid kinase complex. *Proceedings of the National Academy of Sciences of the United States of America*, *114*(52), 13720–13725. https://doi.org/10.1073/pnas.1718471115

Lemmon, M. A. (2003). Phosphoinositide recognition domains. *Traffic*, *4*(4), 201–213. https://doi.org/10.1034/j.1600-0854.2004.00071.x

Li, L., Wang, F., Yan, P., Jing, W., Zhang, C., Kudla, J., & Zhang, W. (2017). A phosphoinositide-specific phospholipase C pathway elicits stress-induced Ca2+ signals and confers salt tolerance to rice. *New Phytologist*, *214*(3), 1172–1187. https://doi.org/10.1111/nph.14426

Lin, F., Krishnamoorthy, P., Schubert, V., Hause, G., Heilmann, M., & Heilmann, I. (2019). A dual role for cell plate-associated PI4Kβ in endocytosis and phragmoplast dynamics during plant somatic cytokinesis. *The EMBO Journal*, *38*(4). https://doi.org/10.15252/embj.2018100303

Löfke, C., König, S., Freitag, S., & Heilmann, I. (2008). Alternative metabolic fates of phosphatidylinositol produced by PI-synthase isoforms in Arabidopsis thaliana. *Arabidopsis Thaliana. Biochemical Journal*, *413*(1). https://doi.org/10.1042/BJ20071371ï

Lou, Y., Ma, H., Lin, W. H., Chu, Z. Q., Mueller-Roeber, B., Xu, Z. H., & Xue, H. W. (2006). The highly charged region of plant β-type phosphatidylinositol 4-kinase is involved in membrane targeting and phospholipid binding. *Plant Molecular Biology*, *60*(5), 729–746. https://doi.org/10.1007/s11103-005-5548-x

Lu, K., Cherng, Y., & Zhou, X. ,. (2022). Pinning down proline-directed phosphorylation signaling. *Trends in Cell Biology*, *4*.

Maheshwari, S., Miller, M. S., O'Meally, R., Cole, R. N., Amzel, L. M., & Gabelli, S. B. (2017a). Kinetic and structural analyses reveal residues in phosphoinositide 3-kinase α that are critical for catalysis and substrate recognition. *Journal of Biological Chemistry*, *292*(33), 13541–13550. https://doi.org/10.1074/jbc.M116.772426

Maheshwari, S., Miller, M. S., O'Meally, R., Cole, R. N., Amzel, L. M., & Gabelli, S. B. (2017b). Kinetic and structural analyses reveal residues in phosphoinositide 3-kinase α that are critical for catalysis and substrate recognition. *Journal of Biological Chemistry*, *292*(33), 13541–13550. https://doi.org/10.1074/jbc.M116.772426

Mamode Cassim, A., Gouguet, P., Gronnier, J., Laurent, N., Germain, V., Grison, M., Boutté, Y., Gerbeau-Pissot, P., Simon-Plas, F., & Mongrand, S. (2019). Plant lipids: Key players of plasma membrane organization and function. In *Progress in Lipid Research* (Vol. 73, pp. 1–27). Elsevier Ltd. https://doi.org/10.1016/j.plipres.2018.11.002

MAPK Group. (2002). Mitogen-activated protein kinase cascades in plants: a new nomenclature. *Trends in Plant Science*. https://doi.org/https://doi.org/10.1016/S1360-1385(02)02302-6

Maszkowska, J., Szymańska, K. P., Kasztelan, A., Krzywińska, E., Sztatelman, O., & Dobrowolska, G. (2021). The multifaceted regulation of SnRK2 kinases. In *Cells* (Vol. 10, Issue 9). MDPI. https://doi.org/10.3390/cells10092180

Meijer, H. J. G., Berrie, C. P., Iurisci, C., Divecha, N., Musgrave, A., & Munnik, T. (2001). Identification of a new polyphosphoinositide in plants, phosphatidylinositol 5-monophosphate (PtdIns5P), and its accumulation upon osmotic stress. *Biochem. J*, *360*, 491–498.

Menzel, W., Stenzel, I., Helbig, L. M., Krishnamoorthy, P., Neumann, S., Eschen-Lippold, L., Heilmann, M., Lee, J., & Heilmann, I. (2019). A PAMP-triggered MAPK cascade inhibits phosphatidylinositol 4,5-bisphosphate production by PIP5K6 in Arabidopsis thaliana. *New Phytologist*, *224*(2), 833–847. https://doi.org/10.1111/nph.16069

Michaelis, L., & Menten, M. M. L. (1913). The kinetics of invertin action. *FEBS Letters*, *587*(17), 2712–2720. https://doi.org/10.1016/j.febslet.2013.07.015

Modi, V., & Dunbrack, R. L. (2019). Defining a new nomenclature for the structures of active and inactive kinases. *PNAS*, *116*(14), 6818–6827. https://doi.org/10.5281/zenodo.2580462

Mueller-Roeber, B., & Pical, C. (2002). Inositol phospholipid metabolism in Arabidopsis. Characterized and putative isoforms of inositol phospholipid kinase and phosphoinositide-specific phospholipase C. *Plant Physiology*, *130*(1), 22–46. https://doi.org/10.1104/pp.004770

Müller, S., & Jürgens, G. (2016). Plant cytokinesis-No ring, No constriction but centrifugal construction of the partitioning membrane. In *Seminars in Cell and Developmental Biology* (Vol. 53, pp. 10–18). Academic Press. https://doi.org/10.1016/j.semcdb.2015.10.037

Munnik, T., & Nielsen, E. (2011). Green light for polyphosphoinositide signals in plants. *Current Opinion in Plant Biology*, *14*(5), 489–497. https://doi.org/10.1016/j.pbi.2011.06.007

Murata, T., Sano, T., Sasabe, M., Nonaka, S., Higashiyama, T., Hasezawa, S., Machida, Y., & Hasebe, M. (2013). Mechanism of microtubule array expansion in the cytokinetic phragmoplast. *Nature Communications*, *4*. https://doi.org/10.1038/ncomms2967

Murphy, A., Peer, W., & Schulz, B. (2010). *The plant plasma membrane* (Vol. 19). http://www.springer.com/series/7089

Musielak, T. J., & Bayer, M. (2014). YODA signalling in the early Arabidopsis embryo. In *Biochemical Society Transactions* (Vol. 42, Issue 2, pp. 408–412). Portland Press Ltd. https://doi.org/10.1042/BST20130230

Newcombe, E. A., Delaforge, E., Hartmann-Petersen, R., Skriver, K., & Kragelund, B. B. (2022). How phosphorylation impacts intrinsically disordered proteins and their function. *Essays in Biochemistry*, *66*(7), 901–913. https://doi.org/10.1042/EBC20220060

Nickels, J. T., Buxeda, R. J., & Carman, G. M. (1992). Purification, Characterization, and Kinetic Analysis of a 55-kDa Form of Phosphatidylinositol 4-Kinase from Saccharomyces cerevisiae. *The Journal of Biologial Chemistry*, *267*(23), 16297–16304.

Nicolson, G. L. (2014). *The Fluid - Mosaic Model of Membrane Structure: Still relevant to understanding the structure, function and dynamics of biological membranes after more than 40 years*. Biochimica et Biophysica Acta - Biomembranes; Elsevier. https://doi.org/10.1016/j.bbamem.2013.10.019

Niemeyer, H., de la Luz CArdenas, M., Rabajille, E., Ureta, T., Clark-Turri, L., & Penaranda, J. (1975). Sigmoidal Kinetics of Glucokinase1. *Enzyme*, *20*, 321–333. https://doi.org/https://doi.org/10.1159/000458957

Noack, L., Bayle, V., Armengot, L., Rozier, F., Mamode-Cassim, A., Stevens, F. D., Caillaud, M. C., Munnik, T., Mongrand, S., Pleskot, R., & Jaillais, Y. (2022). A nanodomain-anchored scaffolding complex is required for the function and localization of phosphatidylinositol 4-kinase alpha in plants. *Plant Cell*, *34*(1), 302–332. https://doi.org/10.1093/plcell/koab135

O'Brien, P. J., & Herschlag, D. (1999). Does the active site arginine change the nature of the transition state for alkaline phosphatase-catalyzed phosphoryl transfer? *Journal of the American Chemical Society*, *121*(47), 11022–11023. https://doi.org/10.1021/ja9932582

O'Brien, P. J., Lassila, J. K., Fenn, T. D., Zalatan, J. G., & Herschlag, D. (2008). Arginine coordination in enzymatic phosphoryl transfer: Evaluation of the effect of Arg166 mutations in Escherichia coli alkaline phosphatase. *Biochemistry*, *47*(29), 7663–7672. https://doi.org/10.1021/bi800545n

Perera, I. Y., Davis, A. J., Galanopoulou, D., Yang, J. I., & Boss, W. F. (2005). Characterization and comparative analysis of Arabidopsis phosphatidylinositol phosphate 5-kinase 10 reveals differences in Arabidopsis and human phosphatidylinositol phosphate kinases. *FEBS Letters*, *579*(16), 3427–3432. https://doi.org/10.1016/j.febslet.2005.05.018

Phillips, J. C., Hardy, D. J., Maia, J. D. C., Stone, J. E., Ribeiro, J. V., Bernardi, R. C., Buch, R., Fiorin, G., Hénin, J., Jiang, W., McGreevy, R., Melo, M. C. R., Radak, B. K., Skeel, R. D., Singharoy, A., Wang, Y., Roux, B., Aksimentiev, A., Luthey-Schulten, Z., … Tajkhorshid, E. (2020). Scalable molecular dynamics on CPU and GPU architectures with NAMD. *Journal of Chemical Physics*, *153*(4). https://doi.org/10.1063/5.0014475

Preuss, M., Schmitz, A., Thole, J., Bonner, H., Otegui, M., & Nielsen; Erik. (2006). A role for the RabA4b effector protein PI-4Kβ1 in polarized expansion of root hair cells in Arabidopsis thaliana. *The Journal of Cell Biology*, *172*(7), 991–998. https://doi.org/https://doi.org/10.1083/jcb.200508116

Rao, V., Misra, S., Boronenkov, I., Anderson, R., & Hurley, J. (1998). Structure of Type II Phosphatidylinositol Phosphate Kinase: A Protein Kinase Fold Flattened for Interfacial Phosphorylation. *Cell*, *94*, 829–839. https://doi.org/10.1016/s0092-8674(00)81741-9

Rentel, M., Lecourieux, D., Ouaked, F., Usher, S., Petersen, L., Okamoto, H., Knight, H., Peck, S., Grierson, C., Hirt, H., & Knight, M. (2004). OXI1 kinase is necessary for oxidative burst-mediated signalling in Arabidopsis. *Nature*, *427*(6977), 853–858. https://doi.org/10.1038/nature02356

Romano, P. G. N., Horton, P., & Gray, J. E. (2004). The arabidopsis cyclophilin gene family. *Plant Physiology*, *134*(4), 1268–1282. https://doi.org/10.1104/pp.103.022160

Sajko, S., Grishkovskaya, I., Kostan, J., Graewert, M., Setiawan, K., Trübestein, L., Niedermüller, K., Gehin, C., Sponga, A., Puchinger, M., Gavin, A. C., Leonard, T. A., Svergun, D. I., Smith, T. K., Morriswood, B., & Djinovic-Carugo, K. (2020). Structures of three MORN repeat proteins and a re-evaluation of the proposed lipid-binding properties of MORN repeats. *PLoS ONE*, *15*(12). https://doi.org/10.1371/journal.pone.0242677

Salomon-Ferrer, R., Case, D. A., & Walker, R. C. (2013). An overview of the Amber biomolecular simulation package. *Wiley Interdisciplinary Reviews: Computational Molecular Science*, *3*(2), 198–210. https://doi.org/10.1002/wcms.1121

Sasabe, M., & Machida, Y. (2012). Regulation of organization and function of microtubules by the mitogen-activated protein kinase cascade during plant cytokinesis. *Cytoskeleton*, *69*(11), 913–918. https://doi.org/10.1002/cm.21072

Schiene, C., Reimer, U., Schutkowski, M., & Fischer, G. (1998). Mapping the stereospecificity of peptidyl prolyl cis/trans isomerases. *FEBS Letters*, *432*(3), 202–206. https://doi.org/10.1016/S0014-5793(98)00871-0

Schutkowski, M., Bernhardt, A., Zhou, X. Z., Shen, M., Reimer, U., Rahfeld, J.-U., Kun, ‡, Lu, P., & Fischer, G. (1998). *Role of Phosphorylation in Determining the Backbone Dynamics of the Serine/ Threonine-Proline Motif and Pin1 Substrate Recognition*. https://pubs.acs.org/sharingguidelines

Schutkowski, M., Reineke, U., & Reimer, U. (2005). Peptide arrays for kinase profiling. In *ChemBioChem* (Vol. 6, Issue 3, pp. 513–521). https://doi.org/10.1002/cbic.200400314

Sciorra, V., Audhya, A., Parsons, A., Segev, N., Boone, C., & Emr, S. (2005). Synthetic Genetic Array Analysis of the PtdIns 4-kinase Pik1p Identifies Components in a Golgi-specific Ypt31/rab-GTPase Signaling Pathway. *Molecular Biology Of the Cell*, *16*, 776–793. https://doi.org/https://doi.org/10.1091/mbc.e04-08-0700

Seethala, R., & Menzel, R. (1997). A Homogeneous, Fluorescence Polarization Assay for Src-Family Tyrosine Kinases. *Analytical Biochemistry*, *253*, 210–218. https://doi.org/https://doi.org/10.1006/abio.1997.2365

SERVA Electrophoresis GmbH. (2024). *Instruction Manual: Bradford Reagent, 5x Reagent for protein quantification*. https://www.serva.de/www_root/documents/39222_e_1.pdf

Shao, C., Zhang, Y., & Sun, W. (2014). Statistical characterization of HCD fragmentation patterns of tryptic peptides on an LTQ Orbitrap Velos mass spectrometer. *Journal of Proteomics*, *109*, 26–37. https://doi.org/10.1016/j.jprot.2014.06.012

Shevchenko, A., Tomas, H., Havliš, J., Olsen, J. V., & Mann, M. (2007). In-gel digestion for mass spectrometric characterization of proteins and proteomes. *Nature Protocols*, *1*(6), 2856–2860. https://doi.org/https://doi.org/10.1038/nprot.2006.468

Shevchenko, A., Wilm, M., Vorm, O., & Mann, M. (1996). Mass spectrometric sequencing of proteins from Silver stained Polyacrylamide gels. *Anal. Chem.*, *68*(5), 850–858. https://doi.org/10.1021/ac950914h

Simon, M. L. A., Platre, M. P., Assil, S., Van Wijk, R., Chen, W. Y., Chory, J., Dreux, M., Munnik, T., & Jaillais, Y. (2014). A multi-colour/multi-affinity marker set to visualize phosphoinositide dynamics in Arabidopsis. *Plant Journal*, *77*(2), 322–337. https://doi.org/10.1111/tpj.12358

Simon, M. L. A., Platre, M. P., Marquès-Bueno, M. M., Armengot, L., Stanislas, T., Bayle, V., Caillaud, M. C., & Jaillais, Y. (2016). A PtdIns(4)P-driven electrostatic field controls cell membrane identity and signalling in plants. *Nature Plants*, *2*(7). https://doi.org/10.1038/NPLANTS.2016.89

Singer, S., & Nicolson, G. (1972). The Fluid Mosaic Model of the Structure of Cell Membranes. *Science*, *175*, 720–731. https://doi.org/10.1126/science.175.4023.720

Sinha, S., Tam, B., & Wang, S. M. (2022). Applications of Molecular Dynamics Simulation in Protein Study. In *Membranes* (Vol. 12, Issue 9). MDPI. https://doi.org/10.3390/membranes12090844

Smékalová, V., Luptovčiak, I., Komis, G., Šamajová, O., Ovečka, M., Doskočilová, A., Takáč, T., Vadovič, P., Novák, O., Pechan, T., Ziemann, A., Košútová, P., & Šamaj, J. (2014). Involvement of YODA and mitogen activated protein kinase 6 in Arabidopsis post-embryogenic root development through auxin up-regulation and cell division plane orientation. *New Phytologist*, *203*(4), 1175–1193. https://doi.org/10.1111/nph.12880

Somvanshi, P. R., & Venkatesh, K. V. (2013). Hill Equation in:Encyclopedia of Systems Biology. In *Encyclopedia of Systems Biology*. Springer New York. https://doi.org/10.1007/978-1-4419-9863-7

Sousa, E., Kost, B., & Malho, R. (2008). Arabidopsis phosphatidylinositol-4-monophosphate 5-kinase 4 regulates pollen tube growth and polarity by modulating membrane recycling. *Plant Cell*, *20*(11), 3050–3064. https://doi.org/10.1105/tpc.108.058826

Soyano, T., Nishihama, R., Morikiyo, K., Ishikawa, M., & Machida, Y. (2003). NQK1/NtMEK1 is a MAPKK that acts in the NPK1 MAPKKK-mediated MAPK cascade and is required for plant cytokinesis. *Genes and Development*, *17*(8), 1055–1067. https://doi.org/10.1101/gad.1071103

Srivastava, A., Idriss, H., Taha, K., Lee, S., & Homouz, D. (2022). Phosphorylation Induced Conformational Transitions in DNA Polymerase β. *Frontiers in Molecular Biosciences*, *9*. https://doi.org/10.3389/fmolb.2022.900771

Starodubtseva, A., Kalachova, T., Retzer, K., Jelínková, A., Dobrev, P., Lacek, J., Pospíchalová, R., Angelini, J., Guivarc'h, A., Pateyron, S., Soubigou-Taconnat, L., Burketová, L., & Ruelland, E. (2022). An Arabidopsis mutant

deficient in phosphatidylinositol-4-phosphate kinases ß1 and ß2 displays altered auxin-related responses in roots. *Scientific Reports*, *12*(1). https://doi.org/10.1038/s41598-022-10458-8

Steinberg, S. F. (2018). Post-translational modifications at the ATP-positioning G-loop that regulate protein kinase activity. In *Pharmacological Research* (Vol. 135, pp. 181–187). Academic Press. https://doi.org/10.1016/j.phrs.2018.07.009

Stenzel, I., Ischebeck, T., König, S., Hołubowska, A., Sporysz, M., Hause, B., & Heilmanna, I. (2008). The type B phosphatidylinositol-4-phosphate 5-kinase 3 is essential for root hair formation in Arabidopsis thaliana. *Plant Cell*, *20*(1), 124–141. https://doi.org/10.1105/tpc.107.052852

Stenzel, I., Ischebeck, T., Quint, M., & Heilmann, I. (2012). Variable regions of PI4P 5-kinases direct PtdIns(4,5)P2 toward alternative regulatory functions in tobacco pollen tubes. *Frontiers in Plant Science*, *2*(JAN). https://doi.org/10.3389/fpls.2011.00114

Stevenson, J. M., Perera, I. Y., & Boss, W. F. (1998). A phosphatidylinositol 4-kinase pleckstrin homology domain that binds phosphatidylinositol 4-monophosphate. *Journal of Biological Chemistry*, *273*(35), 22761–22767. https://doi.org/10.1074/jbc.273.35.22761

Stevenson-Paulik, J., Love, J., & Boss, W. F. (2003). Differential regulation of two Arabidopsis type III phosphatidylinositol 4-kinase isoforms. A regulatory role for the pleckstrin homology domain. *Plant Physiology*, *132*(2), 1053–1064. https://doi.org/10.1104/pp.103.021758

Storer, A. C., & Cornish-Bowden, A. (1977). Kinetic Evidence for a “Mnemonical” Mechanism for Rat Liver Glucokinase. *Biochem. J*, *165*, 61–69. https://doi.org/10.1042/bj1650061

Strong, T. C., Kaur, G., & Thomas, J. H. (2011). Mutations in the catalytic loop HRD motif alter the activity and function of drosophila Src64. *PLoS ONE*, *6*(11). https://doi.org/10.1371/journal.pone.0028100

Sun, T., & Zhang, Y. (2022). MAP kinase cascades in plant development and immune signaling. *EMBO Reports*, *23*(2). https://doi.org/10.15252/embr.202153817

Sussman, M. R., & Harper, J. F. (1989). Molecular Biology of the Plasma Membrane of Higher Plants. *The Plant Cell*, *1*, 953–960.

Takahashi, F., Yoshida, R., Ichimura, K., Mizoguchi, T., Seo, S., Yonezawa, M., Maruyama, K., Yamaguchi-Shinozaki, K., & Shinozakia, K. (2007). The mitogen-activated protein kinase cascade MKK3-MPK6 is an important part of the jasmonate signal transduction pathway in Arabidopsis. *Plant Cell*, *19*(3), 805–818. https://doi.org/10.1105/tpc.106.046581

Takenawa, T., & Itoh, T. (2006). Membrane targeting and remodeling through phosphoinositide-binding domains. *IUBMB Life*, *58*(5–6), 296–303. https://doi.org/10.1080/15216540600732039

Teige, M., Scheikl, E., Eulgem, T., Bert, R., Czi, D., Ichimura, K., & Shinozaki, K. (2004). The MKK2 Pathway Mediates Cold and Salt Stress Signaling in Arabidopsis. *Molecular Cell*, *15*, 141–152. https://doi.org/https://doi.org/10.1016/j.molcel.2004.06.023

Tejos, R., Sauer, M., Vanneste, S., Palacios-Gomez, M., Li, H., Heilmann, M., van Wijk, R., Vermeer, J. E. M., Heilmann, I., Munnik, T., & Friml, J. (2014). Bipolar plasma membrane distribution of phosphoinositides and their requirement for auxin-mediated cell polarity and patterning in Arabidopsis. *Plant Cell*, *26*(5), 2114–2128. https://doi.org/10.1105/tpc.114.126185

Towbin, H., Staehelint, T., & Gordon, J. (1979). Electrophoretic transfer of proteins from polyacrylamide gels to nitrocellulose sheets: Procedure and some applications. *PNAS*, *76*(9), 4350–4354. https://doi.org/10.1073/pnas.76.9.4350

Van der Laan, T., Boom, I., Maliepaard, J., Dubbelman, A. C., Harms, A. C., & Hankemeier, T. (2020). Data-independent acquisition for the quantification and identification of metabolites in plasma. *Metabolites*, *10*(12), 1–14. https://doi.org/10.3390/metabo10120514

Varadi, M., Bertoni, D., Magana, P., Paramval, U., Pidruchna, I., Radhakrishnan, M., Tsenkov, M., Nair, S., Mirdita, M., Yeo, J., Kovalevskiy, O., Tunyasuvunakool, K., Laydon, A., Žídek, A., Tomlinson, H., Hariharan, D., Abrahamson, J., Green, T., Jumper, J., … Velankar, S. (2024). AlphaFold Protein Structure Database in 2024: providing structure coverage for over

214 million protein sequences. *Nucleic Acids Research*, *52*(D1), D368–D375. https://doi.org/10.1093/nar/gkad1011

Vedvik, K. L., Eliason, H. C., Hoffman, R. L., Gibson, J. R., Kupcho, K. R., Somberg, R. L., & Vogel, K. W. (2004). Overcoming Compound Interference in Fluorescence Polarization-Based Kinase Assays Using Far-Red Tracers. In *ASSAY and Drug Development Technologies* (Vol. 2, Issue 2). https://doi.org/10.1089/154065804323056530

Vermeer, J. E. M., Thole, J. M., Goedhart, J., Nielsen, E., Munnik, T., & Gadella, T. W. J. (2009a). Imaging phosphatidylinositol 4-phosphate dynamics in living plant cells. *Plant Journal*, *57*(2), 356–372. https://doi.org/10.1111/j.1365-313X.2008.03679.x

Vermeer, J. E. M., Thole, J. M., Goedhart, J., Nielsen, E., Munnik, T., & Gadella, T. W. J. (2009b). Imaging phosphatidylinositol 4-phosphate dynamics in living plant cells. *Plant Journal*, *57*(2), 356–372. https://doi.org/10.1111/j.1365-313X.2008.03679.x

Walker, E., Peristic, O., Ried, C., Stephens, L., & William, R. (1999). Structural insights into phosphoinositide 3-kinase catalysis and signalling. *Letters to Nature*, *402*, 313–319. https://doi.org/https://doi.org/10.1038/46319

Wang, P., Hsu, C.-C., Du, Y., Zhu, P., Zhao, C., Fu, X., Zhang, C., Sebastian Paez, J., Macho, A. P., Andy Tao, W., & Zhu, J.-K. (2020). Mapping proteome-wide targets of protein kinases in plant stress responses. *The Proceedings of the National Academy of Sciences (PNAS)*, *117*(6), 3270–3280. https://doi.org/10.1073/pnas.1919901117/-/DCSupplemental

Wu, C., Tan, L., van Hooren, M., Tan, X., Liu, F., Li, Y., Zhao, Y., Li, B., Rui, Q., Munnik, T., & Bao, Y. (2017). Arabidopsis EXO70A1 recruits Patellin3 to the cell membrane independent of its role as an exocyst subunit. *Journal of Integrative Plant Biology*, *59*(12), 851–865. https://doi.org/10.1111/jipb.12578

Wu, D., & Wu, Z. (2010). Superimposition of protein structures with dynamically weighted RMSD. *Journal of Molecular Modeling*, *16*(2), 211–222. https://doi.org/10.1007/s00894-009-0538-6

Xue, H. W., Pical, C., Brearley, C., Elge, S., & Müller-Röbert, B. (1999a). A plant 126-kDa phosphatidylinositol 4-kinase with a novel repeat structure.

Cloning and functional expression in baculovirus-infected insect cells. *Journal of Biological Chemistry*, *274*(9), 5738–5745. https://doi.org/10.1074/jbc.274.9.5738

Xue, H. W., Pical, C., Brearley, C., Elge, S., & Müller-Röbert, B. (1999b). A plant 126-kDa phosphatidylinositol 4-kinase with a novel repeat structure. Cloning and functional expression in baculovirus-infected insect cells. *Journal of Biological Chemistry*, *274*(9), 5738–5745. https://doi.org/10.1074/jbc.274.9.5738

Yang, Y., Han, X., Ma, L., Wu, Y., Liu, X., Fu, H., Liu, G., Lei, X., & Guo, Y. (2021). Dynamic changes of phosphatidylinositol and phosphatidylinositol 4-phosphate levels modulate H+-ATPase and Na+/H+ antiporter activities to maintain ion homeostasis in Arabidopsis under salt stress. *Molecular Plant*, *14*(12), 2000–2014. https://doi.org/10.1016/j.molp.2021.07.020

Yon-Kahn, J., & Hervé, G. (2010). *Molecular and Cellular Enzymology Volume I*. Springer-Verlag. http://grenoble-sciences.ujf-grenoble.fr/

Zhang, W., Liu, H. T., & Tu, H. (2002). MAPK signal pathways in the regulation of cell proliferation in mammalian cells. *Cell Research*, *12*, 9–18. https://doi.org/https://doi.org/10.1038/sj.cr.7290105

Zhao, X. H., Bondeva, T., & Balla, T. (2000). Characterization of recombinant phosphatidylinositol 4-kinase β reveals auto- and heterophosphorylation of the enzyme. *Journal of Biological Chemistry*, *275*(19), 14642–14648. https://doi.org/10.1074/jbc.275.19.14642

Zimmermann, P., Hirsch-Hoffmann, M., Hennig, L., & Gruissem, W. (2004). Genevestigator. Arabidopsis microarray database and analysis toolbox. *Plant Physiology*, *136*(1), 2621–2632. https://doi.org/10.1104/pp.104.046367

6. Appendix

6.1. Additional information for results

6.1.1. *E. coli* cell lysates, Western Blots and enriched MBP-PI4Kβ1

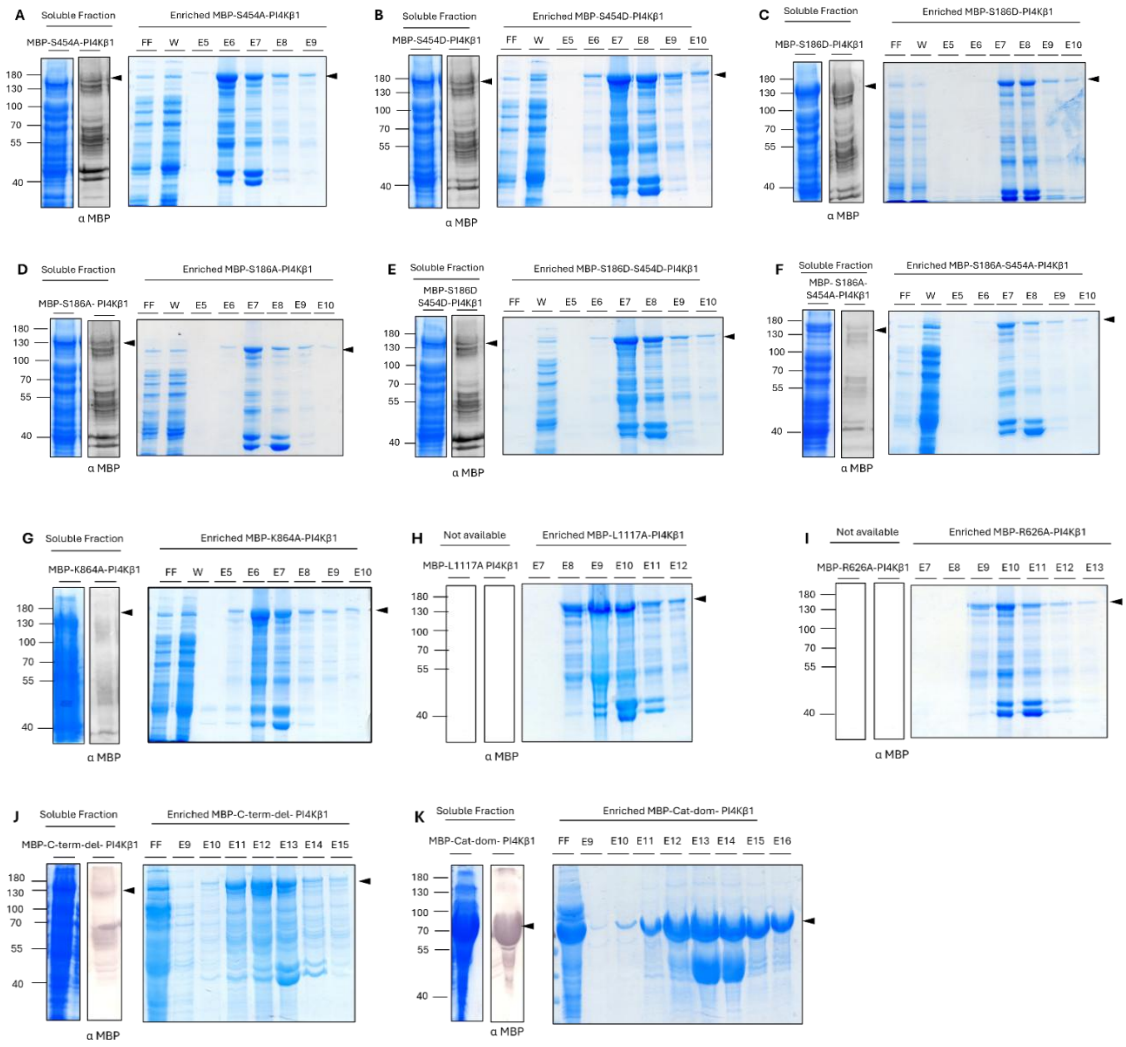

Figure 34.Enrichment of MBP-PI4Kβ1 substitution and truncated variants. The overexpression of all MBP-PI4Kβ1 substitution and truncated variants was first confirmed by SDS-PAGE gel, then immunodetected using a primary antibody against MBP and a secondary antibody against IgG with an AP conjugate for colorimetric detection. The soluble fraction was used for enrichment and different elution fractions were collected (E). **A**. MBP-S454A-PI4Kβ1. **B.** MBP-S454D-PI4Kβ1. **C**. MBP-S186D- PI4Kβ1. **D.** MBP-186A-PI4Kβ1. **E**. MBP-S186D-S454D-PI4Kβ1 **F.** MBP-S186A-S454A-PI4Kβ1. **G.** MBP-K864A-PI4Kβ1-His5x. **H**. MBP-L1117A-PI4Kβ1**. I.** MBP-R626-PI4Kβ1. **J**. MBP-ΔC-terminus-deletion-PI4Kβ1. **K.** MBP-Catalytic-domain-PI4Kβ1. The size of the corresponding MBP-PI4Kβ1 fusion protein is indicated by a black arrowhead. PageRuler™ Prestained Protein Ladder was used as a molecular size marker. Expected molecular sizes of all the full-length MBP-PI4Kβ1 substitution variants was 168 kDa. The expected molecular size for the MBP-ΔC -terminus-deletion-PI4Kβ1 was 166 kDa and for MBP-Catalytic-domain-PI4Kβ1 was 77.5 kDa.

6.1.2. Calibration curve for radiolabeled [γ-^{32}P] ATP

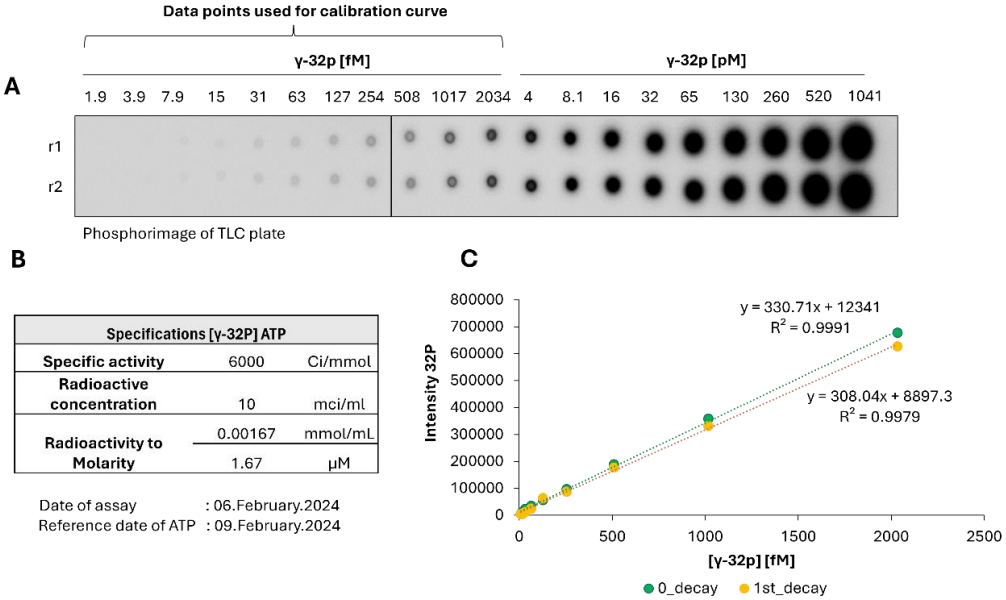

Figure 35.Calibration curve for radiolabeled [γ-^{32}P] ATP. A. Phosphorimage of TLC plate (25 min exposure) showing serial dilutions in duplicates in a ratio of 1:1 of (ddH_2O: γ-^{32}P-ATP). **B.** Table showing the specifications for the [gamma-^{32}P] ATP (Reference: SRP-501) used here. **C.** ATP standard curve showing different γ-^{32}P-ATP concentrations with the corresponding intensities. The linear regression analysis shows a $R^2 > 0.99$ and the slope and y-intercept for 0 and 1st decay.

6.1.3. Lipid Identity test

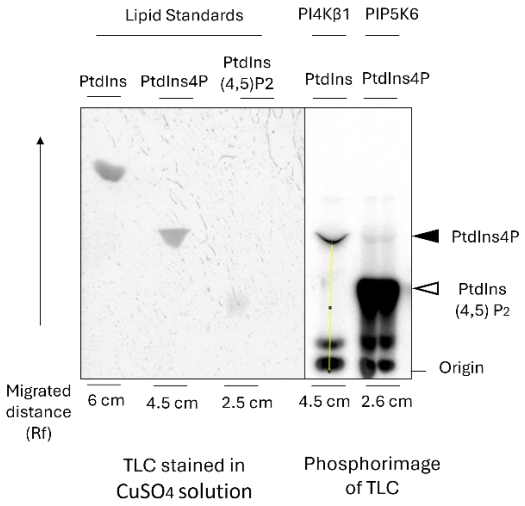

Figure 36. Lipid identity test. The identity of the lipid product PtdIns4P was assessed by TLC analysis by measuring the relative migration values (Rf) between the lipid standards (left) and the unknown lipid samples (right). The lipid standard PtdIns4P showed a Rf= 4.5 cm as well as the unknown lipid sample obtained after incubation of PI4Kβ1 with the substrate PtdIns. The TLC plate containing the lipid standards was dipped in a staining solution, air-dried and heated to visualize the standards. The TLC plate containing the unknown radioalebeled lipid samples was air-dried and the radiolabeled PtdIns4P was visualized by phosphorimaging. PtdIns4P identity could be confirmed after obtaining the same Rf= 4.5 cm as the PtdIns4P standard (yellow line). In parallel PIP5K6 kindly provided by Dr. Schutkowski was assayed using PtdIns4P as a substrate to distinguish migration distance between the products of reaction PtdIns4P and PtdIns (4,5)P_2

6.1.4. Kinetic characterization of catalytic domain PI4Kβ1

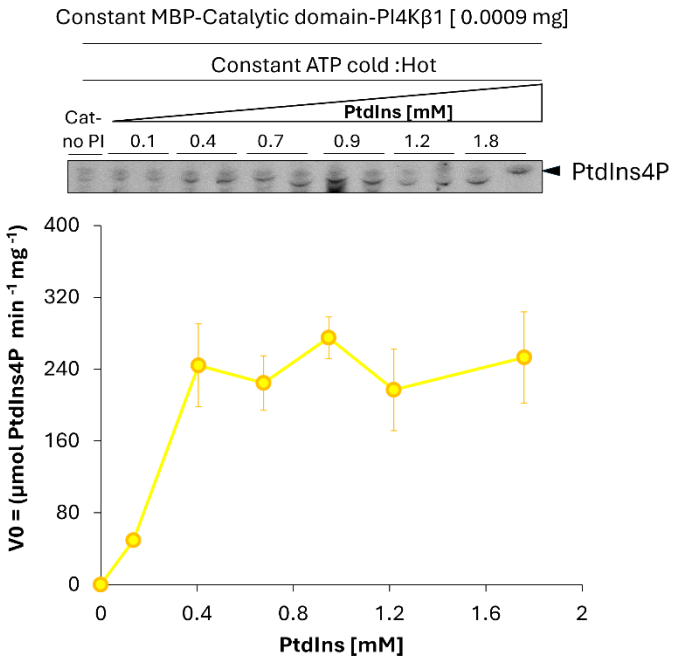

Figure 37.Kinetic characterization of catalytic domain of PI4Kβ1. Non-sigmoidal reaction kinetics was obtained for the recombinantly expressed and enriched MBP-Catalytic-domain-PI4Kβ1 by plotting the initial velocity as a function of increasing PtdIns concentrations. Black arrow shows the product of the reaction (PtdIns4P) resolved by TLC plate and the radioactive lipid was detected by phosphorimaging. Radioactive phosphorylated PtdIns4P was quantified in ImageQuant by densitometry using the calibration curve for radiolabeled [γ-^{32}P] ATP. The exposure time of TLC plate was 24 h. Error bars represent the standard error (SE) of two data points relative to the population mean.. The experiment was performed two times in duplicates.

6.1.5. Control SDS-PAGE gels for kinetics characterization of PI4Kβ1 and variants

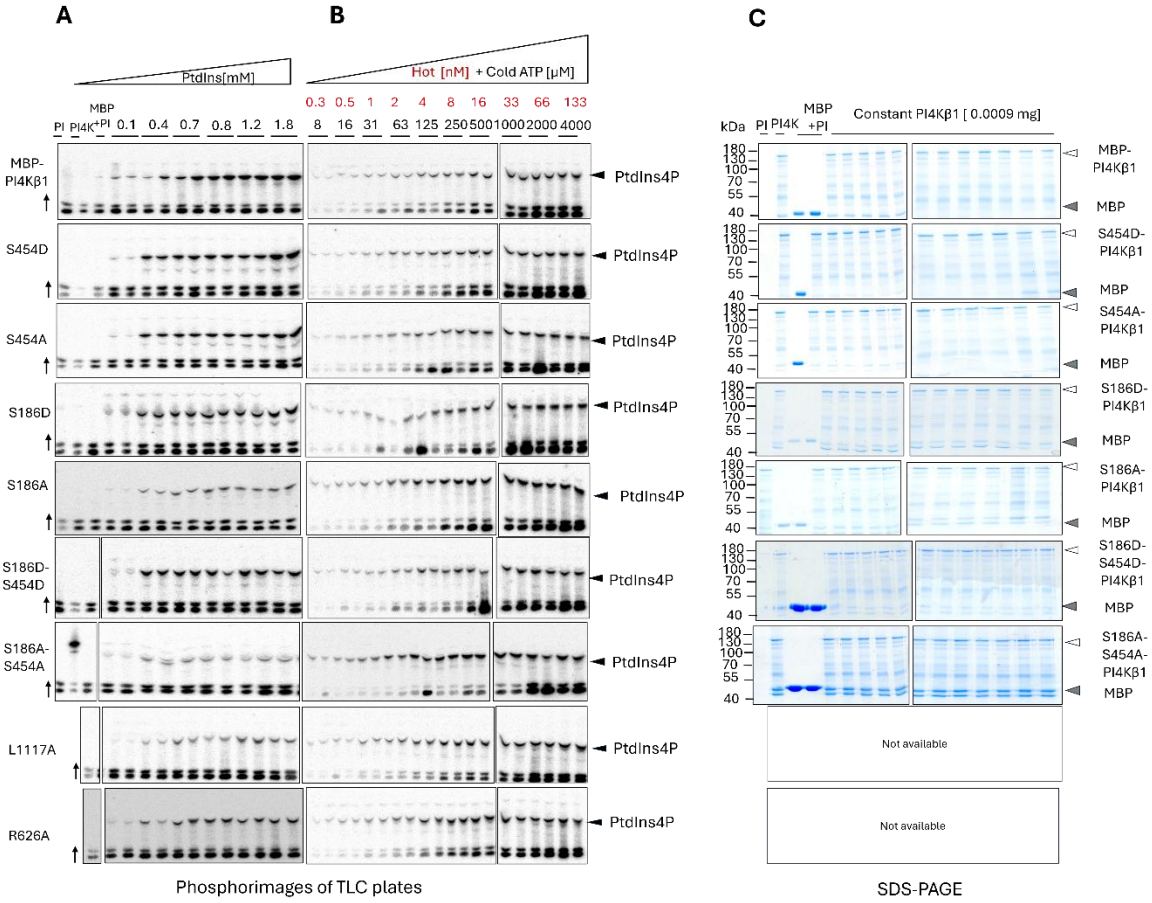

Figure 38. Control SDS-PAGE for kinetic characterization of MBP-PI4Kβ1 for PtdIns and ATP saturation curves. A. Phosphorimages of TLC plates of PtdIns saturation curves for MBP-PI4Kβ1 and substitution variants showing the product of the reaction PtdIns4P (black arrow). **B.** Phosphorimages of TLC plates of ATP saturation curves for MBP-PI4Kβ1 and substitution variants showing the product of the reaction PtdIns4P (black arrow). **C.** Control protein gels for PtdIns and ATP saturation curves showing equal concentrations [0.0009 mg] of MBP-PI4Kβ1 and substitution variants (white arrow) and MBP (gray arrow) used for kinetic characterization. Protein amounts were estimated by densitometry on Coomassie-stained SDS-PAGE gels, using BSA as a known standard. Vertical arrow on the left of the TLC plates indicates the direction in which lipids resolved. Protein sizes were determined according to a the PageRuler™ Prestained Protein Ladder. The expected molecular sizes for the proteins used were as follows, MBP-PI4Kβ1 and all substitution variants, 168 kDa; MBP: 42 kDa;. Assays for MBP- PI4Kβ1 were performed four times and for all substitution variants at least two times.

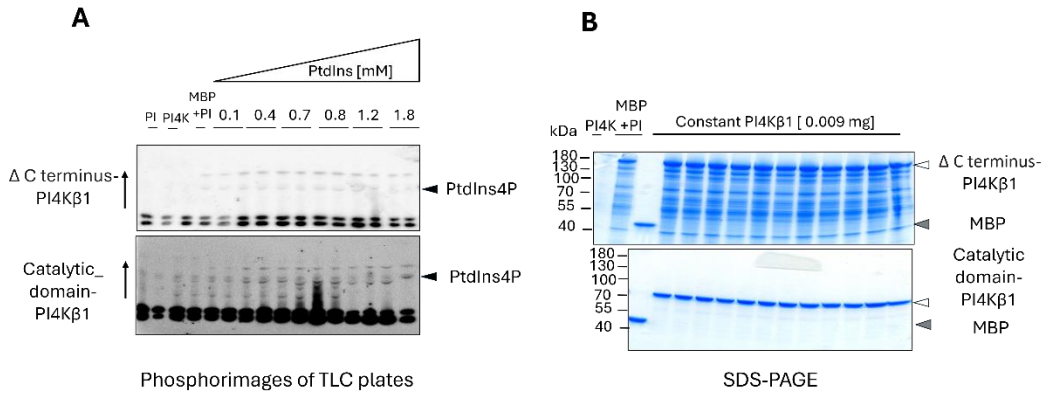

Figure 39. Control SDS-PAGE for kinetic characterization of MBP-PI4Kβ1 variants deleted for PtdIns saturation curves. A. Phosphorimages of TLC plates of PtdIns saturation curves for MBP-PI4Kβ1 variants deleted showing the product of the reaction PtdIns4P (black arrow). **B.** Control protein gels showing equal concentrations [0.0009 mg] of MBP-PI4Kβ1 deleted variants (white arrow) and MBP (gray arrow) used for kinetic characterization. Protein amounts were estimated by densitometry on Coomassie-stained SDS-PAGE gels, using BSA as a known standard. Vertical arrow on the left of the TLC plates indicates the direction in which lipids resolved. Protein sizes were determined according to a the PageRulerTM Prestained Protein Ladder. The expected molecular sizes for the proteins used were as follows Δ C-terminal PI4Kβ1 11107-1121: 167 kDa and catalytic domain $PI4K\beta1_{806\text{-}1121}$ variant: 77 kDa; MBP: 42 kDa;. Assays were performed two times.

6.1.6. Superposition of PI4Kβ1 with PI3K and MD analysis

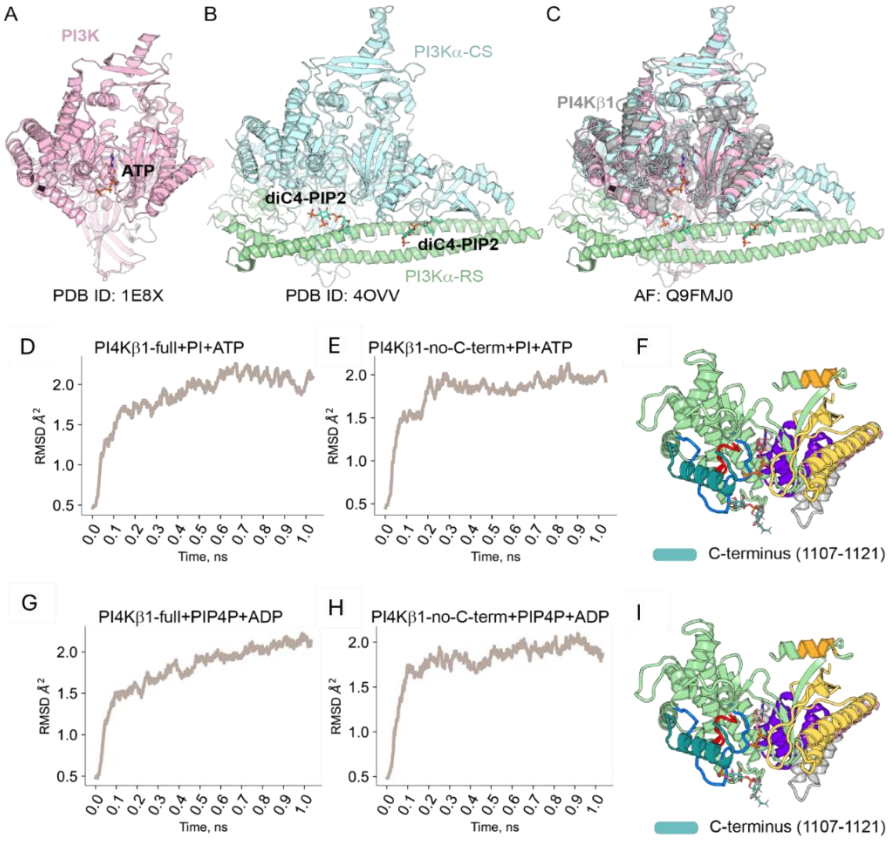

Figure 40.Superposition of Alpha fold model PI4Kβ1 with human PI3K and Root Mean Square deviation (RMSD) after MD analysis. A. Structure of PI3K (phosphatidylinositol 4,5-bisphosphate 3-kinase catalytic subunit gamma

isoform) (PDB:ID 1E8X). **B.** Structure of the PI3Kα-CS (phosphatidylinositol 4,5-bisphosphate 3-kinase catalytic subunit alpha isoform) and the PI3Kα-RS (phosphatidylinositol 3-kinase regulatory subunit alpha) (PDB:ID 4OVV) with diC4-PIP_2. **C.** Superposition of AF-PI4Kβ1 (PDB:ID Q9FMJ09) with both human PI3Ks.**D.** RMSD of the 1.0 ns MD of full-length PI4Kβ1 with ATP and PI (or PtdIns)**. E.** RMSD of the 1.0 ns MD of PI4Kβ1-no-c-term with ATP and PI. **F.** The PI4Kβ1+ATP+PI system with color coded C-terminus. **G.** RMSD of the 1.0 ns MD of full-length-PI4Kβ1 with ADP and PIP4P (or PtdIns4P). **H**. RMSD of the 1.0 ns MD of PI4Kβ1-c-terminus-deletion with ADP and PIP4P. **I.** The PI4Kβ1+ADP+PIP4P system with color coded C-terminus.

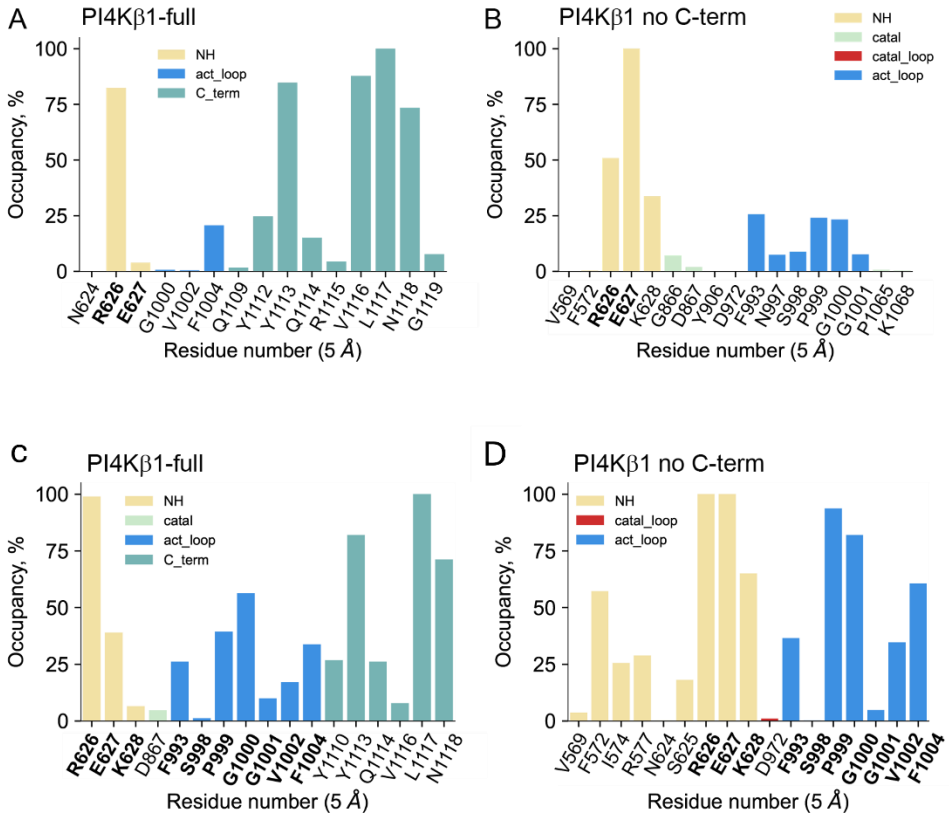

Figure 41. Key residues of PI4Kβ1 interacting with substrate and product during 1 ns MD. A. PI4Kβ1-full length (F46-A143; N541-E641; E835-L1121) interacting with PtdIns **B.** PI4Kβ1-no-C-term interacting with PI (or PtdIns) (F46-A143; N541-E641; E835-D1103). **C**. PI4Kβ1-full interacting with PIP4P (or PtdIns4P). **D.** PI4Kβ1-no-C-term interacting with PIP4P. The occupancy (%) is the proportion of frames in which the residue was 5 Å around the PtdIns. The belonging of each residue to domains is colour coded (NH: new homology; catal: catalytic; catal_loop: catalytic loop; act_loop: activation loop; C_term: C-terminus).

6.1.7. *E. coli* cell lysates, Western Blots and enriched upstream kinases

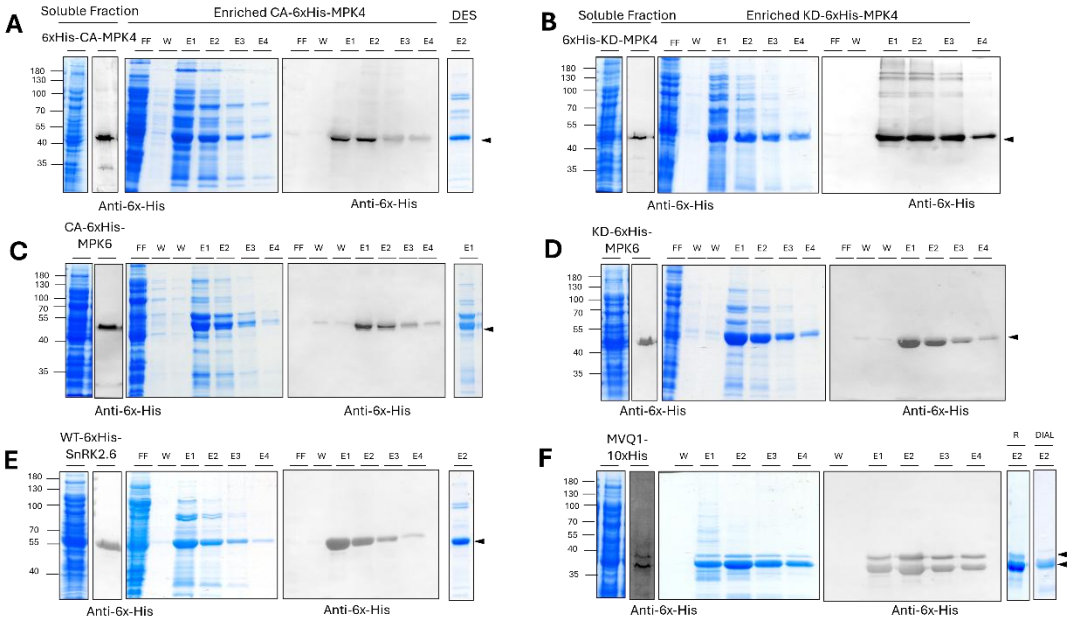

Figure 42. Enrichment of upstream kinases and MVQ1. The overexpression of all upstream kinases and MVQ-1 was first confirmed by SDS-PAGE gel, then immunodetected using a primary antibody against His-tag and a secondary antibody with an AP conjugate for colorimetric detection. The soluble fraction was used for small-scale enrichment using the beads and different elution fractions were collected (E), washing (W), elution after desalting (DES), renaturated (R), after dyalisis (DIAL). **A.** CA-$_{6x}$His-MPK4. **B.** KD-$_{6x}$His-MPK4**. C.** CA-$_{6x}$His-MPK4. **D.** KD-6xHis-MPK4. **E.** WT-6x-SnRK2:6 **F**. MVQ1-His10x. The size of the corresponding upstream kinase is indicated by a black arrowhead. Protein sizes were determined according to the PageRuler™ Prestained Protein Ladder. The expected molecular size for all proteins was: CA-$_{6x}$His-MPK4 (42 kDa), KD-$_{6x}$His-MPK4 (42 kDa), CA-$_{6x}$His-MPK6 (48 kDa), KD-$_{6x}$His-MPK6 (48 kDa), WT-$_{6x}$His-SnRK2.6 (41 kDa), MVQ1-$_{10x}$-His (27 kDa) ; MVQ1 exhibited 2 splice forms (runs higher than expected MW ~ 38 kDa) (klindly provided by Pecher form the Leibniz Institute of Plant Biochemistry, Halle, Germany)

6.1.8. Control gel for MS analysis and coverage of PI4Kβ1

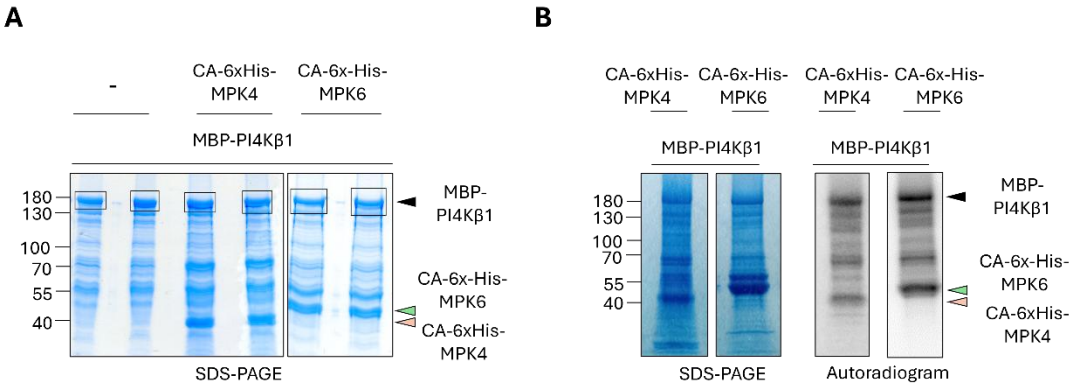

Figure 43. SDS-PAGE control gel used for in-gel digestion of PI4Kβ1 bands for LC-MS/MS. *In vitro* phosphorylation assays were performed by incubating MBP-WT-PI4Kβ1 and the upstream CA-$_{6x}$His-MPK4 or CA-$_{6x}$His-MPK6 together

with cold ATP. A control gel was run in parallel to verify that enriched MAPKs phosphorylated the substrate kinase. **A**. Black squares surround the band excised corresponding to PI4Kβ1 (1.5 µg; ≈ 9.1 µM) running at 168 kDa (Black arrow). The protein gel from left to right in duplicates, shows the control sample by incubating PI4Kβ1 alone without upstream kinase, then PI4Kβ1 with upstream MPK4 (orange arrow) and PI4Kβ1 with upstream MPK6 (green arrow). Bands were excised from the gel, reduced, alkylated and digested with trypsin for LC-MS/MS. **B.** Control protein gel for the enriched proteins used for LC/MS on the left and detection of phosphorylated MBP-WT-PI4Kβ1 by phosphorimaging on the right. Protein sizes were determined according to the PageRuler™ Prestained Protein Ladder. The expected molecular size for all proteins was: CA-$_{6x}$His-MPK4 (42 kDa), CA-$_{6x}$His-MPK6 (48 kDa) and MBP-WT-PI4Kβ1 (168 kDa).

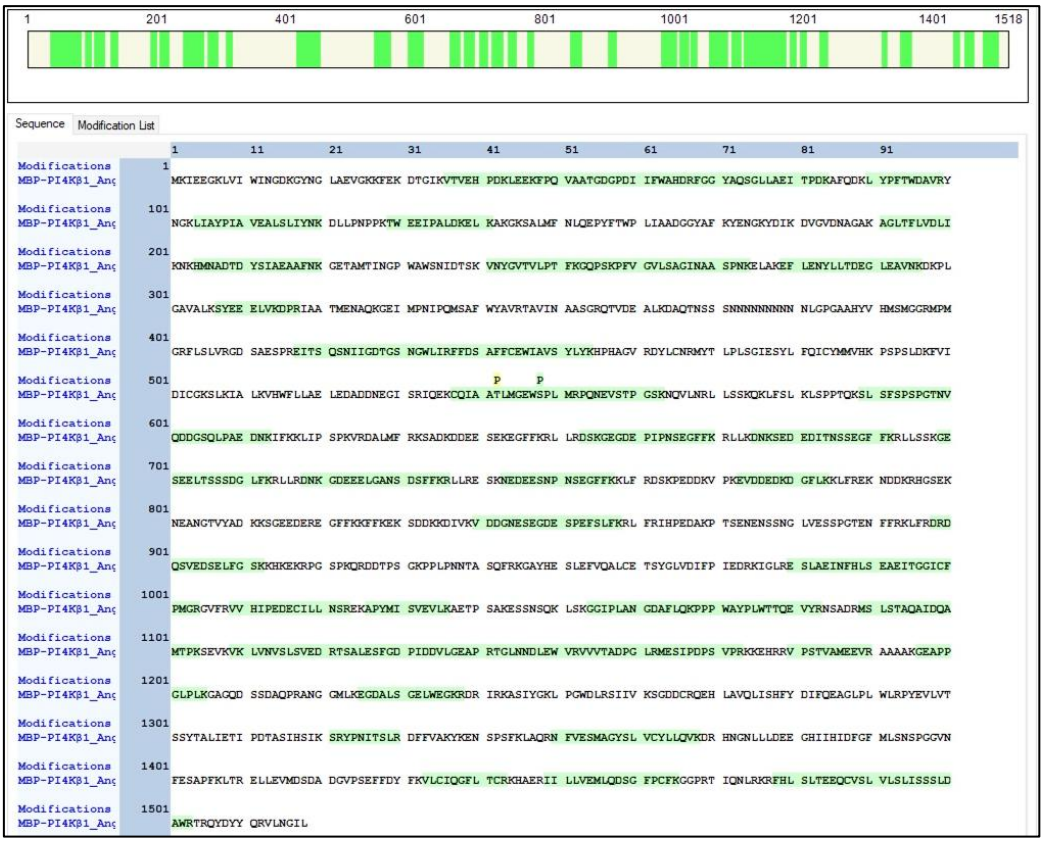

Figure 44. Representative coverage of PI4Kβ1 for MS- analysis of trypsin digested peptides. Recombinant MBP-WT-PI4Kβ1 protein was phosphorylated with recombinant MPK4 or MPK6 *in vitro*. Proteins were separated by SDS-PAGE, bands excised, and in-gel trypsin digestion was performed. The resulting peptides were analyzed by MS. A sequence coverage value of 50% was obtained here. Peptide sequences outlined in green represent the proportion of covered peptides for PI4Kβ1.

6.1.9. Time-course of *in vitro* radioactive lipid phosphorylation by MBP-PI4Kβ1, pre-phosphorylated by MAPK.

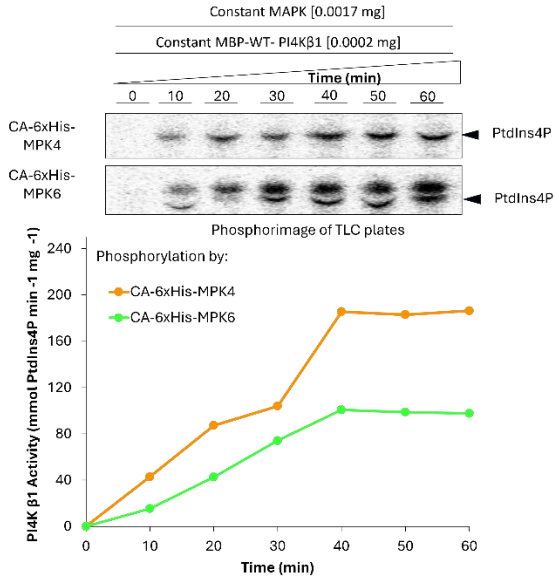

Figure 45. Time-course of *in vitro* radioactive lipid phosphorylation by MBP-PI4Kβ1, pre-phosphorylated by CA-$_{6x}$His-MPK4 or CA-$_{6x}$His-MPK6. The substrate protein, MBP-PI4Kβ1, was pre-phosphorylated for 15 min in the presence of cold ATP by CA-$_{6x}$His-MPK4 or CA-$_{6x}$His-MPK6 and subsequently the lipid substrate PtdIns and [γ-^{32}P]ATP were added to monitor the formation of the radiolabeled product PtdIns4P at 10 min intervals over a period of 60 min. Representative phospohorimages of the TLC plates are shown, where the black arrow head represents the migration of PtdIns4P. The line graph represents the activity of MBP-PI4Kβ1 upon pre-phosphorylation by the respective MAPK, as indicated. Radioactive phosphorylated PtdIns4P was quantified in ImageQuant by densitometry using the calibration curve for radiolabeled γ [32P]ATP. The control assay was performed one time.

6.1.10. Lipid overlay assays: PIP STRIPS

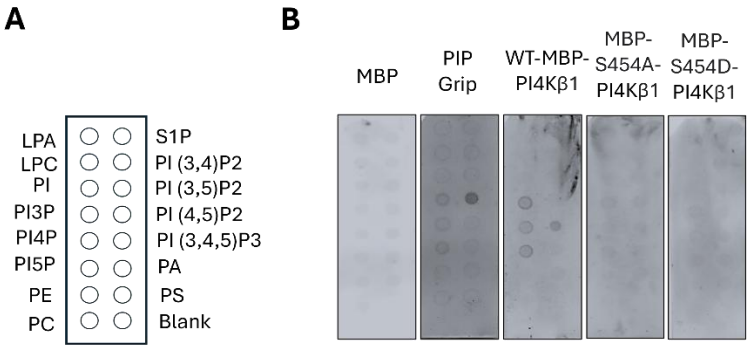

Figure 46. Lipid blots PIP STRIPS. Lipid interaction studies of PI4Kβ1 with PIs. **A.** Schematic representation of the PIP strips used for lipid overlay assays. PIs in plants (PtdIns3P, PtdIns4P, PtdIns(5)P, PtdIns(3,5)P2, PtdIns(4,5)P2). Non-plant specific PIs, phosphatidylinositol 3,4-bisphosphate (PtdIns(3,4)P2), phosphatidylinositol 3,4,5-trisphosphate (PtdIns(3,4,5)P3) and further phospholipids were spotted, lysophosphatidic acid (LPA), lysophosphatidylcholine (LPC), sphingosine 1-phosphate (S1P), phosphatidylinositol (PtdIns), phosphatidylethanolamine (PtdEtn), phosphatidylcholine (PtdCho), phosphatidic acid (PtdOH), phosphatidylserine

(PtdSer). **B**. Lipid overlay assays with MBP, PIP Grip and enriched MBP-PI4Kβ1. Interactions were visualized by using a primary antibody against MBP and a secondary antibody with an AP conjugate for colorimetric detection. The experiment was repeated one time.

6.1.11. Effect of MAPKs phosphorylation on PI4Kβ1 variants activity

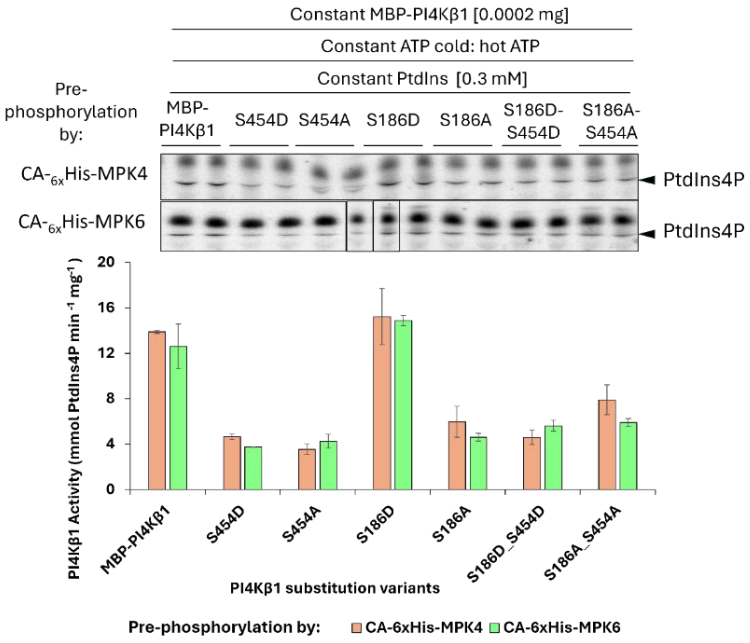

Figure 47. Effect of MAPKs phosphorylation on MBP-PI4Kβ1 and substitution variants activity. The recombinant MAPKs were pre-incubated together MBP-PI4Kβ1 and cold ATP to allow phosphorylation of the target kinase. A control gel was loaded to monitor equal protein concentrations loaded (data not shown). Product of the lipid kinase reaction is indicated by a black arrow (PtdIns4P). Phosphorylated MBP-PI4Kβ1 by CA-6xHis-MPK4 represented in orange bars. Phosphorylated MBP-PI4Kβ1 by CA-6xHis-MPK6, represented in green bars. The experiment was performed three times with similar results. Error bars represent the standard deviation (SD) of six data points relative to the mean.

6.1.12. Summary of identified phosphopeptides for PI4Kβ1

Table 14.Summary of identified phosphopeptides for *Arabidopsis* PI4Kβ1 in LC/MS/MS. The peptides listed were identified from PI4Kβ1 after separate incubations with either MPK4 or MPK6 and identified by a LC-MS-MS setup with the LC ultimate 3000 UHPLC coupled to Orbitrap Exploris ™ 480 Mass Spectrometer (Fisher Scientific, Schwerte, Germany). The Proteome Discoverer 2.5 was used to analyze the data. The table shows the upstream kinase used for the phosphorylation reaction, the putative phosphosites found in the substrate kinase PI4Kβ1, the sequence motif and the post-translational modification) PTM score probability within the peptide. Probability is based on the probability of all possible phosphorylation sites in the peptide sequence based on interpretation of the MS/MS fragment ion pattern.

Upstream Kinase	Putative site in PI4Kβ1	Sequence motif	PTM probability (%)	# of times in 3 repetitions
MPK4	S208	PGTNVQDDGsQLPAEDNKI	48.7	2
MPK4	S224	KIFKKLIPsPKVRDALM	100	4
MPK4	S299	EGFFKRLLsSKGESEEL	49.4	4
MPK4	S300	GFFKRLLSsKGESEELT	49.4	2
MPK4	S304	LSSKGEsEELTSS	98.7	6
MPK4	T308	GESEELtSSSDGL	98	3
MPK4	S309	SKGESEELTsSSDGLFKRL	33.3	2
MPK4	S310	KGESEELTSsSDGLFKRLL	33.3	2
MPK4	S449	IVKVDDGNEsEGDESPEFS	100	1
MPK4	S454	DGNESEGDEsPEFSLFKRL	2	1
MPK4	T531	GSPKQRDDtPSGKPPLP	93.6	2
MPK6	S14	RFLSLVRGDsAESPREITS	100	2
MPK6	S17	SLVRGDSAEsPREITSQSN	98.5	3
MPK6	T145	IQEKCQIAAtLMGEWSPLM	100	1
MPK6	S224	KIFKKLIPsPKVRDALM	100	2
MPK6	S268	EGDEPIPNsEGFFKRLL	100	2
MPK6	S299	SEGFFKRLLsSKGESEELT	98.9	6
MPK6	S300	EGFFKRLLSsKGESEELTS	50	6
MPK6	T308	SSKGESEELtSSSDGLFKR	98.1	4
MPK6	S309	KGESEELTsSSDGLFKR	49.7	2
MPK6	S311	ESEELTSSsDGLFKRLL	99.9	2
MPK6	S333	GDEEELGANsDSFFKRLLR	100	2
MPK6	S344	FFKRLLREsKNEDEESN	100	2
MPK6	S454	DGNESEGDEsPEFSLFKRL	2	1
MPK6	T531	GSPKQRDDtPSGKPPLP	99.8	2
MPK6	S533	PKQRDDTPsGKPPLPNN	50	2
MPK6	T642	SVEVLKAEtPSAKESSN	99.8	1
MPK6	T705	TAQAIDQAMtPKSEVKVKL	100	2
MPK6	T1073	PCFKGGPRtIQNLRKRF	100	1

6.1.13. Summary of identified phosphopeptides PI4Kβ1 in peptide arrays

Table 15.Summary of identified phosphopeptides for *Arabidopsis* PI4Kβ1 in peptide arrays. The peptides listed were identified from PI4Kβ1 after separate incubations with either MPK4 or MPK6 and identified by phosphorimaging of peptide arrays (High-Density PepStar microarray format - JPT). Aminoacids outlined in yellow represent the phosphorylated residue on each respective sequence.

PI4Kβ1 Sequence No.	Position in PI4Kβ1 sequence	Targeted by MPK4	Position in PI4Kβ1 sequence	Targeted by MPK6
3	S8	LSLVRGDSAESPR	S175, S176	RLLSSKQKLFSLK
4	S77	LCNRMYTLPLSGI	None	None
5	S14, S17	VRGDSAESPREIT	None	None

6.2. Additional information for methods

6.2.1. Oligonucleotides used here

Table 16. Oligonucleotides used for cloning.

Vector	Gene of interest	Oligonucleotide sequence 5´ - 3´
pMal-c5G	PI4Kβ1 (Full length)	PI4Kb1**for**NotI AtcgGCGGCCGCatgccgatgggacgctttct PI4kb1**rev**BamHI atgcGGATCCtcacaatattccatttaaga
pGEX4T-1	PI4Kβ1 (Full length)	PI4Kb1**for**BamHI atgcGGATCCatgccgatgggacgctttct PI4Kb1**rev**SalI atgcGTCGACtcacaatattccatttaaga
pMal-c5G	PI4Kβ1 (C-terminus-deletion)	PI4Kb1**for**NotI atcgGCGGCCGCatgccgatgggacgctttct pi4kb1_delCterm_**rev**BamHI_3 atcgGGATCCtcaccgccaagcatctaagctact
pMal-c5G	PI4Kβ1 (Catalytic domain)	PI4Kb1**for**NotI_trunc_Cat_Dom atcgGCGGCCGCatgcctctcaaaggggcggg PI4kb1**rev**BamHI atgcGGATCCtcacaatattccatttaaga
pDONR221	MPK4 (Full length)	B1-MPK4-**for**

		atgcGGGGACAAGTTTGTACAAAAAAGCAGGCTTC atgtcggcggagagttgtttcgg B2-MPK4-**rev** atgcGGGGACCACTTTGTACAAGAAAGCTGGGTCt cacactgagtcttgaggattgaa
pDONR221	SnRK2.6 (Full length)	B1_SNRK2.6 _**for** atgcGGGGACAAGTTTGTACAAAAAAGCAGGCTTC atggatcgaccagcagtgagtgg B2_SNRK2.6 _**rev** atgcGGGGACCACTTTGTACAAGAAAGCTGGGTCt cacattgcgtacacaatctctcc

Table 17. Oligonucleotides used for sequencing

Analyzed_sequence	Name	Oligonucleotide sequence 5´ - 3´
pMal-c5G	pMAL-for pMAL-rev	ATGCCGAACATCCCGCAGAT TTGTCCTACTCAGGAGAGCGTT
pGEX4T-1	pGEX-for pGEX-rev	GGGCTGGCAAGCCACGTTTGGTG CCGGGAGCTGCATGTGTCAGAGG
T7 promoter	T7 for	TAATACGACTCACTATAGGG
T7 terminator	T7 rev	GCTAGTTATTGCTCAGCGG
PDONR221	M13_for M13_rev	GTAAAACGACGGCCAGTG GGAAACAGCTATGACCATG
PI4Kβ1	PI4Kb1_For(own) SeqPI4kB1_For_a1 SeqPI4kB1_For_a2	ATGCCGATGGGACGCTTT GAGGACATAACAAACAGTTCCG CTGCATCACAATTCAGGAAAGGG
MPK4	For1seqmpk4 For2sseqmpk4	ATGTCGGCGGAGAGTTGTTTCGG CGAGGACCAAATCCGAGACTG

Table 18. Oligonucleotides used for site directed-mutagenesis

Vector	Mutation desired	Oligonucleotide sequence 5´ - 3´
PDEST17	V69A_MPK4 (Inactive)	MutVA-MPK4-inact For CGTCCTATCGgcaGAGGCGCTTA MutVA-MPK4-inact Rev TAAGCGCCTCtgcCGATAGGACG
PDEST17	K92R_MPK4 (Inactive)	K92R-MPK4-inact For GGTAGCTATCaggAAGATTGGTAATG K92R-MPK4-inact Rev CATTACCAATCTTcctGATAGCTACC
PDEST17	D160A_SnRK2.6	SnrK2.6_D160A_for CCTCGTCTAAAGATATGTgcaTTCGGATATTC SnrK2.6_D160A_rev GAATATCCGAAtgcACATATCTTTAGACGAGG
pMal-c5G	S454A_PI4Kβ1	Abmut1S454Afor GGGTGATGAAgcaCCAGAATTTTC Abmut1S454Arev GAAAATTCTGGtgcTTCATCACCC
pMal-c5G	S449A_PI4Kβ1	Abmut2S449AFOR CGGGAATGAAgcaGAGGGTGATGAATC Abmut2S449AREV GATTCATCACCCTCtgcTTCATTCCCG
pMal-c5G	S186A_PI4Kβ1	Abmut3S186AFO CTTAAAGCTAgcaCCTCCCACCC Abmut3S186AREV GGGTGGGAGGtgcTAGCTTTAAG
pMal-c5G	S454D_PI4Kβ1	Mimmut1S454DFOR GGGTGATGAAgatCCAGAATTTTCTCTTTTC Mimmut1S454DREV GAAAAGAGAAAATTCTGGatcTTCATCACCC
pMal-c5G	S449D_PI4Kβ1	Mimmut2S449DFOR CGGGAATGAAgatGAGGGTGATGAATC Mimmut2S449DREV GATTCATCACCCTCatcTTCATTCCCG
pMal-c5G	S186D_PI4Kβ1	Mimmut3S186DFOR CTTAAAGCTAgatCCTCCCACCC Mimmut3S186DREV GGGTGGGAGGatcTAGCTTTAAG
pMal-c5G	L1117A_PI4Kβ1	PI4Kβ1_for_L1117A ctaccaacgggtcGCAaatggaata PI4Kβ1_rev_L1117A tattccattTGCgacccgttggtag

pMal-c5G	R626A_PI4Kβ1	PI4Kβ1_for_R626A TtgaattctGCAgaaaaggcgccatac PI4Kβ1_rev_R626A gtatggcgccttttcTGCagaattcaa

6.2.2. Composition of self-cast 8% SDS-PAGE protein gels

Table 19. Composition of self-cast 8% SDS-PAGE protein gels

Stock solution	Volume per 1 gel	Final Conc.	Volume per 1 gel	Final Conc.
ddH2O	3.14 mL	-	2.64 mL	-
Acrylamide/Bis Solution 30% (37.5:1)	1.6 mL	8%	0.52 mL	4%
Tris HCL pH 8.8 (1.8M)	1.2 mL	3.76M	-	-
Tris HCL pH 6.8 (0.625 M)	-	-	0.8	0.08 M
SDS 10% (w/v)	60 µL	0.1 % (w/v)	40 µL	0.1 % (w/v)
APS 10% (w/v)	35 µL	0.06 (w/v)	46 µL	0.1 % (w/v)
TEMED >99% (v/v)	6 µL	0.09 (v/v)	6 µL	0.09 (v/v)
Total volume	6 mL		4 mL	

For separation of MAPKs, 12% self-casted SDS-PAGE protein gels were equally prepared but adding 2.4 mL of Acrylamide/Bis solution to the gel mixture and volumes were adjusted accordingly.

6.2.3. Specification of programs, software and online tools

Table 20.Specification of programs and software

Program/Software	Application	Supplier
UCFS Chimera (Version 1.16)	Analysis of protein molecular structures. Here used for protein visualization and Ramachandran plots	Pettersen EF *et al.,*2004 (National Institutes of Health), California, USA.
PyMOL (Version 2. 5 7)	Molecular visualization system for protein visualization. Here used to analyze surface exposition of mutated sites and display PI4Kβ1 colored domains	The PyMOL Molecular Graphics System, (Schrödinger, L., & DeLano, W., 2020), USA
NAMD (Version 2.13)	Software for molecular dynamics simulation	(Philips *et al*., 2020) Pennsylvania, USA
VMD (Version 1.9.3)	Molecular visualization program for displaying and analyzing protein-ligand complex. Here used to Analyze hydrogen bonds formed and RMSD/RMFD for all atoms	(Humphrey and Schulten, 1996), Illinois, USA
Ligand Reader & Modeler in CHARMM-GUI (CGenFF) (Version 2.4)	Generates the ligand force field parameters and necessary structure files using the general force field (CGenFF)	(Vanommeslaeghe and MacKerell, 2012) Maryland, United States
ImageQuantTL (Version V10.1 – 401)	Phosphorylation image analysis	Cytiva Lifesciences, Stockholm, Sweden
Amersham™ Typhoon™ (Version)	Phosphor imaging scanning	Cytiva Lifesciences, Stockholm, Sweden
UNICORN™ 7 (Version)	Control software for affinity chromatography in ÄKTA pure system	Cytiva Lifesciences, Stockholm, Sweden
Proteome Discoverer (Version 2.5)	Enables comprehensive proteomics data processing workflows	Thermo Scientific, Dreireich, Germany

Table 21.Specification of online tools

Online tool	Application	Supplier
The *Arabidopsis* Information Resource (TAIR)	Online *Arabidopsis* data base: Gene sequences for cloning obtained here	Carnegie Institution, Stanford, CA and National Center for Genome Resources, Santa Fe, NM [http://arabidopsis.org, (April, 2021)].
NetPhos (Version 3.1)	Prediction of phosphorylation sites in eukaryotic proteins	(Blom *et al*., 1999) Glostrup, Denmark.
PhosPhAt (Version 4.0)	Database of phosphorylation sites in *Arabidopsis thaliana* and a plant specific phosphorylation site prediction	(Heazlewood *et al.,* 2007) Potsdam, Germany
The Research Collaboratory for Structural Bioinformatics Protein Data Bank (RCSB PDB)	Database for the 3D structural data of proteins: PI3K in complex with PI and PIP2 used as template for modelling	The Protein Data Bank (Berman et al., 2000) USA.
Alpha fold Data Base	Protein Structure data base used for PI4Kβ1 domain prediction	(Varadi *et al*., 2024) Hinxton, UK
UniProt	Data base for protein sequence and functional information.	(The UniProt consortium, 2023) Geneva, Switzerland
NEBaseChanger (Version 1.3.3)	Site-Directed Mutagenesis primer design	(https://nebasechangerv1.neb.com/) New England Biolabs Inc., Frankfurt, Germany
BoxShade (Version 3.21)	Sequence alignment	K. Hofmann, M. Baron, ExPASy Bioinformatics Resource Portal, SIB Swiss Institute of Bioinformatics, Lausanne, Switzerland
Multalin	Sequence alignment	(Corpet, 1988)

7. Figures

8. Tables

9. Acknowledgements

First of all, I want to thank God and my two guardian Angels my mother and my grandmother, for giving me the strength, wisdom and health to achieve one of my biggest dreams in life “a Doctoral degree” abroad. Thank you for keeping me healthy during Covid times, giving me the strength to overcome the painful appendicitis and for enlightening me in my moments of loneliness by having my family and partner more than 9,000 km away.

I would like to thank my family, my father for being my role model, for his unconditional support, unlimited love, motivation, guidance to become an outstanding professional and for forming me as a person with good values and principles. To my stepmother and four brothers for their full support during these 4 years, advice, unconditional love and motivation to follow my dreams. To my partner Ivan, who always believed in me, who has been walking by my side before I started this PhD journey, for his unconditional love and trust in the whole process. Without their full support and motivation, I would not have completed this journey.

I extend my deepest gratitude to my supervisor, Prof. Dr. Ingo Heilmann, first of all for giving me the opportunity to experience and live the best 4 years of my life so far (my persistence by email was totally worth it). For his incredible trust deposited on my skills as professional and as a person, for giving me the opportunity to achieve one of my biggest dreams in life “to get my Doctoral degree abroad”, for his patience and unlimited support during these four years in Germany. I am immensely grateful for having an excellent supervisor for my research project, for challenging me with interesting research questions, for motivating me to move forward with my experiments, for the interesting discussions in my topic and for making me love science even more thanks to the critical thinking during our meetings. Thank also for not being the usual supervisor, but for being a person that cares for the well-being and work-life balance of your students, which really helped me to cope with research challenges, health issues and life as an international student adapting to a completely new but beautiful culture.

I also want to thank Dr. Mareike Heilmann, not only for training me as a plant biochemist, but also for her constant support, advice and help to move forward with my project. Her help was crucial to finish my doctoral project. Thank you for your immense patience during this whole research journey and for always bringing a nice and contagious happy energy to the research group. I consider you both are a great team, have a clear, efficient plan and interesting ideas for research and that is what I will always aim for once I become an independent researcher.

I am thankful too, to the collaboration partners Prof. Dr. Panos Kastritis and Dr. Marija Sorokina, who helped me with the modelling of the proteins and with their patience helped me to obtain very interesting findings at the end of my doctoral thesis. Also to Dr. Dirk Dobritzsch, Dr. Mathew Fuszard and Henricke for their patience, hard work and persistence to obtain interesting phosphorylation results at the mass spectrometry core facility. Also, to Dr. Justin Lee for providing us with the MAPKs proteins used in this project.

I would also like to thank prof. Ralph Golbik for his crucial contribution to the interpretation of the kinetic data obtained here, for his critical thinking on every aspect of enzymology and for the interesting discussions on the analysis of kinetic parameters obtained during this thesis. His help was crucial to understand the kinetic regulation of the enzyme.

I am also very thankful to my closest colleagues and friends Marta Fratini and Johanna Nordmeier who provided me with unconditional support during my most difficult times and who were also part of my happiest moments in these four years. Thank you for the coffees shared, dinners, advice, academic support and making my everyday life easier in Halle. Very special thanks also goes to my colleagues who helped me during the first years of my PhD when I did not know anyone and I did not even know how to say “Danke”, Johanna U., Monique M., Christoph K., Julia G., Ema B. and Lehnnart S. I am also very thankful to Alexandra S. for her support during my full research, help with peptide microarrays and positive energy and to the colleagues who I got to know more at the end of my PhD Benita, Franzi, Marie, Vera and Irene. Every person in this nice big research group contributed to different stages to this beautiful journey and I am pretty sure my stay would not have been so enjoyable without you around. Finally, a big thank you to my friends around the world and in Halle, Sachi, Daniela, Lizeth y Paola our meetings and our constant talks have been extremely valuable for both my professional and personal life.

My sincere thanks to Marion and Christine, whose expertise in managing laboratory equipment and reagents ready to use was crucial for my experiments. Their patience and readiness to assist at all times were crucial to the completion of my project.

My appreciation also goes to the Martin-Luther-Universität Halle-Wittenberg, for the fully-funded project with core funding, whose resources and assistance have been invaluable and essential for this doctoral project.

10. Curriculum vitae

Angela L. Meza López

Work Until 31.07.2025	PhD Student at Martin-Luther-Universität Halle-Wittenberg

Education

02.2021-07.2025	**PhD student in Plant Biochemistry** Department of Plant Biochemistry (Prof. Dr. Ingo Heilmann) Institut für Biochemie und Biotechnologie Martin-Luther-Universität Halle-Wittenberg 06120 Halle (Saale), Germany
02.2018-12.2020	**Master's Degree in Design and Process Management (Bioprocess)** Engineering Faculty Universidad de La Sabana Chia, Cundinamarca, Colombia.
02.2009-06.2015	**Bachelor's Degree in Biology** Universidad Militar Nueva Granada Faculty of basic and applied sciences Bogotá, Colombia

Publications and conferences

Variation of isoflavone content and DPPH scavenging capacity of phytohormone- treated seedlings after *in vitro* germination of cape broom (*Genista monspessulana*). Authors: A. Meza, P. Rojas, W. Cely-Veloza, C. Guerrero Perilla, E. Coy-Barrera. 2020. Journal: South African Journal of Botany. https://doi.org/10.1016/j.sajb.2019.12.006

Botanik-Tagung, International Conference of our German Society for Plant Sciences. Participation: Poster. Date: 15-19th September., 2024 Halle (Saale), Germany.

International Conference on Biotechnology and Genetic Engineering. Participation: Speaker in oral presentation. Date: October 28- 30, 2019. (Paris, France).

XLIX National Congress of Biological Sciences.Participation: Speaker in oral presentation (Lecturer). Date: 7th to 10th October - 2014. (Sincelejo, Colombia). Project: Relation composition and antioxidant capacity of *Genista monspessulanna* front the effect of hormones in explants *in vitro*. Ángela MEZA, Paola ROJAS, Willy Cely-Celoza, Camilo GUERRERO, Ericsson COY-BARRERA.

11. Erklärung

Hiermit erkläre ich, dass ich die vorliegende Dissertation selbständig und ohne fremde Hilfe verfasst habe, keine anderen als die angegebenen Quellen und Hilfs-mittel benutzt habe und die den benutzten Werken wörtlich oder inhaltlich entnom-menen Stellen als solche kenntlich gemacht habe.

Des Weiteren erkläre ich, bisher keine vergeblichen Promotionsversuche unternom-men zu haben und die Dissertation in der gegenwärtigen bzw. in einer anderen Fassung nicht bereits an einer anderen Fakultät vorgelegt zu haben.

Halle (Saale), _____ _____

Angela L. Meza López